

Remarks

The Official Action dated December 23, 2008 and the Advisory Action of April 14, 2009 have been carefully reviewed. The present remarks, which are responsive to the Official Actions, are being filed as part of the submission required under 37 C.F.R. §1.114, in connection with the Request for Continued Examination, which is submitted concurrently herewith. In view of the amendments submitted herewith and the following remarks, favorable reconsideration and allowance of this application are respectfully requested. Applicants are submitting the previously filed response in its entirety as the Examiner has indicated in the Advisory Action that these amendments and accompanying remarks have not been entered into the present application.

The December 23, 2008 Official Action and the references cited therein have been carefully reviewed. In view of the present amendments and following remarks, favorable reconsideration and allowance of this application are respectfully requested.

At page 2 of the Official Action, the Examiner has rejected claims 9, 10, 12, 19, 36, 37, 52 under 35 U.S.C. §112, first paragraph as allegedly failing to satisfy the written description requirement.

Claims 9, 10, 12, 19, 21, 22, 24, 27, 36, 37, 46, 47, and 52 stand rejected under 35 U.S.C. §112, first paragraph. It is the Examiner's position that the specification fails to provide reasonable enablement for methods employing antisense mediated inhibition of p66shc in vivo.

Applicants respectfully submit that the claims as presently amended are in condition for allowance. Each of the above-noted rejections under 35 U.S.C. §112, first paragraph is, therefore, respectfully traversed.

**THE CLAIMS AS AMENDED FULLY SATISFY THE REQUIREMENTS
OF 35 U.S.C. §112, FIRST PARAGRAPH**

A. Written Description

Claims 9, 10, 12, 19, 36, 37, 52 stand rejected under 35 U.S.C. §112, first paragraph as the specification allegedly fails to adequately describe the genus of agents encompassed by the claims. Applicants respectfully disagree. The skilled person having the sequence information provided in the specification before him or her would readily be able to obtain nucleic acid molecules, either antisense or siRNA which are effective to down modulate p66shc expression and use the same to reduce the expression of p66shc in target cells.

At page 4 of the Official Action, the Examiner acknowledges that the specification does describe an antisense nucleic acid which specifically hybridizes to a nucleotide sequence which encodes p66shc protein and is effective to down modulate expression of p66shc protein. In order to expedite prosecution, claims 9, 10, 12, 19, 36, 37 and 52 have been amended to recite this feature. Applicants reserve the right to file one or more continuing applications on any subject matter canceled in accordance with the present amendment.

It is submitted that the foregoing amendment obviates the rejection of the aforementioned claims based on inadequate written description. Accordingly, Applicants request the rejection be withdrawn. It is noted that the Examiner indicated in the Advisory Action that the foregoing amendment has overcome this ground of rejection.

B. Enablement

The Examiner has rejected claims 9, 10, 12, 19, 21, 22, 24, 27, 36, 37, 46, 47 and 52 asserting that undue experimentation would be required to practice the invention as claimed. Specifically, the Examiner contends that the

specification fails to enable practice of the present method in vivo. Applicants respectfully and strenuously disagree.

At the outset, Applicants do not concur with the Examiner's assertion that the state of the antisense mediated gene inhibition is highly unpredictable. Indeed a search of the USPTO.gov database using the term ACLM/"antisense" reveals hundreds of issued patents directed to antisense molecules for down regulating expression of target genes of interest to treat pathological disorders. Notably, many of these patents are not limited to methods for in vitro administration and frequently exemplify the use of in vivo mouse models to demonstrate efficacy. Applicants appreciate that each case is examined on its own merits however, given the plethora of references, applications and issued patents in this art area, it cannot be reasonably maintained that the skilled person doubts that administration of antisense molecules in vivo are effective for down modulating target gene expression.

In further support of Applicant's position, listed below are several companies actively involved in developing antisense therapeutics for the treatment and prevention of a wide variety of diseases which include viral infection, cancer, multiple sclerosis, cardiovascular disease, diabetes and inflammation.

1. Isis Pharmaceuticals (www.isispharm.com)

Isis Pharmaceuticals is the leading antisense company and "Vitravene" (fomivirsen) is the first antisense drug to achieve marketing clearance. Vitravene treats a condition called cytomegalovirus (CMV) retinitis in people with AIDS.

ISIS has 14 antisense drugs in clinical trials for indications including cancer, cardiovascular, inflammation, Multiple sclerosis and diabetes

2. Genta (www.genta.com)

Genta are currently developing "genesense" for cancer treatment and are in a phase II clinical trial (for Melanoma and CLL).

3. AVI BioPharma (www.avibio.com)

AVI BioPharma are in a phase I/II clinical trial with an antisense molecule for the prevention of restenosis. They also have another antisense molecule in phase I for Duchene Muscular Dystrophy.

4. OncoGenex (www.oncogenex.com)

Oncogenex has 5 antisense products in development (OGX-011, OGX-427, SN2310, CSP-9222 and OGX-223) all of which are undergoing clinical trials in cancer (OGX-011 is currently in Phase II/III)

5. Ester Neurosciences (www.amarincorp.com)

Ester Neurosciences are developing antisense molecules for the treatment of neurological disorders. They are currently in a Phase IIb with EN101 (orally available antisense) for the treatment of Myasthenia Gravis

6. Lorus Therapeutics (www.lorusthera.com)

Lorus Therapeutics have three antisense products in development and LOR 2040 is already undergoing clinical trials in cancer (AML).

Applicants have also performed a search of the PUBMED database using antisense as a search term. This search revealed no less than 28,635 hits. A listing of the first fifty abstracts identified is attached.

Finally, Applicants are also providing copies of several recent publications describing the use of efficacious antisense molecules in vivo. See for example:

1. Cross-species comparison of in vivo PK/PD relationships for second-generation antisense oligonucleotides targeting apolipoprotein B-100

Yu RZ, Lemonidis KM, Graham MJ, Matson JE, Crooke RM, Tribble DL, Wedel MK, Levin AA, Geary RS. Biochem Pharmacol. 2008 Nov 14.

2. Regression of prostate cancer xenografts by RLIP76 depletion. Singhal SS, Roth C, Leake K, Singhal J, Yadav S, Awasthi S.

Biochem Pharmacol. 2008 Nov 25.

3. Antisense inhibition of ATM gene enhances the radiosensitivity of head and neck squamous cell carcinoma in mice Zou J, Qiao X, Ye H, Yang Y, Zheng X, Zhao H, Liu

J Exp Clin Cancer Res. 2008 Oct 26;27:56.

4. Enhanced therapeutic effects for human pancreatic cancer by application K-ras and IGF-IR antisenseoligonucleotides
Shen YM, Yang XC, Yang C, Shen JK.
World J Gastroenterol. 2008 Sep 7;14(33):5176-85

5. Matrix metalloproteinase-9 Inhibition Down-Regulates Radiation-Induced Nuclear Factor-KB Activity Leading to Apoptosis in BreastTumors Kunigal S, Lakka SS, Joseph P, Estes N, Rao JS.
Clin Cancer Res. 2008 Jun 1;14(11):3617-26.

6. Survivin Antisense Oligonucleotides Effectively Radiosensitize Colorectal Cancer Cells in both Tissue Culture and Murine Xenograft Models Rödel F, Frey B, Leitmann W, Capalbo G, Weiss C, Rödel C.
Int J Radiat Oncol Biol Phys. 2008 May 1;71(1):247-55.

Notably, several groups are actively working on antisense technologies for down modulating p66Shc. These include

7. Veeramani et al (Oncogene 24, 7203-7212 (2005)).

8. Wu Z. J Cell. Phys. 209 996-1005 (2006).

9. Tiberi et al BBRC 342 503-508 (2006).

10. Nemoto et al J. Biol.Chem. 281 (15) 10555-10560 (2006).

Copies attached.

In the Advisory Action, the Examiner asserts that references 1-6 were not submitted to the office. A check of PAIR however, indicates that all of these references were submitted in connection with Applicants' response to the Final Official Action. All of these references are being resubmitted as evidence refuting the Examiner's contention that the art of antisense technology is unpredictable. They are not being presented in connection with an information

disclosure statement as they do not comprise prior art that is relevant to the patentability of applicants claims.

In view of all the foregoing, Applicants take exception to the Examiner's assertion that the present claims are not fully enabled by the disclosure in the specification. Indeed, once the antisense molecule for the target is identified, routine methods are available for administering the same to a subject *in vivo* as are methods for assessing the subject for a reduction in symptoms associated with arteriosclerosis, ischemic heart disease, lung emphysema, myocardial infarction, stroke, premature aging, cell senescence, Parkinson's, Alzheimer's, cancers, and vascular complications of diabetes. The Examiner has acknowledged that Applicants have described an antisense sequence which is effective to down modulate production of p66shc protein. Administration of the molecule the invention *in vivo* is well within the purview of the skilled person without resort to undue experimentation.

In In re Wands, 8 USPQ2d 1400 (1988) cited by the Examiner, the Federal Circuit Court of Appeals held that engaging in experimentation to practice a claimed invention does not render the disclosure non-enabling as long as the experimentation required is not "undue". The Court stated that: "The determination of what constitutes undue experimentation in a given case requires the application of a standard of reasonableness . . . The test is not merely quantitative, since a considerable amount of experimentation is permissible, if it is merely routine or if the specification in question provides a reasonable amount of guidance with respect to the direction in which the experimentation should proceed." In re Wands, 8 USPQ2d 1400, 1404 (Fed. Cir. 1988).

In the present case, the experimentation necessary is merely routine and is inherent in the nature of the art.

Therefore, there is no undue burden of experimentation. The level of skill in the art of antisense administration is high as exemplified by the many citations provided herein, and the required techniques for administration of the same are familiar to those skilled in this art area. Indeed, the endpoints to be assessed for efficacy, i.e., the metabolic changes described in Figure 9 and means for assessing the same are all disclosed in the specification.

In view of all the foregoing, it is respectfully submitted that the specification wholly enables practice of the full scope of the currently claimed methods.

RESPONSE TO EXAMINER'S REMARKS IN ADVISORY ACTION

As mentioned above, Applicants note that the Examiner has indicated that the present amendment has overcome the 35 U.S.C. §112, first paragraph rejection based on inadequate written description. Applicants strenuously disagree with the Examiner's contention that the presently claimed subject matter is not fully enabled by the disclosure in the present specification. Indeed at page 13, lines 17 to 21 Applicants provide three references describing *in vivo* administration of antisense oligonucleotides. Attached for the Examiner's consideration is an article entitled "Therapeutic Applications of Oligonucleotides" by Stanley T. Crooke. *In vivo* applications of antisense oligonucleotides are described at several sections of the reference. See for example page 342 where various *in vivo* routes for administration of oligonucleotides are described. Enablement must be assessed using the teachings in the specification as well as the knowledge of those skilled in the art at the time the application was filed. Clearly, methods for administering antisense oligonucleotides *in vivo* were known to the skilled artisan as evidenced by the teachings of Crooke in 1992. The Examiner has acknowledged that Applicants have fully described

a functional antisense molecule which down modulates p66Shc production. Applicants submit that the skilled person having the foregoing before him or her would be readily able to practice the present invention over the full scope of the claims without undue experimentation. Nothing more is required under 35 U.S.C. §112, first paragraph. Accordingly, Applicants respectfully request that the rejection of the present claims for inadequate enablement be withdrawn.

CONCLUSION

It is respectfully requested that the amendments presented herewith be entered in this application, since the amendments are primarily formal, rather than substantive in nature. This amendment is believed to clearly place the pending claims in condition for allowance.

In the event the Examiner is not persuaded as to the allowability of any claim, and it appears that any outstanding issues may be resolved through a telephone interview, the Examiner is requested to telephone the undersigned attorney at the phone number given below.

In the event a fee is required or an overpayment is made, the Commissioner is authorized to charge or credit the deposit account of the undersigned, Account No. 04-1406.

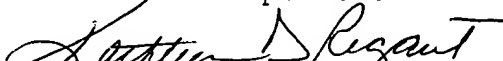
Early and favorable action on the present application is earnestly solicited.

Respectfully submitted,

DANN, DORFMAN, HERRELL AND SKILLMAN

A Professional Corporation

By



Kathleen D. Rigaut, Ph.D., J.D.

PTO Registration No. 43,047

Telephone: (215) 563-4100

Enclosures

All Databases PubMed Nucleotide Protein Genome Structure OMIM PMC
 Journals Books

Search for

[Advanced Search](#)

[Save Search](#)

[Limits](#) [Preview/Index](#) [History](#) [Clipboard](#) [Details](#)

Display Show Sort By Send to

All: 28635 Review: 3060

Items 1 - 20 of 28635

of 1432 Next

1: [Docetaxel plus oblimersen sodium \(Bcl-2 antisense oligonucleotide\): an EORTC multicenter, randomized phase II study in patients with castration-resistant prostate cancer.](#)

Sternberg CN, Dumez H, Van Poppel H, Skoneczna I, Sella A, Daugaard G, Gil T, Graham J, Carpentier P, Calabro F, Collette L, Lacombe D; for the EORTC Genitourinary Tract Cancer Group.

Ann Oncol. 2009 Mar 17. [Epub ahead of print]

PMID: 19297314 [PubMed - as supplied by publisher]

[Related Articles](#)

2: [Targeted Delivery Systems for Oligonucleotide Therapeutics.](#)

Yu B, Zhao X, Lee LJ, Lee RJ.

AAPS J. 2009 Mar 19. [Epub ahead of print]

PMID: 19296227 [PubMed - as supplied by publisher]

[Related Articles](#)

3: [Defensin-like polypeptide LUREs are pollen tube attractants secreted from synergid cells.](#)

Okuda S, Tsutsui H, Shiina K, Sprunck S, Takeuchi H, Yui R, Kasahara RD, Hamamura Y, Mizukami A, Susaki D, Kawano N, Sakakibara T, Namiki S, Itoh K, Otsuka K, Matsuzaki M, Nozaki H, Kuroiwa T, Nakano A, Kanaoka MM, Dresselhaus T, Sasaki N, Higashiyama T.

Nature. 2009 Mar 19;458(7236):357-61.

PMID: 19295610 [PubMed - in process]

[Related Articles](#)

4: [Reverse signaling by glycosylphosphatidylinositol-linked manduca ephrin requires a SRC family kinase to restrict neuronal migration in vivo.](#)

Coate TM, Swanson TL, Copenhaver PF.

J Neurosci. 2009 Mar 18;29(11):3404-18.

PMID: 19295147 [PubMed - in process]

[Related Articles](#)

5: [Strategies for blocking the fibrogenic actions of connective tissue growth factor \(CCN2\): From pharmacological inhibition](#)

Also try:

[antisense oligonucleotides](#)

[natural antisense](#)

[antisense transcripts](#)

[antisense therapy](#)

[antisense oligo](#)

Recent Activity

[Turn Off](#) [Clear](#)

[antisense](#) (28635) [PubMed](#)

in vitro to targeted siRNA therapy in vivo.

Brigstock DR.

J Cell Commun Signal. 2009 Mar 18. [Epub ahead of print]

PMID: 19294531 [PubMed - as supplied by publisher]

[Related Articles](#)

6: T7-based linear amplification of low concentration mRNA samples using beads and microfluidics for global gene expression measurements.

Kralj JG, Player A, Sedrick H, Munson MS, Petersen D, Forry SP, Meltzer P, Kawasaki E, Locascio LE.

Lab Chip. 2009 Apr 7;9(7):917-24. Epub 2008 Dec 15.

PMID: 19294302 [PubMed - in process]

[Related Articles](#)

7: Rational Design of Antisense Oligomers to Induce Dystrophin Exon Skipping.

Mitrapant C, Adams AM, Meloni PL, Muntoni F, Fletcher S, Wilton SD.

Mol Ther. 2009 Mar 17. [Epub ahead of print]

PMID: 19293776 [PubMed - as supplied by publisher]

[Related Articles](#)

8: The Efficiency of CD40 Down Regulation by siRNA and Antisense ODN: Comparison of Lipofectamine and FuGENE6.

Ebadi P, Karimi MH, Pourfathollah AA, Saheb Ghadam Lotfi A, Soheili ZS, Samiee S, Hajati S, Nadali F, Geramizadeh B, Moazzeni SM.

Iran J Immunol. 2009 Mar;6(1):1-11.

PMID: 19293472 [PubMed - in process]

[Related Articles](#)

9: Antisense expression of PKC α improved sensitivity of SGC7901/VCR cells to doxorubicin.

Wu DL, Sui FY, Du C, Zhang CW, Hui B, Xu SL, Lu HZ, Song GJ.

World J Gastroenterol. 2009 Mar 14;15(10):1259-63.

PMID: 19291828 [PubMed - in process]

[Related Articles](#) [From article at journal site](#)

10: A LC-MS/MS Method for the Analysis of Intracellular Nucleoside Triphosphate Levels.

Chen P, Liu Z, Liu S, Xie Z, Aimiuwu J, Pang J, Klisovic R, Blum W, Grever MR, Marcucci G, Chan KK.

Pharm Res. 2009 Mar 17. [Epub ahead of print]

PMID: 19291372 [PubMed - as supplied by publisher]

[Related Articles](#)

11: Transferrin Receptor Targeted Lipopolymplexes for Delivery of Antisense Oligonucleotide G3139 in a Murine K562 Xenograft Model.

Zhang X, Koh CG, Yu B, Liu S, Piao L, Marcucci G, Lee RJ, Lee LJ.

Pharm Res. 2009 Mar 17. [Epub ahead of print]

PMID: 19291371 [PubMed - as supplied by publisher]

12: Is HIV Eradication Feasible?

de Mendoza C.

AIDS Rev. 2009 Jan-Mar;11(1):52-3.

PMID: 19290034 [PubMed - in process]

[Related Articles](#)

 13: Auger Radiation-Induced, Antisense-Mediated Cytotoxicity of Tumor Cells Using a 3-Component Streptavidin-Delivery Nanoparticle with 111In.

Liu X, Wang Y, Nakamura K, Kawauchi S, Akalin A, Cheng D, Chen L, Rusckowski M, Hnatowich DJ.

J Nucl Med. 2009 Mar 16. [Epub ahead of print]

PMID: 19289423 [PubMed - as supplied by publisher]

[Related Articles](#)

 14: Efficacy of systemic morpholino exon-skipping in duchenne dystrophy dogs.

Yokota T, Lu QL, Partridge T, Kobayashi M, Nakamura A, Takeda S, Hoffman E.

Ann Neurol. 2009 Mar 13. [Epub ahead of print]

PMID: 19288467 [PubMed - as supplied by publisher]

[Related Articles](#)

 15: Influence of basic fibroblast growth factor on the growth of HeLa cells and the expression of angiogenin.

Yang J, Wang J, Zhao J, Zuo D, Li X, Wang L.

Oncol Rep. 2009 Apr;21(4):949-55.

PMID: 19287993 [PubMed - in process]

[Related Articles](#)

 16: A natural antisense transcript, BOKAS, regulates the pro-apoptotic activity of human Bok.

Zhang H, Gao S, De Geyter C.

Int J Oncol. 2009 Apr;34(4):1135-8.

PMID: 19287972 [PubMed - in process]

[Related Articles](#)

 17: In silico prediction and experimental validation of natural antisense transcripts in two cancer-associated regions of human chromosome 6.

Monti L, Cinquetti R, Guffanti A, Nicassio F, Cremona M, Lavorgna G, Bianchi F, Vignati F, Cittaro D, Taramelli R, Acquati F.

Int J Oncol. 2009 Apr;34(4):1099-108.

PMID: 19287968 [PubMed - in process]

[Related Articles](#)

 18: Irinotecan-induced ovarian follicular apoptosis is attenuated by deleting the kinase domain of death-associated protein kinase.

Li L, Tanaka T, Yukawa K, Akira S, Umesaki N.

Int J Oncol. 2009 Apr;34(4):905-14.

PMID: 19287947 [PubMed - in process]

[Related Articles](#)



Phase II trial of Belagenpumatucel-L, a TGF-beta2 antisense gene modified allogeneic tumor vaccine in advanced non small cell lung cancer (NSCLC) patients.

Nemunaitis J, Nemunaitis M, Senzer N, Snitz P, Bedell C, Kumar P, Pappen B, Maples PB, Shawler D, Fakhrai H.

Cancer Gene Ther. 2009 Mar 13. [Epub ahead of print]

PMID: 19287371 [PubMed - as supplied by publisher]

[Related Articles](#)

20: MicroRNA 184 regulates expression of NFAT1 in umbilical cord blood CD4+ T-cells.

Weitzel RP, Lesniewski ML, Haviernik P, Kadereit S, Leahy P, Greco NJ, Laughlin MJ.

Blood. 2009 Mar 13. [Epub ahead of print]

PMID: 19286996 [PubMed - as supplied by publisher]

[Related Articles](#)

Items 1 - 20 of 28635

1 of 1432

Display Show Sort By Send to

[Write to the Help Desk](#)

[NCBI](#) | [NLM](#) | [NIH](#)

[Department of Health & Human Services](#)

[Privacy Statement](#) | [Freedom of Information Act](#) | [Disclaimer](#)

All Databases PubMed Nucleotide Protein Genome Structure OMIM PMC
Journals Books

Search for

[Advanced Search](#)

[Save Search](#)

[Limits](#) [Preview/Index](#) [History](#) [Clipboard](#) [Details](#)

Display Show Sort By Send to

All: 28635

Items 21 - 40 of 28635

Previous of
1432 Next

21: [Nested Genes CDA12 and CDA13 Encode Proteins Associated with Membrane Trafficking in the Ciliate Tetrahymena thermophila.](#)

Zweifel E, Smith J, Romero D, Giddings TH Jr, Winey M, Honts J, Dahlseid J, Schneider B, Cole ES.

Eukaryot Cell. 2009 Mar 13. [Epub ahead of print]

PMID: 19286988 [PubMed - as supplied by publisher]

[Related Articles](#)

[Turn Off](#) [Clear](#)

[antisense \(28635\)](#) [PubMed](#)

22: [Microbubble Stability is a Major Determinant of the Efficiency of Ultrasound and Microbubble Mediated In Vivo Gene Transfer.](#)

Alter J, Sennoga CA, Lopes DM, Eckersley RJ, Wells DJ.

Ultrasound Med Biol. 2009 Mar 12. [Epub ahead of print]

PMID: 19285783 [PubMed - as supplied by publisher]

[Related Articles](#)

23: [Both foxj1a and foxj1b are implicated in left-right asymmetric development in zebrafish embryos.](#)

Tian T, Zhao L, Zhang M, Zhao X, Meng A.

Biochem Biophys Res Commun. 2009 Mar 13;380(3):537-42. Epub 2009 Jan 23.

PMID: 19284996 [PubMed - in process]

[Related Articles](#)

24: [Increased expression of heat shock protein 105 in rat uterus of early pregnancy and its significance in embryo implantation.](#)

Yuan JX, Xiao LJ, Lu CL, Zhang XS, Liu T, Chen M, Hu ZY, Gao F, Liu YX.

Reprod Biol Endocrinol. 2009 Mar 13;7(1):23. [Epub ahead of print]

PMID: 19284651 [PubMed - as supplied by publisher]

[Related Articles](#) [From article at journal site](#)

25: [Anti-angiogenesis effect of generation 4 polyamidoamine/vascular endothelial growth factor antisense oligodeoxynucleotide on breast cancer in vitro.](#)

Gu SZ, Zhao XH, Zhang LX, Li L, Wang ZY, Meng M, An GL.

J Zhejiang Univ Sci B. 2009 Mar;10(3):159-67.

PMID: 19283869 [PubMed - in process]

Related Articles Free article in PMC 1st journal site

26: Spermatozoal RNAs: What about their functions?

Dadoune JP.

Microsc Res Tech. 2009 Mar 12. [Epub ahead of print]

PMID: 19283828 [PubMed - as supplied by publisher]

Related Articles

27: A genetic strategy involving a glycosyltransferase promoter and a lipid translocating enzyme to eliminate cancer cells.

Levano K, Sobocki T, Jayman F, Debata PR, Sobocka MB, Banerjee P.

Glycoconj J. 2009 Mar 12. [Epub ahead of print]

PMID: 19283471 [PubMed - as supplied by publisher]

Related Articles

28: Cloning and characterization of a squalene synthase gene from a petroleum plant, *Euphorbia tirucalli* L.

Uchida H, Yamashita H, Kajikawa M, Ohyama K, Nakayachi O, Sugiyama R, Yamato KT, Muranaka T, Fukuzawa H, Takemura M, Ohyama K.

Planta. 2009 Mar 13. [Epub ahead of print]

PMID: 19283408 [PubMed - as supplied by publisher]

Related Articles

29: A large-scale chemical modification screen identifies design rules to generate siRNAs with high activity, high stability and low toxicity.

Bramsen JB, Laursen MB, Nielsen AF, Hansen TB, Bus C, Langkjær N, Babu BR, Højland T, Abramov M, Van Aerschot A, Odadzic D, Smiclus R, Haas J, Andree C, Barman J, Wenska M, Srivastava P, Zhou C, Honcharenko D, Hess S, Müller E, Bobkov GV, Mikhailov SN, Fava E, Meyer TF, Chattopadhyaya J, Zerial M, Engels JW, Herdewijn P, Wengel J, Kjems J.

Nucleic Acids Res. 2009 Mar 12. [Epub ahead of print]

PMID: 19282453 [PubMed - as supplied by publisher]

Related Articles Free article at journal site

30: Disease-causing mutations improving the branch site and polypyrimidine tract: pseudoexon activation of LINE-2 and antisense Alu lacking the poly(T)-tail.

Meili D, Kralovicova J, Zagalak J, Bonafé L, Fiori L, Blau N, Thöny B, Vorechovsky I.

Hum Mutat. 2009 Jan 20. [Epub ahead of print]

PMID: 19280650 [PubMed - as supplied by publisher]

Related Articles

31: Enhanced tolerance to chilling stress in OsMYB3R-2 transgenic rice is mediated by alteration in cell cycle and ectopic expression of stress genes.

Ma Q, Dai X, Xu Y, Guo J, Liu Y, Chen N, Xiao J, Zhang D, Xu Z, Zhang X, Chong K.

Plant Physiol. 2009 Mar 18. [Epub ahead of print]

Related Articles From article at journal site

32: Nitrogen excretion in developing zebrafish (*Danio rerio*): A role for Rh proteins and urea transporters.

Braun MH, Steele SL, Ekker M, Perry SF.

Am J Physiol Renal Physiol. 2009 Mar 11. [Epub ahead of print]

PMID: 19279128 [PubMed - as supplied by publisher]

Related Articles

33: Sensitization of *Campylobacter jejuni* to fluoroquinolone and macrolide antibiotics by antisense inhibition of the CmeABC multidrug efflux transporter.

Jeon B, Zhang Q.

J Antimicrob Chemother. 2009 Mar 11. [Epub ahead of print]

PMID: 19279049 [PubMed - as supplied by publisher]

Related Articles

34: Lin9 is required for mitosis and cell survival during early zebrafish development.

Kleinschmidt MA, Wagner TU, Liedtke D, Spahr S, Samans B, Gaubatz S.

J Biol Chem. 2009 Mar 11. [Epub ahead of print]

PMID: 19278998 [PubMed - as supplied by publisher]

Related Articles From article at journal site

35: Octa-guanidine Morpholino Restores Dystrophin Expression in Cardiac and Skeletal Muscles and Ameliorates Pathology in Dystrophic mdx Mice.

Wu B, Li Y, Morcos PA, Doran TJ, Lu P, Lu QL.

Mol Ther. 2009 Mar 10. [Epub ahead of print]

PMID: 19277018 [PubMed - as supplied by publisher]

Related Articles

36: Modular protein engineering in emerging cancer therapies.

Vázquez E, Ferrer-Miralles N, Mangues R, Corchero JL, Schwartz S Jr, Villaverde A.

Curr Pharm Des. 2009;15(8):893-916.

PMID: 19275653 [PubMed - in process]

Related Articles

37: Microinjection of zebrafish embryos to analyze gene function.

Rosen JN, Sweeney MF, Mably JD.

J Vis Exp. 2009 Mar 9;(25). pii: 1115. doi: 10.3791/1115.

PMID: 19274045 [PubMed - in process]

Related Articles From article at journal site

38: Light-independent cell death induced by accumulation of pheophorbide a in *Arabidopsis thaliana*.

Hirashima M, Tanaka R, Tanaka A.

Plant Cell Physiol. 2009 Mar 8. [Epub ahead of print]

PMID: 19273468 [PubMed - as supplied by publisher]

Related Articles

39: Requirement of focal adhesion kinase in branching tubulogenesis

Wei WC, Kopeck AK, Tang MJ.

J Biomed Sci. 2009 Jan 12;16(1):5.

PMID: 19272169 [PubMed - in process]

Related Articles From article in PMC at journal site

40: Molecular Characterization of a TIA-1-Like RNA-Binding Protein in Cells Derived from the Fall Armyworm *Spodoptera frugiperda* (Lepidoptera: Noctuidae).

Muto S, Tanabe T, Matsumoto E, Mori H, Kotani E.

Biosci Biotechnol Biochem. 2009 Mar 7. [Epub ahead of print]

PMID: 19270389 [PubMed - as supplied by publisher]

Related Articles From article at journal site

Items 21 - 40 of 28635

Previous 2 of

Display Show Next

[Write to the Help Desk](#)

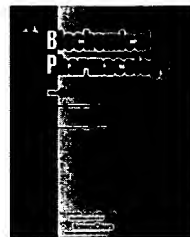
[NCBI](#) | [NLM](#) | [NIH](#)

[Department of Health & Human Services](#)

[Privacy Statement](#) | [Freedom of Information Act](#) | [Disclaimer](#)



ELSEVIER

available at www.sciencedirect.comjournal homepage: www.elsevier.com/locate/biochempharm

Cross-species comparison of in vivo PK/PD relationships for second-generation antisense oligonucleotides targeting apolipoprotein B-100

Rosie Z. Yu ^{*}, Kristina M. Lemonidis, Mark J. Graham, John E. Matson, Rosanne M. Crooke, Diane L. Tribble, Mark K. Wedel, Arthur A. Levin, Richard S. Geary

Primary Laboratory of Origin, Isis Pharmaceuticals, Inc., 1896 Rutherford Road, Carlsbad, CA 92008, United States

ARTICLE INFO

Article history:

Received 24 July 2008

Accepted 6 November 2008

Keywords:

Pharmacokinetics

Pharmacodynamics

ApoB

Lipid lowering

Cross-species

Antisense

ABSTRACT

The in vivo pharmacokinetics/pharmacodynamics of 2'-O-(2-methoxyethyl) (2'-MOE) modified antisense oligonucleotides (ASOs), targeting apolipoprotein B-100 (apoB-100), were characterized in multiple species. The species-specific apoB antisense inhibitors demonstrated target apoB mRNA reduction in a drug concentration and time-dependent fashion in mice, monkeys, and humans. Consistent with the concentration-dependent decreases in liver apoB mRNA, reductions in serum apoB, and LDL-C, and total cholesterol were concurrently observed in animal models and humans. Additionally, the long duration of effect after cessation of dosing correlated well with the elimination half-life of 2'-MOE modified apoB ASOs studied in mice ($t_{1/2} \cong 20$ days) and humans ($t_{1/2} \cong 30$ days) following parental administrations. The plasma concentrations of ISIS 301012, observed in the terminal elimination phase of both mice and monkeys were in equilibrium with liver. The partition ratios between liver and plasma were similar, approximately 6000:1, across species, and thus provide a surrogate for tissue exposure in humans. Using an inhibitory E_{max} model, the ASO liver EC_{50} were 101 ± 32 , 119 ± 15 , and 300 ± 191 $\mu\text{g/g}$ of ASO in high-fat-fed (HF) mice, transgenic mice containing the human apoB transgene, and monkeys, respectively. The estimated liver EC_{50} in man, extrapolated from trough plasma exposure, was 81 ± 122 $\mu\text{g/g}$. Therefore, extraordinary consistency of the exposure-response relationship for the apoB antisense inhibitor was observed across species, including human. The cross-species PK/PD relationships provide confidence in the use of pharmacology animal models to predict human dosing for second-generation ASOs targeting the liver.

© 2008 Elsevier Inc. All rights reserved.

1. Introduction

Applying pharmacokinetic and pharmacodynamic analyses to guide and expedite drug development is well recognized and

has received increasing interest in recent years [1]. Although these principles are well accepted and widely used for low molecular weight drugs and proteins, there have been a growing number of reports describing pharmacokinetic and

^{*} Corresponding author. Tel.: +1 760 603 2549; fax: +1 760 603 3862.

E-mail address: Ryu@isisph.com (R.Z. Yu).

Abbreviations: ASO, antisense oligonucleotide; ApoB-100, apolipoprotein B-100; VLDL-C, very low density lipoprotein cholesterol; IDL-C, intermediate density lipoprotein cholesterol; LDL-C, low-density lipoprotein cholesterol; HF-fed, high-fat diet fed; IACUC, Institutional Animal Care and Use Committee; s.c., subcutaneous; i.p., intraperitoneal; ELISA, enzyme-linked immunosorbent assay; LLOQ, the lower limit of quantitation; CGE, capillary gel electrophoresis; SPE, solid phase extraction; MOE, 2'-O-(2-methoxy) ethyl.

0006-2952/\$ - see front matter © 2008 Elsevier Inc. All rights reserved.

[doi:10.1016/j.bcp.2008.11.005](https://doi.org/10.1016/j.bcp.2008.11.005)

pharmacodynamic relationships with antisense therapeutic agents [2-5].

The pharmacokinetics of 2'-methoxyethyl (2'-MOE) chimeric phosphorothioate antisense oligonucleotides (ASOs), or second-generation ASOs, have been described in a number of species including man [6-10]. The structure of the second-generation ASOs is characterized by five 2'-MOE modifications on the ribose sugar at both 5'- and 3'-termini, flanking a 10-nucleotide oligodeoxynucleotide gap (5-10-5 2'MOE chimeras) with phosphorothioate backbone. Although there are slight sequence dependent differences, the pharmacokinetics of the second-generation ASOs are remarkably similar and are characterized by predictable distribution and prolonged tissue elimination (14-30 days) as compared to first-generation oligonucleotides.

Although, ASOs have been shown to be able to work by multiple mechanisms once bound to the target RNA [11], all of the 2'MOE chimeric ASOs in development have been shown to work by forming RNA-ASO duplexes that serve as a substrate for RNase H₁ [12,13]. RNase H₁ cleaves the RNA to which the ASO is bound, resulting in loss of the target RNA and eventually the protein, both of which have been measured as a direct means of evaluating pharmacodynamic effects.

Consequently, the ASO prevents the translation of the encoded protein product in a highly sequence-specific manner. Because of the unique mechanism of action of antisense therapeutics, investigations of the pharmacological effects of antisense oligonucleotide *in vivo* have focused primarily on target mRNA reduction and the subsequent reduction in protein translation and the downstream effects resulting from target protein reduction, which are dependent on the target studied. Moreover, establishment of the correlation between plasma equilibrium concentrations with the concentrations at the target sites is pertinent, enabling plasma concentrations to be used as a surrogate in clinical studies to establish the pharmacodynamics and pharmacokinetics relationships. Translation of preclinical to clinical PK/PD relationships require predictive pharmacokinetics and reliable PD biomarkers that can be assessed in real time. In this report, we present data from multiple species for potent apolipoprotein B-100 (apoB-100) 2'-MOE chimeric antisense compounds that provides both of these prerequisites; predictable cross-species pharmacokinetics [9] and reliable biomarkers, apoB itself and its related LDL-cholesterol particles measured in serum in real time.

ApoB-100 is the protein component of atherogenic lipids and triglycerides, including LDL-cholesterol. ApoB-100 is synthesized and packaged into lipoprotein particles principally in the liver of all species [14-16]. Circulating LDL-C, which typically constitutes 60-70% of serum cholesterol, is widely recognized as a major risk factor for coronary heart disease (CHD) and has been implicated in the inflammation associated with the pathogenesis of atherosclerosis. Similarly, apoB-100 is now recognized as a risk factor for atherosclerosis. This led to the development of an antisense inhibitor of the molecular target, apolipoprotein B (apoB), for use in lowering apoB-100 and subsequent lowering LDL-C.

Since the sequence of mRNAs for apoB-100 differs depending on the species and 2'-MOE ASOs are highly specific, we have used species-specific apoB-100 ASOs to demonstrate

potent dose-dependent reduction of apoB-100 mRNA and protein in the liver of all species tested and concomitant reductions in plasma apoB and apoB-100 containing lipoproteins [17,18]. Species-specific apoB antisense inhibitors had been evaluated in multiple animal species, including mice, hamsters, rabbits and monkeys (lean and HF-fed) and it had been demonstrated that administration of the apoB-100 antisense inhibitor produced significant pharmacological effects, i.e., significant reductions in mRNA and liver protein with concomitant reductions in serum apoB, LDL-C, and total cholesterol [18]. All the apoB antisense inhibitors evaluated are 20-mer phosphorothioate oligonucleotide with 2'-O-(2-methoxy) ethyl (MOE) modification on the 5 nucleotides on both 3' and 5' termini. MOE modifications provide enhanced resistance to nucleases, a longer target organ half-life, and reduced toxicity [19,20]. In addition, these modifications increase the affinity of an antisense oligonucleotide for complementary target mRNA, resulting in enhanced potency and specificity [20-22].

ISIS 301012 (Mipomersen), the human specific apoB-100 antisense inhibitor, is currently in Phase 3 clinical development in familial hypercholesterolemia. ISIS 301012 has been shown to produce consistent and predictable dose-dependent and exposure-dependent reduction in serum atherogenic lipids and lipoproteins in human subjects [23-26]. These dose- and exposure-response correlations have been demonstrated in all clinical subject populations studied to date, including healthy volunteers, subjects with mild hypercholesterolemia, polygenic hypercholesterolemia subjects on stable statin therapy, and homozygous familial hypercholesterolemia subjects on stable statin therapy.

In this paper, we present for the first time remarkable cross-species correlates of PK/PD associations at the molecular level for apoB-100 antisense oligonucleotides. Herein we will summarize the pharmacokinetics and pharmacodynamics of apoB antisense inhibitors in fat fed mice, transgenic human apoB-100 mice, monkeys and humans using species-specific apoB antisense inhibitors. The comparisons in pharmacodynamics across species provide guidance in selection of predictive animal models for the development of future antisense oligonucleotides in this chemical class.

2. Methods and materials

2.1. Materials and reagents

2.1.1. Oligonucleotides

ISIS 147764, ISIS 326358 and ISIS 301012 are 20-nucleotide second-generation antisense oligonucleotides targeting apoB mRNA in mice, monkeys and humans, respectively. All the compounds have MOE modifications at positions 1-5 and 15-20 (Table 1). ISIS 13866, a 2'MOE -modified oligonucleotide at positions 15-21 (underlined) with a sequence of 5'-GCG TTT GCT CTT CTTMCTTGMCG TTT TTT-3', was used as the internal standard for quantitation of ASO in tissues. In addition, all the cytosines of the compounds were modified to contain a 5-methyl group (5-methyl cytosine, ³M). The sequence of the binding site in the monkey differs by only two nucleotides in the region that binds the 3'-MOE wing. Thus, ISIS 301012 is

Table 1 – Testing compounds targeting apoB mRNA across species.

Isis compound number	Species	Sequence (5' → 3')
ISIS 147764	Mouse	<u>G</u> T ^M C ^M C ^M CTGAAGATGT ^M CAAT <u>G</u> ^M C
ISIS 326358	Monkey	<u>G</u> ^M C ^M CT ^M CAGT ^M CTG ^M CTT <u>A</u> ^M CA ^M C ^M C
ISIS 301012	Human	<u>G</u> ^M C ^M CT ^M CAGT ^M CTG ^M CTT <u>C</u> ^M CA ^M C ^M C

Underline denotes 2'-O-methoxyethyl-modification. The cytosines in the compounds were modified to contain a 5-methyl group (5-methyl cytosine, ^MC).

pharmacologically active in the monkey, albeit much lower potency than the monkey-specific ASO, ISIS 326358.

All the studied ASOs were synthesized using an automated DNA synthesizer Model 380B (Applied Biosystems, Inc., Foster City, CA) and purified as previously described [22]. The purity of the compounds used in this study was >90%.

2.1.2. Chemicals and reagents

Tween 20 and phenol:chloroform:isoamyl alcohol 25:24:1 was obtained from SIGMA Chemical Co. (St. Louis, MO). Reacti-BindTM NeutrAvidin coated polystyrene 96-well plates and SuperBlock TBS Blocking Buffer were purchased from Pierce (Rockford, IL). Tris-HCl and Na₂HPO₄ was obtained from J.T. Baker, (Phillipsburg, NJ), NaCl from Fisher Scientific (Fair Lawn, NJ), anti-digoxigenin-AP (conjugated with alkaline phosphatase, Fab fragments) was obtained from Roche Diagnostics Corporation (Indianapolis, IN). The alkaline phosphatase fluorescent substrate AttoPhos[®] and its reconstitution solution were purchased from Promega Life Science (Madison, WI).

2.2. Animals and treatments

All animal studies were conducted utilizing protocols and methods approved by the Institutional Animal Care and Use Committee (IACUC) and carried out in accordance with the Guide for the Care and Use of Laboratory Animals adopted and promulgated by the U.S. National Institutes of Health.

2.2.1. Mice

2.2.1.1. HF-fed C57BL/6 mice. Four to 6-week-old male C57BL/6 mice (Charles River Laboratories, Inc., Wilmington, MA) fed a HF diet were administered ISIS 147764 5, 25, or 50 mg/kg or control ASO at 50 mg/kg intraperitoneally (i.p.), twice weekly for 6 weeks. Animals were sacrificed at 48 h and 1, 2, 4, and 6 weeks after the last dose. Oligonucleotide concentrations in the liver, hepatic apoB mRNA and protein levels, serum apoB-100, total-C, and LDL-C levels were measured at each time point.

2.2.1.2. Human apoB expressing transgenic mice. Six-week old female human apoB expressing transgenic mice (C57BL/6 hemizygous for full length human gene-Taconic, Hudson, NY) were administered ISIS 301012 at 2.5, 5, 10 and 25 mg/kg or control ASO at 25 mg/kg i.p., twice weekly for 6 weeks. Animals were sacrificed 48 h after receiving the last dose and samples collected were measured for hepatic oligonucleotide concentrations and human apoB mRNA expression.

2.2.2. Monkeys

2.2.2.1. Lean cynomolgus monkeys. ISIS 301012 was administered to male and female cynomolgus monkeys (*Macaca*

fascicularis; Sierra Biomedical Animal Colony, Sparks, NV) at 4 mg/kg by 1-h i.v. infusion every other day for 4 doses (1 week). On Days 7, blood was collected for quantitation of ISIS 301012 in plasma by peripheral venipuncture into EDTA containing vacutainers just prior to dosing and at 1, 2, 4, 8, 24 and 48 h following i.v. infusion. Following the 4th dose of 4 mg/kg ISIS 301012, monkeys were euthanized and additional plasma samples and liver samples were taken 3, 4, 8, 16, 32 and 48 days after the fourth dose to assess the terminal elimination half-life in plasma and liver (1/sex/time point).

2.2.2.2. High-fat-fed (HF-fed) cynomolgus monkeys. The cynomolgus monkeys (*M. fascicularis*; Charles River Laboratories Animal Colony, Sparks, NV) were fed an HF diet (~43.9% fat, 21.3% protein, and 35.2% carbohydrate), monkeys for 3 weeks prior to treatment and continued throughout the study period. Monkey-specific apoB antisense inhibitor, ISIS 326358 was administered subcutaneously (s.c.) at 5, 10 or 35 mg/kg/week, to monkeys for 5 weeks. The oligonucleotide sequences for ISIS 326358 and ISIS 301012 (human apoB inhibitor) differ by only two bases. Doses were given on alternate days for the first 3 doses (loading) and twice weekly thereafter (maintenance). Oligonucleotide concentrations in the liver, liver apoB mRNA/protein levels, serum apoB-100, total-C, and LDL-C levels were measured at various time points.

2.2.3. Humans

Healthy human volunteers received ISIS 301012 as a 2-h i.v. infusion and s.c. injections at doses that ranged from 50 to 400 mg [9,26] in a Phase I clinical study. Briefly, 29 healthy volunteer subjects in this study received either 50 mg (n = 8), 100 mg (n = 8), 200 mg (n = 9), or 400 mg (n = 4) per dose day; seven subjects received placebo. The multiple-dose (MD) period consisted of three i.v. infusions (on Days 1, 3 and 5) over 2 h every other day during the first week, followed by once weekly s.c. injections for 3 weeks (total of 6 doses over 22 days on Days 8, 15 and 22). Intensive pharmacokinetic blood sampling occurred for 24 h following the first i.v. dose (at 0, 0.5, 1, 2, 2.25, 2.5, 3, 4, 6, 8, and 24 h), and again following the last s.c. dose (at 0, 0.5, 1, 1.5, 2, 3, 4, 6, 8, 12 and 24 h). Additionally, trough blood samples for determination of elimination half-life were collected at 3, 17, 33, 47, 61, 75 and 89 days after the last s.c. dose. Serum lipoprotein and cholesterol profiling was performed after fasting at pre-dose on Days 1, 8, 15, and 22 and during all the follow-up time points. Selected pharmacokinetic and pharmacodynamic data from the Phase I study are included in this report to compare with preclinical data.

2.3. Methods

2.3.1. Sample extraction and analysis of oligonucleotide concentrations in liver

Liver samples from mice and monkeys were analyzed using a quantitative capillary gel electrophoresis method which is a variation on the method reported previously [27]. The assay was validated for precision, accuracy, selectivity, sensitivity and stability of ISIS 301012 in liver tissues. Quantitation of the other species-specific apoB antisense inhibitors in liver were qualified but not fully validated. These analyses were conducted at Southwest Bio-Labs (Las Cruces, NM) and Isis Pharmaceuticals, Inc. (Carlsbad, CA). Briefly, liver samples were weighed, homogenized in a Bio Savant (Bio 101, Inc., Vista, CA) and then the material was extracted as described [27] with the exception that a phenyl-bonded SPE column (Supelco Inc., Bellefonte, PA) was used. An internal standard (ISIS 13866, a 27-mer 2'-O-methoxyethyl modified phosphorothioate oligonucleotide) was added prior to extraction. Extracted samples were analyzed by CGE using a Beckman P/ACE Model 5010 capillary electrophoresis instrument (Beckman Instruments, Irvine, CA) with UV detection at 260 nm. The limit of quantitation for this assay has been estimated to be 1.52 μ g/g oligonucleotide in liver.

2.3.2. Analysis of oligonucleotide concentrations in plasma

Plasma samples in mice, monkeys and humans were analyzed using a quantitative, sensitive hybridization ELISA method which is a variation on the method reported previously [28]. The assay was validated for precision, accuracy, selectivity, sensitivity and stability of ISIS 301012 in plasma. Quantitation of the other species-specific apoB antisense inhibitors in plasma were qualified but not fully validated. Plasma sample analyses were conducted at PPD Development (Richmond, VA) and Isis Pharmaceuticals, Inc. (Carlsbad, CA). The assay conducted with synthesized putative shortened oligonucleotide metabolite standards showed no measurable cross-reactivity confirming the assays specificity for the parent oligonucleotide. The lower limit of quantitation (LLOQ) was determined to be 1.52 ng/mL.

2.3.3. RNA isolation and RT-PCR analysis

Total RNAs were extracted from liver samples using the RNeasy kit (Qiagen, Santa Clarita, CA). RT-PCR analysis was performed using a Prism 7700 Sequence Detector (Applied Biosystems, Inc., Foster City, CA). The species-specific primer probe sets for apoB quantitation were used and values were normalized to glyceraldehyde-3-phosphate dehydrogenase (G3PDH) and/or Ribogreen levels.

2.3.4. Lipid and lipoprotein analysis

Serum lipoprotein cholesterol in animal studies was analyzed using a Beckman System Gold 126 HPLC system, with 126 photodiode array detector (Beckman Instruments; Fullerton, CA) on a Superose 6 HR 10/30 column (Pfizer, Chicago, IL). VLDL, LDL, and HDL fractions were measured at a wavelength of 505 nm and validated with a cholesterol calibration kit (Sigma). For each experiment, a three-point standard curve was performed in triplicate to determine the absolute concentration of each lipoprotein fraction [18]. For clinical

samples, apoB levels were determined by an immunoturbimetric method (MDS PharmaServices, Belfast). Total cholesterol, LDL-C, HDL-C and triglycerides were measured using standard enzyme based colorimetric assays (MDS PharmaServices, Belfast; and LipoScience, Raleigh, NC) [26].

2.3.5. Pharmacokinetic analysis

Both compartmental and non-compartmental analysis methods were used for pharmacokinetic characterization of the plasma concentration data (WinNonlin 4.0 or 5.0, Pharsight Corporation, Mountain View, CA). First-order elimination rate constants for apoB antisense inhibitors in plasma or liver were calculated using non-compartmental nonlinear regression of the decay curves for plasma or liver. Half-life was calculated by dividing 0.693 by the first-order elimination rate. In animals, the elimination of apoB antisense inhibitors from liver was measured directly, and the liver concentration-time data were analyzed using a non-compartmental model.

2.3.6. Pharmacodynamic analysis

The relation between apoB mRNA, serum apoB reductions and liver concentrations or plasma trough concentrations of ASOs was characterized using a pharmacodynamic model. ApoB mRNA levels following apoB antisense inhibitor treatment were normalized with the ApoB mRNA levels from control animals (treated with saline):

$$E = \frac{\text{mRNA}_{\text{treatment}}}{\text{mRNA}_{\text{control}}} \times 100 \quad (1)$$

Similarly, serum apoB levels following ASO treatment were normalized with the baseline serum apoB levels of the same animal or subject.

The relationship between inhibitory activity of apoB mRNA or serum apoB (E) and liver concentrations or plasma trough concentrations of ASOs was best described by adopting an inhibitory sigmoidal E_{max} model:

$$E = E_0 - \frac{E_{\text{max}}C^n}{EC_{50}^n + C^n} \quad (2)$$

where E_0 is the baseline level; E_{max} is the maximum reduction of apoB mRNA; EC_{50} is the concentration of ISIS 301012 required for half-maximal reduction of apoB mRNA; C is liver concentrations or plasma trough concentrations of ASOs; and n is the sigmoidicity factor.

3. Results

3.1. Pharmacokinetics

The clearance of apoB ASOs from tissues was slow in all species studied. The elimination half-life for the mouse-specific apoB antisense inhibitor, ISIS 147764 in mouse liver was 20 days, while the elimination half-lives for ISIS 301012 were 24 and 34 days in mice and monkeys, respectively (Table 2). Elimination half-life was not determined for ISIS 326358 because ISIS 326358 is a monkey-specific apoB inhibitor and is not going to be developed for use in humans. The

Table 2 – Estimated elimination half-life (in days) of apoB ASOs in mice, monkeys and man.

Species	Compound	Dose	Elimination half-life (days)		Liver/plasma trough concentration ratio
			Plasma	Liver	
Mouse	ISIS 147764	25 mg/kg	NA	20	NM
Mouse	ISIS 301012	2.5–25 mg/kg	NM	24 ^a	5861 ± 2342
Monkey	ISIS 301012	4 mg/kg	31.3 ± 0.3 ^b	34 ^b	5825 ± 2882
Human	ISIS 301012	200 mg (~2.7 mg/kg)	31 ± 11 ^c	NA	NM

NA = not applicable; NM = not measured.
^a Measured in CD-1 mice (internal data).
^b Animals received 30 mg/kg/week doses of ISIS 301012 for 1 year. For determination of plasma elimination half-life, plasma samples were collected at various time points up to 182 days after last dose (n = 3).
^c Data presented are mean ± standard deviation (n = 8).

monkey study with ISIS 326358 was to demonstrate pharmacology and evaluate target knock down-related toxicities. The plasma concentration-time profile for ISIS 301012 was multi-phasic with a rapid distribution phase and at least one additional much slower elimination phase (Fig. 1). The plasma concentrations of ISIS 301012 observed in the terminal elimination phase in monkeys represent ISIS 301012 that is in equilibrium with liver (Fig. 1) as well as other tissues and thus, equilibrium plasma concentrations provide a measure of tissue elimination rate. Because such a high fraction of the administered dose is retained by the liver and kidney, the majority of the oligonucleotide in circulation at equilibrium should be proportional to the concentrations in those tissues. Indeed, the elimination half-life of ISIS 301012 studied in monkey liver of approximately 30 days was very similar to the elimination half-life observed in monkey plasma, as well as in human plasma (Table 2). Moreover, a similar partition ratio of ISIS 301012 between liver and plasma at equilibrium was observed across species, and was 5861 and 5825 in mice and monkeys, respectively (Table 2). Therefore, it is reasonable to assume this liver to plasma partition ratio at equilibrium in humans would be similar, thus providing a surrogate for liver exposure in the clinic. Taken together, these results suggest

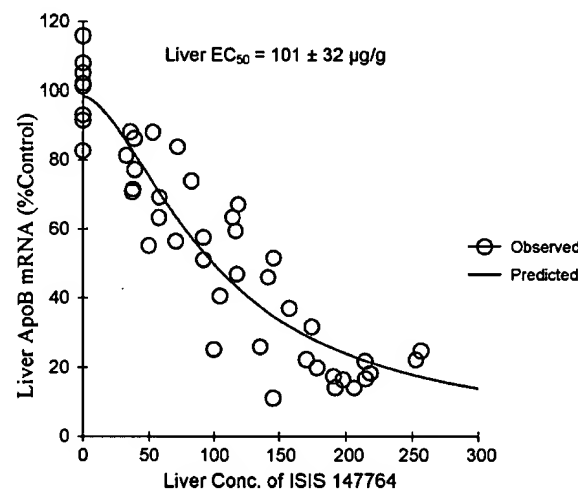


Fig. 2 – Best fit inhibitory effect E_{max} model of ApoB mRNA levels in liver as a function of liver concentrations of ISIS 147764 in HF-fed mice. Each data point represents a single animal (n = 48). Solid lines represent predicted apoB mRNA levels using nonlinear regression.

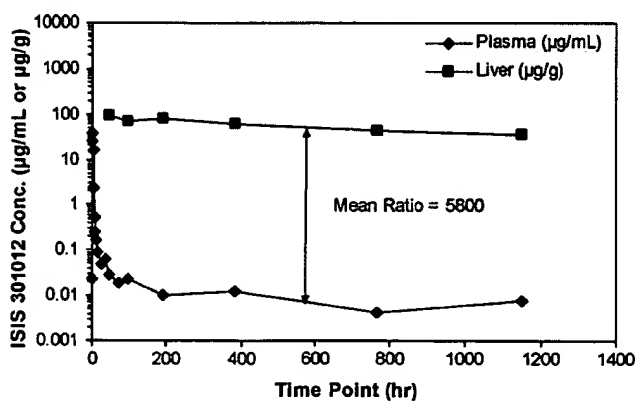


Fig. 1 – Post-distributional phase plasma and liver concentrations of ISIS 301012 in monkeys. Each tissue data point represents average concentrations in two animals. Note that both plasma and tissue concentrations decay similarly over time following cessation of intravenous administration.

that the pharmacokinetic behavior of ISIS 301012 in animals is predictive of that in man.

3.2. Pharmacodynamics of ApoB ASO inhibitors in various species

ApoB antisense inhibitors act as antagonists to apoB-100 mRNA expression. To elicit their effect on mRNA, they must by definition gain access to the target cell, in this case the hepatocyte. ApoB antisense inhibitors bind to apoB mRNA via Watson-Crick hybridization to form RNA-DNA duplex, subsequently, RNases H cleave apoB RNA strand of the duplex [12,13]. Therefore, the relationships between liver apoB mRNA levels to ASO concentrations in the liver can be described by a typical sigmoidal inhibitory effect E_{max} model after administration of apoB-100 ASOs in animals. The obtained EC_{50} in high-fat-fed mice administered ISIS 147764 was $101 \pm 32 \mu\text{g}$ of ISIS 147764 per gram of liver (Fig. 2). Furthermore, the duration of effect was correlated with the tissue elimination half-life from liver ($t_{1/2} = 20$ days) in this model (Fig. 3). Approximately 8 weeks after cessation of treatment, apoB mRNA levels had returned to their

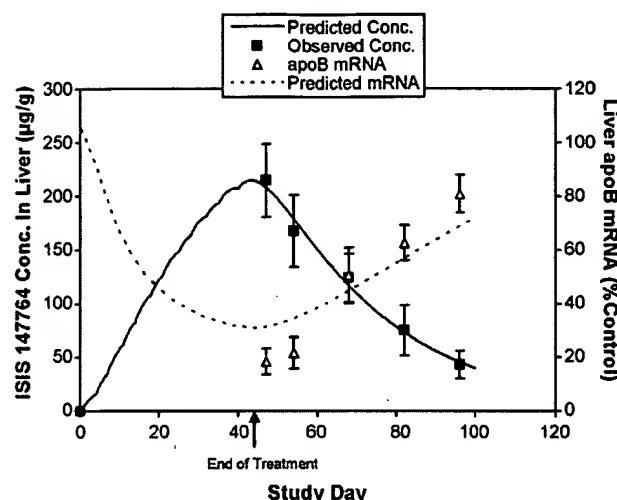


Fig. 3 – Pharmacokinetic/pharmacodynamic relationship of ISIS 147764 in mouse liver following 6 weeks of treatment with mouse specific ApoB antisense oligonucleotide ISIS 147764 (error bars representing standard deviation, $n = 3$). Solid lines represent predicted concentrations in liver using nonlinear regression.

pre-dose levels in mice. Similarly, in the human apoB transgenic mouse model, the relationship between human apoB hepatic mRNA expression and concentrations of ISIS 301012 in the mouse liver and in trough plasma (C_{min}) was observed with estimated EC_{50} of $119 \pm 15 \mu\text{g/g}$ in liver and $18 \pm 4 \text{ ng/mL}$ in plasma (Fig. 4, Table 3). The ratio of the EC_{50} in liver to plasma was consistent with the partition ratio of ISIS 301012 between liver and plasma at equilibrium (Tables 2 and 3). The apoB mRNA reductions in human transgenic mice treated with human specific ISIS 301012 were specific for human apoB mRNA, as no change in murine apoB mRNA was observed in this model (Fig. 5). Additionally, in these animals, the reduction in hepatic apoB mRNA also produced corresponding reductions in liver apoB protein, serum apoB, LDL-C, and total cholesterol (data not shown). In all experiments, control ASOs had no effect on apoB mRNA in the liver, indicating that inhibition of apoB expression was both target- and sequence-dependent.

The liver EC_{50} determined in high-fat-fed monkeys was $300 \pm 191 \mu\text{g/g}$ of species-specific apoB ASO (ISIS 326358) per gram of liver (Table 3, Fig. 6a). Although the estimate of EC_{50} was two-fold higher when compared to the EC_{50} measured in mice, it is not possible to assign a real difference because of the large

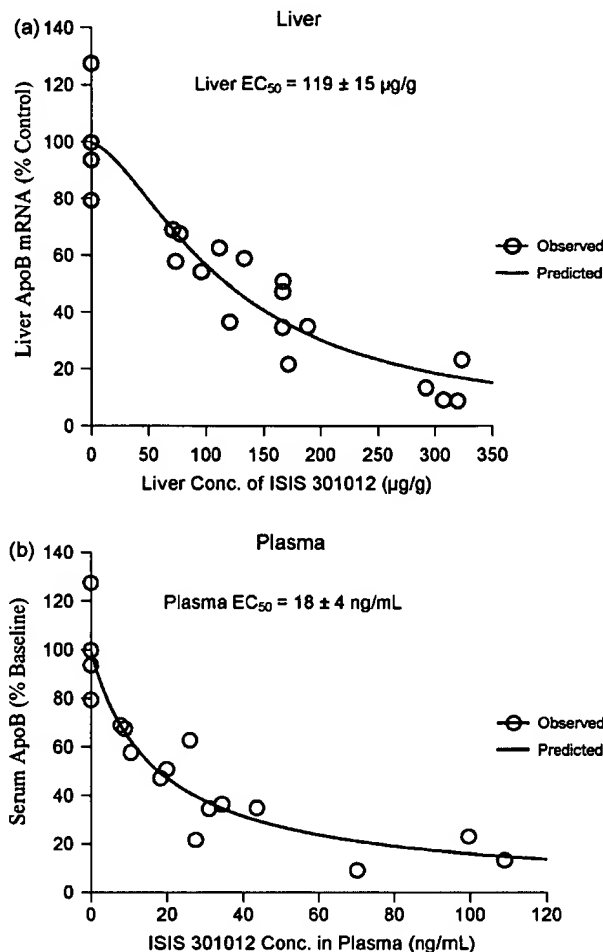


Fig. 4 – Best fit inhibitory effect E_{max} model of ApoB mRNA levels in liver as a function of liver concentrations of ISIS 301012 (a) or plasma trough concentrations of ISIS 301012 (b) in human ApoB transgenic mice. Each data point represents a single animal ($n = 20$). Solid lines represent predicted apoB mRNA levels using nonlinear regression.

standard error associated with the estimates. Treatment with ISIS 326358, the monkey-specific ASO, produced a dose- and liver concentration-dependent decrease in liver apoB mRNA, with the corresponding downstream effects, such as serum apoB (Fig. 6a and b) and LDL-C following 5 weeks of treatment at doses ranging from 5 to 33 mg/kg/week . Indeed, by the end of

Table 3 – In vivo pharmacodynamics of ApoB antisense inhibitors across species.

Species	Isis compound number	Liver EC_{50} ($\mu\text{g/g}$) (estimate \pm SE)	Plasma EC_{50} (ng/mL) (estimate \pm SE)
Mouse	ISIS 147764	101 ± 32	NM
Human ApoB transgenic mouse	ISIS 301012	119 ± 15	18 ± 4
Monkey	ISIS 326358	300 ± 191	52 ± 33^b
Human ^a	ISIS 301012	81 ± 122^b	14 ± 21

SE = standard error of the estimate; NM = not measured.

^a Phase 1 healthy volunteer study.

^b A liver/plasma partition ratio of 5800 was used.

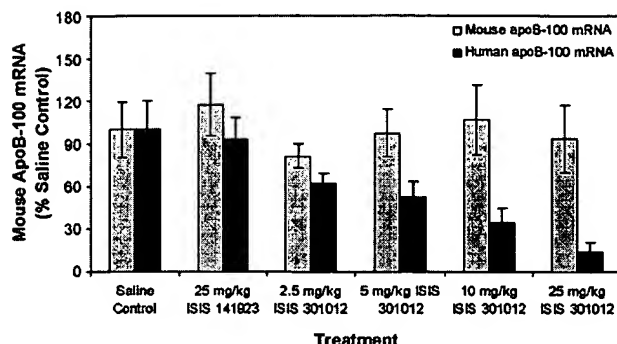


Fig. 5 – Lack of inhibitory effects of control ASO (ISIS 141923) and ISIS 301012 treatment on mouse ApoB-100 mRNA in human apoB transgenic mice following 6 weeks of treatment administered twice a week (error bars representing standard deviation, $n = 4$).

treatment, the mean reduction in serum apoB and LDL-C ranged from 39% to 60% and 46% to 71%, respectively.

The exposure-response relationships were ultimately studied in human volunteer subjects administered ISIS

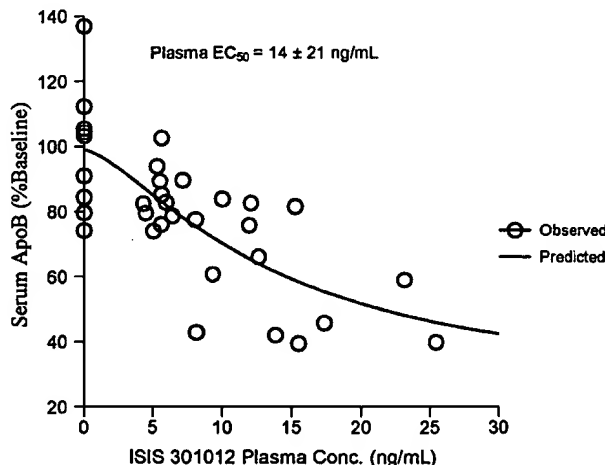


Fig. 7 – Best fit inhibitory effect E_{max} model of serum ApoB (%baseline) as a function of plasma trough concentrations of ISIS 301012 measured at the end of treatment (on MD25) in healthy human volunteers. Each data point represents an individual volunteer subject ($n = 33$). Solid lines represent predicted apoB mRNA levels using nonlinear regression.

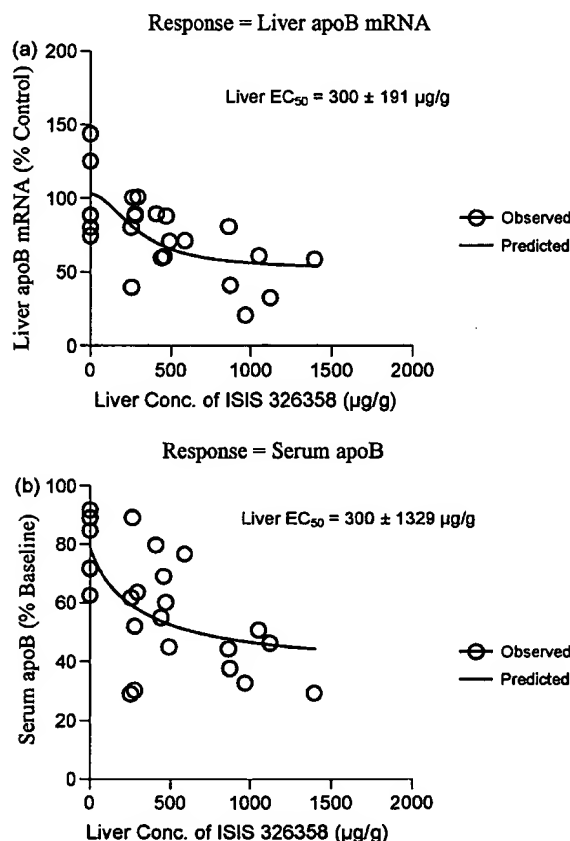


Fig. 6 – Best fit inhibitory effect E_{max} model of ApoB mRNA levels in liver as a function of liver concentrations of ISIS 326358 (a) and serum ApoB levels as a function of liver concentrations of ISIS 326358 in HF-fed monkeys (b). Each data point represents a single animal ($n = 24$). Solid lines represent predicted apoB mRNA levels using nonlinear regression.

301012 in a Phase 1 study in healthy volunteers with mildly elevated LDL-C. ISIS 301012 demonstrated dose-dependent exposure/responses as measured by reductions in both serum apoB and LDL-C [26]. Because ISIS 301012 concentrations in human liver cannot be directly measured easily, the correlation between plasma and liver drug concentrations measured in preclinical models was utilized to estimate the levels of ISIS 301012 in the livers of human subjects (Table 3).

The disposition relationship between ASO plasma trough levels and liver levels were the same as observed in preclinical animal models which led us to determine the relationship between serum apoB levels and plasma trough levels in man. The relationship between serum apoB levels and plasma trough concentrations of ISIS 301012 were effectively described with a sigmoidal inhibitory effect E_{max} model using the data collected on PD14 (17 days after last treatment). The estimated trough plasma concentration that produced 50% of maximum effect (EC_{50}) and predicted liver concentrations, were 14 ng/mL (Table 3, Fig. 7). This plasma level corresponds to an estimated liver exposure of approximately 81 μ g/g.

The duration of effects on apoB and related lipids in plasma following cessation of treatment was highly correlated with the slow elimination of ISIS 301012 (Fig. 8). For example, significant reduction ($p < 0.02$) of serum apoB levels from baseline for the 200-mg treatment cohort was achieved for up to 75 days after last dose, consistent with the slow elimination of ISIS 301012 (elimination $t_{1/2}$ of approximately 31 days) (Table 2). Therefore, the pharmacologic effects were prolonged, consistent with the long tissue half-life of the drug.

4. Discussion

Because the direct pharmacological response of antisense therapeutics is target mRNA reduction, establishment of the

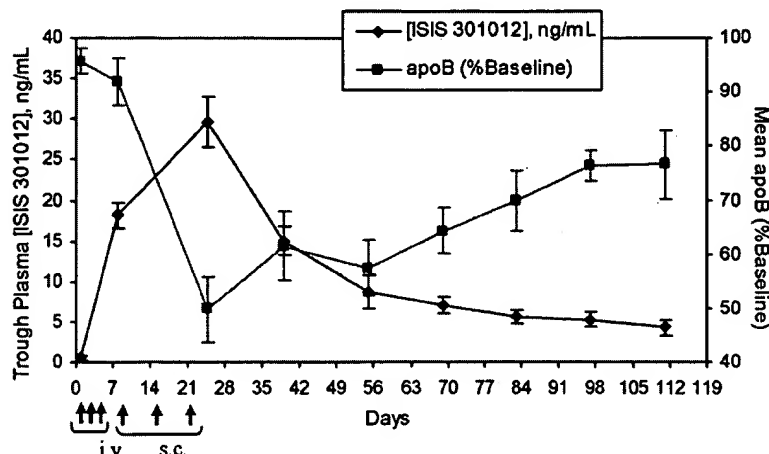


Fig. 8 – Prolonged exposure-response relationships between ISIS 301012 trough plasma concentrations and serum ApoB levels (%baseline) with time in human healthy volunteers during and following six (6) doses of ISIS 301012 at 200 mg per injection. Trough plasma concentrations of ISIS 301012 were measured at ≥ 72 h from last dose. Data presented are mean \pm standard error. Arrows represent dosing times. Last dose was administered on Day 22.

correlation of target organ concentration and target mRNA reduction is most widely used in studying the pharmacokinetic/pharmacodynamic relationships of antisense oligonucleotides in animal models. The pharmacological effect of antisense inhibitors occurs in cells when the antisense inhibitor binds to its cognate mRNA and the RNA strand of the heteroduplex is degraded by RNase H [13]. RNase H₁ cleavage is very rapid, occurring within minutes [13]. Therefore, a direct response pharmacodynamic model was used to describe the liver concentration (exposure) relationship with liver apoB mRNA expression (response) in all species.

We have previously reported that the pharmacokinetics of ISIS 301012 in monkeys is predictive for man on the basis of body weight. Thus a dose of 2 mg/kg ISIS 301012 in the monkey results in similar plasma concentrations at the same dosage (2 mg/kg) in man [9]. It is this remarkable similarity in pharmacokinetics across species that allows for the prediction of exposure from animals models and further, based on these studies across species, allows prediction of response in humans from the preclinical models. Additionally, the lack of impact of mode of parenteral administration on the ultimate tissue pharmacokinetics independent of species has been established for multiple antisense oligonucleotide molecules in this chemical class [8,9,29,30] as well as for ISIS 301012 [9]. The predictive pharmacokinetic behavior of these molecules, independent of their sequence, has been shown in these published accounts to be primarily a consequence of their common biopharmaceutical and physical chemical properties.

Similarities in the pharmacodynamics and potency of apoB antisense inhibitors between species were observed for the apoB-100 ASOs, including mice (both wild type and human transgenic), monkeys, and humans. The observed similarities in pharmacodynamics across species related to the previously observed similarities in pharmacokinetics for ASOs across species [10,31–33]. Peak plasma concentrations of the antisense oligonucleotides like ISIS 301012 do not correlate with drug effect as the effect is post-distribution and intracellular, not in the plasma compartment. This is unlike small

molecules and protein therapeutics where plasma concentrations (C_{max} or AUC) directly correlate the drug response [34–37] due to either a rapid equilibrium with intracellular compartments or direct effects occurring in the circulation. Antisense oligonucleotides rapidly and extensively transfer from plasma to tissues following parenteral administrations. However, distribution to the ultimate site of action within the cells of interest takes hours with maximum activity seen 24–48 h after administration [38]. Since the site of activity for the antisense oligonucleotides is intracellular, ASO drug effects are closely related with target tissue concentrations only after distribution from circulation [2–5,33]. Thus, the plasma concentrations of ASO observed in post-distribution phase (plasma trough ASO concentration) represent the ASO that is in equilibrium with target tissue. Because tissue concentrations in human are not usually accessible, establishing the relationship of plasma trough concentration of ASOs with target tissue concentrations (liver) is required to provide a surrogate of target tissue drug exposure. As shown in mice and monkeys, plasma trough concentrations directly correlated with target organ (liver) concentrations with similar partition ratios. This similarity across species provides confidence that similar relationships may exist for humans. It is this relationship that was used to estimate human liver concentrations based on measured plasma trough levels in human clinical trials. Comparison of the measured trough plasma EC₅₀ values in humans ultimately confirmed that data generated in animal models are predictive of the potency of the human apoB antisense inhibitor (ISIS 301012). Because the mechanism of action and ADME characteristics are similar for other ASOs in the same chemical class as ISIS 301012, these data further provide confidence in the use of preclinical models for prediction of clinical effect for other ASOs.

The strength of the human volunteer data has been extended to hypercholesterolemic subjects in multiple Phase 2 studies. Consistent with the Phase I healthy volunteer study, similar exposure-response relationships in patients with hypercholesterolemia, either used alone or when co-adminis-

tered with statins, had been demonstrated in several Phase II studies [23–25].

ISIS 301012 has a long tissue half-life in animals and humans. The elimination half-lives observed in monkeys were highly predictive of the half-lives measured in humans (greater than 30 days). Consistent with the long elimination half-life of ISIS 301012, it had a long duration of action in lipid lowering effect. Based on the long half-life coupled with the duration of action of ISIS 301012, current dosing regimens being evaluated in clinical development involve once weekly s.c. injection. Furthermore, the excellent relationship of trough plasma levels to apoB-100 and other downstream effects allows for the design of more complex PK/PD models. As clinical experience with this compound grows, development of predictive population models that further incorporate demographic or physiologic covariates should be possible. The use of these models in clinical trial planning and design has been widely adapted in novel drug development strategies and shown to greatly expedite drug development process [39].

In conclusion, these data demonstrated that apoB antisense inhibitors have consistently exhibited exposure-dependent reduction on liver apoB mRNA, as well as the downstream effects such as serum apoB, LDL-C and total cholesterol in multiple preclinical models and human. The exposure-response relationships in HF-fed mice using the mouse-specific apoB antisense inhibitor, ISIS 147764, in human apoB transgenic mice using human-specific apoB antisense inhibitor, ISIS 301012, and monkeys using monkey-specific apoB antisense inhibitor, ISIS 326358, were predictive of the effects of ISIS 301012 in man. The long duration of action of apoB antisense inhibitors in animals and humans is consistent with the prolonged tissue half-lives. These favorable PK/PD properties for apoB antisense inhibitors provide guidance for clinical development and appear to support infrequent dose administration.

Acknowledgements

The authors wish to thank Drs. Stanley Crooke and Jeff Jonas for scientific discussion and critical review of the manuscript. Finally, this manuscript would not be possible without the administrative support provided by Robert Saunders, for which we are grateful.

Authors are employees of ISIS Pharmaceuticals and own shares in ISIS Pharmaceuticals.

REFERENCES

- Galluppi GR, Rogge MC, Roskos LK, Lesko LJ, Green MD, Feigal Jr DW, et al. Integration of pharmacokinetic and pharmacodynamic studies in the discovery, development, and review of protein therapeutic agents: a conference report. *Clin Pharmacol Ther* 2001;69:387–99.
- Geary RS, Yu RZ, Siwkowski A, Levin AA. Pharmacokinetic/pharmacodynamic properties of phosphorothioate 2'-O-(2-methoxyethyl)-modified antisense oligonucleotides in animals and man. In: Crooke ST, editor. *Antisense drug technology: principles, strategies and applications*. Boca Raton, FL: Taylor & Francis Group; 2007. p. 305–26.
- Callies S, Andre V, Vick A-M, Graff J, Patel B, Brail L, et al. Modelling pharmacokinetic and pharmacodynamic properties of second generation antisense-oligonucleotides (ASOs). Copenhagen: PAGE (Population Approach Group in Europe); 2007.
- Yu RZ, Gibiansky L, Gibiansky E, Geary RS. Population pharmacokinetics and pharmacodynamics of ISIS 2302 (Role of Population Analysis in Drug Development). ASCPT Annual Meeting. Orlando, Florida; 2001.
- Yu RZ, Matson J, Geary RS. Terminal elimination rates for antisense oligonucleotides in plasma correlate with tissue clearance rates in mice and monkeys. Annual Meeting of American Association of Pharmaceutical Scientists. Denver, Colorado; 2001.
- Geary RS, Mathison B, Ushiro-Watanabe T, Savides MC, Henry SP, Levin AA. Second generation antisense oligonucleotide pharmacokinetics and mass balance following intravenous administration in rats. San Francisco, CA: Society of Toxicology, Oxford University Press; 2001. p. 343.
- Geary RS, Ushiro-Watanabe T, Truong L, Freier SM, Lesnik EA, Sioufi NB, et al. Pharmacokinetic properties of 2'-O-(2-methoxyethyl)-modified oligonucleotide analogs in rats. *J Pharmacol Exp Ther* 2001;296:890–7.
- Geary RS, Yu RZ, Watanabe T, Henry SP, Hardee GE, Chappell A, et al. Pharmacokinetics of a tumor necrosis factor-alpha phosphorothioate 2'-O-(2-methoxyethyl)-modified antisense oligonucleotide: comparison across species. *Drug Metab Dispos* 2003;31:1419–28.
- Yu RZ, Kim T-W, Hong A, Watanabe TA, Gaus HJ, Geary RS. Cross-species pharmacokinetic comparison from mouse to man of a second generation antisense oligonucleotide ISIS 301012. Targeting human ApoB-100. *Drug Metab Dispos* 2007;35:460–8.
- Levin AA, Yu RZ, Geary RS. Basic principles of the pharmacokinetics of antisense oligonucleotide drugs. In: Crooke ST, editor. *Antisense drug technology: principles, strategies and applications*. Boca Raton, FL: Taylor & Francis Group; 2007. p. 183–215.
- Crooke ST, Vickers T, Lima W, Wu H. Mechanisms of antisense drug action, an introduction. In: Crooke ST, editor. *Antisense drug technology: principles, strategies and applications*. Boca Raton, FL: Taylor & Francis Group; 2007. p. 5–46.
- Wu H, Lima W, Crooke ST. Molecular cloning and expression of cDNA for human RNase H. *Antisense Nucleic Acid Drug Dev* 1998;8:53–61.
- Wu H, MacLeod AR, Lima WF, Crooke ST. Identification and partial purification of human double strand RNase activity: a novel terminating mechanism for oligoribonucleotide antisense drugs. *J Biol Chem* 1998;273:2532–42.
- Davidson NO, Shelness GS. Apolipoprotein B: mRNA editing, lipoprotein assembly, and presecretory degradation. *Annu Rev Nutr* 2000;20:169–93.
- Marsh JB, Welty FK, Lichtenstein AH, Lamon-Fava S, Schaefer EJ. Apolipoprotein B metabolism in humans: studies with stable isotope-labeled amino acid precursors. *Atherosclerosis* 2002;162:227–44.
- Das HK, Leff T, Breslow JL. Cell type-specific expression of the human apoB gene is controlled by two cis-acting regulatory regions. *J Biol Chem* 1988;263:11452–8.
- Crooke R. Second-generation antisense drug for cardiovascular disease demonstrates significant and durable reductions in cholesterol. In: The 9th Drug Discovery Technology World Congress; 2004.
- Crooke RM, Graham MJ, Lemonidis KM, Whipple CP, Koo S, Perera RJ. An apolipoprotein B antisense oligonucleotide

lowers LDL cholesterol in hyperlipidemic mice without causing hepatic steatosis. *J Lipid Res* 2005;46:872-84.

[19] Henry SP, Stecker K, Brooks D, Monteith D, Conklin B, Bennett CF. Chemically modified oligonucleotides exhibit decreased immune stimulation in mice. *J Pharmacol Exp Ther* 2000;292:468-79.

[20] McKay RA, Miraglia LJ, Cummins LL, Owens SR, Sasmor H, Dean NM. Characterization of a potent and specific class of antisense oligonucleotide inhibitor of human protein kinase C- α expression. *J Biol Chem* 1999;274:1715-22.

[21] Altmann K-H, Fabbro D, Dean NM, Geiger T, Monia BP, Mueller M, et al. Second-generation antisense oligonucleotides: structure-activity relationships and the design of improved signal transduction inhibitors. *Biochem Soc Trans* 1996;24:630-7.

[22] Baker BF, Lot SS, Condon TP, Cheng-Flournoy S, Lesnik EA, Sasmor HM, et al. 2'-O-(2-Methoxy)ethyl-modified anti-intercellular adhesion molecule 1 (ICAM-1) oligonucleotides selectively increase the ICAM-1 mRNA level and inhibit formation of the ICAM-1 translation initiation complex in human umbilical vein endothelial cells. *J Biol Chem* 1997;272:11994-2000.

[23] Stein E. High low-density lipoprotein cholesterol on three drugs. ACC06: 56th Scientific Session of the American College of Cardiology ACC Symposium: Common challenges in preventive cardiology; 2007. p. 603-8.

[24] Stein E, Wedel M, Bradley J. Statin-like dose-dependent reductions in LDL cholesterol and apolipoprotein B with ISIS, 301012, an antisense inhibitor of apolipoprotein B, in subjects with polygenic hypercholesterolemia. *J Am Coll Cardiol* 2007;49:1206-78.

[25] Kastelein J, Akdim F, Trip M. ISIS, 301012, an antisense inhibitor of apolipoprotein B, produces significant additional reduction of low-density lipoprotein cholesterol and apolipoprotein B in hypercholesterolemic subjects on statins not meeting target. *J Am Coll Cardiol* 2007;49:820-7.

[26] Kastelein JJ, Wedel MK, Baker BF, Su J, Bradley JD, Yu RZ, et al. Potent reduction of apolipoprotein B and low-density lipoprotein cholesterol by short-term administration of an antisense inhibitor of apolipoprotein B. *Circulation* 2006;114:1729-35.

[27] Leeds JM, Graham MJ, Troung L, Cummins LL. Quantitation of phosphorothioate oligonucleotides in human plasma. *Anal Biochem* 1996;235:36-43.

[28] Yu RZ, Baker B, Chappel A, Geary RS, Chueng E, Levin AA. Development of an ultrasensitive noncompetitive hybridization-ligation enzyme-linked immunosorbent assay for the determination of phosphorothioate oligodeoxynucleotide in plasma. *Anal Biochem* 2002;304:19-25.

[29] Geary RS, Leeds JM, Henry SP, Monteith DK, Levin AA. Antisense oligonucleotide inhibitors for the treatment of cancer. 1. Pharmacokinetic properties of phosphorothioate oligodeoxynucleotides. *Anticancer Drug Des* 1997;12:383-93.

[30] Zhang RW, Iyer RP, Yu D, Tan WT, Zhang XS, Lu ZH, et al. Pharmacokinetics and tissue disposition of a chimeric oligodeoxynucleoside phosphorothioate in rats after intravenous administration. *J Pharmacol Exp Ther* 1996;278:971-9.

[31] Geary RS, Yu RZ, Leeds JM, Ushiro-Watanabe T, Henry SP, Levin AA, et al. Pharmacokinetic properties in animals. In: Crooke ST, editor. *Antisense drug technology: principles, strategies, and applications*. New York: Marcel Dekker Inc.; 2001. p. 119-54.

[32] Geary RS, Yu RZ, Levin AA. Pharmacokinetics of phosphorothioate antisense oligodeoxynucleotides. *Curr Opin Investig Drugs* 2001;2:562-73.

[33] Yu RZ, Geary RS, Levin AA. Pharmacokinetics and pharmacodynamics of antisense oligonucleotides. In: Meyers RA, editor. *Encyclopedia of molecular cell biology and molecular medicine*. Weinheim, Germany: Wiley-VCH; 2007.

[34] Boothe DM, Boeckh A, Simpson RB, Dubose K. Comparison of pharmacodynamic and pharmacokinetic indices of efficacy for 5 fluoroquinolones toward pathogens of dogs and cats. *J Vet Intern Med* 2006;20:1297-306.

[35] Svetyi LI, Alekhin SN. Pharmacokinetic and pharmacodynamic effects of isradipine in patients with arterial hypertension. *Eksp Klin Farmakol* 2002;65:35-8.

[36] Zhou H, Choi L, Lau H, Bruntsch U, Vries EE, Eckhardt G, et al. Population pharmacokinetics/toxicodynamics (PK/TD) relationship of SAM486A in phase I studies in patients with advanced cancers. *J Clin Pharmacol* 2000;40:275-83.

[37] Ebert U, Grossmann M, Oertel R, Gramatte T, Kirch W. Pharmacokinetic-pharmacodynamic modeling of the electroencephalogram effects of scopolamine in healthy volunteers. *J Clin Pharmacol* 2001;41:51-60.

[38] Yu RZ, Zhang H, Geary RS, Graham M, Masarjian L, Lemonidis K, et al. Pharmacokinetics and pharmacodynamics of an antisense phosphorothioate oligonucleotide targeting Fas mRNA in mice. *J Pharmacol Exp Ther* 2001;296:388-95.

[39] Barrett JS, Gupta M, Mondick JT. Model-based drug development applied to oncology. *Expert Opin Drug Discov* 2007;2:185-209.

Research

Open Access

Antisense inhibition of ATM gene enhances the radiosensitivity of head and neck squamous cell carcinoma in mice

Jian Zou^{†,2}, Xiaoming Qiao^{†,1}, Huiping Ye¹, Yuqiong Yang³, Xuelian Zheng², Houyu Zhao¹ and Shixi Liu^{*1,2}

Address: ¹Department of Otolaryngology, West China Hospital, Sichuan University, Chengdu, 610041, PR China, ²State Key Laboratory of Biotherapy, West China Hospital, Sichuan University, Chengdu, 610041, PR China and ³Department of Oncology, West China Hospital, Sichuan University, Chengdu, 610041, PR China

Email: Jian Zou - zoujian926@gmail.com; Xiaoming Qiao - xmqiaoent@gmail.com; Huiping Ye - yehuiping888@yahoo.com.cn; Yuqiong Yang - westhuaxi@163.com; Xuelian Zheng - schoolhua@yahoo.cn; Houyu Zhao - chengduent@sohu.com; Shixi Liu* - liushixi999@gmail.com

* Corresponding author †Equal contributors

Published: 26 October 2008

Journal of Experimental & Clinical Cancer Research 2008, **27**:56 doi:10.1186/1756-9966-27-56

Received: 25 August 2008

Accepted: 26 October 2008

This article is available from: <http://www.jeccr.com/content/27/1/56>

© 2008 Zou et al; licensee BioMed Central Ltd.

This is an Open Access article distributed under the terms of the Creative Commons Attribution License (<http://creativecommons.org/licenses/by/2.0>), which permits unrestricted use, distribution, and reproduction in any medium, provided the original work is properly cited.

Abstract

Background: Treatment failure after radiotherapy of head and neck squamous cell carcinoma (HNSCC) could be a significant problem. Our objective is to sensitize SCCVII cells to ionizing radiation *in vitro* and *in vivo* through inhibiting ATM expression using antisense oligodeoxynucleotides (AS-ODNs), and investigate the potential mechanism of radiosensitization.

Methods: We designed and synthesized AS-ODNs that target ATM mRNA to reduce the ATM expression. The influence on the expression of ATM mRNA and protein in SCCVII cells were analysed by real-time quantitative PCR and western blotting respectively. Clonogenic survival assay was performed to detect the survival ability of SCCVII cells after irradiation, while flow cytometry used to analyse the cell cycle and apoptosis. The volume of solid tumors generated with SCCVII cells was measured, and cell apoptosis was analysed by TUNEL assay after irradiation.

Results: The relative ATM mRNA and protein expression in SCCVII cells treated with ATM AS-ODNs were decreased to $25.7 \pm 3.1\%$ and $24.1 \pm 2.8\%$ of that in untreated cells respectively ($P < 0.05$). After irradiation, the survival fraction (SF) of cells treated with ATM AS-ODNs was lower than that of other groups at the same dose of radiation ($P < 0.05$), while the percentage of cells in G2/M phase decreased and apoptotic rate of cells increased ($P < 0.05$). The inhibition rate in SCCVII cells solid tumor exposed to X-ray alone was $23.2 \pm 2.7\%$, while it was $56.1 \pm 3.8\%$ in the group which irradiated in combination with the treatment of ATM AS-ODNs ($P < 0.05$). The apoptotic index for the group irradiated in combination with ATM AS-ODNs injection was 19.6 ± 3.2 , which was significantly higher than that of others ($P < 0.05$).

Conclusion: Inhibition of ATM expression sensitized SCCVII cells to ionizing radiation *in vitro* and *in vivo*. The potential mechanism should be the defective G2/M cell cycle checkpoint control and enhanced radiation-induced apoptosis.

Background

Despite advances in surgical treatments, radiotherapy is superior in its ability to preserve function and appearance in the treatment of head and neck squamous cell carcinoma (HNSCC). But some kinds of HNSCC are refractory to ionizing radiation, which results in the low effectiveness of radiotherapy alone[1,2]. SCCVII cell line, is a spontaneously arising head and neck squamous carcinoma cell line from syngeneic C3H/HeJ mice[3]. An oral cancer murine model using the SCCVII cell line shares characteristics such as initial locoregional tumor invasion, direct extension into the neck, and early cervical metastases with human head and neck tumors[4]. So SCCVII cell line could be a good object to study the biological behavior of HNSCC.

One strategy to improve the effectiveness of radiotherapy is augmenting of tumour radiosensitivity[5]. In the latter study, SCCVII cells were found to be resistant to ionizing radiation. The cytotoxicity of ionizing radiation is mainly mediated through the generation of DNA-double strand break (DSB) as evidenced by the pronounced radiosensitivity of cells and organisms defective in the machinery of DSB repair[6-8]. Thus, inhibition of DSB repair provides a mechanism to enhance the cytotoxicity of IR in tumour cells. The ataxia-telangiectasia mutated (ATM) protein kinase is a critical component in these pathways and integrates the cellular response to damage by phosphorylating key proteins involved in cell cycle regulation and DSB repair[9,10]. Lack of the normal ATM function in the inherited ataxia telangiectasia (AT) syndrome results in the profound hypersensitivity to ionizing radiation[11-13]. As mentioned elsewhere p53-wild-type cell lines with dysfunctional ATM, when irradiated, either show a lack of or delayed activation of p53, resulting in a defective G1/S cell-cycle checkpoint[14]. However, in p53 mutated cell lines, disruption of ATM resulted in defective G2/M checkpoint control, radio-resistant DNA synthesis, retarded cell proliferation and enhanced radiosensitivity[15,16]. Therefore, we manage to examine whether reduction of ATM expression after antisense oligodeoxynucleotides (AS-ODNs) treatment would result in enhanced radiosensitivity of p53-mutated SCCVII cells from C3H/He mice through the aberrant G2/M checkpoint.

Methods

Reagents

RPMI-1640 media and 10% heat-inactivated fetal bovine serum (FBS) were purchased from Gibco Company (Eggenstein, Germany). Lipofectamine 2000, Opti-MEM medium and Trizol kit were bought from Invitrogen Company (Carlsbad, CA, USA). SYBR ExScript RT-PCR Kit and SYBR Green Master Mix were purchased from Takara Biotechnology Company (Dalian, China). ATM monoclonal antibodies was bought from Santa Cruz Biotechnology

(Santa Cruz, CA, USA), and β -actin monoclonal antibodies from Sigma (St Louis, MO, USA). BCIP/NBT alkaline phosphatase substrate kit IV was purchased from Vector laboratories (Burlingame, CA, USA). TUNEL apoptosis detection kit was bought from Roche Company (Shanghai, China)

Cell lines and mice

SCCVII cell line was generously obtained from the laboratory of gene therapy at Johns Hopkins University. SCCVII cells were cultured in complete RPMI-1640 media containing 10% heat-inactivated FBS, 2 mM L-glutamine, 100 IU/mL penicillin, 100 μ g/mL streptomycin. Cells were cultured as a monolayer at 37°C in a humidified atmosphere containing 5% CO₂. Female C3H/He mice, aged 6-8 weeks, weighing 18-22 g, were obtained from Vital River Laboratories (Beijing, China) and were maintained in the animal facility at West China Medical School, Sichuan University in accordance with nation's related regulations and animal welfare requirements.

Synthesis of oligodeoxynucleotides(ODNs) and selection of target sequences

A 25-mer AS-ODN which was previously reported to inhibit ATM expression in mouse cerebrovascular endothelial cells[17], and its associated controls, sense (Sen) and mismatch (Mis) ODNs, were synthesized by Shanghai Sangon Biological Engineering Technology & Services (Shanghai, China). The sequences were as follows: AS, 5'-GTGCTAGACTCATCGTTAACATT-3'; Sen, 5'-AAATCTAAACCATGAGTCTAGCAC-3' and Mis, 5'-CCCCAGCAGCTCCATTGGCGTAA-3'. All the ODNs were chemically modified to phosphorothioate ODNs by substituting the oxygen molecules of the phosphate backbone with sulfur.

Transfection of ODNs in SCCVII cells

SCCVII cells at a density of 5×10^4 cells/ml were plated for overnight incubation. Cells were maintained in RPMI-1640 medium supplemented with 10% FBS at 37°C and 5% CO₂. After grew to 80%-90% fill, cells were replenished with incompletely RPMI-1640 medium, then treated with ATM AS-ODNs, ATM Sen-ODNs and Mis-ODNs. The procedures were as follows: 200 nM of ATM AS-ODNs, Sen-ODNs, Mis-ODNs and 2 mg/ml Lipofectamine 2000 were added to Opti-MEM medium separately, and incubated for 5 min at room temperature. Then liposome and ODNs were mixed together respectively and incubated at room temperature for 20 min. SCCVII cells were washed again with Opti-MEM medium before transfection. The liposome ODNs complexes were carefully plated on the cells, and incubated at 37°C, 5% CO₂. After 6 hours transfected cells were washed twice with PBS, the medium was replaced with fresh RPMI-1640 medium supplemented with 10% FBS, cells were incubated at 37°C overnight. A

second ODNs incubation was performed before cells were exposed to radiation.

Real-time quantitative PCR analysis

Total RNAs were extracted from cultured SCCVII cells using Trizol reagent according to the manufacturer's protocol. RNA concentration and purity were determined on a UV spectrophotometer (BioRad Inc., Hercules, CA, USA) by the 260 nm absorbance and 260–280 nm absorbance ratio, respectively. Synthesis of cDNA was conducted using SYBR ExScript RT-PCR Kit according to manufacturer's instructions. Real-time quantitative RT-PCR for the ATM mRNA was performed on an ABI PRISM 7300 Sequence Detection System (Applied Biosystems, Foster City, CA, USA) using SYBR Green Master Mix. For normalization the gene GAPDH was used. Final reaction volume is 25 μ l. Cycling conditions were as follows: initial denaturation at 95°C for 10 s, followed by 40 cycles of 95°C for 5 s and 59°C for 31 s. Each measurement was performed in triplicate. The gene expression levels obtained were normalized by mRNA expression of GAPDH. The relative mRNA expression was then presented in relation to the untreated control group. All oligonucleotide primers were designed and synthesized by Sangon (Shanghai, China). The primer sequences are listed as follows: ATM, forward, 5'-CCAGGGAAAGATGATGAAGA-3' reverse 5'-CTACAATGAGCTGCGTGTGG-3'; GAPDH, forward, 5'-CCTCAAGATTCTCAGCAAT-3' reverse, 5'-CCATCACAGTCTTCTGAGT-3'.

Western blot analysis

Total proteins extracted from SCCVII cells were separated on 10% or 15% SDS-polyacrylamide gels. Fifty micrograms each of the preparations were fractionated by 12.5% SDS-PAGE and transferred to nitrocellulose membrane (Millipore, Bedford, MA). The membrane was blocked with 3% milk powder in PBS at room temperature for 3 hours, washed with TBS (PBS containing 0.1% Tween-20) for 10 min three times, then incubated with the ATM monoclonal antibodies (1:1000 dilution) or β -actin monoclonal antibodies (1:2000 dilution) in TBS containing 1% milk powder at 4°C overnight. After three washes with TBS, the membrane was incubated with alkaline phosphatase-labeled anti-mouse IgG antibody in TBS containing 1% milk powder at room temperature for 3 hours and washed again with TBS three times. The membrane was briefly equilibrated with PBS and visualized with the BCIP/NBT alkaline phosphatases substrate kit IV. Reactive bands were scanned by Gel Doc 1000 (Bio-Rad). The experiment was repeated three times.

Irradiation

ELEKTA Precise radiation system (Elekta, Sweden) was used to irradiate cells and solid tumor. X-ray irradiation was performed at room temperature at a dose rate of 200

cGy/min and equipped with an external 0.5-mm copper filter.

Clonogenic survival assay

The SCCVII cells were seeded in triplicate at limiting dilutions in 6-well plates for about 24 hours in RPMI-1640 medium supplemented with 10% FBS until attached. Then the cells were transfected with ATM AS-ODNs, ATM Sen-ODNs and Mis-ODNs respectively. About 18 hours after transfection, they were irradiated with different doses of X-ray radiation (0, 2, 4, 6, and 8 Gy) respectively. The medium was replaced with a fresh one 24 hours after irradiation. After 7 days of incubation, the colonies were fixed with methanol, stained with 0.5% crystal violet in absolute ethanol and colonies with >50 cells were counted under dissection microscope. In each irradiation dose group, surviving fraction (SF) of cells was calculated as plating efficiency of the irradiated cells divided by the plating efficiency of the irradiated cells by that of the untreated control.

Cell cycle and apoptosis analyzed by flow cytometry

After 48 hours exposed to 2 Gy radiation, cells were harvested, and centrifuged at 1500 rpm for 2 min. Then cells were washed with PBS twice, and fixed with 70% icy-cold ethanol at 4°C overnight. Cells were stained with PI at 4°C for 30 min. Cell cycle progression and apoptotic rate were analyzed by flow cytometry (Elite ESP, Beckman Coulter, USA).

Animal experiment of radiosensitization

Female C3H/He mice were used to investigate the effect of ATM AS-ODNs on radiosensitivity of SCCVII cells solid tumor. All surgical procedures and care administered to the animals were in accordance with institutional guidelines. Animal surgeries and radiotherapy were performed under general anesthesia, 50 mg/kg ip injection of pentobarbital sodium. About 5×10^6 SCCVII cells were subcutaneously inoculated in submental space of the mice. Tumor growth rates were determined by measuring two orthogonal dimensional diameters of each tumor twice a week. Tumour volumes were estimated according to the formula $V = \pi/6 \times a^2 \times b$, where a is the short axis, and b the long axis. When tumors reached an average volume of about 200 mm³, the tumor-bearing C3H/He mice were divided into four groups: (a) control group, no treatment; (b) ATM AS-ODNs group, tumors were treated with ATM AS-ODNs alone but not exposed to irradiation for each time; (c) irradiation group, tumors were exposed to X-ray of 2 Gy alone for each time; and (d) combination group, 2.5 mg/kg of ATM AS-ODNs was injected into the solid tumor the day before X-ray exposure, another dosage of ATM AS-ODNs was injected right before exposure to 2 Gy of X-ray for each time. The same treatment for each group were repeated 3 times (the interval time was 5 days). C3H/

He mice were killed 3 weeks later. The ATM protein expression of the tumor in the different groups were analysed by western blot using the procedures described as above. The tumor inhibition rate was evaluated using the following formula: (1-average tumor volume of experimental group/average tumor volume of control group) \times 100%.

Terminal deoxynucleotidyltransferase-mediated dUTP-digoxigenin nick-end-labeling (TUNEL) assay

TUNEL staining of tumour sections was performed using an *in situ* apoptosis detection kit (Roche, Shanghai, China) according to the manufacturer's protocol. The total number of apoptotic cells in 10 randomly selected fields was counted. The apoptotic index (AI) was calculated as the percentage of positive staining cells, namely AI = number of apoptotic cells \times 100/total number of nucleated cells.

Statistics

Results were expressed as mean \pm standard deviation (SD). SPSS 12.0 software package was used to perform statistical analysis. One-way ANOVA test was used to determine statistical difference between the experimental groups with others. Differences were considered statistically significant at $P < 0.05$.

Results

Expression of ATM in ATM AS-ODNs transfected SCCVII cells

We analyzed the expression of ATM in mRNA and protein level in SCCVII cells using real-time fluorescent quantitative PCR and western blot assay respectively. After 48 hours treatment, there were no significant difference among the group treated with liposome alone, the group treated with Sen-ODNs and the group treated with Mis-ODNs ($P > 0.05$; Figure. 1). However when incubating with liposome formulations of ATM AS-ODNs, the relative ATM mRNA expression was only about $25.7 \pm 3.1\%$ to the untreated SCCVII cells, which demonstrated a significantly reduced expression of ATM mRNA ($P < 0.05$; Figure. 1). As shown in Figure. 2, ATM protein expression was also significantly reduced by ATM AS-ODNs compared with Sen-ODNs and Mis-ODNs after 72 hours treatment (Figure. 2A). The relative ATM protein expression of SCCVII cells treated with ATM AS-ODNs was only about $24.1 \pm 2.8\%$ to the untreated cells ($P < 0.05$; Figure. 2B). But there was no significant difference among the group treated with liposome alone, the group treated with Sen-ODNs and the group treated with Mis-ODNs ($P > 0.05$; Figure. 2B).

Effect of ATM AS-ODNs on clonogenic survival ability of SCCVII cells after irradiation

Cellular response to ionizing radiation was evaluated by clonogenic survival assay. Compared with untreated cells or cells treated with control ODNs, cloning efficiency declined notably in cells which transfected with ATM AS-ODNs at the same dose of radiation (Figure. 3). The survival fraction after 2 Gy (SF2) reflect the cellular intrinsic radiosensitivity. The SF2 of cells transfected with ATM AS-ODNs was $53.3 \pm 3.1\%$, definitely lower than that of other cells, which indicated a significant increase in the radiosensitivity ($P < 0.05$; Figure. 3). There were no obvious differences among the other groups about clonogenic survival ability ($P > 0.05$; Figure. 3).

Effect of ATM AS-ODNs on apoptosis and cell cycle of SCCVII cells after irradiation in vitro

After 2 Gy irradiation, the apoptotic rate in ATM AS-ODNs transfected cells was $24.7 \pm 2.5\%$, which was higher than that in Sen-ODNs and Mis-ODNs transfected cells ($P < 0.05$; Figure. 4). It was also found that cell percentage of G2/M phase was decreased dramatically in ATM AS-ODNs transfected cells at 48 hours after 2 Gy irradiation compared with that of other groups ($P < 0.05$; Figure. 5).

Inhibitory effect of ATM AS-ODNs on tumor growth in vivo after irradiation

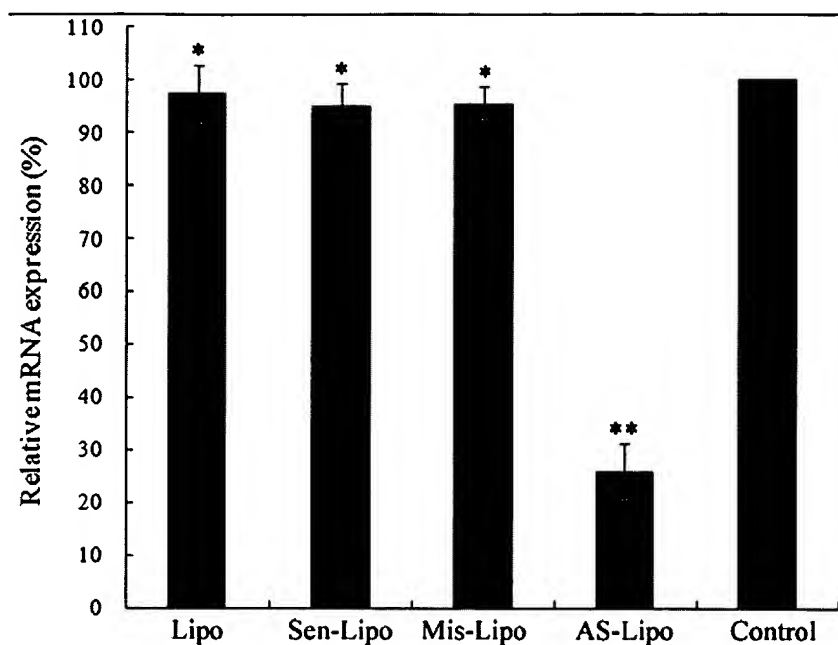
In the group treated with ATM AS-ODNs alone and the group irradiated in combination with the treatment of ATM AS-ODNs, the relative ATM protein expression were only $63.4 \pm 5.6\%$ and $62.1 \pm 6.1\%$ to the untreated group respectively ($P < 0.05$; Figure. 6). Tumor growth of the mice in four groups were shown in Figure. 7. The inhibition rate in SCCVII cells solid tumor exposed to X-ray alone was $23.2 \pm 2.7\%$, while it was $56.1 \pm 3.8\%$ in solid tumor irradiated in combination with the treatment of ATM AS-ODNs at the experimental endpoint ($P < 0.05$; Figure. 7).

Enhancement of tumour apoptosis by irradiation combined with ATM AS-ODNs treatment in vivo

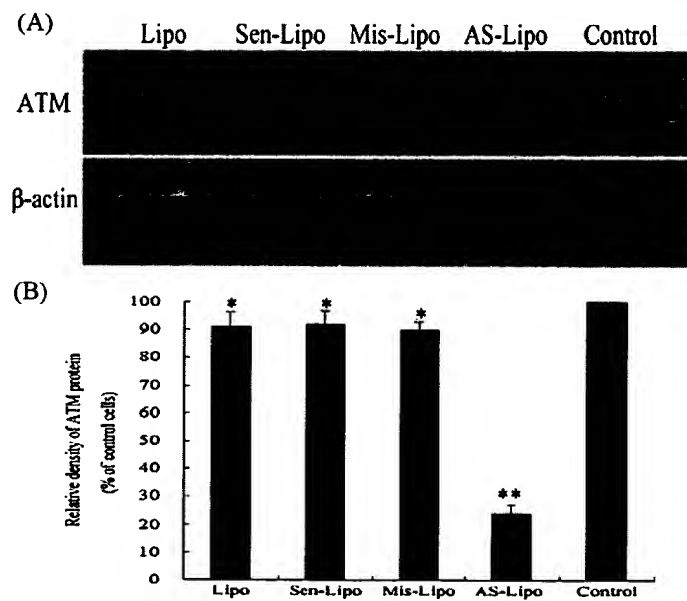
Only small numbers of apoptotic cells were detected by TUNEL analysis in tumors treated with irradiation alone. In contrast with irradiation alone, tumor cell apoptosis was doubled following irradiation in combination with ATM AS-ODNs treatment (Figure. 8A). Accordingly, the AI for tumors from ATM AS-ODNs treated mice was 19.6 ± 3.2 , significantly higher than that of the other groups ($P < 0.05$; Figure. 8B).

Discussion

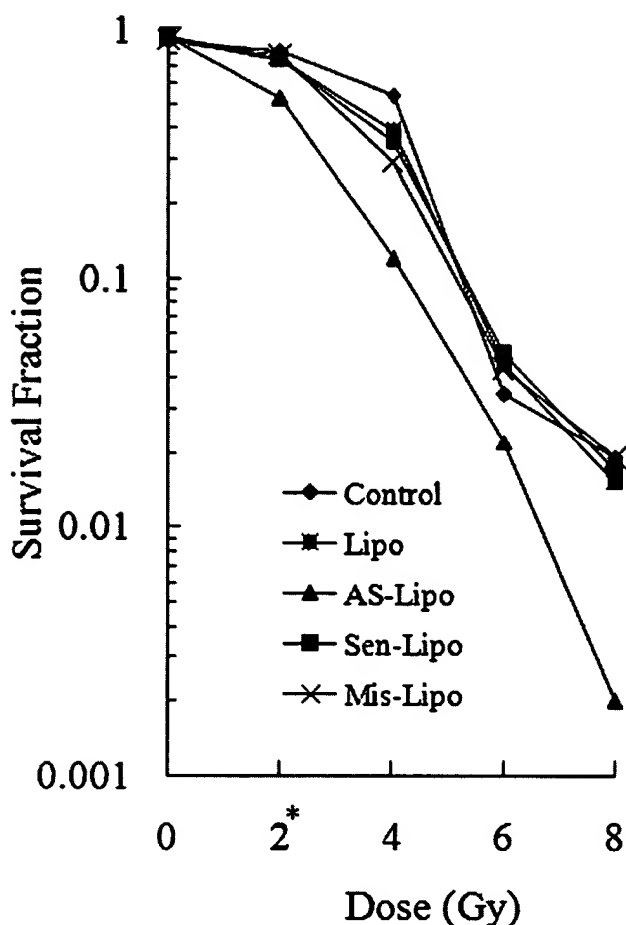
Damage to cellular DNA evokes a wide range of cellular responses that lead to activation of a variety of genes necessary for cellular survival, delay in cell-cycle progression, and induction of DNA repair [18-20]. ATM protein is a key

**Figure 1**

Real-time quantitative PCR analysis of ATM mRNA expression. Reduced expression of ATM mRNA in the presence of liposome formulations of ATM AS-ODNs (AS-Lipo) was observed. * $P > 0.05$, no significantly difference among liposome-treated group (Lipo), and Sen-ODNs (Sen-Lipo) treated group and Mis-ODNs (Mis-Lipo) treated group. ** $P < 0.05$, compared with other groups.

**Figure 2**

Effect of ATM AS-ODNs on the expression of ATM protein *in vitro*. (A) Liposome formulations of ATM AS-ODNs significantly reduced the expression of ATM protein compared with other groups. (B) * $P > 0.05$, no significantly difference among liposome-treated group (Lipo), and Sen-ODNs (Sen-Lipo) treated group and Mis-ODNs (Mis-Lipo) treated group. ** $P < 0.05$, compared with other groups.

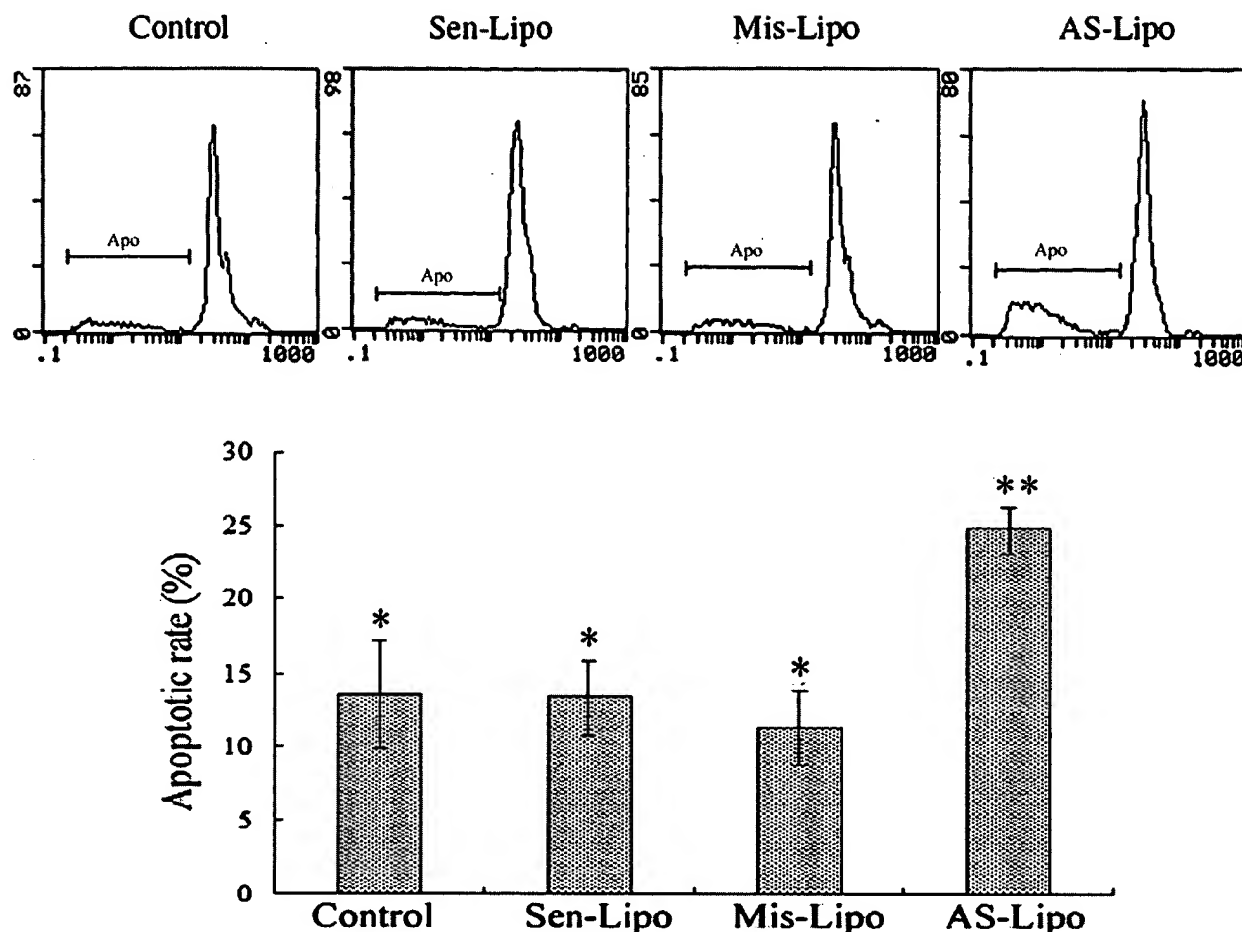
**Figure 3**

Survival curves for SCCVII cells after irradiation. Survival fractions at each dose point were normalized to untreated cells. * $P < 0.05$, The mean of SF2 in the cells transfected with ATM AS-ODNs was significantly lower than that of other cells.

mediator of the radioprotective machinery inducing a signaling network that is responsible for repair of radiation-induced damaged DNA and for cellular recovery and survival [21-23]. Rasheed had found that disruption of the ATM gene in mice resulted in exquisite sensitivity to low doses of ionizing radiation[24]. Yin demonstrated that treatment of mouse cerebrovascular endothelial cells with ATM AS-ODNs led to specific inhibition of ATM induction, and increased radiation-induced apoptosis *in vitro*[17]. Therefore we designed the experiment to test the hypothesis whether ATM AS-ODNs could inhibit the expression of ATM in SCCVII cells and furthermore increase the radiosensitivity by enhancing radiation-induced apoptosis *in vitro* and *in vivo*.

In the present study, we successfully transfected ATM AS-ODNs into SCCVII cells using liposome as delivery car-

rier, and detected the inhibitory expression of ATM at mRNA and protein level in SCCVII cells. We found that expression of ATM was dramatically reduced after cells were transfected with ATM AS-ODNs compared with that Sen-ODNs and Mis-ODNs treated groups, which indicated that the inhibition was specific for the ATM antisense sequence. Then we investigated whether the reduction of ATM expression resulted in radiosensitization in SCCVII cells. The results of clonogenic survival assay *in vitro* demonstrated that the cloning efficiency declined notably in cells which transfected with ATM AS-ODNs at the same dose of radiation ($P < 0.05$) compared with untreated cells or cells treated with control ODNs. While the SF2 of cells transfected with ATM AS-ODNs was $53.3 \pm 3.1\%$, definitely lower than that of other cells, which means the increase of cell intrinsic radiosensitivity. Furthermore we investigated whether the increased radio-

**Figure 4**

The apoptotic rate of SCCVII cells after 2 Gy irradiation. The apoptotic rate (Apo) in ATM AS-ODNs transfected cells was higher than that in Sen-ODNs and Mis-ODNs transfected cells after 2 Gy irradiation. * $P > 0.05$, no significant difference among these groups. ** $P < 0.05$, compared with other groups.

sensitivity in SCCVII cells was due to the enhanced radiation-induced apoptosis and defective cell-cycle checkpoint. As we known, in p53 mutated cell lines, ATM mainly regulates the G2/M checkpoint to arrest cells in G2 phase at the time of irradiation where the radiation-induced DSBs can be repaired[15,16]. From flow cytometry, we found that the cells did not accumulate in the G2/M phase following irradiation in cells transfected with ATM AS-ODNs, which mean the reduced ATM expression resulted in the defective G2/M checkpoint control. Moreover, we found that radiation-induced apoptosis increased among the cells lack of ATM expression compared with those cells that have impact ATM expression.

In our study, we also investigated the effects of ATM AS-ODNs on the apoptotic responses to ionizing radiation *in vivo*. It was found that the tumors irradiated in combination with the treatment of ATM AS-ODNs were effective in controlling tumor growth and showed higher apoptotic rate. The inhibition rate in the tumors injected with ATM AS-ODNs before exposure to X-ray was $56.1 \pm 3.8\%$, whereas it was $23.2 \pm 2.7\%$ in tumors exposed to radiation alone, and a significant difference was found between these two groups ($P < 0.05$). The results of TUNEL assay demonstrated that the apoptotic rate of the tumors irradiated in combination with the treatment of ATM AS-ODNs was obviously higher than that of control groups. The results of *in vivo* experiments indicated that the radiosensitivity of SCCVII cells solid tumors were enhanced by the

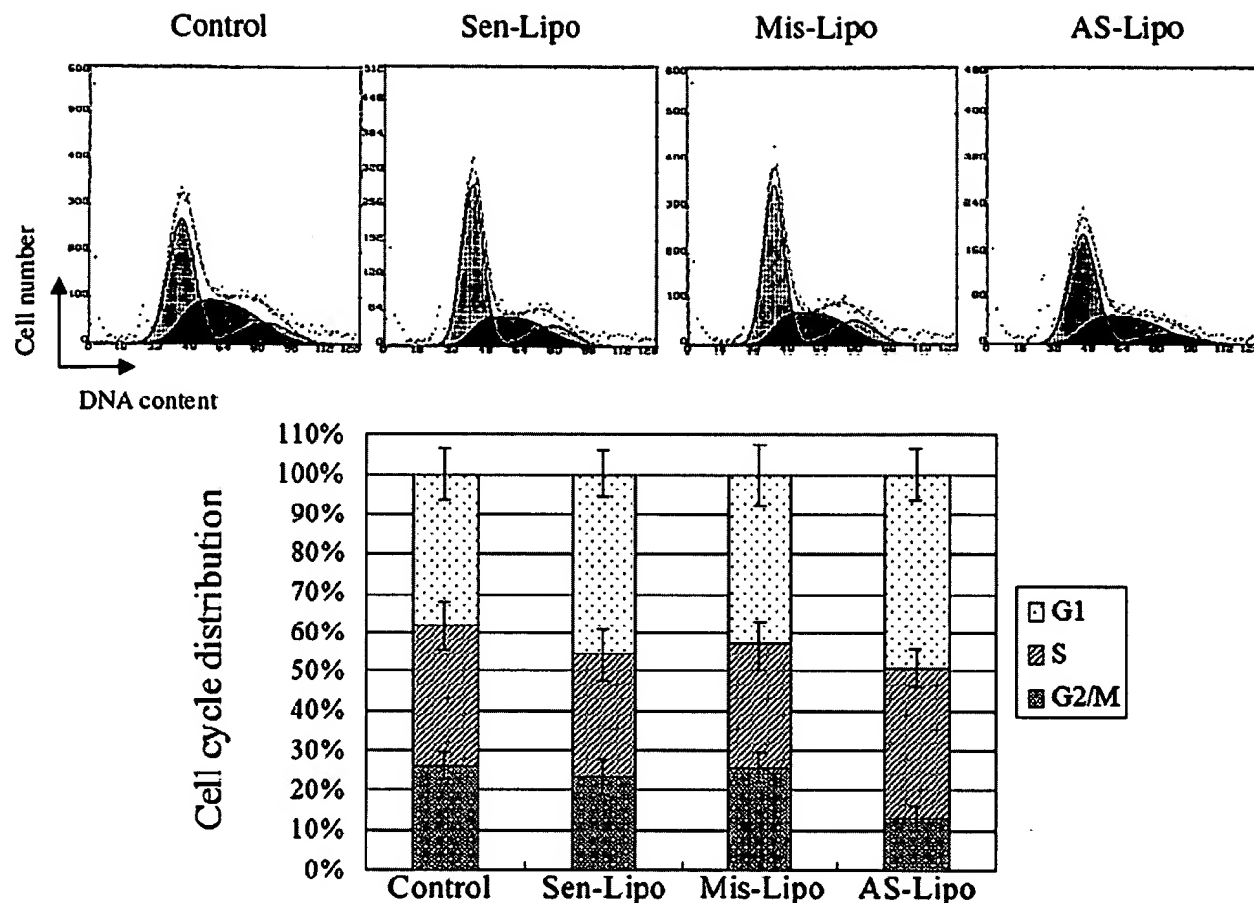


Figure 5
Distribution of the cell cycle in SCCVII cells after 2 Gy irradiation. The cell percentage of G2/M phase decreased dramatically in ATM AS-ODNs transfected cells at 48 hours after 2 Gy irradiation compared with that of other groups ($P < 0.05$).

treatment of ATM AS-ODNs and related with the increased radiation-induced apoptosis.

Conclusion

We had demonstrated that the ATM AS-ODNs used in our study could specifically reduce the ATM expression and further result in an increased radiosensitivity in SCCVII cells *in vitro* and *in vivo*. The potential mechanism of radiosensitization related with reduced ATM expression should be the defective G2/M cell-cycle checkpoint control and enhanced radiation-induced apoptosis.

Competing interests

The authors declare that they have no competing interests.

Authors' contributions

XQ carried out cell culture, participated in the design of the study and performed the statistical analysis. HY carried out flow cytometry assay, participated in the animal experiment. YY participated in irradiation for cells and animals. XZ participated in the clonogenic survival assay. HZ carried out the TUNEL assays. SL conceived of the study, and participated in its design and coordination and helped to draft the manuscript. JZ designed the study, per-

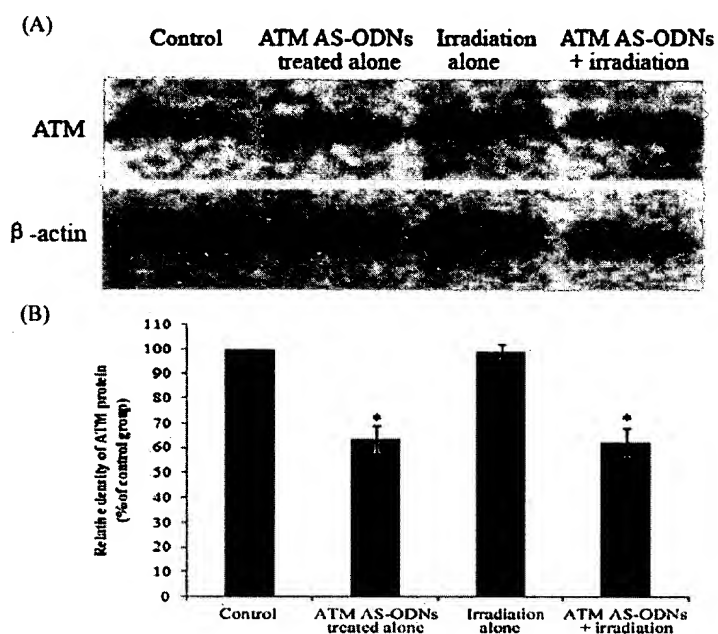


Figure 6
Effect of ATM AS-ODNs on the ATM protein expression *in vivo*. (A) In the group treated with ATM AS-ODNs alone (ATM AS-ODNs treated alone) and the group irradiated in combination with ATM AS-ODNs (ATM AS-ODNs + irradiation), the expression of ATM protein were decreased. (B) * $P < 0.05$, compared with the untreated group and the group irradiated alone.

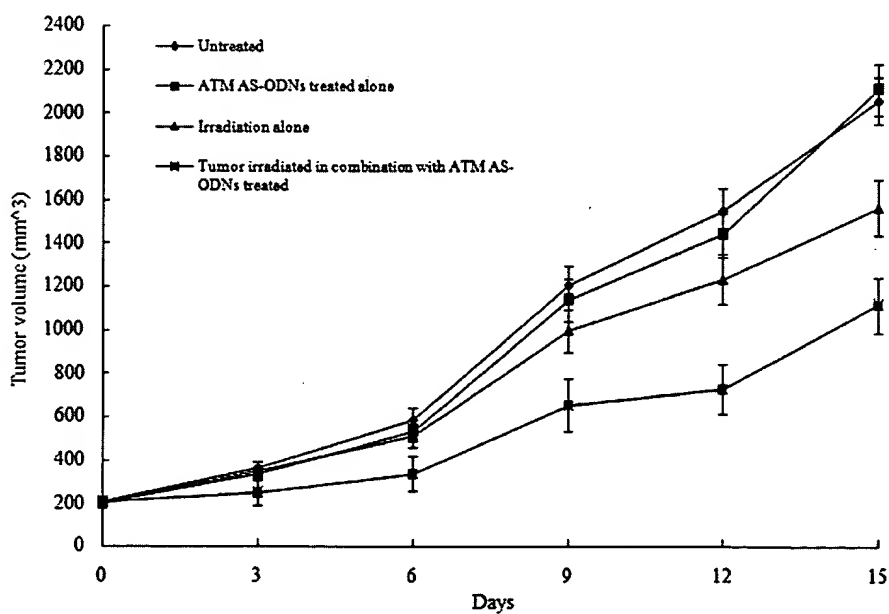
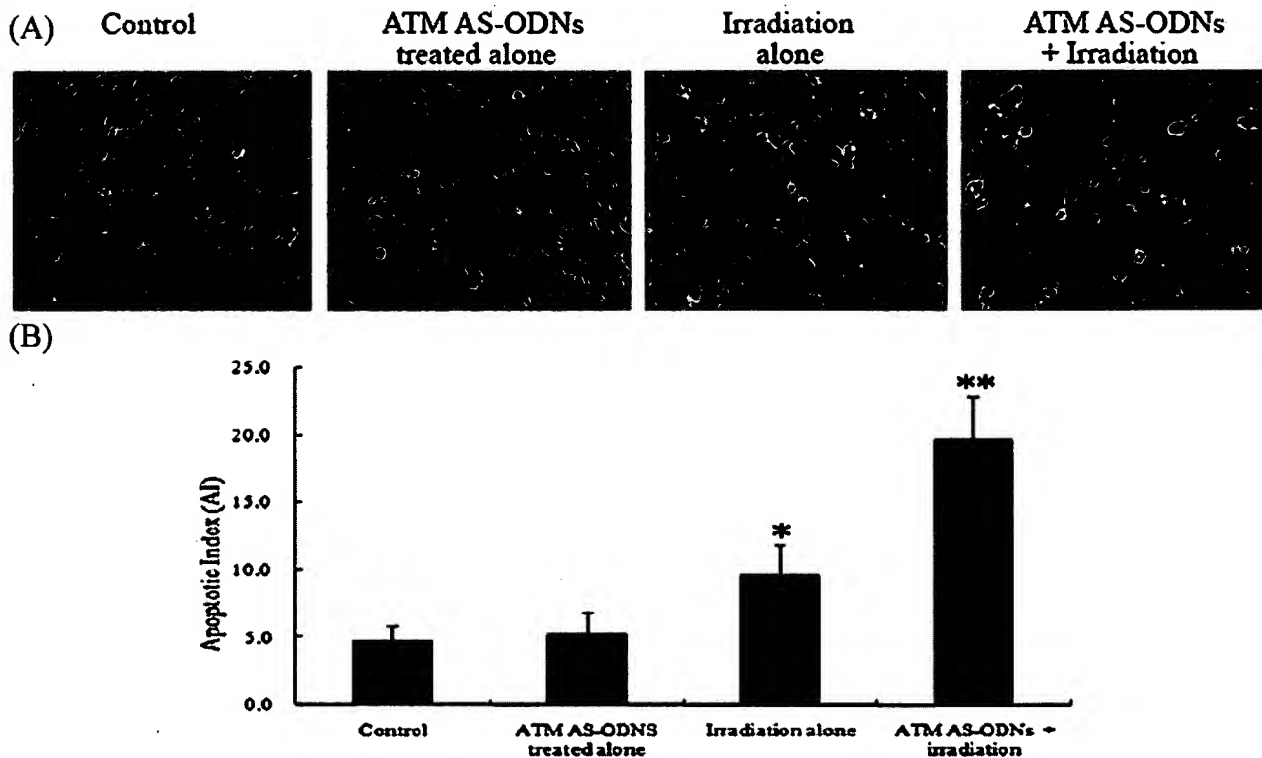


Figure 7
Tumor growth in ATM AS-ODNs treated SCCVII cells in C3H/He mice with or without irradiation.

**Figure 8**

The apoptosis of SCCVII cells *in vivo* after irradiation. (A) Apoptotic cells are detected by TUNEL. The nuclei of apoptotic cells were stained brown as observed under light microscopy (magnification, $\times 400$). (B) The treatment by irradiation in combination with ATM AS-ODNs injection enhanced the apoptotic rate of tumor cells. * $P < 0.05$, there was a significant difference in the AI of tumors treated with irradiation alone compared with the untreated group and the group treated with ATM AS-ODNs alone. ** $P < 0.05$, compared with the other groups.

formed the rest of the experiments and wrote the manuscript. All authors read and approved the final manuscript.

Acknowledgements

This work was supported by the National Natural Science Foundation of China (No. 30572013). We thank the Laboratory of gene therapy at Johns Hopkins University for generous gift of SCCVII cell line. We also thank Dr. Shan Hai (Department of Geriatrics, West China Hospital, Sichuan University, Chengdu, Sichuan, 610041, China) for correcting English of the manuscript.

References

- Rhee JG, Li D, O'Malley BW Jr, Suntharalingam M: **Combination radiation and adenovirus-mediated P16(INK4A) gene therapy in a murine model for head and neck cancer.** *ORL journal for oto-rhino-laryngology and its related specialties* 2003, **65**:144-54.
- Rhee JG, Li D, Suntharalingam M, Guo C, O'Malley BW Jr, Carney JP: **Radiosensitization of head/neck squamous cell carcinoma by adenovirus-mediated expression of the Nbs1 protein.** *International journal of radiation oncology, biology, physics* 2007, **67**:273-8.
- O'Malley BW Jr, Cope KA, Johnson CS, Schwartz MR: **A new immunocompetent murine model for oral cancer.** *Arch Otolaryngol Head Neck Surg* 1997, **123**(1):20-24.
- Khurana D, Martin EA, Kasperbauer JL, et al: **Characterization of a spontaneously arising murine squamous cell carcinoma (SCC VII) as a prerequisite for head and neck cancer immunotherapy.** *Head & neck* 2001, **23**:899-906.
- Dunne AL, Price ME, Mothersill C, McKeown SR, Robson T, Hirst DG: **Relationship between clonogenic radiosensitivity, radiation-induced apoptosis and DNA damage/repair in human colon cancer cells.** *British journal of cancer* 2003, **89**:2277-83.
- Li Y, Carty MP, Oakley GG, Seidman MM, Medvedovic M, Dixon K: **Expression of ATM in ataxia telangiectasia fibroblasts rescues defects in DNA double-strand break repair in nuclear extracts.** *Environmental and molecular mutagenesis* 2001, **37**:128-40.
- El-Awady RA, Dikomey E, Dahn-Daphi J: **Radiosensitivity of human tumour cells is correlated with the induction but not with the repair of DNA double-strand breaks.** *British journal of cancer* 2003, **89**:593-601.
- Sakata K, Someya M, Matsumoto Y, Hareyama M: **Ability to repair DNA double-strand breaks related to cancer susceptibility and radiosensitivity.** *Radiation medicine* 2007, **25**:433-8.
- Shiloh Y: **ATM and related protein kinases: safeguarding genome integrity.** *Nature reviews* 2003, **3**:155-68.
- Shiloh Y, Lehmann AR: **Maintaining integrity.** *Nature cell biology* 2004, **6**:923-8.

11. Berkovich E, Monnat RJ Jr, Kastan MB: Roles of ATM and NBS1 in chromatin structure modulation and DNA double-strand break repair. *Nature cell biology* 2007, 9:683-90.
12. Peng Y, Woods RG, Beamish H, et al: Deficiency in the catalytic subunit of DNA-dependent protein kinase causes down-regulation of ATM. *Cancer research* 2005, 65:1670-7.
13. Morales M, Theunissen JW, Kim CF, Kitagawa R, Kastan MB, Petrini JH: The Rad50S allele promotes ATM-dependent DNA damage responses and suppresses ATM deficiency: implications for the Mre11 complex as a DNA damage sensor. *Genes & development* 2005, 19:3043-54.
14. Mirzayans R, Severin D, Murray D: Relationship between DNA double-strand break rejoining and cell survival after exposure to ionizing radiation in human fibroblast strains with differing ATM/p53 status: implications for evaluation of clinical radiosensitivity. *International journal of radiation oncology, biology, physics* 2006, 66:1498-505.
15. Delia D, Fontanella E, Ferrario C, Chessa L, Mizutani S: DNA damage-induced cell-cycle phase regulation of p53 and p21waf1 in normal and ATM-defective cells. *Oncogene* 2003, 22:7866-9.
16. Gaul L, Mandl-Weber S, Baumann P, Emmerich B, Schmidmaier R: Bendamustine induces G2 cell cycle arrest and apoptosis in myeloma cells: the role of ATM-Chk2-Cdc25A and ATM-p53-p21-pathways. *Journal of cancer research and clinical oncology* 2008, 134:245-53.
17. Yin KJ, Chen SD, Lee JM, Xu J, Hsu CY: ATM gene regulates oxygen-glucose deprivation-induced nuclear factor-kappaB DNA-binding activity and downstream apoptotic cascade in mouse cerebrovascular endothelial cells. *Stroke; a journal of cerebral circulation* 2002, 33:2471-7.
18. Eastham AM, Atkinson J, West CM: Relationships between clonogenic cell survival, DNA damage and chromosomal radiosensitivity in nine human cervix carcinoma cell lines. *International journal of radiation biology* 2001, 77:295-302.
19. Wada S, Kurabayashi H, Kobayashi Y, et al: The relationship between cellular radiosensitivity and radiation-induced DNA damage measured by the comet assay. *The Journal of veterinary medical science/the Japanese Society of Veterinary Science* 2003, 65:471-7.
20. Wada S, Van Khoa T, Kobayashi Y, et al: Prediction of cellular radiosensitivity from DNA damage induced by gamma-rays and carbon ion irradiation in canine tumor cells. *The Journal of veterinary medical science/the Japanese Society of Veterinary Science* 2005, 67:1089-95.
21. Savitsky K, Bar-Shira A, Gilad S, et al: A single ataxia telangiectasia gene with a product similar to PI-3 kinase. *Science* 1995, 268(5218):1749-1753.
22. Riballo E, Kuhne M, Rief N, et al: A pathway of double-strand break rejoining dependent upon ATM, Artemis, and proteins locating to gamma-H2AX foci. *Molecular cell* 2004, 16:715-24.
23. Lavin MF: The Mre11 complex and ATM: a two-way functional interaction in recognising and signaling DNA double strand breaks. *DNA repair* 2004, 3:1515-20.
24. Rasheed N, Wang X, Niu QT, Yeh J, Li B: Atm-deficient mice: an osteoporosis model with defective osteoblast differentiation and increased osteoclastogenesis. *Human molecular genetics* 2006, 15:1938-48.

Publish with **BioMed Central** and every scientist can read your work free of charge

"BioMed Central will be the most significant development for disseminating the results of biomedical research in our lifetime."

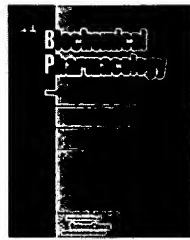
Sir Paul Nurse, Cancer Research UK

Your research papers will be:

- available free of charge to the entire biomedical community
- peer reviewed and published immediately upon acceptance
- cited in PubMed and archived on PubMed Central
- yours — you keep the copyright

Submit your manuscript here:
http://www.biomedcentral.com/info/publishing_adv.asp



available at www.sciencedirect.comjournal homepage: www.elsevier.com/locate/biochempharm

Regression of prostate cancer xenografts by RLIP76 depletion

Sharad S. Singhal*, Cherice Roth, Kathryn Leake, Jyotsana Singhal,
Sushma Yadav, Sanjay Awasthi

Department of Molecular Biology and Immunology, University of North Texas Health Science Center, Fort Worth, TX 76107, United States

ARTICLE INFO

Article history:

Received 5 October 2008

Accepted 18 November 2008

Keywords:

RLIP76

Cancer

Drug-resistance

Xenografts

Glutathione-conjugate transport

ABSTRACT

RLIP76 plays a central role in radiation and chemotherapy resistance through its activity as a multi-specific ATP-dependent transporter which is over-expressed in a number of types of cancers. RLIP76 appears to be necessary for cancer cell survival because both *in vitro* cell culture and *in vivo* animal tumor studies show that depletion or inhibition of RLIP76 causes selective toxicity in malignant cells. RLIP76 induces apoptosis in cancer cells through the accumulation of endogenously formed GS-E. The results of our *in vivo* studies demonstrate that administration of RLIP76 antibodies, siRNA or anti-sense to mice bearing xenografts of PC-3 prostate cancer cells leads to near complete regression of established subcutaneous xenografts with no apparent toxic effects. Since anti-RLIP76 IgG (which inhibit RLIP76-mediated transport), siRNA and antisense (which deplete RLIP76) showed similar tumor regressing activities, our results indicate that the inhibition of RLIP76 transport activity at the cell surface is sufficient for observed anti-tumor activity. These studies indicate that RLIP76 serves a key effector function for the survival of prostate cancer cells and that it is a valid target for cancer therapy.

© 2008 Elsevier Inc. All rights reserved.

1. Introduction

Prostate cancer is the most frequently diagnosed malignancy and the second leading cause of cancer-related deaths in men in the U.S. In the early stage of the disease, the treatments of choice are extensive surgery and/or radiation therapy. Although both treatment modalities are effective, they are associated with significant morbidity and mortality. Despite striking improvements in drug therapy targeting kinase signaling pathways, prostate cancer remains a deadly malignancy if not found and removed in early stages. It is characteristically so highly drug-resistant, that no effective

and life-prolonging regimen of cytotoxic chemotherapy has been demonstrated for prostate cancer despite several decades of effort. Although prostate cells characteristically express high levels of transporter proteins in their membranes that can contribute to drug-resistance, and may also play some role in radiation resistance, targeting the ATP Binding Cassette (ABC)-transporter family protein has not been effective reversing drug-resistance in prostate cancer [1,2]. Prostate cancer is being detected with increasing frequency, and many patients are receiving such treatments as radical prostatectomy and radiation therapy. The highly drug and radiation-resistant nature of prostate cancer, as compared

* Corresponding author at: Department of Molecular Biology and Immunology, 3500 Camp Bowie Boulevard, 416 S RES Building, University of North Texas Health Science Center, Fort Worth, TX 76107-2699, United States. Tel.: +1 817 735 0459; fax: +1 817 735 2118.

E-mail address: ssinghal@hsc.unt.edu (S.S. Singhal).

Abbreviations: RLIP76 (RalBP1), Ral-interacting protein; GSH, glutathione; GS-E, glutathione-electrophile-conjugates; DNP-SG, dinitrophenyl S-glutathione; DOX, doxorubicin; 4HNE, 4-hydroxy- α -nonenal; IOVs, in-side out vesicles; MDR, multi-drug-resistance; Pgp, P-glycoprotein; MRP1, multi-drug-resistance associated protein; SCLC, small cell lung cancer; NSCLC, non-small cell lung cancer; POB1, partner of RalBP1; TUNEL, TdT-mediated dUTP nick end labeling assay.

0006-2952/\$ - see front matter © 2008 Elsevier Inc. All rights reserved.

[doi:10.1016/j.bcp.2008.11.013](https://doi.org/10.1016/j.bcp.2008.11.013)

with other neoplasm such as lung or breast cancer, is a major reason why there is still no effective and life-prolonging traditional cytotoxic chemotherapy for prostate cancer [3-5].

Clinically, however, inhibitors of ABC-transporters have not yet been successful in improving therapeutic outcomes [6,7], though alternative targeting strategies may ultimately prove clinically efficacious [8]. Clearly, other transport and resistance mechanisms are involved [9]. In contrast, genetic deletion of the non-ABC transporter, RLIP76, causes loss of about 4/5 of total transport activity for glutathione-conjugates (GS-E), along with major phenotypic effects due to sensitivity to stress or toxin mediated apoptosis. The loss of this transport activity for GS-E resulted in demonstrated accumulation of GS-E and their electrophilic precursors (e.g., GS-HNE and 4HNE) in the tissues of these animals [10].

Cell-line, animal and human clinical data indicate that the ABC-transporters MRP, P-glycoprotein (Pgp) and related transporters are clearly able to mediate drug-accumulation defects in cultured malignant cells, but correlations with pathology, clinical resistance and outcomes in prostate cancer are poor, and attempts at improving therapeutic efficacy by targeting these have not been successful [1,3-5]. Our approach will supply a missing piece of the puzzle to the understanding of multi-specific transport mechanisms in prostate cancer, a stress-responsive non-ABC, high capacity transporter, which must have had significant confounding effect in studies of ABC-transporters. Cancer cells appear significantly more sensitive to apoptosis triggered by blocking RLIP76 than normal cells, suggesting the feasibility of targeting RLIP76 in prostate cancer therapy.

RLIP76 was characterized as a human GTPase-activating protein, Ral-interacting protein. It was cloned as a Ral-binding GAP through a yeast two-hybrid screen [11]. It is a 76 kDa protein, but it appears as a 95 kDa band in SDS-PAGE [12]. Complete and sustained regression of human lung and colon cancer xenografts by systemic depletion clearly demonstrates the effectiveness of targeting the mercapturic acid pathway through RLIP76 [13]. Present studies were therefore designed to examine the effect of inhibiting transport activity of RLIP76 on PC-3 cells in culture and on tumor xenografts in nude mice. The focus of our present studies is to develop a novel therapeutic strategy for the treatment of prostate cancer by using RLIP76 antibody, siRNA or antisense.

2. Materials and methods

2.1. Materials

Bacterial strains DH5 α and BL21(DE3) were purchased from Invitrogen Life Tech. (Carlsbad, CA). pET30a(+), the T7 promoter based expression vector was purchased from Novagen, Inc. (Madison, WI). Restriction enzymes, thermostable DNA polymerase (Vent polymerase) and DNA ligase were from New England Biolabs (Beverly, MA). dNTPs were from Applied Biosystems (Foster city, CA). RPMI-1640 and DMEM medium, phosphate buffered saline (PBS), penicillin/streptomycin solution (P/S), fetal bovine serum (FBS), trypsin/EDTA, and trypan blue were purchased from GIBCO BRL Inc.,

Grand Island, NY. Dimethylsulfoxide (DMSO), G418 (geneticin) and 3-(4,5-dimethylthiazol-2-yl)-2,5-diphenyltetrazolium bromide (MTT) were obtained from sigma (St Louis, MO). Doxorubicin (DOX, adriamycin) was obtained from Adria Laboratories (Columbus, OH). 3 H-GSH (3000 Ci/mmol) was purchased from Pharmacia Biotech (Piscataway, NJ). 14 C-DOX (specific activity 44.8 Ci/mmol) was purchased from NEN Life Sciences (Boston, MA). Polyclonal rabbit-anti-human recombinant RLIP76 IgG as well as pre-immune IgG were prepared and purified as described previously [12]. Secondary antibody for Western blots, goat anti-rabbit IgG horseradish peroxidase conjugate was purchased from Sigma (St. Louis, MO). TUNEL fluorescence detection kit was purchased from Promega (Madison, WI). DNP-SG was synthesized from CDNB and GSH according to the method described by us previously [14]. The sources of other chemicals used in this study were same as described previously [12].

2.2. Cell lines and cultures

Human SCLC H82, NSCLC H226 (squamous cell carcinoma), kidney Caki-2, prostate PC-3 and colon SW-480 from American Type Culture Collection (Manassas, VA), were used in these studies. Human aortic vascular smooth muscle cells (HAVSMC) and human umbilical vascular endothelial cells (HUVEC) were kindly provided by Dr. Paul Boor (UTMB, Galveston, TX) and Dr. Fiemu Nwariaku (UTSWMC, Dallas, TX), respectively. All cells were cultured at 37 °C in a humidified atmosphere of 5% CO₂ in the appropriate medium: RPMI 1640 (H82, H226, Caki-2, and SW-480), Ham's F12K (PC-3), DMEM (HAVSMC), and EGM-2 bullet kit (HUVEC) medium supplemented with 10% (v/v) heat-inactivated FBS and 1% (v/v) P/S solution.

2.3. Anti-RLIP76 antibodies

We have raised and purified polyclonal rabbit-anti-human RLIP76 IgG and aliquots were stored at -86 °C. All reagents for the preparation of antibodies and storage were filtered through 0.22 μ m filters and handled under laminar flow hoods in a sterile manner. Aerobic, anaerobic and fungal cultures of random aliquots were performed at 2-month intervals. The integrity and purity of the antibodies were consistently checked by SDS-PAGE and Western-blot analysis against anti-IgG antibodies during these studies. Protein-A affinity purified immunoglobulin fraction obtained from the pre-immune serum was used as control. Anti-RLIP76 IgG used in these experiments was previously shown by Ouchterlony double immuno-diffusion assay to be non-cross-reactive with any other proteins including Pgp or MRP [15,16].

2.4. RLIP76 siRNA preparation

We chose aa 171-185 (nucleotide 510-555 starting from 1 AUG codon in the open reading frame) in the N-terminal region of RLIP76 as the target region to design for siRNA because of lack of homology with other proteins or nucleotide sequences. We searched for 23-nucleotide sequence motif, AA(N19)TT or NA(N21) (N, any nucleotide) and selected hits with approximately 50% GC contents. The sequence of sense siRNA

corresponds to N21. We converted 3' end of the sense siRNA to TT. The rationale for this sequence conversion was to generate a symmetric duplex with respect to the sequence composition of sense and antisense 3' overhangs. The antisense siRNA was synthesized as the complement to position 1-21 of the 23-nucleotide motif. The selected siRNA sequence was blast-search (NCBI database) against EST libraries, to ensure that only one gene is targeted. Chemically synthesized siRNA duplex in the 2' de-protected and desalted forms, was purchased from Dharmacon Research (Lafayette, CO). A 23 nucleotide long scrambled siRNA duplex was used as a control. The scrambled siRNA sequence was not homologous with RLIP76 mRNA in a blast-search against RLIP76. The siRNA duplex was re-suspended in 1X universal buffer, provided by Dharmacon Research Laboratory (Lafayette, CO). The targeted cDNA sequence (AAGAAAAAGCCAATTTCAGGAGCC) corresponds to aa 170-176 (nt 508-528). The corresponding sense and antisense siRNA sequences are GAAAAAGCCAUUUCAG-GAGCCdTdT and GGCUCUGAAUUGGCUUUUCdTdT, respectively. The sequence of the scrambled siRNA in the sense and antisense directions are GUAACUGCAACGAAUUCGAU-GdTdT and CAUCGAAAUCGUUGCAGUUCdTdT, respectively. Transfection of siRNA duplexes was performed using Trans-messenger Transfection Reagent kit (Qiagen) and assay for silencing 24 h after transfection.

2.5. RLIP76 phosphorothioate anti-sense DNA preparation

The region spanning amino acid residues 171-185 (nucleotide 510-555 starting from 1 AUG codon in the open reading frame) in the N-terminal region of RLIP76 was chosen as the target region for synthesis of phosphorothioate DNA. The oxygen in the backbone of the DNA molecules was replaced by sulfur in each phosphate group, which makes the DNA backbone resistant to nucleases. However, the macromolecule remains electrically charged, impeding its passage across cell membrane. Selected DNA sequence was subjected to blast-search (NCBI database) against EST libraries, to ensure that only the selected gene was targeted. Chemically synthesized phosphorothioate DNA in desalted form was purchased from Biosynthesis Inc (Lewisville, TX). A 21 nucleotide long scrambled phosphorothioate DNA was used as a control. The scrambled DNA sequence was not homologous with RLIP76 cDNA in a blast-search against RLIP76. The targeted cDNA sequence (AAGAAAAAGCCAATTTCAGGAGCC) corresponds to nt 508-528. The corresponding phosphorothioate DNA sequence was GGCTCCTGAATTGGCTTTTC. The sequence of the scrambled DNA was CATCGAAATCGTTGCAGT-TAC. Transfection of phosphorothioate DNA was performed using Maxfect transfection reagent (MoleculA) and assayed for silencing 24 h after transfection.

2.6. Drug sensitivity (MTT) assay

Cell number/ml in an aliquot of cells growing in log phase was determined by counting trypan blue excluding cells in a hemocytometer and 20,000 cells were plated into each well of 96-well flat-bottomed micro-titer plates. After 12 h incubation at 37 °C, medium containing either pre-immune IgG or anti-

RLIP76 IgG were added to cells. After 24-48 h incubation, 20 µl of 5 mg/ml MTT were introduced to each well and incubated for 2 h of exposure. The plates were centrifuged and medium was decanted. Cells were subsequently dissolved in 100 µl DMSO with gentle shaking for 2 h at room temperature, followed by measurement of optical density at 570 nm [17,18]. Eight replicate wells were used in each point in each of three separate measurements. Measured absorbance values were directly linked with a spreadsheet for calculation of IC₅₀, defined as the drug concentration that reduced formazan formation by 50%. Depletion of RLIP76 expression in cells by RLIP76 siRNA and RLIP76 antisense were measured as follows: cells were incubated for 3 h with 0-4 µg/well either RLIP76 siRNA or anti-sense in Transmessenger Transfection Reagent (Qiagen) and Maxfect transfection reagent (MoleculA), respectively, according to the manufacturer provided protocol.

2.7. Cloning, prokaryotic expression, and purification of RLIP76

Purified RLIP76 protein (1965 bp; 655 aa) was obtained from *E. coli* BL21(DE3) expressing the pET30a(+) plasmid containing full-length cDNA corresponding to the sequence of RLIP76. The purification was carried out using DNPSG-affinity resin as described previously and purity was confirmed by SDS-PAGE and Western blot analyses [12].

2.8. Functional reconstitution of purified rec-RLIP76 into artificial liposomes and transport studies

Purified RLIP76 was dialyzed against reconstitution buffer (10 mM Tris-HCl, pH 7.4, 2 mM MgCl₂, 1 mM EGTA, 100 mM KCl, 40 mM sucrose, 2.8 mM BME, 0.05 mM BHT, and 0.025% polidocanol). An aqueous emulsion of soybean asolectin (40 mg/ml) and cholesterol (10 mg/ml) was prepared in the reconstitution buffer by sonication and 0.1 ml of this mixture was added to 0.9 ml aliquot of dialyzed purified rec-RLIP76 protein. The reaction mixture was sonicated at 50 W for 30 s. Vesiculation was initiated by addition of 200 mg SM-2 Bio-beads pre-equilibrated in the reconstitution buffer without polidocanol. Vesiculation was carried out for 4 h at 4 °C, followed by removal of SM-2 Bio-beads by centrifugation and the vesicles (RLIP76-liposomes) were collected, and yields primarily unilamellar vesicles with median diameter of 0.25 µm, and intravesicular/extravesicular volume ratio of 18 µl/ml. Control vesicles (control-liposomes) were prepared using an equal amount of albumin or crude protein from *E. coli* not expressing RLIP76. ATP-dependent transport of ¹⁴C-DOX and ³H-DNPSG in the rec-RLIP76 reconstituted proteoliposomes was performed by rapid filtration technique using the exact protocol described by us previously [12]. Efficiency of delivery for proteoliposomes has been established previously [12,18].

2.9. Preparations of crude membrane fractions for Western blot analyses

Crude membrane fractions were prepared from the normal and cancer cell lines using established procedures as described previously [19]. Levels of RLIP76 protein in normal and

cancer cells was measured by Western blot and ELISA assay using anti-RLIP76 IgG as previously described [18,19]. Purified rec-RLIP76 with purity assessed by amino acid composition analysis was used to generate calibration curves.

2.10. Transport studies in IOVs

Crude membrane vesicles (inside-out vesicles, IOV) were prepared from the normal (H9SMC and HUVEC) and malignant (H82, H226, Caki-2, PC-3 and SW-480) cell lines using established procedures as described by us for the K562 cells [12,20]. Transport studies of DOX and DNP-SG in IOV were performed by the method as described previously [20]. ATP-dependent uptake of ¹⁴C-DOX was determined by subtracting the radioactivity (cpm) of the control without ATP from that of the experimental containing ATP and the transport of DOX was calculated in terms of pmol/min/mg IOV protein. The transport of ³H-DNP-SG was measured in a similar manner.

2.11. Animal model

Hsd: Athymic nude nu/nu mice (~12 weeks old) were obtained from Harlan, Indianapolis, IN. All animal experiments were carried out in accordance with a protocol approved by the Institutional Animal Care and Use Committee (IACUC). Twenty-four mice were divided into six groups of 4 animals (treatments with pre-immune serum, scrambled siRNA, scrambled anti-sense DNA, RLIP76 antibodies, RLIP76 siRNA and RLIP76 antisense). All 24 animals were injected with 2×10^6 human prostate cancer cells (PC-3) suspensions in 100 μ l of PBS, subcutaneously into one flank of each mouse. Animals were examined daily for signs of tumor growth. Treatment were administered when the tumor surface area exceeded $\sim 42 \text{ mm}^2$ (~ day 27). Treatment consisted of 200 μ g of RLIP76 antibodies, siRNA or antisense in 100 μ l PBS. Control groups were treated with 200 μ g/100 μ l pre-immune serum, scrambled siRNA or scrambled anti-sense DNA. Tumors were measured in two dimensions by calipers using Study Director Software V1.6, from Studylog System, San Francisco, CA.

2.12. Colony forming assay

Cells (0.1×10^6 cells/500 μ l) were irradiated at 100, 200, 500 and 1000 cGy using Varian Clinac 2100C Linear Accelerator with 6 MeV photon beam, for 1.25 min at the Texas Cancer Center, Arlington, TX, then aliquots 50 and 100 μ l in 60 mm size petri dishes, separately, in a total volume of 4 ml by adding medium in each Petri dish. After 7 days, un-irradiated and irradiated cells were stained with methylene blue for 30 min. and colonies were counted using Innotech Alpha Imager HP [21].

2.13. Effect of RLIP76 antibody, siRNA and antisense on apoptosis by TUNEL assay

In these studies, we assessed whether cellular levels of RLIP76 could be depleted by RLIP76 antibody, siRNA or antisense mediated delivery to cultured prostate cancer cells, and assessed whether uptake is correlated with apoptosis by the TUNEL assay. The PC-3 prostate cancer cells (1×10^6 cells) were grown on the cover slips. The cells were treated with

RLIP76 antibody (40 μ g/ml final conc.) or transfected with either RLIP76 siRNA (20 μ g/ml final conc.) or RLIP76 antisense (10 μ g/ml final conc.). After 24 h incubation, the medium was removed, and cells were washed with PBS. TdT-mediated dUTP nick end labeling (TUNEL) assay was performed using Promega fluorescence detection kit according to the protocol provided by the manufacturer and described by us previously [21]. Briefly, cells were fixed by immersing slides in freshly prepared 4% paraformaldehyde solution for 30 min at 4 °C followed by washing with PBS. The cells were permeabilized by immersing the slides in 0.2% Triton X-100 solution in PBS for 5 min followed by washing with PBS. Cells were equilibrated with equilibration buffer (provided by Promega Company) for 10 min. The equilibrated areas were blotted with tissue paper and TdT incubation buffer was added to the cells, and placed in humidified chamber. The chamber was covered with aluminum foil to protect from direct light. Slides were incubated at 37 °C for 60 min and the reaction was terminated by immersing the slides in 2× SSC buffer for 15 min followed by washing with PBS. The slides were stained in propidium iodide solution for 10 min in the dark and washed with distilled water several times. Slides were analyzed under a fluorescence microscope using a standard fluorescein filter set to view the green fluorescence at 520 nm, and red fluorescence of propidium iodide at >620 nm. Fluorescence micrographs were taken using Zeiss LSM 510 META (Germany) laser scanning fluorescence microscope at 400× magnification.

2.14. Statistical methods

All data were evaluated with a two-tailed unpaired student's *t* test or compared by one-way ANOVA and are expressed as the mean \pm SD. A value of $P < 0.05$ was considered statistically significant.

3. Results and discussion

3.1. Expression of RLIP76

Western-blot analyses of membrane protein extracts from various human normal and cancer cells were performed against anti-RLIP76 IgG indicated relatively larger amounts of RLIP76 in cancer versus normal cells (Fig. 1).

The results of RLIP76 protein and transport-activity are presented in Table 1 show that the amounts of total crude membrane proteins obtained from 100×10^6 cells in log-phase growth were comparable for normal and cancer cells. RLIP76 protein represented 0.21% and 0.66% of the total detergent soluble protein from the membranes of normal and cancer cells, respectively. These values of % of total membrane protein are in the range of those seen in various cell lines previously [15,19]. We have shown that proteoliposomes reconstituted with RLIP76, mediate ATP-dependent transport of DOX and other drugs [12,17,22]. In order to examine whether differential RLIP76 protein in normal and cancer cells was reflected in their transport activity, we compared the ATP-dependent uptake of DOX and DNP-SG in crude membrane inside-out vesicles (IOV) prepared separately from the mem-

Table 1 – RLIP76 protein and transport activity in human normal and cancer cells.

	Total crude protein (mg/10 ⁸ cells)	RLIP76 protein		Transport-activity (pmol/min/mg)	
		µg/10 ⁸ cells	% of total crude protein	¹⁴ C-DOX	³ H-DNP-SG
Non-malignant					
HAVSMC (aorta smooth muscle)	7.73 ± 0.61	17 ± 2	0.22	38 ± 5	114 ± 10
HUVEC (umbilical endothelial)	7.14 ± 0.48	15 ± 2	0.21	33 ± 5	104 ± 12
Malignant					
Caki-2 (kidney)	7.21 ± 0.72	44 ± 3	0.61	189 ± 12	684 ± 54
H-82 (lung, SCLC)	7.08 ± 0.47	34 ± 3	0.48	102 ± 8	316 ± 21
PC-3 (prostate)	7.88 ± 0.68	52 ± 3	0.66	257 ± 18	946 ± 42
H-226 (lung, NSCLC)	7.17 ± 0.82	38 ± 3	0.53	174 ± 14	594 ± 32
SW-480 (colon)	7.91 ± 0.86	49 ± 3	0.62	228 ± 21	744 ± 41

Cell lines were cultured in respective medium and homogenate was prepared from 100 × 10⁶ cells. RLIP76 was purified from total crude membrane fraction using DNPSG-affinity column chromatography, and quantified by ELISA. For transport studies, in-side-out vesicles (IOVs) prepared from 20 × 10⁶ cells was enriched for IOVs by wheat-germ-agglutinin affinity chromatography [20]. Transport-activity was calculated from measurements of uptake of ¹⁴C-DOX (sp. activity, 8.5 × 10⁴ cpm/nmol) and ³H-DNP-SG (sp. activity, 3.6 × 10³ cpm/nmol) into the IOVs (20 µg/30 µl reaction mixture) in the absence or presence of 4 mM ATP. Each transport experiment was done in triplicates in three separate experiments (n = 9).

branes of control and cancer cells. The results presented in Table 1 clearly demonstrated that the ATP-dependent transport of DOX and DNP-SG was significantly higher in IOVs prepared from cancer cells than from normal cells. Results of

measurements of ATP-dependent transport of ¹⁴C-DOX and ³H-DNPSG revealed greater transport of both substrates in cancer cells containing greater amounts of RLIP76 protein, and a general correlation between RLIP76 protein level and transport-activity. Thus, greater RLIP76 expression corresponded to greater transport-activity.

3.2. Relative contribution of RLIP76 towards DOX-transport

DOX is a common allocrite transported by RLIP76 [12,18], MRP1 [23,24] and MDR1 [25]. We therefore, quantified the relative contribution of these transporters in the ATP-dependent transport of DOX in PC-3 cells using an immunological approach. We have previously shown that anti-RLIP76 IgG inhibit DOX-transport in IOVs [20,26]. Likewise, antibodies against MRP and Pgp also inhibit transport-activity in IOVs [26–28]. We therefore, designed experiments in which IOVs prepared from PC-3 cells and separately coated with anti-RLIP76 IgG, anti-MRP1 IgG, or anti-MDR1 IgG were used to measure the ATP-dependent uptake of ¹⁴C-DOX. Optimal concentration of antibody to be used for specific inhibition of DOX-transport was determined in titration studies where varying concentration of each antibody was used to coat the membrane-vesicles. Anti-RLIP76 IgG, which recognized only RLIP76 in crude extracts of PC-3 cells, inhibited 61 ± 8% of total DOX-transport in IOVs prepared from PC-3 cells. Anti-MRP IgG also inhibited DOX-transport in a saturable manner, but maximal inhibition was less (28 ± 5%) as compared to that observed with anti-RLIP76 IgG. Anti-Pgp IgG had a small but detectable inhibitory effect on DOX-transport (5 ± 2%). These results also established that <40 µg/ml of each of the antibody quantitatively inhibited transport-activity of their respective antigen present in the amount of vesicles used in these experiments. In the vesicle coated with the mixture of the three antibodies almost complete abrogation (92 ± 6%) of DOX-transport was observed. In control vesicles coated with pre-immune IgG, the transport-activity remained unaffected. These results demonstrated that RLIP76, MRP, and Pgp together

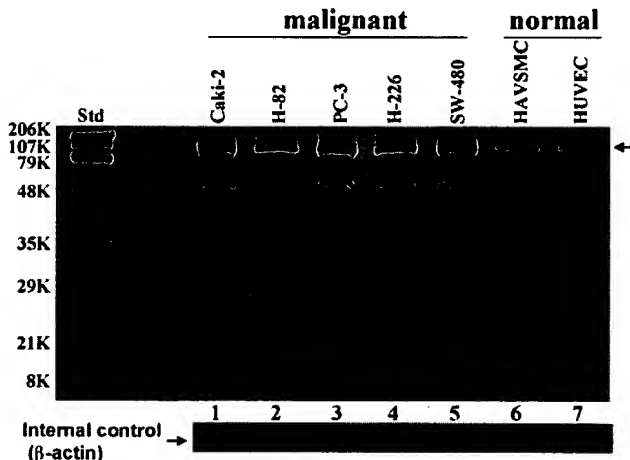


Fig. 1 – Comparison of RLIP76 levels in cultured malignant versus non-malignant cells Aliquots of crude membrane fractions of malignant cells (human kidney, Caki-2; small cell lung, H-82; prostate, PC-3; non-small cell lung, H-226 and colon, SW-480) and non-malignant cells (human aortic vascular-smooth-muscle cells, HAVSMC and human umbilical vascular-endothelial cells, HUVEC) containing 200 µg protein were used for SDS-PAGE and Western-blotting against anti-RLIP76-IgG as primary-antibody and horseradish peroxidase-conjugated goat-anti-rabbit-IgG as secondary-antibody and developed with 4-chloro-1-naphthol as chromogenic substrate. Intensity of the full-length RLIP76 protein (~95 kDa, denoted by arrow) band was quantified by scanning densitometry as shown by integrated density values (IDV), for lanes 1–7 values are 32,259, 25,588, 35,597, 27,810, 33,377, 11,569, and 11,124, respectively, using Innotech Alpha Imager HP. β-actin was used as an internal control.

constitute nearly all ATP-dependent transport-activity in these membranes. Furthermore, these results established that RLIP76 accounted for a major portion (about two-third) of the ATP-dependent transport of DOX in prostate cancer cells.

3.3. RLIP76 inhibition or depletion caused cytotoxicity in malignant cells

The cytotoxic effects of RLIP76 inhibition by anti-RLIP76 IgG or the depletion of RLIP76 by either siRNA or antisense phosphorothioate were assessed by an established MTT-cytotoxicity method [13,18,19]. Cells were treated with pre-immune IgG, scrambled siRNA, scrambled antisense, anti-RLIP76 IgG, RLIP76 siRNA or RLIP76 antisense for 24 h. The preferential toxicity of all three targeting agents was preferentially directed to the malignant cells as compared with non-malignant cells, an observation we have seen with other malignant (lung, ovary, melanoma, breast) as compared with non-malignant cell lines [13,19]. In contrast with the results seen with lung or colon cancer previously (in which all three modalities gave similar results), antisense was significantly more effective in killing prostate cancer cells than the antibody (Fig. 2); this difference could be related to factors in prostate cancers that reduce the effectiveness of the antibody, or perhaps due a relatively greater role of some intracellular function of RLIP76 in prostate cancers.

3.4. Apoptosis caused by inhibition or depletion of RLIP76

The mechanism of cytotoxicity was assessed by determining apoptosis through an immuno-histochemical TUNEL assay.

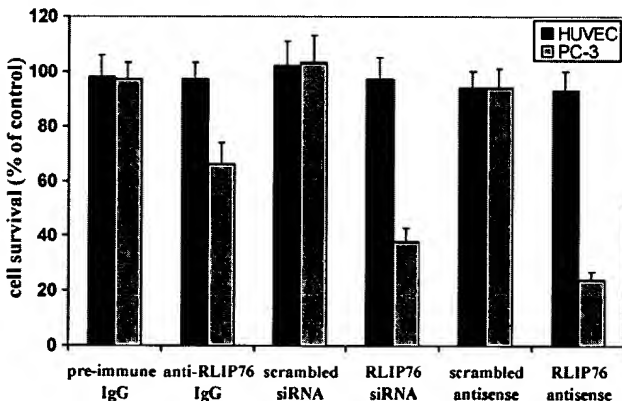


Fig. 2 – Selective toxicity of anti-RLIP76 IgG, RLIP76 siRNA and RLIP76 antisense toward PC-3 prostate cancer cells
Effect of anti-RLIP76 IgG (40 µg/ml final concentration) on cell survival was determined by MTT assay. Depletion of RLIP76 expression by RLIP76 siRNA (20 µg/ml final conc.) and RLIP76 antisense (10 µg/ml final conc.) was done, using Transmessenger Transfection-Reagent-kit (Qiagen), and Maxfect Transfection-Reagent (Molecular, Inc.), according to the manufacturer's instructions, respectively.
Cell survival was measured by MTT cytotoxicity-assay 48 h after treatment [18]. The values are presented as mean ± SD from two separate determinations with eight-replicates each (n = 16). black bars, HUVEC (normal) cells; gray bars, PC-3 prostate cancer cells.

The results of the TUNEL assay showed no detectable apoptosis in the PC-3 cells treated with pre-immune IgG, scrambled siRNA or scrambled antisense. Apoptosis was however, seen in cells treated with anti-RLIP76 IgG, RLIP76 siRNA or RLIP76 antisense (Fig. 3A).

3.5. RLIP76 depletion caused regression of prostate cancer xenografts in nude mice

The ultimate pre-clinical test for the potential utility of an anti-neoplastic agent is effectiveness in an animal model. The above observations of the anti-neoplastic effects of RLIP76 depletion were examined in a xenografts model of prostate cancer. Tumor-bearing animals with established s.c. implanted tumors (~42 mm³) were treated with 200 µg of either RLIP76 antibody, RLIP76 siRNA or RLIP76 antisense therapy by i.p. injection. Treated animals had rapid and dramatic reductions in tumors, whereas uncontrolled growth was observed in the control groups. The remarkable contrast in the outcome of tumors in animals treated with RLIP76 antibody, RLIP76 siRNA or RLIP76 antisense versus pre-immune serum, scrambled siRNA or antisense was clearly evident for prostate cancer cell lines (Fig. 3B) (for animal pictures, see supplementary data). The RLIP76 antibody, RLIP76 siRNA or RLIP76 antisense treated animals with prostate cancer are still alive at 261 days without evidence of recurrence. In comparison, all control animals were censored by day 41. Weight gain was comparable to non-tumor-bearing controls, and no overt-toxicity was evident. Present studies demonstrate nearly complete and sustained regression of xenografts of PC-3 prostate cancer by targeted depletion of the mercapturic acid pathway transporter protein, RLIP76.

The marked effectiveness of this targeted therapy compares quite favorably with other promising targeted agents in prostate cancer. ZD6126, a vascular targeting agent, caused reduction in the growth of xenografts in nude mice when administered by i.v. (100 mg/kg) daily for 5 days, resulted in ~18% body weight loss; the combination of cisplatin and ZD6126 resulted in greater than additive in growth delay, but regression was not observed [29]. Vitamin D3 analog (1,25-dihydroxyvitamin D3), anti-PSMA (prostate specific membrane antigen) and anti-interleukin-6 (IL-6) monoclonal antibodies were found effective in xenografts of LNCaP prostate cancer carcinoma, but growth inhibition occurred rather than regression [30–32]. PTEN (phosphatase and tensin homolog), a protein known to inhibit Bcl-2 expression, caused reduction in the rate of growth of PC-3 xenografts; the combination of PTEN with radiation therapy (5 Gy) was more effective in slowing growth, but regression was not observed [33]. CKBM is a combination of herbs and yeasts, a drug product targeting prostate cancer, did cause delayed and incomplete regression by 28 days in xenografts of PC-3 prostate cell carcinoma, when treatment was started before established visible tumor was present [34]. Polyamine analogues containing cyclopropane rings caused reduction in the rate of growth of DU-145 prostate cancer xenografts, but regression was not observed [35]. Combination of doxorubicin (4 mg/kg, i.p.) and Apo2L/TRAIL (0.5 mg/kg, i.p.) did cause regression of very small tumors, but if treatment was started at the time of established PC-3 prostate tumors at least 6 mm in each dimension (as in our case), only relatively little growth inhibition was seen [36]. The

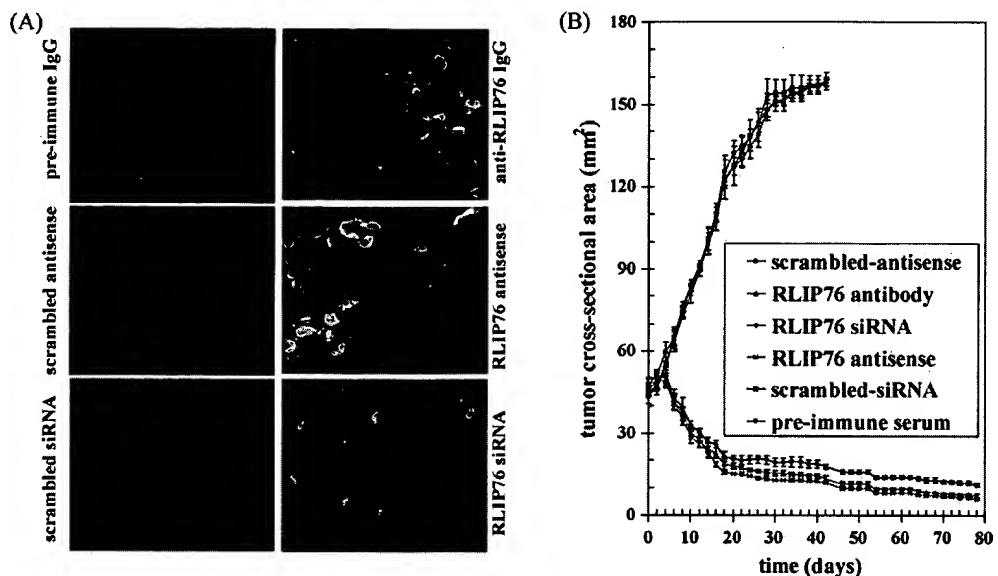


Fig. 3 – Effect of RLIP76 antibody, siRNA or antisense on apoptosis and on the regression of established PC-3 prostate cancer xenografts Effect of anti-RLIP76 IgG, RLIP76 siRNA and RLIP76 antisense on apoptosis was performed by TUNEL assay. Human prostate cancer cells were grown on cover-slips. For anti-RLIP76 IgG treatment, cells were incubated with RLIP76 antibody for 24 h; for siRNA treatment, cells were transfected with Transmessenger Transfection Reagent (Qiagen); for antisense treatment, cells were transfected with Maxfect Transfection Reagent (Molecula, Inc.), prior to TUNEL assay, using Promega fluorescence detection kit and examined using Zeiss LSM 510 META (Germany) laser scanning fluorescence microscope with filters 520 nm and >620 nm. Photographs taken at identical exposure at 400× magnification are presented. Apoptotic cells showed green fluorescence (panel A). For xenografts studies, we used twenty-four 12-week-old Hsd: Athymic nude nu/nu mice (Harlan, Indianapolis, IN) randomized 4 animals each into six groups as follow: (1) pre-immune serum, (2) scrambled siRNA, (3) scrambled anti-sense DNA, (4) RLIP76 antibodies, (5) RLIP76 siRNA and (6) RLIP76 antisense. All 24 animals were injected with 2×10^6 human prostate cancer cells (PC-3) suspensions in 100 μ l of PBS, subcutaneously into one flank of each nu/nu nude mouse. Animals were examined daily for signs of tumor growth. When tumors reached a cross-sectional area of $\sim 42 \text{ mm}^2$ (27 days later), animals were randomized treatment groups as indicated in the figure (for animal pictures, see supplementary data). Treatment consisted of 200 μ g of RLIP76 antibodies, siRNA or antisense in 100 μ l PBS. Control groups were treated with 200 μ g/100 μ l pre-immune serum, scrambled siRNA or scrambled anti-sense DNA. Tumors were measured in two dimensions using calipers. Tumor measurements are presented with all control groups (pre-immune IgG, scrambled siRNA or antisense) versus all treated groups (anti-RLIP76 IgG, RLIP76 siRNA, or anti-sense) (panel B).

therapeutic and toxicological effect of cesium chloride ($\sim 1000 \text{ mg/kg}$ by oral gavage for 30 consecutive days) administration has recently been shown to nearly completely inhibit the growth of established PC-3 cell lines in xenografts, but also did not cause regression. Cesium chloride had no effect on LNCaP tumors [37]. Incomplete regression was seen by day 32 in xenografts of PC-3 cell carcinoma treated with 2-methoxyestradiol (2ME2, 75 mg/kg, p.o.) and 2 Gy radiation delivered each day for 5 days inhibits microtubule polymerization and angiogenesis, and celecoxib, COX-2 inhibitor [38,39]. Thus, targeted therapeutics for prostate cancer aimed at Bcl-2, 2ME2, COX-2, CKBM, IL-6, Apo2L/TRAIL, or PTEN do not appear as effective as RLIP76 inhibition or depletion in comparable animal xenografts models.

3.6. Radiation-sensitivity

We have shown that RLIP76 knockout mice are extremely sensitive to irradiation [10,40], and in recent studies, we have also demonstrated that the overall effect of RLIP76-depletion is

almost an order of magnitude greater than the effects exerted by important signaling proteins including Akt, JNK and MEK [10]. Based on these previous studies in knockout-animals and other histologies of cancer cells, we reasoned that RLIP76 modulation would directly affect radiation-sensitivity and resistance of prostate cancer cells. To test this postulate, we determined X-irradiation sensitivity of the human prostate cancer cells in dose-response studies utilizing 100–1000 cGy single dose X-irradiation, followed by colony-forming assays. Cells pretreated with RLIP76-liposomes were least sensitive to radiation. Delivery of RLIP76 to cells via a liposomal-delivery system completely reversed radiation-sensitivity. At each radiation-dose, survival was significantly more when the cells were pretreated with RLIP76-liposomes before radiation exposure (Fig. 4). The physiological significance of RLIP76-mediated transport of endogenously generated GS-E (e.g., conjugate of 4HNE) is further indicated by results of our studies showing that RLIP76-enriched cells are resistant to radiation-toxicity. In these studies, prostate cancer cells were loaded with RLIP76 by incubating with RLIP76-liposomes. As

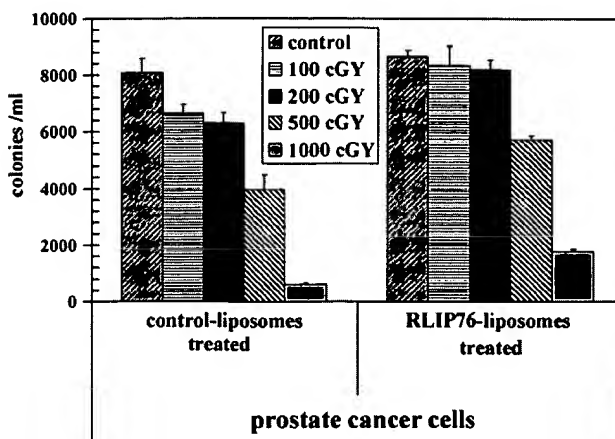


Fig. 4 – Radiation-protection by RLIP76 liposomal delivery
 2.5×10^3 human prostate cancer cells grown in Ham's F12 medium, were treated with control and RLIP76-liposomes (50 μ g/ml final conc.) for 24 h prior to radiation at 100, 200, 500 and 1000 cGy (6 MeV photons, 1.25 min) at the Texas Cancer Center, Arlington, TX. After 7 days, cells were stained with methylene-blue and the colonies were counted using Alpha Imager HP [21]. The results presented are the mean and s.d. from three separate experiments.

shown in Fig. 4, cells enriched with RLIP76 were resistant to radiation as compared to controls. These results suggest that the electrophilic-products of lipid-peroxide caused by reactive-oxygen species (ROS) generated during radiation may account for the cell killing by radiation and that RLIP76-mediated transport of GSH-conjugates of these electrophiles provides protection from radiation. These findings confirmed prior findings that RLIP76-liposomes are excellent radio-protective agents [10,40].

Cancer therapy target proteins must be expressed differentially in cancer as compared with normal cells, and the necessity for the presence of the target protein must differ between cancers vs. normal cells. Ideally, the target should be understood in context of existing biochemical and physiological frameworks and pathways known to play a direct role in carcinogenesis or in thwarting cancer therapy. In the present studies, we demonstrate that RLIP76 is a very promising target for therapy of prostate and other cancers, but important additional mechanistic and pre-clinical data is necessary to understand the role of RLIP76 in regulating key signaling pathways known to be important in carcinogenesis, drug-resistance, and the mechanisms of intrinsic drug-resistance in cancer. Other investigators have shown that binding of cdc2 to RLIP76 is essential to shut off endocytosis during mitosis, and yet others that over-expression of POB1 (partner of RLIP76) triggers apoptosis in prostate cancer cells [41,42]. Results of our present studies are in strong support of our hypothesis that prostate cancer cell depend on the function of RLIP76 for survival. The RLIP76 antibody, siRNA or antisense, is a novel and promising therapeutic agent for the treatment of human prostate cancers. Further studies are required to elucidate its mechanism of action.

4. Conclusions

The results of the present study clearly demonstrate that RLIP76 protein and activity is greater in cancer cells as compared with normal cells and that apoptosis triggered by RLIP76 depletion will be manifested preferentially in cancer as compared with normal cells. Studies demonstrating the marked enhancement of vinorelbine efficacy in lung cancer xenografts by concomitant depletion of RLIP76 have confirmed the *in vivo* relevance of these observations [13]. Present studies have shown that human cancers (lung, colon, kidney and prostate) express higher levels of RLIP76 than non-cancerous cell, and that depletion or inhibition of RLIP76 in these cancer cell types caused marked apoptosis, whereas non-cancerous cells were spared. Because human prostate cancers have a relatively high expression of RLIP76, we reasoned that it may be functioning as a defense mechanism in prostate cancer cells as well. RLIP76 plays a central role in radiation and chemotherapy-resistance through its activity as a multi-specific ATP-dependent transporter. In conclusion, present studies demonstrate that depletion of RLIP76 exerts anti-neoplastic effects in prostate cancer. This study should help lay the foundation for clinical studies. These outstanding findings will have obvious translational implications for the treatment of prostate cancer and potentially other malignancies.

Acknowledgements

This work was supported in part by National Institutes of Health Grants CA 77495 and CA 104661, Cancer Research Foundation of North Texas, Institute for Cancer Research and the Joe & Jessie Crump Fund for Medical Education.

Appendix A. Supplementary data

Supplementary data associated with this article can be found, in the online version, at doi:10.1016/j.bcp.2008.11.013.

REFERENCES

- [1] Sirotnak FM, Wendel HG, Bornmann WG, Tong WP, Miller VA, Scher HI, et al. Co-administration of probenecid, an inhibitor of a CMOAT/MRP-like plasma membrane ATPase, greatly enhanced the efficacy of a new 10-deazaaminopterin against human solid tumors *in vivo*. *Clin Cancer Res* 2000;6:3705-12.
- [2] Zhang Y, Bressler JP, Neal J, Lal B, Bhang HE, Laterra J, et al. ABCG2/BCRP expression modulates D-Luciferin based bioluminescence imaging. *Cancer Res* 2007;67:9389-97.
- [3] Grant S. Cotargeting survival signaling pathways in cancer. *J Clin Invest* 2007;118:3003-6.
- [4] Shen MM, Abate-Shen C. Pten inactivation and the emergence of androgen-independent prostate cancer. *Cancer Res* 2007;67:6535-8.
- [5] Kinkade CW, Castillo-Martin M, Puzio-Kuter A, Yan J, Foster TH, Gao H, et al. Targeting AKT/mTOR and ERK MAPK signaling inhibits hormone-refractory prostate cancer in a preclinical mouse model. *J Clin Invest* 2008;118:3051-64.

[6] Pusztai L, Wagner P, Ibrahim N, Rivera E, Theriault R. Phase II study of tariquidar, a selective P-glycoprotein inhibitor, in patients with chemotherapy-resistant, advanced breast carcinoma. *Cancer* 2005;104:682-91.

[7] Modok S, Mellor HR, Callaghan R. Modulation of multidrug resistance efflux pump activity to overcome chemoresistance in cancer. *Curr Opin Pharmacol* 2006;6:350-4.

[8] Robey RW, Shukla S, Finley EM, Oldham RK, Barnett D, Ambudkar SV, et al. Inhibition of P-glycoprotein (ABCB1)- and multidrug resistance-associated protein 1 (ABCC1)-mediated transport by the orally administered inhibitor, CBT-1((R)). *Biochem Pharmacol* 2008;75:1302-12.

[9] Shukla S, Wu CP, Ambudkar SV. Development of inhibitors of ATP-binding cassette drug transporters: present status and challenges. *Expert Opin Drug Metab Toxicol* 2008;4: 205-23.

[10] Singhal J, Singhal SS, Yadav S, Warnke M, Yacoub A, Dent P, et al. RLIP76 in defense of radiation poisoning. *Int J Rad Oncol Biol Phys* 2008;72:553-61.

[11] Jullien-Flores V, Dorseuil O, Romero F, Letourneur F, Saragosti S, Berger R, et al. Bridging Ral-GTPase to Rho-pathways. RLIP76, a Ral-effector with CDC42/RacGTPase activating protein activity. *J Biol Chem* 1995;270:22473-7.

[12] Awasthi S, Cheng J, Singhal SS, Saini MK, Pandya U, Pikula S, et al. Novel function of human RLIP76: ATP-dependent transport of glutathione-conjugates and doxorubicin. *Biochemistry* 2000;39:9327-34.

[13] Singhal SS, Singhal J, Yadav S, Dwivedi S, Boor P, Awasthi YC, et al. Regression of lung and colon cancer xenografts by depleting or inhibiting RLIP76. *Cancer Res* 2007;67: 4382-9.

[14] Awasthi YC, Garg HS, Dao DD, Partridge CA, Srivastava SK. Enzymatic conjugation of erythrocyte glutathione with 1-chloro-2,4-dinitrobenzene: the fate of glutathione conjugate in erythrocytes and the effect of glutathione depletion on hemoglobin. *Blood* 1981;58:733-8.

[15] Singhal SS, Singhal J, Sharma R, Singh SV, Zimniak P, Awasthi YC, et al. Role of RLIP76 in lung cancer doxorubicin-resistance. I. The ATPase activity of RLIP76 correlates with doxorubicin and 4HNE-resistance in lung cancer cells. *Int J Oncol* 2003;22:365-75.

[16] Awasthi S, Singhal SS, Sharma R, Zimniak P, Awasthi YC. Transport of glutathione-conjugates and chemotherapeutic drugs by RLIP76: a novel link between G-protein and tyrosine-kinase signaling and drug-resistance. *Int J Cancer* 2003;106:635-46.

[17] Stuckler D, Singhal J, Singhal SS, Yadav S, Awasthi YC, Awasthi S. RLIP76 transports vinorelbine and mediates drug-resistance in non-small cell lung cancer. *Cancer Res* 2005;65:991-8.

[18] Singhal SS, Yadav S, Singhal J, Zajac E, Awasthi YC, Awasthi S. Depletion of RLIP76 sensitizes lung cancer cells to doxorubicin. *Biochem Pharmacol* 2005;70:481-8.

[19] Singhal SS, Awasthi YC, Awasthi S. Regression of melanoma in a murine model by RLIP76-depletion. *Cancer Res* 2006;66:2354-60.

[20] Awasthi S, Singhal SS, Srivastava SK, Zimniak P, Bajpai KK, Saxena M, et al. Adenosine-triphosphate-dependent transport of doxorubicin, daunomycin, and vinblastine in human tissues by a mechanism distinct from the P-glycoprotein. *J Clin Invest* 1994;93:958-65.

[21] Singhal SS, Yadav S, Drake K, Singhal J, Awasthi S. Hsf-1 and POB1 induce drug-sensitivity and apoptosis by inhibiting Ralbp1. *J Biol Chem* 2008;283:19714-29.

[22] Sharma R, Singhal SS, Wickramarachchi D, Awasthi YC, Awasthi S. RLIP76-mediated transport of leukotriene C₄ in cancer cells: implications in drug-resistance. *Int J Cancer* 2004;112:934-42.

[23] Cole SPC, Bhardwaj G, Gerlach JH, Mackie JE, Grant CE, Almquist KC, et al. Over-expression of a transporter gene in a multidrug-resistant human lung cancer cell line. *Science* 1992;258:1650-4.

[24] Lautier D, Canitrot Y, Deeley RG, Cole SPC. Multidrug-resistance mediated by the multidrug-resistance protein (MRP) gene. *Biochem Pharmacol* 1996;52: 967-77.

[25] Gottesman MM, Pastan I. Biochemistry of multidrug-resistance mediated by the multidrug-transporter. *Annu Rev Biochem* 1993;62:385-427.

[26] Awasthi S, Singhal SS, Singhal J, Cheng J, Zimniak P, Awasthi YC. Role of RLIP76 in lung cancer doxorubicin-resistance. II. Doxorubicin-transport in lung cancer by RLIP76. *Int J Oncol* 2003;22:713-20.

[27] Hipfner DR, Mao Q, Qiu W, Leslie EM, Gao M, Deeley RG, et al. Monoclonal-antibodies that inhibit the transport function of the 190-kDa multidrug-resistance protein, MRP. Localization of their epitopes to the nucleotide-binding-domains of the protein. *J Biol Chem* 1999;274: 15420-6.

[28] Kokubu N, Cohen D, Watanabe T. Functional modulation of ATPase of P-glycoprotein by C219, a monoclonal-antibody against P-glycoprotein. *Biochem Biophys Res Commun* 1997;230:398-401.

[29] Blakey DC, Westwood FR, Walker M, Hughes GD, Davis PD, Ashton SE, et al. Antitumor activity of the novel vascular targeting agent ZD6126 in a panel of tumor models. *Clin Cancer Res* 2002;8:1974-83.

[30] Vegenas V, O'Kelly J, Said J, Uskokovic M, Binderup L, Koeffle HP. Ability of potent vitamin D3 analogs to inhibit growth of prostate cancer cells in vivo. *Anticancer Res* 2003;23:283-9.

[31] Vallabhajosula S, Smith-Jones PM, Navarro V, Goldsmith SJ, Bander NH. Radio-immunotherapy of prostate cancer in human xenografts using monoclonal antibodies specific to prostate specific membrane antigen (PSMA): studies in nude mice. *Prostate* 2004;58:145-55.

[32] Smith PC, Keller ET. Anti-interleukin-6 monoclonal antibody induces regression of human prostate cancer xenografts in nude mice. *Prostate* 2001;48:47-53.

[33] Anai S, Goodison S, Shiverick K, Iczkowski K, Tanaka M, Rosser CJ. Combination of PTEN gene therapy and radiation inhibits the growth of human prostate cancer xenografts. *Hum Gene Ther* 2006;17:975-84.

[34] Liu ES, Luk SC, Leung ET, Lee WH, Yuen WF, Kwok KM, et al. Effect of CKBM on prostate cancer cell growth in vitro and in vivo. *J Chemother* 2008;20:246-52.

[35] Frydman B, Blokhin AV, Brummel S, Wilding G, Maxuitenko Y, Sarkar A, et al. Cyclopropane-containing polyamine analogues are efficient growth inhibitors of a human prostate tumor xenograft in nude mice. *J Med Chem* 2003;46:4586-600.

[36] El-Zawahry A, McKillop J, Voelkel-Johnson C. Doxorubicin increases the effectiveness of Apo2L/TRAIL for tumor growth inhibition of prostate cancer xenografts. *BMC Cancer* 2005;5:2.

[37] Low JC, Wasan KM, Fazli L, Eberding A, Adomat H, Guns ES. Assessing the therapeutic and toxicological effects of cesium chloride following administration to nude mice bearing PC-3 or LNCaP prostate cancer xenografts. *Cancer Chemother Pharmacol* 2007;60:821-9.

[38] Casarez EV, Dunlap-Brown ME, Conaway MR, Amorino GP. Radio-sensitization and modulation of p44/42 mitogen-activated protein kinase by 2-Methoxyestradiol in prostate cancer models. *Cancer Res* 2007;67: 8316-24.

[39] Patel MI, Subbaramaiah K, Du B, Chang M, Yang P, Newman RA, et al. Celecoxib inhibits prostate cancer growth:

evidence of a cyclooxygenase-2-independent mechanism. *Clin Cancer Res* 2005;11:1999–2007.

[40] Awasthi S, Singhal SS, Yadav S, Singhal J, Drake K, Nadkar A, et al. RLIP76 is a major determinant of radiation-sensitivity. *Cancer Res* 2005;65:6022–8.

[41] Oosterhoff JK, Penninkhof F, Brinkmann AO, Grootegoed JA, Blok LG. POB1 is down-regulated during human prostate cancer progression and inhibits growth factor signaling in prostate cancer cells. *Oncogene* 2003;22:2920–5.

[42] Rosse C, L'Hoste S, Offner N, Picard A, Camonis JH. RLIP, an effector of the Ral-GTPases, is a platform for Cdk1 to phosphorylate epsin during the switch off of endocytosis in mitosis. *J Biol Chem* 2003;278: 30597–604.

BIOLOGY CONTRIBUTION

SURVIVIN ANTISENSE OLIGONUCLEOTIDES EFFECTIVELY RADIOSENSITIZE COLORECTAL CANCER CELLS IN BOTH TISSUE CULTURE AND MURINE XENOGRAFT MODELS

FRANZ RÖDEL, PH.D.,* BENJAMIN FREY, PH.D.,† WERNER LEITMANN, M.S.,‡ GIANNI CAPALBO, PH.D.,* CHRISTIAN WEISS, M.D.,* AND CLAUS RÖDEL, M.D.*

*Department of Radiation Therapy and Oncology, University of Frankfurt/Main, Frankfurt, Germany; †Department of Radiation Oncology, University of Erlangen, Erlangen, Germany; and ‡Lilly Deutschland GmbH, Bad Homburg, Germany

Purpose: Survivin shows a radiation resistance factor in colorectal cancer. In the present study, we determined whether survivin messenger RNA levels in patients with rectal cancer predict tumor response after neoadjuvant radiochemotherapy and whether inhibition of survivin by the use of antisense oligonucleotides (ASOs) enhances radiation responses.

Methods and Materials: SW480 colorectal carcinoma cells were transfected with survivin ASO (LY2181308) and irradiated with doses ranging from 0–8 Gy. Survivin expression, cell-cycle distribution, γ H2AX fluorescence, and induction of apoptosis were monitored by means of immunoblotting, flow cytometry, and caspase 3/7 activity. Clonogenic survival was determined by using a colony-forming assay. An SW480 xenograft model was used to investigate the effect of survivin attenuation and irradiation on tumor growth. Furthermore, survivin messenger RNA levels were studied in patient biopsy specimens by using Affymetrix microarray analysis.

Results: In the translational study of 20 patients with rectal cancer, increased survivin levels were associated with significantly greater risk of local tumor recurrence ($p = 0.009$). Treatment of SW480 cells with survivin ASOs and irradiation resulted in an increased percentage of apoptotic cells, caspase 3/7 activity, fraction of cells in the G₂/M phase, and H2AX phosphorylation. Clonogenic survival decreased compared with control-treated cells. Furthermore, treatment of SW480 xenografts with survivin ASOs and irradiation resulted in a significant delay in tumor growth.

Conclusion: Survivin appears to be a molecular biomarker in patients with rectal cancer. Furthermore, *in vitro* and *in vivo* data suggest a potential role of survivin as a molecular target to improve treatment response to radiotherapy in patients with rectal cancer. © 2008 Elsevier Inc.

Survivin, Apoptosis, Radiosensitization, Rectal cancer, Animal model.

INTRODUCTION

The success of radiation therapy is dependent on its ability to control tumor proliferation and induce cell death by causing irreparable cellular damage that finally triggers apoptosis (1–3). For patients with rectal cancer treated by using neoadjuvant radiochemotherapy, we and others previously showed that a high level of apoptotic tumor cells in pretreatment biopsy specimens emerged as a significant predictor for tumor response and long-term local control (4, 5). Close correlation between spontaneous and radiation-induced apoptosis and radiosensitivity also was confirmed in a panel of colorectal cancer cell lines *in vitro* (6).

Although it is clear that apoptosis propensity is regulated by a variety of intrinsic factors, including p53 and members

of the bcl-2 family (3, 7, 8), a prominent role of survivin, the smallest and structurally unique member of the inhibitor of apoptosis (IAP) family (9), recently was shown for colorectal cancer tumorigenesis and prognosis (10–12). Survivin, originally identified in the late 1990s, shows regulatory functions for both control of cell division and inhibition of apoptosis (9, 13). Compared with most noncancerous tissues, survivin is overexpressed in human tumors and appears to be highly related to resistance of tumor cells to anticancer treatment (14–16). In a retrospective analysis of patients with rectal cancer, we previously showed that immunohistochemically determined expression of survivin protein inversely correlated with pretreatment apoptosis and was associated with an unfavorable local control rate after preoperative 5-fluorouracil-based radiochemotherapy

Reprint requests to: Franz Rödel, Ph.D., Department of Radiation Therapy and Oncology, University of Frankfurt, Theodor-Stern-Kai 7, 60590 Frankfurt, Germany. Tel: (+49) 69-6301-6637; Fax: (+49) 69-6301-5091; E-mail: franz.roedel@kgu.de

This work was supported in part by a noneducational grant from Eli Lilly Company Germany and the German Research Foundation

(DFG RO 3482/1-1).

Conflict of interest: none.

Acknowledgments—The authors thank R. Sieber and B. Müller for excellent technical assistance.

Received Nov 15, 2007, and in revised form Feb 7, 2008.
Accepted for publication Feb 11, 2008.

(17). In the clinical part of the present study, we sought to confirm these findings on messenger RNA (mRNA) levels by prospectively collecting fresh-frozen pretreatment tumor tissues from 20 patients with rectal cancer treated with a neoadjuvant protocol of radiotherapy combined with capecitabine and oxaliplatin (18).

In recent years, several strategies were developed to interfere with survivin function or expression. These include ribozymes, small interfering RNAs, dominant-negative mutants, and cyclin-dependent kinase inhibitors (15, 19). The first survivin inhibitors have now entered Phase I clinical trials. In the second part of this study, we therefore investigated the effects of combining irradiation with attenuation of survivin expression in colorectal cancer cells both *in vitro* and in mice, accomplished by using the Eli Lilly product LY2181308 (Eli Lilly and Company, Indianapolis, IN), an antisense oligonucleotide (ASO) against survivin mRNA.

METHODS AND MATERIALS

Patient characteristics and biopsy samples

Pretreatment tumor tissue samples were obtained from 20 consecutive patients with locally advanced rectal cancer (Union Internationale Contre le Cancer Stages II and III) treated with preoperative radiotherapy and combined capecitabine (Xeloda) and oxaliplatin (Elotaxin) within a prospective Phase I/II protocol (XELOX-RT). Details of this study were previously published (18). Median follow-up for the 20 patients at the time of analysis was 49 months (range, 7–69 months). Biopsy specimens of macroscopically normal mucosa were also obtained at a distance of 2 cm surrounding the tumor location. Tissue specimens were flash-frozen in liquid nitrogen and stored until extraction of mRNA after removal of portions needed for pathologic diagnosis to ensure that tumor specimens contained greater than 60% tumor cells.

Microarray expression analysis

Ten micrograms of total RNA were used to prepare biotinylated complementary RNAs. Hybridization of 15 μ g of labeled complementary RNA was performed on HG-U133A Affymetrix microarrays (Affymetrix, Santa Clara, CA) as described (20). All arrays were globally scaled to a target value of 1,000, and intracellular survivin mRNA values (Affymetrix average difference units) were derived by using Microarray Suite 5.0 software.

Immunohistochemical staining for survivin on tumor biopsies

Before labeling, paraffin-embedded tumor samples were deparaffinized and heated in 10 mM of citrate buffer (pH 6.0) for 20 minutes in a pressure cooker. Next, slides were blocked in 5% nonfat dry milk in phosphate-buffered saline (PBS), and primary antisurvivin antibodies (R&D Systems, Wiesbaden, Germany) were applied at a 1:50 dilution and incubated at 4°C overnight, followed by a biotinylated anti-rabbit secondary antibody (Dianova, Hamburg, Germany; dilution, 1:50; 1 hour at room temperature) and streptavidin/biotinylated alkaline phosphatase for 30 minutes. Finally 3-amino-9-ethyl-carbazole (AEC) solution was used as chromogen, and hematoxylin (37%), for counterstaining. Mean percentage of positive tumor cells and intensity of survivin staining were quantitated by using an Image-System (Optimas 6.2; Stemmer PC Systeme, Puchheim, Germany) and assigned to one of the following cate-

gories: 0 (<5%), 1 (5–25%), 2 (25–50%), 3 (50–75%), and 4 (>75%) and 1⁺ (weak), 2⁺ (moderate), and 3⁺ (intense), resulting in a weighted score ranging from 0–12 (17).

Cell culture

The human colorectal adenocarcinoma cell line SW480 was obtained from the American Type Culture Collection (LGC-Promochem, Wiesbaden, Germany) and maintained in Dulbecco's modified Eagle's medium (DMEM; Biochrom, Berlin, Germany) supplemented with 10% heat-inactivated fetal calf serum (FCS), 1% sodium pyruvate, 2 mM of glutamine, 100 U/mL of penicillin, and 100 μ g/mL of streptomycin (all supplements from Biochrom) at 37°C in 5% carbon dioxide and 95% humidity.

In vitro transfection of ASOs and irradiation

SW480 cells (5×10^5) were seeded in 25-cm² flasks 24 hours before transfection, resulting in a confluence of the cell monolayer of 50–60%. For cell culture experiments, 12 μ L of Lipofectin reagent was incubated in 1,000 μ L of OptiMEM reduced serum medium (Invitrogen, Karlsruhe, Germany) for 30 minutes, and survivin-specific synthetic, single-stranded DNA-ASO (LY 2181308), or a scrambled control ASO (LY 2293329; each 400 nM) was added to the mixture for 15 minutes. Next, cells were incubated for 24 hours at 37°C, and DMEM, supplemented with 20% heat-inactivated fetal calf serum, was added. Cells were irradiated an additional 24 hours later at room temperature by using X-ray orthovoltage-irradiation (Stabilipan; Siemens, Munich, Germany) at 250 kV/15 mA/40 cm focus–surface distance at a dose rate of 1.15 Gy/min with single doses of 0, 1, 2, 4, 6, and 8 Gy.

Western immunoblotting

For immunoblotting, SW480 cells were lysed in RIPA buffer (50 mM of Tris, pH 7.4, 150 mM of sodium chloride, 1% Triton X-100, 1% deoxycholate) supplemented with protease inhibitors (1 mM of phenylmethyl-sulfonylfluoride, 10 μ g/mL of pepstatin, 10 μ g/mL of aprotinin, and 5 μ g/mL of leupeptin; all Sigma, Deisenhofen, Germany). Protein concentrations were determined by using a BCA-protein assay (Pierce, Rockford, IL); equal amounts of protein (10 μ g) were separated on a 12.5% sodium dodecyl sulfate-polyacrylamide gel and transferred to a nitrocellulose membrane (Hybond C; Amersham, Freiburg, Germany). Membranes were blocked in 5% nonfat dry milk in PBS for 30 minutes at room temperature and probed with rabbit antisurvivin antibodies (dilution, 1:1000; R&D Systems, Wiesbaden, Germany) overnight at 4°C. Next, membranes were incubated with horseradish-peroxidase-linked secondary antibodies (1:200; Dako, Hamburg, Germany) and developed by using an enhanced chemiluminescence detection system (Amersham) and autoradiography (BiomaxR Film; Kodak, Rochester, NY). To confirm equal protein loading, membranes were probed in parallel with a 1:2,000 dilution of an anti- β -tubulin antibody (Biozol, Eching, Germany).

Quantification of apoptosis, caspase 3/7 assay

For quantification of apoptotic tumor cells, fluorescein isothiocyanate (FITC)-labeled recombinant chicken AnnexinV (Responsif GmbH, Erlangen, Germany) was used in combination with propidium iodide (PI) to discriminate necrotic cells. In brief, 10⁵ cells were resuspended in 500 μ L of Ringer's solution, incubated for 30 minutes at 4°C in the dark with 1 μ g of AxV-FITC/1 μ g of PI, subsequently analyzed by using a Coulter EPICS-XL-flow cytometer (Coulter, Hialeah, FL) and SystemXL-II software (Coulter). Caspase 3/7 activity was analyzed in a 96-well microplate format using the Apo-ONE assay (Promega, Mannheim, Germany) according to

the manufacturer's recommendations. SW480 cells ($1-3 \times 10^5$) were incubated for 90 minutes in a luciferase substrate mix, and luminescence activity was measured in a luminometer (Berthold, Bad Wildbad, Germany).

Cell-cycle analysis

Both adherent and detached SW480 cells (1×10^6 /ml) were collected by means of trypsinization and washed with PBS for 10 minutes by centrifugation at $120 \times g$. Cells were resuspended in a hypertonic solution containing 1 μ g/mL of PI, 4 mmol/L of sodium citrate, 1 mg/mL of RNaseA (Boehringer, Mannheim, Germany), and 0.1% Triton X-100. Fluorescence activated cell sorter (FACS) analysis was performed using a Coulter EPICS-XL-flow cytometer (Coulter) and SystemXL-II software.

Flow cytometry for phospho-histone γ H2AX

For analysis of serine-139 phosphorylated histone H2AX, cells were irradiated with 2 Gy, detached by using Accutase treatment for 15 minutes (PAA, Pasching, Austria), pelleted by centrifugation (5 minutes at $120 \times g$), and fixed in 70% ethanol for 2 hours at -20°C . Before antibody labeling, samples were rehydrated with 0.05 M of Tris-buffer (pH 7.4), centrifuged, and incubated in Tris buffer and 0.1% Triton X-100 for 10 minutes on ice. Next, cells were incubated with either an FITC-conjugated anti- γ H2AX antibody at a 1:250 dilution or an isotype control antibody (both Up-state, Lake Placid, NY). Cells were fixed in 1% paraformaldehyde in PBS and analyzed using a Coulter EPICS-flow cytometer XL. Mean fluorescence of the isotype control was subtracted to eliminate unspecific background staining for every sample.

3-(4,5-Methylthiazol-2-yl)-2,5-diphenyl-tetrazolium bromide assay

Cells transfected 24 hours before with either survivin ASO or scrambled ASO were seeded at a density of $2-10 \times 10^3$ cells/200 μL in a 96-well microplate, grown for 6 hours, and subsequently exposed to 8 Gy of irradiation. After 24, 48, and 72 hours of incubation at 37°C , 3-(4,5-methylthiazol-2-yl)-2,5-diphenyl-tetrazolium bromide (MTT; 20 μL /well of a 5-mg/mL solution in PBS) was added for 4 hours. Solubilization of the converted purple formazan dye was accomplished by adding 50 μL /well of 0.01 N hydrogen chloride/20% sodium dodecyl sulfate, incubating overnight at 37°C , and quantitated by measuring the absorbance at 570 nm using an enzyme-linked immunosorbent assay reader (HTS 7000; Perkin Elmer, Rodgau, Germany) and Software HTS-Soft (Perkin Elmer).

Clonogenic survival assay

After transfection with either survivin ASO or scrambled ASO, SW480 cells were plated in complete DMEM medium into culture dishes and irradiated as previously described (7). After 10–14 days, colonies were stained with methylene-blue solution for 30 minutes and counted using an Automatic Colony Analyzing Machine (ACAM, Erlangen, Germany). Calculation of survival fractions (SFs) was performed using the equation: SF = colonies counted/cells seeded \times (plating efficiency/100), taking into consideration the individual plating efficiency.

In vivo ASO treatment and X-irradiation

Female athymic Naval Medical Research Institute (NMRI) nude mice (8–10 weeks old; Charles River, Sulzfeld, Germany) were kept in laminar flow rooms with a constant temperature of $22^{\circ}\text{C} \pm 0.5^{\circ}\text{C}$, 55% humidity, and a 12-hour light/dark cycle in accordance with the requirements of the German Animal Welfare Act. For measurement

of the *in vivo* radiosensitizing effect of survivin-specific synthetic single-stranded DNA-ASO, animals received a subcutaneous injection of exponentially growing SW480 cells (4×10^6 /mice) into the right flank regions. After 7–9 days, when average tumor volume reached approximately $0.05-0.1 \text{ cm}^3$ (or 50–100 mg), mice were stratified into five groups of 5–10 animals each. Group 1 indicates no treatment; Group 2, irradiation with 3×3 Gy; Group 3, LY2181308-ASO monotherapy; Group 4, LSN2293329 mismatch control; and Group 5, combined treatment with X-irradiation and LY2181308-ASO. The ASOs were dissolved in PBS and injected intraperitoneally into mice starting with 50 mg/kg body weight (BW) 1 day before irradiation and 25 mg/kg BW at Days 3 and 4 at 2–4 hours before radiation therapy, followed by a single administration of 25 mg/kg BW on Days 7 and 9 of treatment. Irradiation of tumors was performed under inhalation anesthesia with isoflurane using a linear accelerator (Primart; Siemens) at a dose rate of 0.8 Gy/min on Days 2, 3, and 4 of treatment. Measurement of tumor volumes was started at Day 8 after inoculation of cells and tumor volume was calculated according to the formula: volume (mm^3) = length/width²/2. Percentage of tumor growth inhibition was calculated as follows: Inhibitory rate (%) = (V_{control} – V_{treat})/V_{control} \times 100, where V represents tumor volume.

Statistical evaluation

Local failure rates were calculated by using the Kaplan-Meier method, and differences were analyzed by means of log-rank test. Experimental *in vitro* data are presented as mean \pm SD from three or more independent experiments. Levels of significance were calculated using Student's *t*-test (Excel program; Microsoft, Unterschleißheim, Germany). The level of significance was 0.05 (two sided) in all statistical testing.

RESULTS

Survivin mRNA levels as a predictor for treatment response to preoperative radiochemotherapy

Intracellular survivin mRNA levels in 20 tumor biopsy specimens and the corresponding noncancerous mucosa of patients with rectal cancer treated within a prospective protocol of preoperative XELOX-RT were determined by using Affymetrix HGU133 microarrays. A significantly increased median intracellular mRNA level was observed in tumor biopsy specimens compared with normal mucosa: 2012.8 ± 943.5 vs. 474.2 ± 295.2 Affymetrix average difference units ($p < 0.001$). Levels of intracellular survivin mRNA significantly correlated (KK = 0.763; $p = 0.01$) with levels of immunohistochemically detected protein expression in the same biopsy specimen (Fig. 1a). As shown in Fig. 1b, high survivin mRNA levels (greater than median = 1,845.50 Affymetrix average difference units) were significantly related to increased risk of local relapse compared with tumors showing low intracellular survivin levels ($p = 0.009$).

Inhibition of survivin by LY2181308 ASO in SW480 cells results in increased apoptosis and caspase 3/7 activity, decreased cell proliferation, altered cell-cycle distribution, and increased phospho-histone γ H2AX

Survivin-specific synthetic single-stranded DNA-ASO (LY 2181308) was used to knock down its expression in SW480 colorectal cell lines previously described to harbor

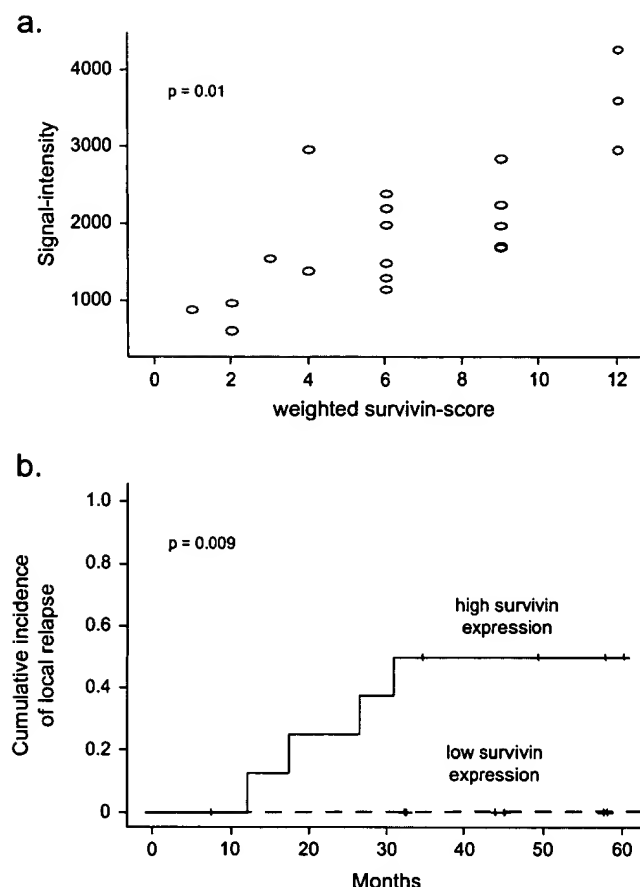


Fig. 1. Survivin messenger RNA (mRNA) level as a predictive marker of local control after neoadjuvant radiochemotherapy in patients with rectal cancer. (a) Intracellular mRNA levels in 20 patients with locally advanced rectal cancer significantly correlated with immunohistochemically determined protein level (labeling score) in the corresponding tumor biopsy specimens ($p = 0.01$). (b) Cumulative incidence plot of local relapses in 20 patients treated uniformly with a preoperative combination of radiotherapy and chemotherapy (XELOX-RT) according to a high (greater than median) or low (less than median) survivin mRNA level, determined in pretreatment biopsy specimens by using Affymetrix HGU133 microarray.

high amounts of the protein (6). Western blot analysis of total cellular extracts 48 hours after transfection of ASO showed an 80% decrease in survivin protein expression compared with mock or mismatch ASO control (LY 2293329) transfected cells (Fig. 2a).

To analyze whether survivin attenuation functionally affects the level of apoptosis, SW480 cells were irradiated with 8 Gy 48 hours after transfection with LY2181308-ASO and analyzed by using either AnnexinV-PI-staining or caspase 3/7 activity. As shown in Fig. 2b, the fraction of spontaneous and radiation-induced apoptotic cells was significantly greater ($p < 0.02$) in survivin ASO-treated SW480 cells at 24 and 48 hours after irradiation compared with nontreated or mismatch ASO-treated controls. Moreover, survivin ASO treatment resulted in a significant ($p = 0.01$) increase in caspase 3/7 activity in nonirradiated cells and more pronounced in irradiated SW480 cells (Fig. 2c). In parallel, metabolic activity and cell viability significantly ($p <$

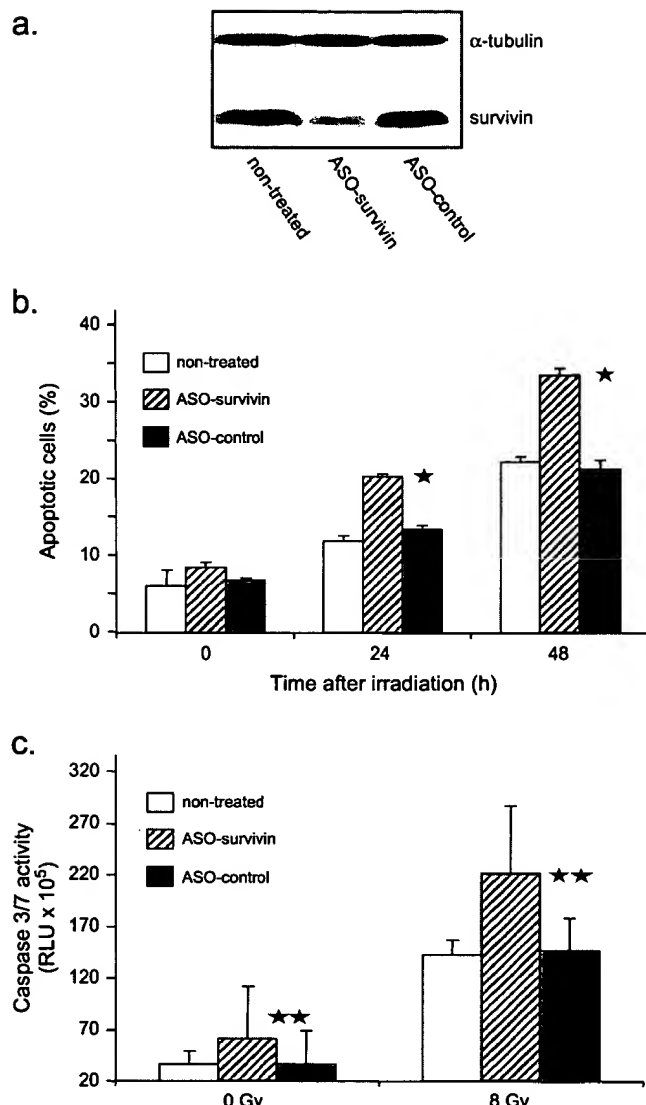


Fig. 2. Survivin antisense oligonucleotide (ASO) treatment attenuates survivin protein expression in SW480 colorectal cells and affects spontaneous and radiation-induced apoptosis and caspase 3/7 activity. (a) Western immunoblots from total cellular proteins extracted 48 hours after transfection with survivin-specific synthetic single-stranded DNA-ASO (LY2181308) using antibodies against survivin (1:750 dilution) and α -tubulin (1:1,000 dilution). (b) Apoptotic cells were determined by using AnnexinV FACS analysis in nontreated SW480 cells, as well as 24 and 48 hours after irradiation with 8 Gy. * $p < 0.01$ vs. mock-treated cells. (c) Caspase activity was quantitated by using a luciferase-based Apo-Glo assay (Promega, Mannheim, Germany) 48 hours after irradiation with 8 Gy. ** $p < 0.03$ vs. nontreated cells. Data expressed as mean \pm SD from three independent experiments.

0.01) decreased in nonirradiated survivin ASO-transfected cells, as well as 24 and 48 hours after irradiation (MTT assay; Fig. 3a). Cell-cycle analyses performed at 48 hours after ASO transfection showed a further increase in G₂/M fraction in LY2181308-treated SW480 cells, indicating that a larger fraction of carcinoma cells was blocked in a more radiosensitive stage of the cell cycle compared with mock-treated or mismatch ASO control-treated cells (Fig. 3b).

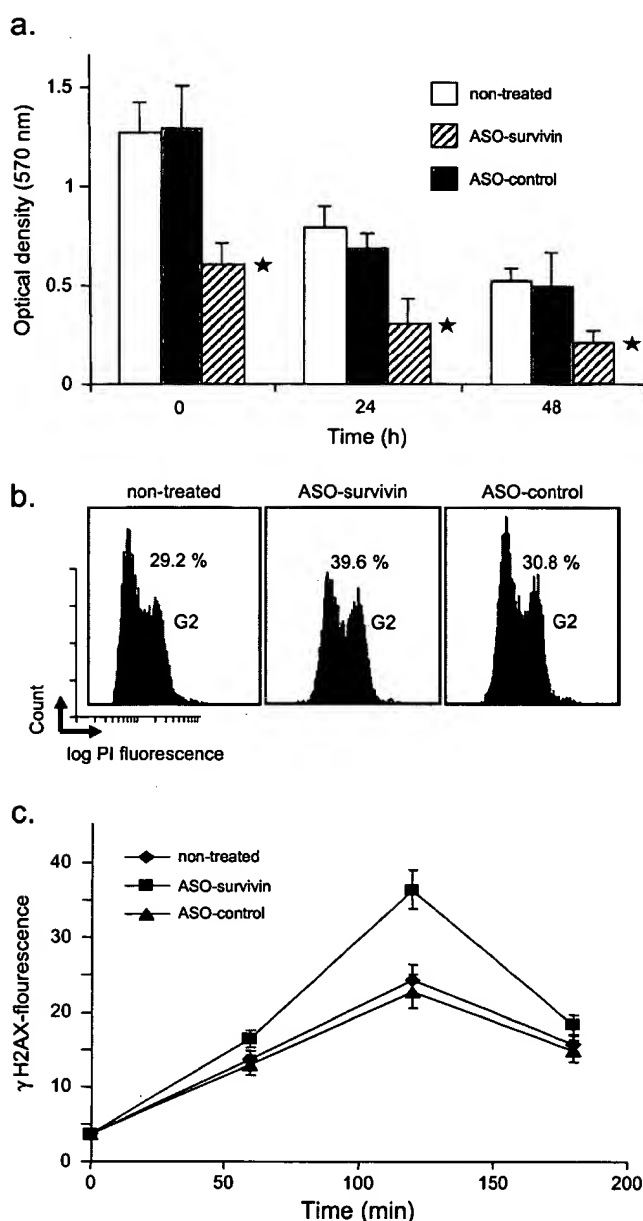


Fig. 3. Survivin attenuation by LY 2181308 antisense oligonucleotide (ASO) affects cell viability and cell-cycle distribution and increases phospho-histone H2AX. (a) Metabolic activity determined using a 3-(4,5-methylthiazol-2-yl)-2,5-diphenyl-tetrazolium bromide (MTT) assay after transfection of survivin-specific ASO, ASO control, or nontreated cells without (0 Gy) and 24 or 48 hours after irradiation with 8 Gy. * $p < 0.004$. Data presented as mean \pm SD from three repeated experiments. (b) Fixed SW480 carcinoma cells were labeled with propidium iodide (PI), and flow cytometry was used to measure DNA content 24 hours after transfection. Percentages of cells in G₂/M phase are shown in the individual plots. Data shown as one representative of three experiments. (c) Percentage of serine-139 phosphorylated-histone γ H2AX fluorescence after transfection with survivin-specific synthetic ASO, mismatch control ASO, or mock-treated cells and irradiation with 2 Gy as assessed by using FACS analysis. Data expressed as mean relative value \pm SD from two independent experiments. * $p = 0.02$ vs. non-treated controls.

Next, we analyzed whether attenuation of survivin also may affect radiosensitivity by mechanisms other than increasing apoptosis and caspase activity. Initial H2AX serine-139 phosphorylation was analyzed after ASO treatment and irradiation. As shown in Fig. 3c, induction of phospho-histone γ H2AX, a marker of recognized DNA double-strand breaks, increased after survivin-specific ASO treatment in SW480 cells 60–120 minutes after irradiation compared with mismatch ASO control-treated or nontreated cells.

Survivin as a radioresistance factor in both cell culture and a murine xenograft model system

Clonogenic assays were performed after irradiation with 1–8 Gy of SW480 cells treated with either survivin ASO or mismatch ASO control. Non-ASO-treated cells served as a control. As shown in Fig. 4a, inhibition of survivin shifted the survival curves down for SW480 cells with a reduction in the shoulder. Survival at 2-Gy irradiation (SF = 2) significantly decreased (0.28 vs. 0.44; $p = 0.005$) in survivin ASO-treated cells, resulting in a radiation-induced cytotoxicity enhancement factor of 1.8–2.

On the basis of the radiosensitizing effect of survivin attenuation *in vitro*, we next investigated the pharmacologic activity of survivin-specific synthetic ASO in a murine SW480 xenograft model in which tumor volumes were measured using a calliper. SW480 tumor-bearing mice were treated with 3 Gy/d fractions for 3 consecutive days starting on Day 2 of treatment. The ASO was administered intraperitoneally at an initial dose of 50 mg/kg BW 1 day before irradiation (Day 1) and at Days 3 and 4 at 2–4 hours before radiation therapy, followed by a single administration of 25 mg/kg BW on Days 7 and 9 of treatment. Mismatch ASO control- and mock-treated animals were used to determine nonspecific effects of oligonucleotide treatment and tumor growth, respectively. Results (Fig. 4b) showed that both single administration of survivin ASO or fractionated irradiation alone resulted in decreased tumor volumes. Combining survivin ASO and irradiation resulted in significant inhibition ($p = 0.0001$) of tumor growth that was more pronounced than treatment with either irradiation or survivin ASO monotherapy.

Inhibition of survivin protein expression by ASO in tumor xenografts

To provide evidence that inhibition of tumor growth by survivin ASO was caused by its ability to specifically abrogate protein levels *in vivo*, survivin expression was assayed in paraffin-embedded tumor samples of respective mice on Day 6 after the start of treatment. Consistent with results *in vitro*, tumors treated with LY 2181308 showed decreased expression of survivin protein compared with tumors derived from mismatch control ASO- and mock-treated animals. Immunoreactivity of survivin (Fig. 5a) and survivin-expressing tumor cells was significantly decreased in tumors treated with survivin ASO and more pronounced after combined survivin ASO treatment and irradiation ($p < 0.0001$; Fig. 5b). These results suggest that inhibition of tumor growth is attributable

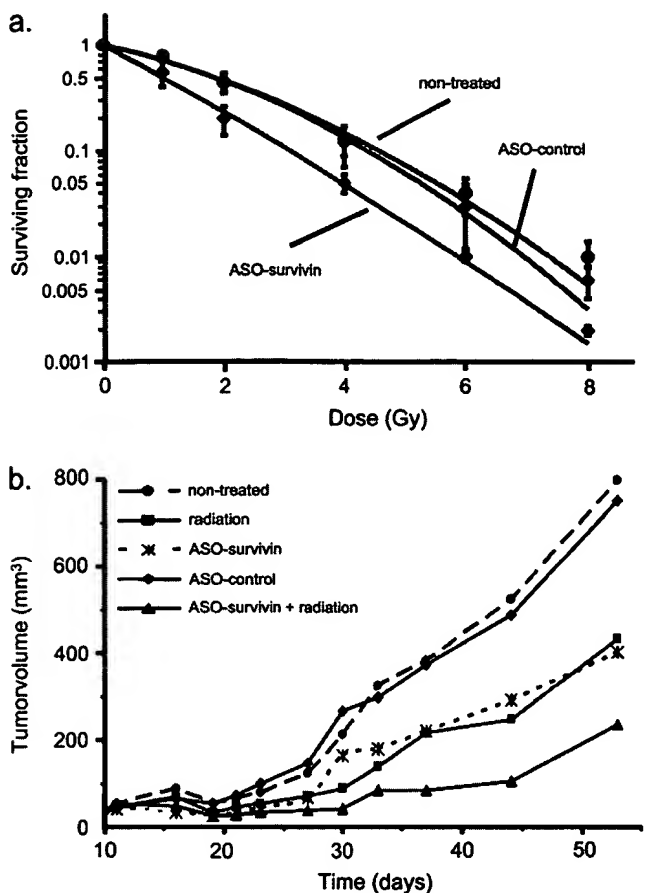


Fig. 4. Survivin as a radioresistance gene in both cell culture and a murine xenograft model system. (a) Effect of survivin attenuation on clonogenic survival of SW480 cells transfected with either survivin-specific single-stranded DNA–antisense oligonucleotide (ASO) or ASO control. Nontreated cells served as a control. After 12–14 days, colonies greater than 50 cells were counted and survival fractions normalized to the plating efficiency were fitted according to the linear quadratic equation. Data shown as mean \pm SD from three experiments. (b) SW480 adenocarcinoma were injected subcutaneously into NMRI nude mice and tumor growth was monitored by using callipers. When average tumor volume reached approximately $0.05\text{--}0.1\text{ cm}^3$, mice were stratified into five groups of 5–10 animals each. Group 1 indicates no treatment; Group 2, X-irradiation with $3 \times 3\text{ Gy}$; Group 3, LY2181308-ASO monotherapy; Group 4, LY2293329 mismatch control; and Group 5, combined treatment with X-irradiation and LY2181308-ASO. ASO was injected intraperitoneally starting with 50 mg/kg of body weight (BW) 1 day before irradiation and 25 mg/kg BW at Days 3 and 4 at 2–4 hours before irradiation and on Days 7 and 9. Mean values of tumor volumes for each treatment group are shown.

to decreased levels of the antiapoptotic protein in tumor xenografts.

DISCUSSION

By disturbing the balance between proliferation and cell death, defects in the apoptosis pathway contribute to a variety of diseases, including cancer (21). In this context, alterations in expression of apoptosis-related proteins, such as the IAP family, show a pivotal pathway by which cancer cells acquire resistance to therapeutic treatment (22–24). Of these

antiapoptotic and prosurvival factors, survivin, the smallest member of the IAP family, deserves growing attention as an interesting biomarker and ideal molecular target for cancer therapy because of its universal overexpression in human tumors and its prominent role in the regulation of both tumor cell apoptosis and cell proliferation (25–27).

In patients with rectal cancer, immunohistochemically determined expression of survivin protein previously was associated with unfavorable local control rates after preoperative 5-fluorouracil-based radiochemotherapy in a retrospective analysis (28). In line with that, our prospectively collected microarray gene profiling data for tumor biopsy specimens from 20 patients with rectal cancer treated by using an innovative combination of radiotherapy and capecitabine/oxaliplatin showed that increased intracellular survivin mRNA levels were associated with a significantly greater risk of local tumor relapse. These data agree with molecular profiling studies and retrospective analyses in a variety of patient cohorts that consistently identified survivin as a risk factor for cancer progression and poor prognosis (29, 30). Increased survivin levels emerged as a prognostic marker and seem to confer tumor cells greater adaptability, proliferative capacity, and resistance to cell death, which translates into clinically worse disease (27). This was strengthened further by the discovery that compared with normal tissues, survivin constituted the fourth top “transcriptome” in colorectal, lung, brain, and breast cancer, shown by genome-wide searches (30). This reflects an “oncofetal” pattern of expression because survivin is highly expressed in embryonic organs, is nearly undetectable in most differentiated normal tissues, and becomes dramatically reexpressed during tumor development (11, 27). Additionally, survivin participates in the cellular stress response, in which binding of the protein to the molecular chaperone heat shock protein (HSP) 90 helps tumor cells cope with unfavorable environments and other exogenous stresses and thus preserve cell proliferation and cell viability (26, 31). Conversely, global suppression of HSP90 chaperone function or disruption of the survivin–HSP90 interaction results in proteasomal degradation of survivin, initiates mitochondrial apoptosis and cell-cycle arrest, and suppresses cell proliferation (31).

Given such strong evidence implicating the role of survivin in enhancing the progression and malignant potential of cancer cells, we further investigated whether survivin attenuation may increase tumor response of SW480 colorectal cancer cells toward irradiation. We showed that inhibition of survivin by the Eli-Lilly product survivin-specific synthetic single-stranded DNA-ASO (LY2181308) resulted in significant inhibition of metabolic activity, increased apoptosis, and decreased clonogenic survival when combined with irradiation. These radiosensitization effects were confirmed in an orthotopic xenograft transplant model in nude mice by significantly decreasing tumor growth of SW480 colorectal cancer cells when treated with survivin-specific ASO and irradiation. The observation that survivin ASO produces a radiosensitizing effect is consistent with previous studies in which survivin was specifically targeted by a panel of molecular antagonists.

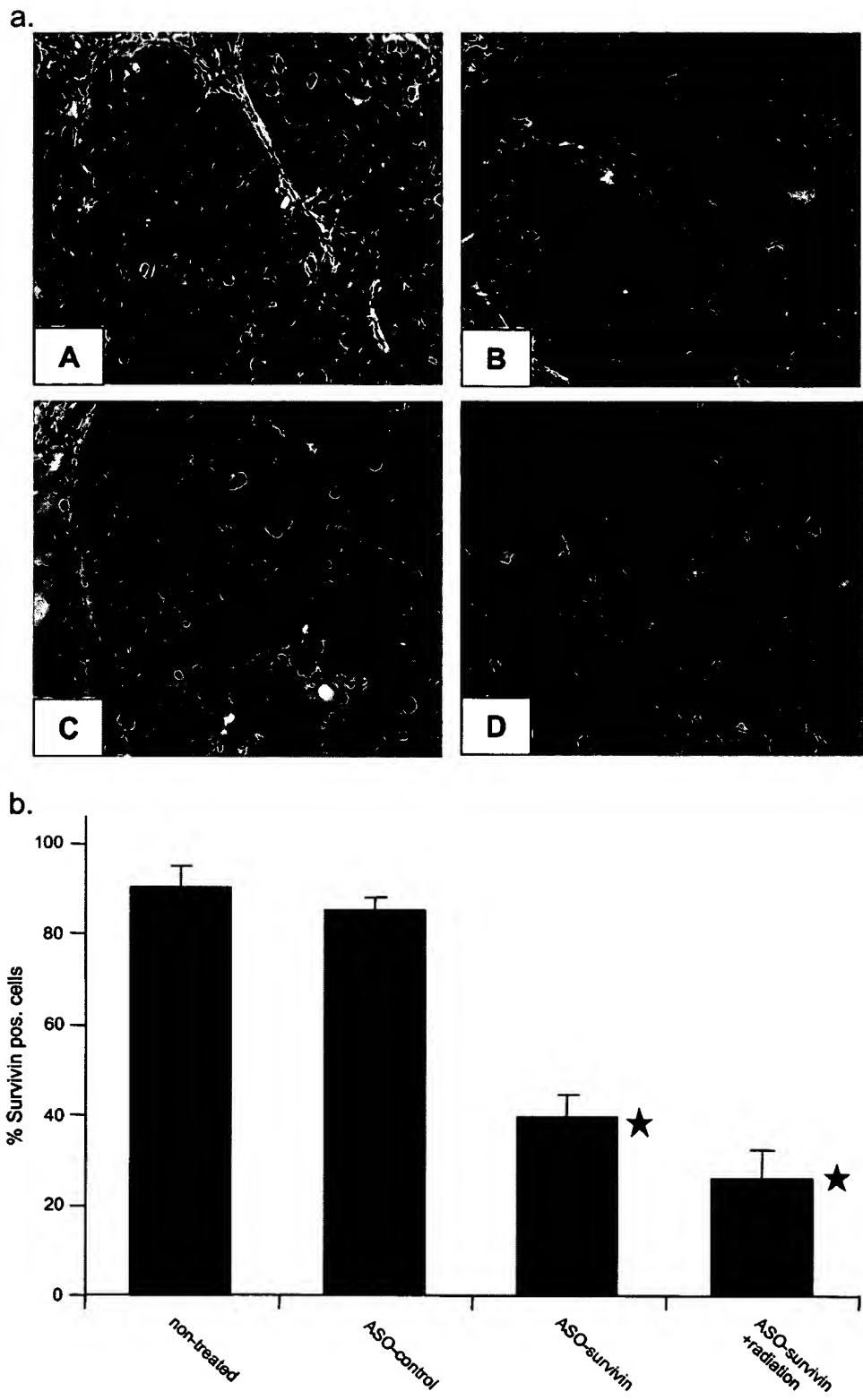


Fig. 5. Inhibition of survivin protein levels by antisense oligonucleotide (ASO) in tumor xenografts. (a) To provide evidence that inhibition of tumor growth by survivin ASO was caused by its ability to specifically aggregate protein levels *in vivo*, survivin expression was immunohistochemically assayed in paraffin-embedded tumor samples of mice (A) without treatment, (B) treated with mismatch ASO control, (C) survivin ASO monotherapy, and (D) treated with survivin ASO and radiation on Day 6 after the start of therapy. (b) Quantitative data obtained by using immunohistochemical analysis given as mean \pm SD from three to four individual tumors/group. * p < 0.0001.

Several groups, including our own, showed that suppression of survivin by using synthetic ASO (32, 33), ribozymes (34), small interfering RNA (28, 35, 36), or dominant-negative mutants (37) effectively radiosensitized human tumor cells. However, the underlying mechanisms by which antisurvivin strategies may improve radiation response appear to be multifaceted and may involve caspase-dependent and caspase-independent mechanisms, such as impaired DNA repair, altered cell-cycle distribution, mitotic arrest, and subsequent cell death (28, 37). Interestingly, a greater incidence of DNA double-strand breaks after irradiation was observed in our study, indicated by a greater amount of Ser¹³⁹-phosphorylated histone γH2AX staining 60–120 minutes after survivin-specific ASO treatment and radiation. Decreased DNA repair capacity on radiation exposure in the presence of survivin inhibitors was also reported by Chakravarti *et al.* (37). Using a dominant-negative survivin construct, this group reported

a significantly greater degree of double-strand DNA damage, which may contribute to decreased clonogenic survival after irradiation in the presence of survivin inhibitors.

In conclusion, our results suggest that survivin shows a radioresistance factor and molecular biomarker, predicting tumor response in patients with rectal cancer treated with neoadjuvant radiochemotherapy. Pharmacologic approaches targeting survivin in tumors overexpressing this protein may strongly increase the therapeutic ratio of radiotherapy. Supported by a favorable safety profile, the survivin ASO LY2181308 has already entered the clinic and currently is planned to undergo Phase I/II evaluation as monotherapy in patients with hepatocellular cancer. Our clinical, *in vitro*, and animal data provide a strong rationale for combining molecular survivin antagonists and radiotherapy in future clinical trials specifically for patients with rectal cancer.

REFERENCES

1. Dewey WC, Ling CC, Meyn RE. Radiation-induced apoptosis: Relevance to radiotherapy. *Int J Radiat Oncol Biol Phys* 1995; 33:781–796.
2. Meyn RE, Stephens LC, Milas L. Programmed cell death and radioresistance. *Cancer Metastasis Rev* 1996;15:119–131.
3. Gudkov AV, Komarova EA. The role of p53 in determining sensitivity to radiotherapy. *Nat Rev Cancer* 2003;3:117–129.
4. Rödel C, Grabenbauer GG, Papadopoulos T, *et al.* Apoptosis as a cellular predictor for histopathologic response to neoadjuvant radiochemotherapy in patients with rectal cancer. *Int J Radiat Oncol Biol Phys* 2002;52:294–303.
5. Scott N, Hale A, Deakin M, *et al.* A histopathological assessment of the response of rectal adenocarcinoma to combination chemo-radiotherapy: Relationship to apoptotic activity, p53 and bcl-2 expression. *Eur J Surg Oncol* 1998;24:169–173.
6. Rödel C, Haas J, Groth A, *et al.* Spontaneous and radiation-induced apoptosis in colorectal carcinoma cells with different intrinsic radiosensitivities: Survivin as a radioresistance factor. *Int J Radiat Oncol Biol Phys* 2003;55:1341–1347.
7. Hengartner MO. The biochemistry of apoptosis. *Nature* 2000; 407:770–776.
8. Adams JM, Cory S. Bcl-2-regulated apoptosis: Mechanism and therapeutic potential. *Curr Opin Immunol* 2007;19:488–496.
9. Ambrosini G, Adida C, Altieri DC. A novel anti-apoptosis gene, survivin, expressed in cancer and lymphoma. *Nat Med* 1997;3: 917–921.
10. Sarela AI, Verbeke CS, Ramsdale J, *et al.* Expression of survivin, a novel inhibitor of apoptosis and cell cycle regulatory protein, in pancreatic adenocarcinoma. *Br J Cancer* 2002;86: 886–892.
11. Kim PJ, Plescia J, Clevers H, *et al.* Survivin and molecular pathogenesis of colorectal cancer. *Lancet* 2003;362:205–209.
12. Kawasaki H, Toyoda M, Shinohara H, *et al.* Expression of survivin correlates with apoptosis, proliferation, and angiogenesis during human colorectal tumorigenesis. *Cancer* 2001;91: 2026–2032.
13. Altieri DC. Molecular circuits of apoptosis regulation and cell division control: The survivin paradigm. *J Cell Biochem* 2004;92:656–663.
14. Altieri DC. Validating survivin as a cancer therapeutic target. *Nat Rev Cancer* 2003;3:46–54.
15. Pennati M, Folini M, Zaffaroni N. Targeting survivin in cancer therapy: Fulfilled promises and open questions. *Carcinogenesis* 2007;28:1133–1139.
16. Capalbo G, Rödel C, Stauber RH, *et al.* The role of survivin for radiation therapy. Prognostic and predictive factor and therapeutic target. *Strahlenther Onkol* 2007;183:593–599.
17. Rödel F, Hoffmann J, Grabenbauer GG, *et al.* High survivin expression is associated with reduced apoptosis in rectal cancer and may predict disease-free survival after preoperative radiochemotherapy and surgical resection. *Strahlenther Onkol* 2002;178:426–435.
18. Rödel C, Grabenbauer GG, Papadopoulos T, *et al.* Phase I/II trial of capecitabine, oxaliplatin, and radiation for rectal cancer. *J Clin Oncol* 2003;21:3098–3104.
19. Zaffaroni N, Pennati M, Daidone MG. Survivin as a target for new anticancer interventions. *J Cell Mol Med* 2005;9:360–372.
20. Schlingemann J, Habtemichael N, Ittrich C, *et al.* Patient-based cross-platform comparison of oligonucleotide microarray expression profiles. *Lab Invest* 2005;85:1024–1039.
21. Hanahan D, Weinberg RA. The hallmarks of cancer. *Cell* 2000; 100:57–70.
22. Hunter AM, Lacasse EC, Korneluk RG. The inhibitors of apoptosis (IAPs) as cancer targets. *Apoptosis* 2007;12:1543–1568.
23. LaCasse EC, Baird S, Korneluk RG, *et al.* The inhibitors of apoptosis (IAPs) and their emerging role in cancer. *Oncogene* 1998;17:3247–3259.
24. Salvesen GS, Duckett CS. IAP proteins: Blocking the road to death's door. *Nat Rev Mol Cell Biol* 2002;3:401–410.
25. Li F, Ambrosini G, Chu EY, *et al.* Control of apoptosis and mitotic spindle checkpoint by survivin. *Nature* 1998;396: 580–584.
26. Altieri DC. Coupling apoptosis resistance to the cellular stress response: The IAP-Hsp90 connection in cancer. *Cell Cycle* 2004;3:255–256.
27. Altieri DC. Survivin, cancer networks and pathway-directed drug discovery. *Nat Rev Cancer* 2008;8:61–70.
28. Rödel F, Hoffmann J, Distel L, *et al.* Survivin as a radioresistance factor, and prognostic and therapeutic target for radiotherapy in rectal cancer. *Cancer Res* 2005;65:4881–4887.
29. van 't Veer LJ, Dai H, van de Vijver MJ, *et al.* Gene expression profiling predicts clinical outcome of breast cancer. *Nature* 2002;415:530–536.
30. Velculescu VE, Madden SL, Zhang L, *et al.* Analysis of human transcriptomes. *Nat Genet* 1999;23:387–388.
31. Fortugno P, Beltrami E, Plescia J, *et al.* Regulation of survivin function by Hsp90. *Proc Natl Acad Sci U S A* 2003;100: 13791–13796.

32. Lu B, Mu Y, Cao C, *et al.* Survivin as a therapeutic target for radiation sensitization in lung cancer. *Cancer Res* 2004;64: 2840–2845.
33. Guan HT, Xue XH, Dai ZJ, *et al.* Down-regulation of survivin expression by small interfering RNA induces pancreatic cancer cell apoptosis and enhances its radiosensitivity. *World J Gastroenterol* 2006;12:2901–2907.
34. Pennati M, Binda M, Colella G, *et al.* Radiosensitization of human melanoma cells by ribozyme-mediated inhibition of survivin expression. *J Invest Dermatol* 2003;120: 648–654.
35. Kappler M, Taubert H, Bartel F, *et al.* Radiosensitization, after a combined treatment of survivin siRNA and irradiation, is correlated with the activation of caspases 3 and 7 in a wt-p53 sarcoma cell line, but not in a mt-p53 sarcoma cell line. *Oncol Rep* 2005;13:167–172.
36. Kami K, Doi R, Koizumi M, *et al.* Downregulation of survivin by siRNA diminishes radioresistance of pancreatic cancer cells. *Surgery* 2005;138:299–305.
37. Chakravarti A, Zhai GG, Zhang M, *et al.* Survivin enhances radiation resistance in primary human glioblastoma cells via caspase-independent mechanisms. *Oncogene* 2004;23:7494–7506.

Matrix metalloproteinase-9 Inhibition Down-Regulates Radiation-Induced Nuclear Factor- κ B Activity Leading to Apoptosis in Breast Tumors

Sateesh Kunigal,¹ Sajani S. Lakka,¹ Pushpa Joseph,² Norman Estes,³ and Jasti S. Rao^{1,4}

Abstract

Purpose: Novel strategies are needed to prevent the high mortality rates of several types of cancer. These high rates stem from tumor resistance to radiation therapy, which is thought to result from the induction of matrix metalloproteinases (MMP) and plasminogen activators. In the present study, we show that the modulation of MMP-9 expression, using adenoviral-mediated transfer of the antisense MMP-9 gene (MMP-9 adenoviral construct, Ad-MMP-9), affects breast cancer sensitivity to radiation.

Experimental Design: In the present study, we used antisense Ad-MMP-9 to down-regulate the expression of MMP-9 in MDA MB 231 breast cancer cell lines *in vitro* before irradiation and subsequently incubated cells in hypoxic condition. *In vivo* studies were done with orthotopic breast tumors, and radiosensitivity was evaluated both *in vitro* and *in vivo*.

Results: Ad-MMP-9 infection resulted in down-regulation of radiation-induced levels of hypoxia-inducible factor 1 α and MMP-9 under hypoxic conditions in MDA MB 231 breast cancer cells. In addition, Ad-MMP-9, in combination with radiation, decreased levels of the transcription factors nuclear factor- κ B and activator protein 1, both of which contribute to the radioresistance of breast tumors. Finally, the triggering of the Fas–Fas ligand apoptotic cascade, which resulted in the cleavage of PARP-1 and caspase-10, caspase-3, and caspase-7, signifies the efficiency of combined treatment of Ad-MMP-9 and radiation. Treatment with Ad-MMP-9 plus radiation completely regressed tumor growth in orthotopic breast cancer model.

Conclusions: In summary, integrating gene therapy (adenovirus-mediated inhibition of MMP-9) with radiotherapy could have a synergistic effect, thereby improving the survival of patients with breast cancer.

Radiotherapy provides a key management strategy for many epithelial tumor types, forms part of the multidisciplinary approach for breast cancer treatment, and is now of routine value after conservative surgery to reduce locoregional tumor recurrence. However, the significant limitations of radiotherapy make it inefficient as the sole treatment for breast and many other cancers. Some cancer cells are intrinsically resistant to damage by ionizing radiation, and treatment can actually induce tumor cell proliferation and repopulation, resulting in a diminished response to radiation, resistant growth, and poor local control (1). Hypoxia-driven cellular modifications have

been shown to contribute to this poor prognostic outlook, giving rise to more aggressive locoregional disease, invasive capacity, and angiogenesis (2).

Intratumoral hypoxia plays a pivotal role in activating the key transcription factor, hypoxia-inducible factor (HIF), which mediates activation of the “survival machinery” in cancer cells. Specifically, HIF1 regulates the expression of numerous genes and controls glycolysis, erythropoiesis, apoptosis, and angiogenesis (3). Studies have shown that HIF1 α activity promotes tumor growth *in vivo* (4). Hypoxic tumor regions show increased gene expression caused by hypoxia-induced activation of transcription machinery (5, 6). Several of the gene products induced or up-regulated under hypoxic conditions play pivotal roles in the metastatic process, and studies have suggested that hypoxia could promote metastasis in human cancer (5). Hypoxia also activates nuclear factor- κ B (NF- κ B) (7), a transcription factor important in the promotion and progression of tumor development and survival (8). As such, inhibition of these pathways represents a potentially important cancer therapeutic.

Cancer cells often develop radioresistance mechanisms related to the DNA repair response. By combining chemotherapy and radiation therapy, radiation efficiency may be strengthened by inhibiting DNA repair and overcome resistance to apoptosis. NF- κ B is activated by DNA-damaging agents and could be involved in cell cycle arrest and prevention of

Authors' Affiliations: Departments of ¹Cancer Biology and Pharmacology, ²Pathology, ³Surgery, and ⁴Neurosurgery, University of Illinois College of Medicine at Peoria, Peoria, Illinois

Received 8/21/07; revised 12/14/07; accepted 1/22/08.

Grant support: National Cancer Institute grants CA 75557, CA 92393, CA 95058, CA 116708, National Institute of Neurological Disorders and Stroke grants NS47699 and NS57529, Caterpillar, Inc., and OSF Saint Francis, Inc. (J.S. Rao).

The costs of publication of this article were defrayed in part by the payment of page charges. This article must therefore be hereby marked *advertisement* in accordance with 18 U.S.C. Section 1734 solely to indicate this fact.

Requests for reprints: Jasti S. Rao, Department of Cancer Biology and Pharmacology, University of Illinois College of Medicine at Peoria, One Illini Drive, Peoria, IL 61605. Phone: 309-671-3445; Fax: 309-671-3442; E-mail: jsrao@uic.edu.

© 2008 American Association for Cancer Research.
doi:10.1158/1078-0432.CCR-07-2060

apoptosis, allowing DNA repair (9). However, sustained NF- κ B activation could permit cells with accumulated radiation-induced DNA damage to escape elimination by apoptosis (10). Indeed, high constitutive NF- κ B activity prevents cancerous cells from apoptosis (11), resulting in a more aggressive potential seen in prostate cancer (12), malignant melanomas, Hodgkin's disease, leukemia, breast cancer, and cutaneous T-cell lymphoma cancer cell lines (13).

The transcription factor activator protein 1 (AP-1) comprises members of the Jun and Fos families and has been implicated in the regulation of apoptosis and cell proliferation (14). Studies suggest that Jun B and c-Jun may trigger apoptosis and promote proliferation of erythroid cells, respectively (15). Activation of Sp1, another key transcription factor, occurs under hypoxic conditions in various cancer cells, including breast carcinoma (16, 17). Thus, agents that enhance apoptosis in irradiated tumor cells could have significant therapeutic benefits.

Degradation of the extracellular matrix plays an important role in tumor metastasis. Matrix metalloproteinases (MMP) have been primarily associated with matrix remodeling, a necessary component of invasion. It has been reported that preoperative, short-course radiotherapy decreases local recurrence rates (e.g., rectal cancer) and, combined with optimal surgery, improves patient survival. Although radiotherapy has proved benefits, several reports show an increase in expression and activation of gelatinase MMPs (18). Initially, MMPs were thought to simply breakdown components of the extracellular matrix, allowing for invasion and metastasis. However, recent studies confirmed that MMP activity involves precise MMP localization on a cell's invasive front, exposure of key components in the extracellular matrix transform it from a barrier into a scaffold for invasion, and cleavage of free insulin-like growth factors result in cell growth, division, and inhibition of apoptosis (19).

Hypoxia-targeted gene therapy presents a number of interesting developments and applications in modern oncology. Attempts are currently being made to overcome the adverse effects and limitations of radiation and exploit resistant hypoxic tumor cells using combination gene therapy and radiotherapy. In this study, we combined radiation with down-regulated MMP-9, which reduced hypoxia by using a replication-deficient recombinant adenovirus containing a 528-bp antisense expression segment for human MMP-9 (Ad-MMP-9AS or Ad-MMP-9; ref. 20) to treat breast cancer tumors. Our results indicated that, after the combined treatment, transcription factor activity controlling the expression of the oncoproteins was reduced and proapoptotic molecules were up-regulated, resulting in increased apoptosis and tumor suppression.

Materials and Methods

Cell culture and treatments. MDA MB 231 human breast cancer cells were purchased from the American Type Culture Collection and cultured in DMEM supplemented with 10% fetal bovine serum in a humidified CO₂ incubator at 37°C. MDA MB 231 cells were serum-starved for 12 to 18 h and treated with 100 multiplicity of infection of the empty vector (Ad-CMV) or antisense MMP-9 adenoviral construct (Ad-MMP-9). Either Ad-MMP-9 or Ad-CMV was added to the cell monolayer (1.0 mL/60-mm dish or 3 mL/100-mm dish), and cells were incubated at 37°C for 60 min with brief agitation every 5 min. The necessary amount of culture medium was then added, and cells were returned to the incubator. For the radiation treatment, the cells were

starved of serum, exposed to 5 Gy, and returned to the incubator after the addition of the necessary amount of complete culture medium. For the treatment combination of virus and radiation, the cells were first infected with 100 multiplicity of infection of Ad-MMP-9 or Ad-CMV, and 24 h later, the cells were irradiated with 5 Gy. After the above-described treatments, the cells were incubated in hypoxic condition for a period of 12 to 16 h. The hypoxic condition was accomplished with the Anaerocult mini setup (EM Science).

Reverse transcription-PCR. Total RNA was isolated from cells in all treatment conditions using TRIzol per standard protocol. Total RNA was treated with DNase I (Invitrogen) to remove contaminating genomic DNA. PCR analysis was done using the one-step reverse transcription-PCR kit (Invitrogen). Glyceraldehyde-3-phosphate dehydrogenase (GAPDH) was used as an internal control. The following primers were used:

HIF1 α 5'-AGCTCTGCAACATGGAGG-3' sense,
5'-CACGACTTGTATTCTCCC-3' antisense;
MMP-9 5'-TGGACCATGCCTGCAACCTG-3' sense,
5'-CTCCTGCGTCTCAAAGGCA-3' antisense;
GAPDH 5'-CGGAGTCACGGATTCGTCGTAT-3' sense,
5'-AGCCTTCTCCATGGTGGTGAAGAC-3' antisense.

The PCR conditions were as follows: 95°C for 5 min, followed by 30 cycles of 95°C for 1 min, annealing temperature set according to the AT and GC content of the primers, respectively, for 1 min and 72°C for 1 min. The final extension was at 72°C for 5 min.

Electromobility shift assay. Nuclear extracts were prepared from MDA MB 231 cells that were treated with Ad-MMP-9, radiation, or both. Cells were detached with EDTA, resuspended in buffer A [10 mmol/L HEPES (N-2-hydroxyethylenepiperazine-N'-2-ethanesulfonic acid; pH 7.9), 1.5 mmol/L MgCl₂, 10 mmol/L KCl, 0.5 mmol/L DTT] containing protease inhibitors (1 mmol/L phenylmethylsulfonyl fluoride, 5 mmol/L iodoacetamide, 0.1 mmol/L quercetin, 10 μ g/mL aprotinin, 10 μ g/mL leupeptin, 0.3 mmol/L sodium vanadate), and incubated on ice for 15 min. After homogenization in a Wheaton 0.1-mL homogenizer, the nuclei were collected by centrifugation. The pellet was resuspended in buffer B [20 mmol/L HEPES (pH 7.9), 25% glycerol, 1.5 mmol/L MgCl₂, 420 mmol/L NaCl, 0.2 mmol/L EDTA, 0.5 mmol/L DTT] containing protease inhibitors and incubated on ice for 30 min, followed by centrifugation at 13,000 \times g (5 min at 4°C). The supernatant was dialyzed against buffer C (20 mmol/L HEPES, 20% glycerol, 100 mmol/L KCl, 0.2 mmol/L EDTA, 0.5 mmol/L DTT) containing protease inhibitors for 2 h at 4°C, followed by centrifugation at 13,000 \times g (5 min at 4°C). The supernatant proteins were used immediately or aliquoted and stored at -80°C.

Binding reaction was done for 30 min on ice in a volume of 20 μ L, containing 4 μ g nuclear protein extracts, 40 ng poly(dI-dC), 4 μ L 5 \times binding buffer [1 \times binding buffer: 20 mmol/L HEPES (pH 7.9), 50 mmol/L KCl, 5 mmol/L MgCl₂, 1 mmol/L EDTA, 1 mmol/L DTT, 10% glycerol] with or without 20-fold to 50-fold excess of cold competitor or unrelated competitor and a ³²P-labeled probe (3 \times 10⁴ cpm). For supershift electrophoretic mobility shift assay, protein extracts were incubated with 6 μ g SP1 monoclonal antibody or isotype control before the addition of the ³²P-labeled probe. DNA-protein complexes were separated on 5% polyacrylamide gel in Tris/glycine buffer at 4°C. The following double-stranded oligonucleotides (Santa Cruz Biotechnology) were used in this study:

NF- κ B 5'-AGT TGA GGG GAC TTT CCC AGG C-3' and 3'-TCA ACT CCC CTG AAA GGG TCC G-5';
AP-1 5'-CCC TTG ATG ACT CAG CCG GAA-3' and 3' GCG AAC TAC TGA GTC CCC CTT-5'.

End-labeled probes were prepared with 40 μ Ci (1,480 MBq) [γ -³²P] ATP using T4 polynucleotide kinase and were gel-purified on NAP-5 Sephadex G-25 DNA-grade columns.

Western blot analysis. MDA MB 231 cells were treated with Ad-CMV, Ad-MMP-9, radiation of 5 Gy, or a combination (Ad-MMP-9 plus radiation) and incubated under hypoxic conditions as described earlier. After the incubation period, the cells were washed with ice-cold PBS and lysed in radioimmunoprecipitation assay buffer containing protease inhibitors. Whole-cell extracts were subjected to SDS-PAGE and subsequently transferred to a polyvinylidene difluoride membrane (Bio-Rad). The membranes were blocked with 7% nonfat dry milk and probed with antibodies for the following molecules: MMP-9, HIF1 α , extracellular signal-regulated kinase 1/2 (ERK1/2), phosphorylated ERK, NF- κ B, p50, p65, c-fos, jun D, AP-1, Fas, Fas ligand (Fas-L), caspase-10, caspase-3, caspase-7, and PARP-1. Appropriate antibody conjugate with horseradish peroxidase was used as the secondary antibody. Membranes were developed according to an enhanced chemiluminescence protocol as per the manufacturer's instructions (Amersham Biosciences). Nuclear and cytoplasmic fractions for Western blotting were prepared as described elsewhere (21).

Gelatin zymography. Gelatin-substrate gel electrophoresis was done as described previously (22). MDA MB 231 cells were transfected with Ad-CMV, Ad-MMP-9, radiation of 5 Gy, or a combination (Ad-MMP-9 plus radiation) and incubated under hypoxic conditions as described earlier. To collect conditioned media, cells were washed once with serum-free medium and incubated with fresh serum-free medium. After 12 to 14 h, conditioned medium was collected and centrifuged to remove cellular debris, and protein concentrations were determined. Equal amounts of protein were subjected to 0.1% gelatin SDS-PAGE under nonreducing conditions. Gels were washed in 2.5% Triton X-100 and incubated overnight in Tris-CaCl₂ buffer. The gels were then stained with 0.2% Coomassie blue for 30 min and destained in 20% methanol and 10% acetic acid. The clear bands represent gelatinase activity.

Clonogenic survival assay. A clonogenic survival assay was used to investigate the sensitivity of MDA MB 231 cells infected with Ad-MMP-9 to radiation therapy as described previously (23). Briefly, the cells were treated as described earlier. The MDA MB 231 cells were trypsinized and plated in 100-mm dishes to assay for their colony-forming ability immediately after irradiation under hypoxic condition. Colonies were counted 10 to 15 d later. Survival curves were plotted using the GraphPad Prism 3.0 software program.

Animal experiments. MDA MB 231 cells were cultured in complete medium until a 70% to 80% density was obtained. At this point, cells were trypsinized, washed once with serum-free medium, and counted. Cells were injected bilaterally into the second mammary fat pads of athymic, female, 4-wk-old to 6-wk-old *nu/nu* mice (5.6×10^6 /100 μ L serum-free culture medium). Tumor growth was monitored daily. Once the tumor reached ~6 to 8 mm in size, the animals were divided into five groups of five animals each. Group 1 received PBS injections, group 2 received three doses of 5×10^8 plaque-forming units intratumorally on alternate days, group 3 received three doses of 5×10^8 plaque-forming units intratumorally on alternate days, group 4 was irradiated with two doses of 5 Gy on alternate days, and group 5 received Ad-MMP-9 and radiation treatments. In the case of the combined treatment, the tumors were first given intratumoral injections of Ad-MMP-9 on alternate days. Then, after the third dosage, the tumors were given two doses of 5 Gy on alternate days. The regression in the orthotopic tumor growth was followed for up to 8 wk. Mice were euthanized when the tumor diameter in control mice measured between 1.2 and 1.5 cm were removed and further processed. Additionally, as there was no tumor in animal treated with the Ad-MMP-9 infection in combination with irradiation, we included one more group of five animals that received combined treatment. The animals with tumor were euthanized after 15 d post combined treatment. Finally, the tumor volume was calculated using the formula $V = \pi / 6 (a \times b \times c)$.

Immunohistochemistry. Tumor samples fixed in 10% neutral buffered formalin were embedded in paraffin using automatic embedding equipment, after which 5- μ m sections were prepared. Immunohisto-

chemical analysis for MMP-9, HIF1 α , and caspase-3 was done on paraffin-embedded breast tumor sections of mice treated with Ad-CMV, Ad-MMP-9, irradiation, and Ad-MMP-9 infection in combination with irradiation.

Terminal deoxynucleotidyl transferase biotin-dUTP nick end labeling assay. Terminal deoxynucleotidyl transferase biotin-dUTP nick end labeling (TUNEL) assay was done with paraformaldehyde-fixed, paraffin-embedded breast tumor sections as per the manufacturer's protocol. Briefly, the TUNEL method identifies apoptotic cells *in situ* by using terminal deoxynucleotidyl transferase to transfer biotin-dUTP to the free 3'-OH of cleaved DNA. The biotin-labeled cleavage sites are then visualized by reaction with fluorescein-conjugated avidin (avidin-FITC). The cells were visualized using a fluorescent microscope with appropriate filter sets. DNA fragmentation in these treated tumors is indicative of apoptotic cell population.

Results

Ad-MMP-9 infection inhibits radiation-induced MMP-9 and HIF1 α expression at both the mRNA and protein levels in breast cancer cells. We analyzed the effect of Ad-MMP-9 (adenoviral construct of antisense to MMP-9 gene) on the MDA MB 231 cell line, which is the most aggressive breast cancer cell line for MMP-9 and HIF1 α expression at the mRNA level. Reverse transcription-PCR analysis showed that Ad-MMP-9 infection inhibited MMP-9 and HIF1 α at the mRNA level when compared with control or Ad-CMV (empty vector)-infected MDA MB 231 cells under hypoxic conditions (Fig. 1A). In contrast, radiation alone augmented the expression level of these molecules. Treatment with Ad-MMP-9 plus radiation inhibited expression levels more than Ad-MMP-9 infection alone. The level of MMP-9 was reduced by nearly 40% in the Ad-MMP-9-treated cells when compared with mock and Ad-CMV treatments; MMP-9 level was reduced by >50% when cells were treated with Ad-MMP-9 plus radiation. Conversely, in the cells that were treated with radiation alone, the level of MMP-9 was 50% higher than in the control cells (Fig. 1A).

Similarly, the expression level of HIF1 α at the mRNA level in the irradiated cells was increased by 30% compared with the control and Ad-CMV-infected cells. Ad-MMP-9 treatment alone inhibited the expression of HIF1 α by 25% compared with the controls; combined treatment of Ad-MMP-9 and radiation resulted in a 60% reduction of HIF1 α compared with the controls. These results support the earlier findings of Moeller et al. (24) that radiation increased the levels of active HIF1 and that the hypoxic condition is responsible for the poor response of the tumors to radiotherapy (Fig. 1A and B). Western blot analyses using respective antibodies against MMP-9 and HIF1 α support the reverse transcription-PCR analysis results, where the level of MMP-9 was reduced nearly 40% to 45% in the Ad-MMP-9-treated cells compared with the control and Ad-CMV treatment and by more than 60% to 70% when cells were infected with Ad-MMP-9 in combination with radiation. Conversely, in the cells treated with radiation alone, the level of MMP-9 was 30% more than in the control cells (Fig. 1C and D).

In addition, analysis of MMP-9 activity by gelatin zymography using conditioned medium from the treated cells revealed decreased levels of MMP-9 activity in Ad-MMP-9-infected cells compared with the controls. MMP-9 activity was even further reduced with the combined treatment. In contrast, we observed an almost 2-fold increase in MMP-9 activity in the

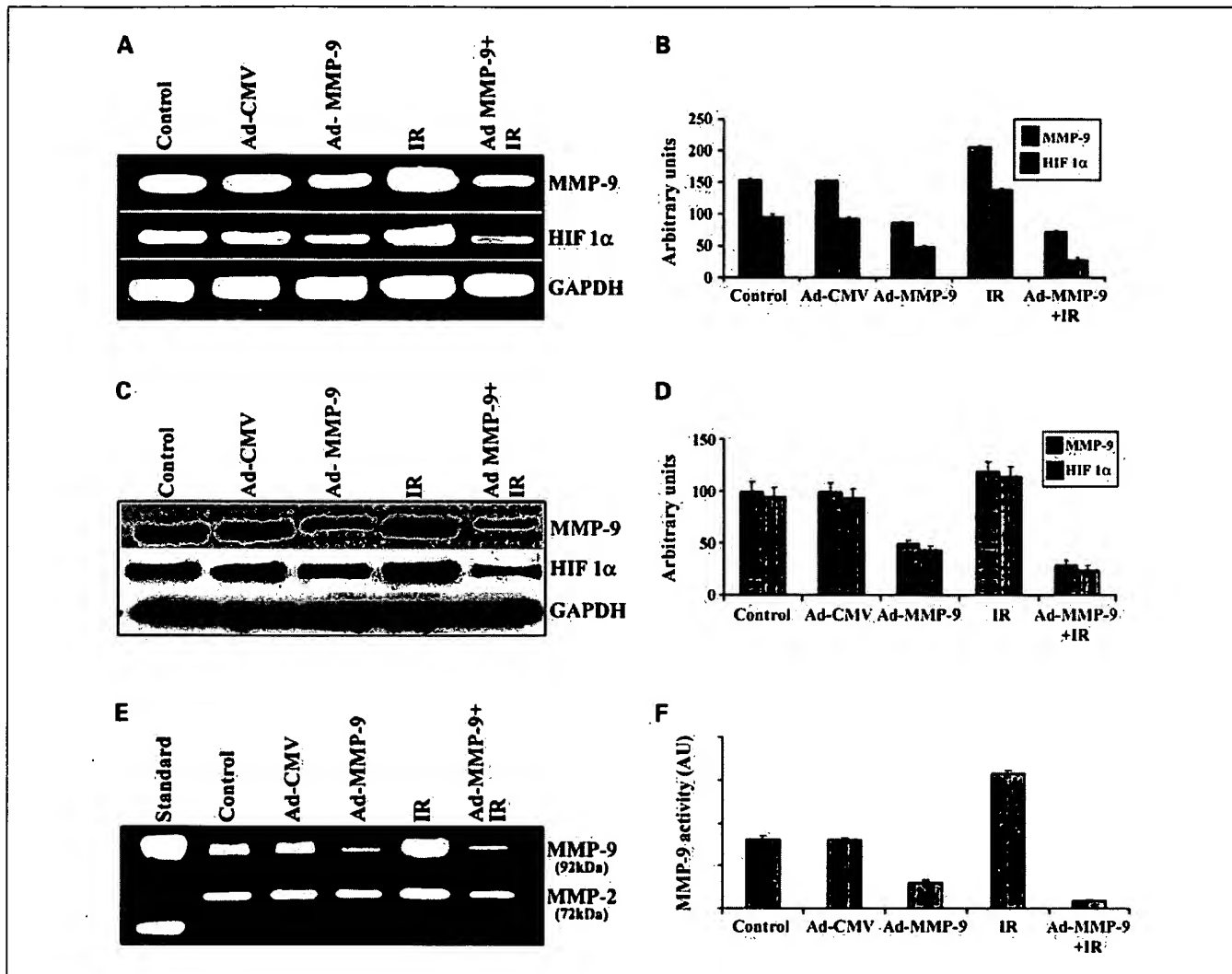


Fig. 1. Ad-MMP-9 infection inhibits radiation-induced MMP-9 and HIF1 α expression at both the mRNA and protein levels in breast cancer cells. *A*, briefly, MDA MB 231 cells were infected with Ad-CMV (100 multiplicity of infection), Ad-MMP-9 (100 multiplicity of infection), irradiation (IR; 5 Gy), or a combination of Ad-MMP-9 (100 multiplicity of infection) and irradiation (5 Gy), and incubated under hypoxic conditions as described in Materials and Methods. After 12 to 16 h of incubation, total RNA was extracted using TRIzol reagent and quantitated, and reverse transcription – PCR was done for assessment of MMP-9 and HIF1 α levels. Expression of GAPDH was verified for the equal loading of cDNA. *B*, densitometric analysis of MMP-9 and HIF1 α expression at the mRNA level (mean \pm SE; $n = 3$). *C*, after incubation, cell lysates were prepared and used for Western blot analysis to determine the levels of MMP-9 and HIF1 α . GAPDH was also used as a control to confirm equal loading of cell lysates. *D*, densitometric analysis of MMP-9 and HIF1 α expression at the protein level (mean \pm SE; $n = 3$). *E*, MMP-9 activity was analyzed by gelatin zymography using equal amounts of protein from the conditioned medium as described in Materials and Methods. *F*, densitometric analysis of MMP-9 activity (mean \pm SE; $n = 4$).

irradiated cells when compared with the control and Ad-CMV-treated cells (Fig. 1E and F).

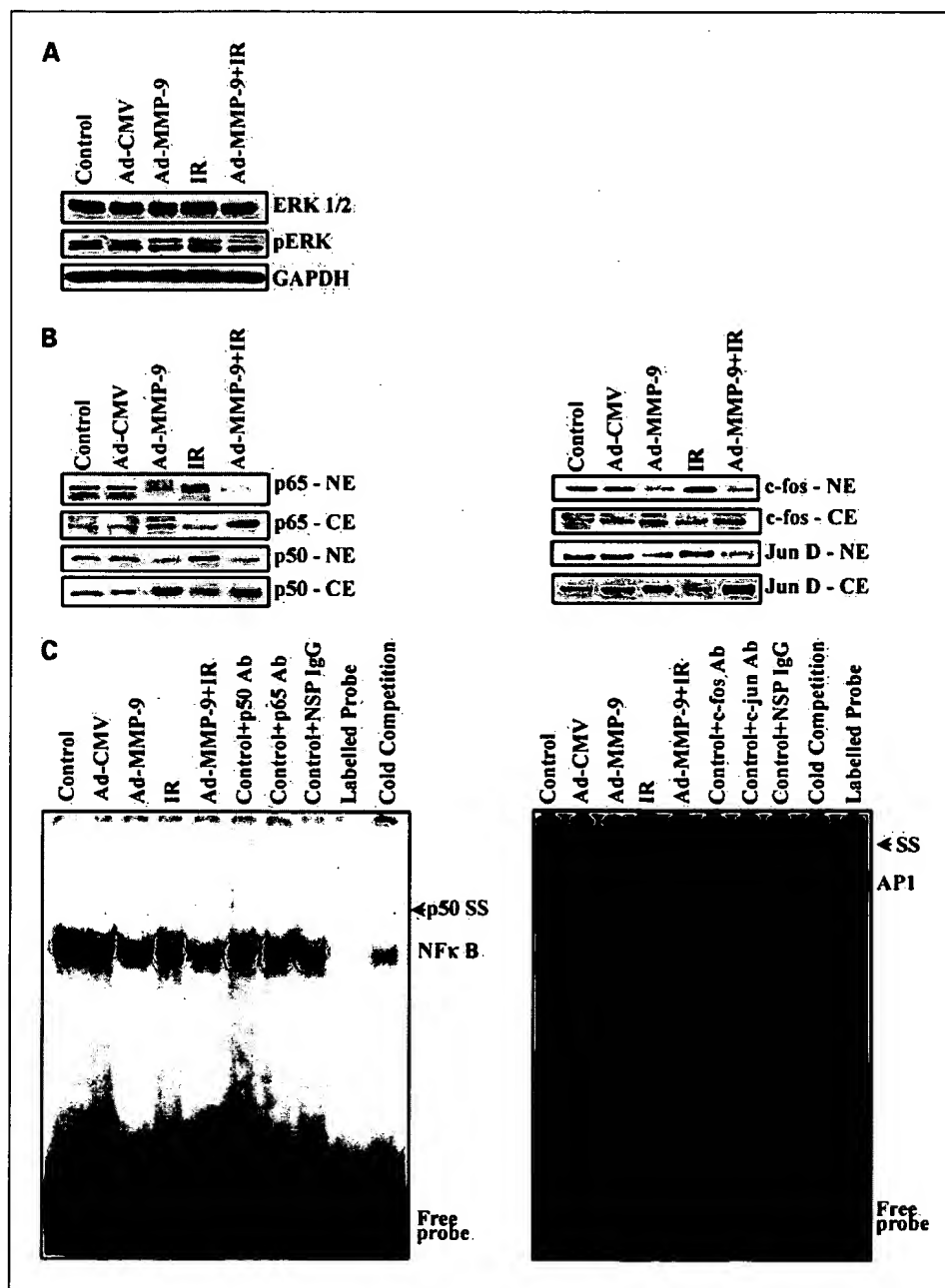
Treatment with Ad-MMP-9 and radiation decreases the binding activity of NF- κ B and AP-1. Ionizing radiation is reported to induce activation of NF- κ B and AP-1 (25). Poynter et al. have reported on the phosphorylation and dephosphorylation of members of the ERK family of the mitogen-activated protein kinase cascade and the events leading to activation of the transcription factor NF- κ B. These cascades are critical for the transcriptional up-regulation of genes important for cell survival, apoptosis, proliferation, transformation, and inflammation (26). Furthermore, it is known that ionizing radiation augments phosphorylation of ERK (27). Western blot analysis using whole-cell extracts of the cells treated with Ad-MMP-9 and Ad-MMP-9 in combination with radiation showed reduced phosphorylation of ERK, whereas irradiated cells

showed increased phosphorylation when compared with the controls (Fig. 2A). Activation of the binding activities of these transcription factors in tumor cells contributes to MMP-9 transcription and cell invasion (28). Western immunoblot analysis using the nuclear fractions from the treated cells showed reduced translocation of p50 and p65 (subunits of NF- κ B) and c-fos and Jun D (subunits of AP-1) to the nucleus in the Ad-MMP-9-treated cells, and further reduction in the cells was treated with Ad-MMP-9 in combination with radiation compared with the controls. In contrast, analysis of the cytoplasmic fractions showed reduced signals for the above-said molecules in the Ad-MMP-9-treated cells, and further reduction in the cells treated with Ad-MMP-9 in combination with radiation compared with the controls (Fig. 2B). However, a slight increase of NF- κ B and AP-1 translocation to the nucleus was seen in irradiated cells alone when compared

with the controls. Furthermore, we analyzed the DNA-binding activities of NF- κ B and AP-1 in the nuclear extracts using NF- κ B and AP-1-specific oligonucleotide probes (electrophoretic mobility shift assay). In the cells treated with Ad-MMP-9 or Ad-MMP-9 plus radiation, the DNA-protein complex was decreased when compared with the control and irradiated cells. The specificity of the NF- κ B-DNA and AP-1-DNA complexes was confirmed by supershift assay using specific antibodies (Fig. 2C).

Down-regulation of MMP-9 and radiation induces apoptosis in breast cancer cells. Because radiation-induced NF- κ B activation leads to cell survival, we next examined whether Ad-MMP-9 treatment in combination with radiation could cause apoptosis. Western immunoblot analysis showed the up-regulation of Fas

in the Ad-MMP-9, radiation, and combination treatments. However, Fas-L was up-regulated only in the Ad-MMP-9-treated and Ad-MMP-9 plus radiation-treated cells compared with the controls and radiation alone treatment (Fig. 3A). The densitometric analysis also revealed an increase of Fas (~1.5-fold) and Fas-L (~1.8-fold) expression in the Ad-MMP-9-infected cells, in combination with irradiation compared with the irradiation alone. We also looked downstream of this cascade. Western blot analysis revealed the cleavage of PARP-1 and caspase-10, caspase-3, and caspase-7 in Ad-MMP-9, radiation, and combination treatments compared with the control and Ad-CMV-treated cells (Fig. 3B). To confirm these initial observations, we analyzed apoptosis by looking for DNA fragmentation (TUNEL) assay. TUNEL-positive, apoptotic MDA



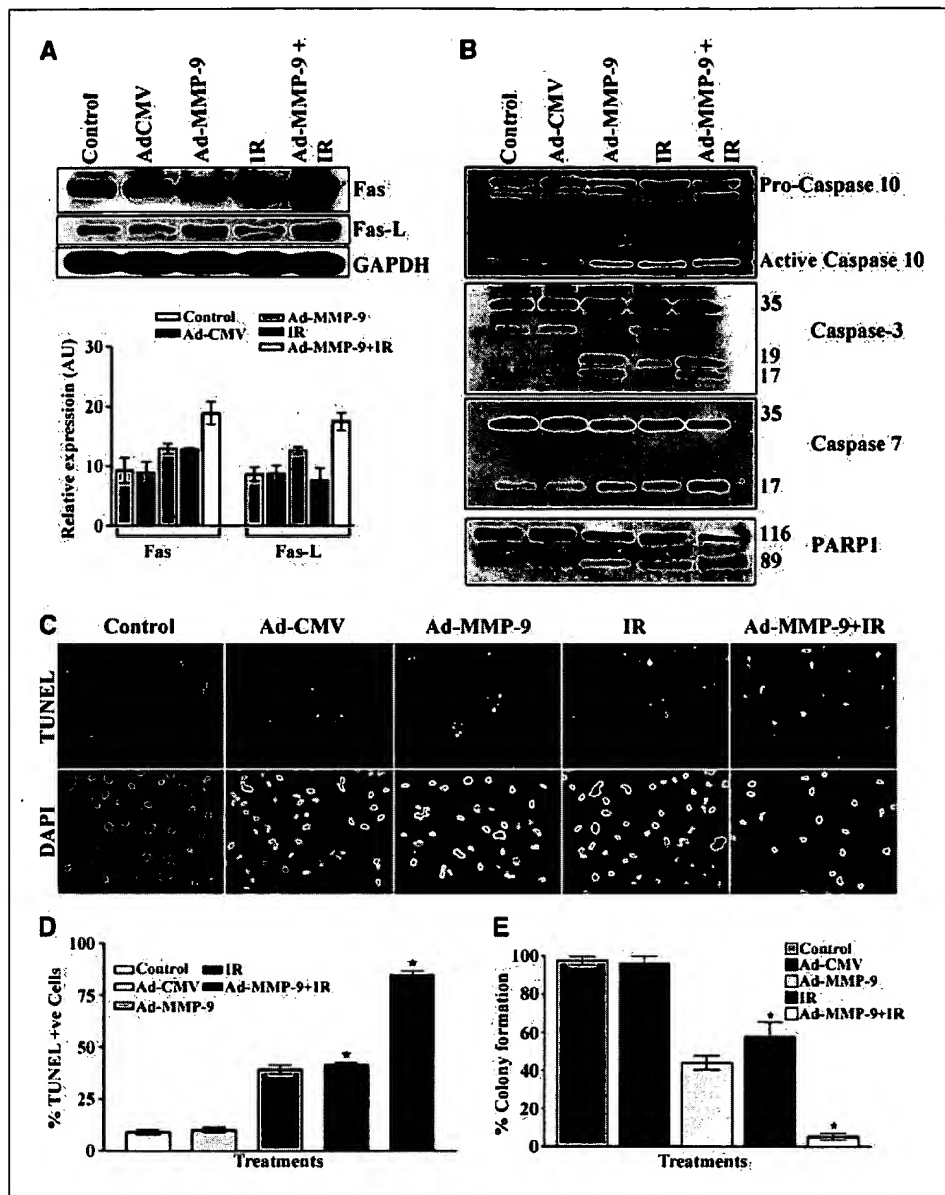


Fig. 3. Down-regulation of MMP-9 and radiation induces apoptosis in breast cancer cells. *A*, Western blot results for Fas and Fas-L. Representation of densitometric analysis of the expression of Fas and Fas-L (mean \pm SE; $n = 4$). *B*, Western blot results for caspase-10, caspase-3, and caspase-7 show active caspase and PARP cleavage. *C* and *D*, TUNEL assay was done with MDA MB 231 cells with the earlier said treatments as per the manufacturer's protocol and the densitometric analysis of percentage of TUNEL-positive cells are represented (mean \pm SE; $n = 3$). *, significant difference between irradiated alone cells and combination treatment of Ad-MMP-9 infection with irradiation ($P \leq 0.05$). *E*, clonogenic survival was assessed between 15 d after radiation exposure. Each experiment was done at least four times, and triplicates were done for each experiment. Clonogenic survival was assessed between 15 d after radiation exposure. Each experiment was done at least four times, and triplicates were done for each experiment. Statistical analysis was done using PRISM and ANOVA. *, significant difference between irradiated alone cells and combination treatment of Ad-MMP-9 infection with irradiation ($P \leq 0.01$).

MB 231 cells were meagerly present in control or Ad-CMV-infected cells. Ad-MMP-9 infection, in combination with irradiation, resulted in a distinct increase of TUNEL-positive cells compared with the Ad-MMP-9 alone-treated and irradiation alone-treated cells (Fig. 3C). Quantitation of TUNEL-positive cells indicated that Ad-MMP-9 infection in combination with irradiation (~85%) had 2-fold more compared with irradiation alone (~40%; Fig. 3D). A clonogenic survival assay was done to determine the influence of the down-regulation of MMP-9 in breast tumor cell to ionizing radiation. Figure 3E indicates that down-regulation of MMP-9 in MDA-MB-231 cells increased the radiosensitivity than uninfected and controls in terms of clonogenic survival. Statistical analysis shows that clonogenic survival in irradiated MDA-MB-231 cells that has reduced MMP-9 activity is significantly reduced compared with irradiated control MDA-MB-231 cells. These data confirm that the down-regulation of active MMP-9 increase sensitivity to ionizing radiation.

MMP-9 and HIF1 α mediate the inhibition of tumor growth after treatment with Ad-MMP-9 plus radiation. MDA MB 231 cells were chosen for animal studies because these cells form aggressive primary tumors. We compared the effect of the three treatments (Ad-MMP-9, radiation, and a combination) on tumor growth. Tumors that received radiation (two doses of 5 Gy) showed tumor regression of >50% when compared with the control and Ad-CMV-treated tumors. Analysis of tumor size revealed that tumors injected with 5×10^8 plaque-forming units of Ad-MMP-9 displayed a more delayed tumor growth than those of control mice. These tumors were suppressed by nearly 40% to 45% when compared with the controls. However, the combined treatment of Ad-MMP-9 and radiation completely regressed tumor growth in all of the mice by the end of the experiment (after 8 weeks; Fig. 4A). Furthermore, to show the efficacy of the combined treatment, we also did another set of experiment where the animals were sacrificed after 15 days of the combined treatment.

Additionally, to show the efficiency of the treatments, we analyzed the activity of MMP-9 in the tumor tissues using zymography. The densitometric analysis showed that the irradiated tumors had a 2-fold to 3-fold increase in MMP-9 activity compared with the controls. In contrast, Ad-MMP-9

treatment reduced activity by 2-fold to 2.5-fold than the control. MMP-9 activity was further reduced by 4-fold to 5-fold even after only 15 days of treatment with Ad-MMP-9 plus radiation (Fig. 4B). Furthermore, we analyzed the tumor sections from control, Ad-CMV, Ad-MMP-9, irradiation, and

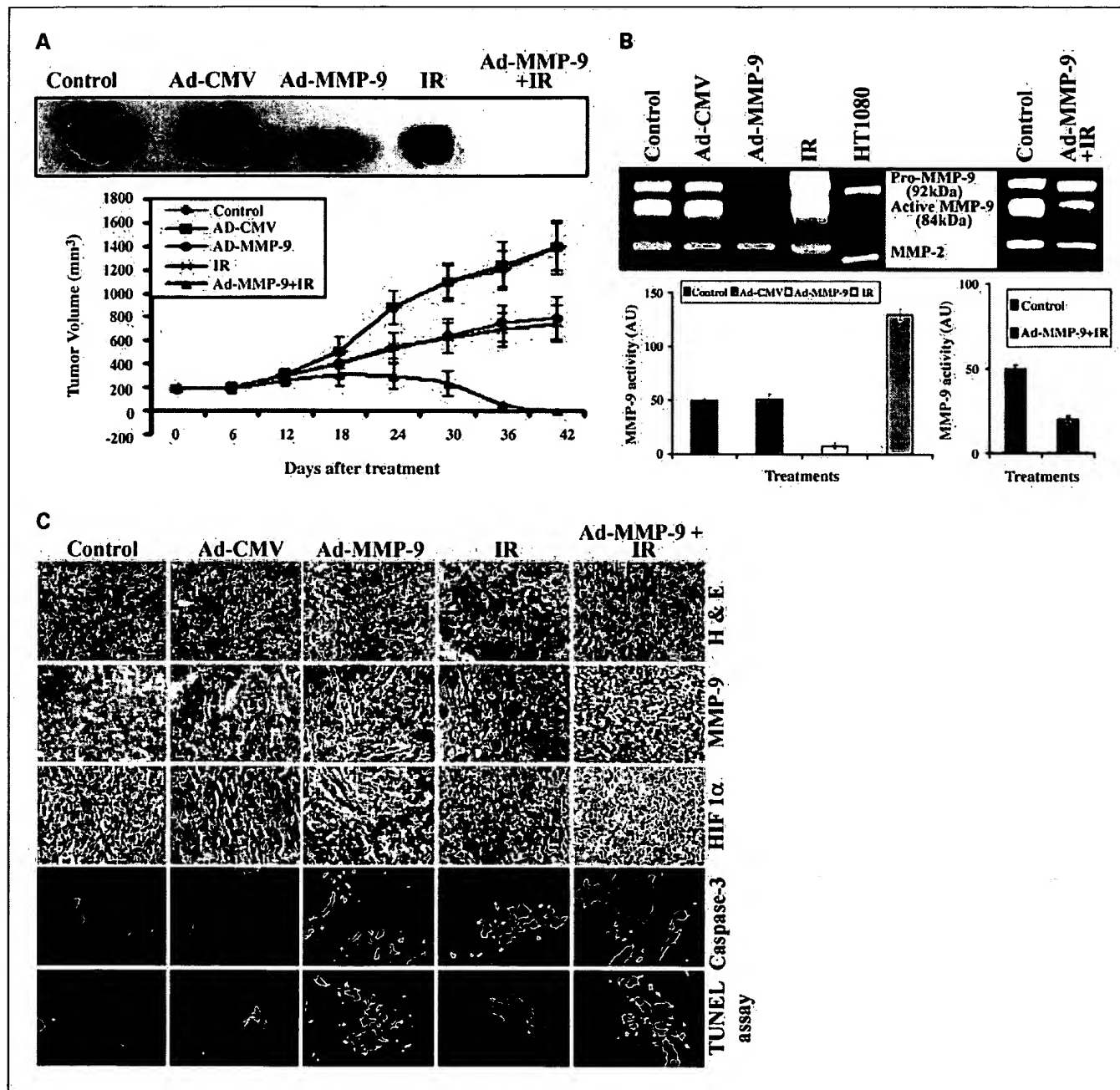


Fig. 4. MMP-9 and HIF1 α mediate the inhibition of tumor growth after treatment with Ad-MMP-9 plus radiation. **A**, representative tumors from animals treated with Ad-CMV, Ad-MMP-9, irradiation, and Ad-MMP-9 in combination with irradiation. Growth delay curve of tumors from animals treated with Ad-CMV, Ad-MMP-9, irradiation, and Ad-MMP-9 in combination with irradiation. Tumor size was measured using calipers as described in Materials and Methods. Finally, the tumor volume was calculated using the formula $V = \pi/6 (a \times b \times c)$. The data represent the mean \pm SD ($n = 5$) for each treatment at the said time point. **B**, MMP-9 activity was analyzed using gelatin zymography by loading equal amounts of protein from the tissue lysates from the tumors treated with Ad-MMP-9, irradiation, and controls. Additionally, the second panel in the zymogram shows MMP-9 activity in the tumor harvested after 15 d of the combination treatment compared with the control. MMP-9 activity is represented densitometrically. **C**, H&E staining and immunohistochemical analysis for MMP-9 and HIF1 α was done on paraffin-embedded breast tumor sections of mice treated with Ad-CMV, Ad-MMP-9, irradiation, and Ad-MMP-9 plus radiation using specific antibodies for these molecules. Paraffin-embedded breast tumor sections of mice treated with Ad-CMV, Ad-MMP-9, irradiation, and Ad-MMP-9 plus radiation were immunostained for proteolytically cleaved caspase-3 active subunits, which exist only when cells undergo apoptosis. TUNEL assay was done with paraformaldehyde-fixed, paraffin-embedded breast tumor sections as per the manufacturer's protocol.

Ad-MMP-9, plus radiation treatment groups for MMP-9 and HIF1 α using immunohistochemistry. We observed more apoptotic cells and necrotic areas in the sections from treated tumors compared with the control tumors. The sections from control and Ad-CMV–treated tumors revealed a highly aggressive tumor nature and many mitotic dividing cells (Fig. 4C). We observed significant expression of MMP-9 and HIF1 α in control, Ad-CMV, and radiation-treated tumor sections. However, expression levels were drastically reduced in breast tumor sections of mice treated with Ad-MMP-9 and Ad-MMP-9 plus radiation. After the *in vitro* studies for apoptosis, we analyzed the effect of these treatments *in vivo*. Paraffin-embedded breast tumor sections of mice treated with Ad-CMV, Ad-MMP-9, radiation, and Ad-MMP-9 plus radiation were immunostained for proteolytically cleaved active subunits of caspase-3, which exist only when cells undergo apoptosis. The combination-treated tumors showed more active subunits of caspase-3 compared with the controls and irradiation alone treated tumors, thereby suggesting more apoptosis in the combined treated tumors even at 15 days after treatment (Fig. 4C). In addition, TUNEL assay indicated DNA fragmentation, which is indicative of apoptotic cell population, in Ad-MMP-9–treated and irradiated tumors (Fig. 4C). In tumors treated with Ad-MMP-9 and radiation, we observed a significantly higher presence of DNA fragmentation compared with the controls. This high level of apoptosis accounts for the 50% to 60% regression of tumors after treatment with Ad-MMP-9 plus radiation.

Discussion

The goal of this study was to investigate the effect of combining MMP-9 inhibition along with radiation on orthotopic breast tumors. We found that Ad-MMP-9 treatment before radiation augmented the effects of radiation and successfully regressed tumors. In recent years, there has been a consensus that hypoxia can influence a broad spectrum of physiologic and pathologic cellular mechanisms (29). In particular, the combination of hypoxia gene therapy with ionizing radiation represents an exciting and promising approach to overcome and exploit resistant hypoxic tumor cells. Here, we also show that Ad-MMP-9 infection in irradiated cells decreased HIF 1, which is associated with reduction in sensitivity to radiation and causes disease failure after radiation therapy (30). We further show that Ad-MMP-9 infection augmented apoptosis in irradiated cells *in vitro* and *in vivo*. In our *in vitro* studies, we observed increases in HIF1 α , both at the mRNA expression and protein levels, in control and irradiated cells. However, in cells treated with Ad-MMP-9 alone and Ad-MMP-9 plus radiation, levels of HIF1 α were drastically reduced. Furthermore, the immunohistochemical analysis of tumor tissue sections supported the *in vitro* results. HIF1 is a key transcription factor that regulates the expression of a variety of genes, which control glycolysis, erythropoiesis, apoptosis, and angiogenesis (3). A direct correlation between tumor grade and HIF-1 expression in breast tumors has been shown (31). The role of HIF-1 in solid tumor growth is still not entirely clear, but previous work suggests that this transcription factor is necessary for the growth and angiogenesis of these tumors.

Radiation-induced MMP-9 leads to enhanced tumor growth and metastasis (32). Recent studies have implicated MMPs in

multiple roles, including tumor growth (33), regulation of apoptosis (34), and angiogenesis (35). Thus, the observed radiation-induced augmentation in MMP-9 activity is not only integral to tumor invasion, but may also aid survival in a relatively hostile setting. Our results show down-regulation of MMP-9 in irradiated breast cancer cells decreased MMP activity at both the mRNA and protein levels.

Ionizing radiation acts through the induction of double-strand breaks to DNA to induce elimination of cancerous cells via apoptosis (36). The efficiency of radiotherapy for cancer treatment is limited by toxic side effects, which impede dose escalation. Moreover, cancer cells often develop radioresistance mechanisms that are related to the DNA repair response. The aim of combining gene therapy and radiation is to strengthen the efficiency of radiation by inhibition of DNA repair, overcoming the clonogenic survival in irradiated cells and in turn apoptotic resistance. Transcription factors like NF- κ B and AP-1 are activated by DNA-damaging agents and could be involved in cell cycle arrest and prevention of apoptosis to allow DNA repair (9, 37). Not only does NF- κ B promote survival of cancer cells, but it also contributes to abnormal proliferation and metastasis (25, 38–40). Our Western immunoblot analysis showed a decrease in the translocation of NF- κ B subunits (p50 and p65) and AP-1 subunits (c-fos and Jun D) in the cells that received the combined treatment of Ad-MMP-9 and radiation. Furthermore, we did the electrophoretic mobility shift assay to analyze the protein-DNA interaction for NF- κ B and AP-1. The results indicated that in the case of cells treated with Ad-MMP-9 alone and Ad-MMP-9 combined with radiation, the protein-DNA interaction was reduced compared with the control and Ad-CMV–treated cells. This observation was supported by the supershift assay using specific antibodies against NF- κ B and AP-1, respectively (41).

Apoptosis is induced by different stimuli, such as death ligands and chemotherapeutic drugs that lead to the activation of caspases (42). Recently, researchers have shown that inhibition of NF- κ B activity restores sensitivity to Fas-mediated

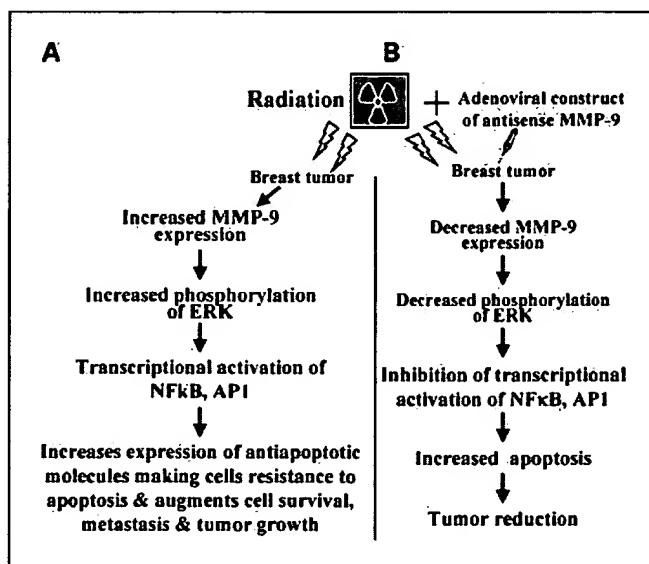


Fig. 5. Schematic representations of the effect of irradiation (A) and Ad-MMP-9 in combination with irradiation (B) on breast tumor growth.

apoptosis (43, 44). Treatment of breast cancer cells with Ad-MMP-9, radiation, or both induced caspase-dependent apoptosis, which is associated with the activation of several individual caspases. Our results show that the caspase-10 pathway may be responsible for induction of apoptosis where Fas and Fas-L are involved at the cell membrane. The Fas–Fas-L death pathway is an important mediator of apoptosis. Deregulation of the Fas pathway is reported to be involved in the immune escape of breast cancer and the resistance to anticancer drugs (45). It has been reported that the resistance of leukemic eosinophils to Fas-mediated apoptosis is due to induced NF-κB activation (46). The results of the present study corroborate the findings of these studies; we observed that the reduction in NF-κB activation led to increased expression of Fas-L and directed apoptosis via the Fas–Fas-L mediated pathway. This led to the activation of caspase-10, a death effector domain-containing initiator caspase, which, in turn, cleaves or activates caspase-3 and caspase-7 (effector caspases capable of cleaving PARP-1). Caspase-3 immunofluorescent staining and TUNEL assay revealed the increased apoptosis in the tumors treated with Ad-MMP-9 and radiation compared with the control and irradiation alone–treated tumors. The TUNEL assay using the tissue sections shows synergistic effect when Ad-MMP-9 was given in combination with radiation. Furthermore, the clonogenic survival assay supported the results obtained involving activation of apoptotic cascade.

We suggest a new strategy for improving the radiosensitivity of breast tumors in treating breast cancer through down-regulation of MMP-9 using adenoviral constructs of antisense MMP-9 before radiation (Fig. 5). The decreased MMP-9 activity of the tumors inhibited phosphorylation of ERK, which reduced the transcriptional activity of NF-κB and AP-1. This in turn led to increased apoptosis, thereby regressing the tumor. The precise and rapid propagation of this signaling cascade demands strict and flexible regulatory processes that still remain unexplored. The nature of the regulators involved may have therapeutic implications. Our schematic is based on our *in vitro* and *in vivo* model data showing an increase in apoptosis and tumor reduction.

In summary, the present study indicates that MMP-9 might be a potential target candidate as an inducer of the HIF-regulated molecular cascade. Down-regulating MMP-9 activity augments the effect of radiotherapy by directly or indirectly reducing HIF transcription machinery. Because HIF1α is involved in the pathogenesis of several human diseases (e.g., myocardial and cerebral ischemia, pulmonary hypertension), Ad-MMP-9 may have a future therapeutic role as an HIF1α activity inhibitor.

Acknowledgments

We thank Shellee Abraham for preparing the manuscript, Diana Meister and Sushma Jasti for reviewing the manuscript, and Noorjehan Ali for technical assistance.

References

- Brown JM, Giaccia AJ. The unique physiology of solid tumors: opportunities (and problems) for cancer therapy. *Cancer Res* 1998;58:1408–16.
- Chakraborty G, Rangaswami H, Jain S, Kundu GC. Hypoxia regulates cross-talk between Syk and Lck leading to breast cancer progression and angiogenesis. *J Biol Chem* 2006;281:11322–31.
- Semenza GL. Hypoxia-inducible factor 1: master regulator of O₂ homeostasis. *Curr Opin Genet Dev* 1998;8:588–94.
- Unruh A, Ressel A, Mohamed HG, et al. The hypoxia-inducible factor-1α is a negative factor for tumor therapy. *Oncogene* 2003;22:3213–20.
- Rofstad EK. Microenvironment-induced cancer metastasis. *Int J Radiat Biol* 2000;76:589–605.
- Semenza GL. Hypoxia, clonal selection, and the role of HIF-1 in tumor progression. *Crit Rev Biochem Mol Biol* 2000;35:71–103.
- Cummins EP, Taylor CT. Hypoxia-responsive transcription factors. *Pflugers Arch* 2005;450:363–71.
- Karin M, Greten FR. NF-κB: linking inflammation and immunity to cancer development and progression. *Nat Rev Immunol* 2005;5:749–59.
- Russell JS, Raju U, Gumin GJ, et al. Inhibition of radiation-induced nuclear factor-κB activation by an anti-Ras single-chain antibody fragment: lack of involvement in radiosensitization. *Cancer Res* 2002;62:2318–26.
- Jung M, Dritschilo A. NF-κB signaling pathway as a target for human tumor radiosensitization. *Semin Radiat Oncol* 2001;11:346–51.
- Smirnov AS, Ruzov AS, Budanov AV, Prokhortchouk AV, Ivanov AV, Prokhortchouk EB. High constitutive level of NF-κB is crucial for viability of adenocarcinoma cells. *Cell Death Differ* 2001;8:621–30.
- Lindholm PF, Bub J, Kaul S, Shidham VB, Kajdacsy-Balla A. The role of constitutive NF-κB activity in PC-3 human prostate cancer cell invasive behavior. *Clin Exp Metastasis* 2000;18:471–9.
- Giri DK, Aggarwal BB. Constitutive activation of NF-κB causes resistance to apoptosis in human cutaneous T cell lymphoma HuT-78 cells. Autocrine role of tumor necrosis factor and reactive oxygen intermediates. *J Biol Chem* 1998;273:14008–14.
- Karin M, Liu Z, Zandi E. AP-1 function and regulation. *Curr Opin Cell Biol* 1997;9:240–6.
- Jacobs-Helber SM, Wickrema A, Birrer MJ, Sawyer ST. AP-1 regulation of proliferation and initiation of apoptosis in erythropoietin-dependent erythroid cells. *Mol Cell Biol* 1998;18:3699–707.
- Blasi F. Proteolysis, cell adhesion, chemotaxis, and invasiveness are regulated by the u-PA-u-PAR-PAI-1 system. *Thromb Haemost* 1999;82:298–304.
- Bradbury D, Clarke D, Seedhouse C, Corbett L, Stocks J, Knox A. Vascular endothelial growth factor induction by prostaglandin E2 in human airway smooth muscle cells is mediated by E prostanoid EP2/EP4 receptors and SP-1 transcription factor binding sites. *J Biol Chem* 2005;280:29993–30000.
- Kumar A, Collins H, Van TJ, Scholefield JH, Watson SA. Effect of preoperative radiotherapy on matrix metalloproteinase gene expression in rectal cancer. *Eur J Cancer* 2002;38:505–10.
- Stetler-Stevenson WG, Yu AE. Proteases in invasion: matrix metalloproteinases. *Semin Cancer Biol* 2001;11:143–52.
- Lakka SS, Rajan M, Gondi CS, et al. Adenovirus-mediated expression of antisense MMP-9 in glioma cells inhibits tumor growth and invasion. *Oncogene* 2002;21:8011–9.
- Bacqueville D, Deleris P, Mende C, et al. Characterization of a G protein-activated phosphoinositide 3-kinase in vascular smooth muscle cell nuclei. *J Biol Chem* 2001;276:22170–6.
- Lakka SS, Jasti SL, Kyritsis AP, et al. Regulation of MMP-9 (type IV collagenase) production and invasiveness in gliomas by the extracellular signal-regulated kinase and jun amino-terminal kinase signaling cascades. *Clin Exp Metastasis* 2000;18:245–52.
- Raju U, Nakata E, Mason KA, Ang KK, Milas L. Flavopiridol, a cyclin-dependent kinase inhibitor, enhances radiosensitivity of ovarian carcinoma cells. *Cancer Res* 2003;63:3263–7.
- Moeller BJ, Dreher MR, Rabbani ZN, et al. Pleiotropic effects of HIF-1 blockade on tumor radiosensitivity. *Cancer Cell* 2005;8:99–110.
- Magne N, Toillon RA, Bottero V, et al. NF-κB modulation and ionizing radiation: mechanisms and future directions for cancer treatment. *Cancer Lett* 2006;231:158–68.
- Poynter ME, Janssen-Heininger YM, Budermann Hoffmann S, Taatjes DJ, Mossman BT. Measurement of oxidant-induced signal transduction proteins using cell imaging. *Free Radic Biol Med* 1999;27:1164–72.
- Wang T, Hu YC, Dong S, et al. Co-activation of ERK, NF-κB, GADD45β in response to ionizing radiation. *J Biol Chem* 2005;280:12593–601.
- Himelstein BP, Canete-Soler R, Bernhard EJ, Muschel RJ. Induction of fibroblast 92 kDa gelatinase/type IV collagenase expression by direct contact with metastatic tumor cells. *J Cell Sci* 1994;107:477–86.
- Shih SC, Claffey KP. Hypoxia-mediated regulation of gene expression in mammalian cells. *Int J Exp Pathol* 1998;79:347–57.
- Harrison LB, Chadha M, Hill RJ, Hu K, Shasha D. Impact of tumor hypoxia and anemia on radiation therapy outcomes. *Oncologist* 2002;7:492–508.
- Kimbro KS, Simons JW. Hypoxia-inducible factor-1 in human breast and prostate cancer. *Endocr Relat Cancer* 2006;13:739–49.
- Jadhav U, Mohanam S. Response of neuroblastoma cells to ionizing radiation: modulation of *in vitro* invasiveness and angiogenesis of human microvascular endothelial cells. *Int J Oncol* 2006;29:1525–31.
- Coussens LM, Tinkle CL, Hanahan D, Werb Z. MMP-9 supplied by bone marrow-derived cells contributes to skin carcinogenesis. *Cell* 2000;103:481–90.
- Bergers G, Brekken R, McMahon G, et al. Matrix metalloproteinase-9 triggers the angiogenic switch during carcinogenesis. *Nat Cell Biol* 2000;2:737–44.

35. Martin DC, Sanchez-Sweatman OH, Ho AT, Inderdeo DS, Tsao MS, Khokha R. Transgenic TIMP-1 inhibits simian virus 40 T antigen-induced hepatocarcinogenesis by impairment of hepatocellular proliferation and tumor angiogenesis. *Lab Invest* 1999;79:225–34.

36. Li L, Story M, Legerski RJ. Cellular responses to ionizing radiation damage. *Int J Radiat Oncol Biol Phys* 2001;49:1157–62.

37. Takeuchi K, Motoda Y, Ito F. Role of transcription factor activator protein 1 (AP-1) in epidermal growth factor-mediated protection against apoptosis induced by a DNA-damaging agent. *FEBS J* 2006;273:3743–55.

38. Aggarwal BB, Shishodia S, Takada Y, et al. Curcumin suppresses the paclitaxel-induced nuclear factor- κ B pathway in breast cancer cells and inhibits lung metastasis of human breast cancer in nude mice. *Clin Cancer Res* 2005;11:7490–8.

39. Helbig G, Christopherson KW, Bhat-Nakshatri P, et al. NF- κ B promotes breast cancer cell migration and metastasis by inducing the expression of the chemokine receptor CXCR4. *J Biol Chem* 2003;278: 21631–8.

40. Shah N, Thomas T, Shirahata A, Sigal LH, Thomas TJ. Activation of nuclear factor κ B by polyamines in breast cancer cells. *Biochemistry* 1999;38: 14763–74.

41. Ho E, Ames BN. Low intracellular zinc induces oxidative DNA damage, disrupts p53, NF κ B, AP-1 DNA binding, and affects DNA repair in a rat glioma cell line. *Proc Natl Acad Sci USA* 2002;99:16770–5.

42. Nicholson DW. Caspase structure, proteolytic substrates, and function during apoptotic cell death. *Cell Death Differ* 1999;6:1028–42.

43. Meli M, D'Alessandro N, Tolomeo M, Rausa L, Notarbartolo M, Dusonchet L. NF- κ B inhibition restores sensitivity to Fas-mediated apoptosis in lymphoma cell lines. *Ann N Y Acad Sci* 2003;1010: 232–6.

44. Shimada K, Nakamura M, Ishida E, Kishi M, Matsuyoshi S, Konishi N. The molecular mechanism of sensitization to Fas-mediated apoptosis by 2-methoxyestradiol in PC3 prostate cancer cells. *Mol Carcinog* 2004;39:1–9.

45. Kim R, Tanabe K, Emi M, Uchida Y, Toge T. Death receptor-dependent and -independent pathways in anticancer drug-induced apoptosis of breast cancer cells. *Oncol Rep* 2003;10:1925–30.

46. Qin Y, Camoretti-Mercado B, Blokh L, Long CG, Ko FD, Hamann KJ. Fas resistance of leukemic eosinophils is due to activation of NF- κ B by Fas ligation. *J Immunol* 2002;169:3536–44.



BASIC RESEARCH

Enhanced therapeutic effects for human pancreatic cancer by application K-ras and IGF-IR antisense oligodeoxynucleotides

Yong-Mei Shen, Xiao-Chun Yang, Chen Yang, Jun-Kang Shen

Yong-Mei Shen, Radioimmunoassay Center & Clinical Laboratory, the Second Affiliated Hospital of Soochow University, Suzhou 215004, Jiangsu Province, China

Xiao-Chun Yang, Jun-Kang Shen, Department of MRI, the Second Affiliated Hospital of Soochow University, Suzhou 215004, Jiangsu Province, China

Chen Yang, Radioimmunoassay Center, the Municipal Hospital of Suzhou, Suzhou 215002, Jiangsu Province, China

Author contributions: Shen YM, Yang XC and Yang C contributed equally to this work; Shen YM, Yang XC, Yang C designed research and performed research; Shen YM, Yang XC, Yang C and Shen JK analyzed data; and Shen YM and Yang XC wrote the paper.

Supported by Social development foundation of Suzhou, China, No. SZD0614; Young teacher foundation of Soochow University; Foundation of health department of Jiangsu Province, China, No. Z200622

Correspondence to: Dr. Xiao-Chun Yang, Department of MRI, the Second Affiliated Hospital of Soochow University, Suzhou 215004, Jiangsu Province, China. szyxc@yahoo.com.cn

Telephone: +86-512-67783460 Fax: +86-512-68284303

Received: April 9, 2008

Revised: July 21, 2008

Accepted: July 28, 2008

Published online: September 7, 2008

Abstract

AIM: To investigate the combined effects of K-ras antisense oligodeoxynucleotide (K-ras ASODN) specific to GTT point mutation at codon 12 and type I insulin-like growth factor receptor (IGF-IR) antisense oligodeoxynucleotide (IGF-IR ASODN) on proliferation and apoptosis of human pancreatic cancer Patu8988 cells *in vitro* and *in vivo*.

METHODS: K-ras gene point mutation and its style at codon 12 of human pancreatic cancer cell line Patu8988 were detected by using polymerase chain reaction with special sequence primers (PCR-SSP) and sequence analysis. According to the mutation style, K-ras mutation ASODN specific to K-ras point mutation at codon 12 was designed and composed. After K-ras ASODN and IGF-IR ASODN treated on Patu8988 cells respectively or cooperatively, the proliferation and morphological change of Patu8988 cells were analyzed by 3-(4,5-dimethylthiazol-2-yl)-2,5-diphenyltetrazolium bromide (MTT) assay, colony forming assay and

transmission electron microscopy; the expression of K-ras and IGF-IR mRNA and protein in the treated cells was measured by reverse-transcript polymerase chain reaction (RT-PCR) and flow cytometry respectively; apoptosis was determined by flow cytometry. The combined antitumor activity of K-ras ASODN and IGF-IR ASODN was evaluated in BALB/c nude mice bearing human pancreatic cancer inoculated with Patu8988 cells.

RESULTS: The results of PCR-SSP and sequence analysis showed that the human pancreatic cancer cell line Patu8988 had point mutation at codon 12, and the mutation style was GGT→GTT. 2-32 µg/mL K-ras ASODN and 2-32 µg/mL IGF-IR ASODN could inhibit Patu8988 cells' growth, induce apoptosis and decrease the expression of K-ras and IGF-IR mRNA and protein alone. However, there was much more effective inhibition of growth and induction of apoptosis by their combination than by each one alone. In tumor bearing mice, the combination of K-ras ASODN and IGF-IR ASODN showed a significant inhibitory effect on the growth of transplanted pancreatic cancer, resulting in a statistically significant difference compared with each alone.

CONCLUSION: It has been found that K-ras ASODN combined with IGF-IR ASODN could cooperatively inhibit the growth of Patu8988 cells, and induce their apoptosis *via* reinforcing specific down regulation of K-ras and IGF-IR mRNA and protein expression.

© 2008 The WJG Press. All rights reserved.

Key words: Pancreatic cancer; Antisense oligodeoxynucleotide; K-ras; Type I insulin-like growth factor receptor; Patu8988

Peer reviewer: Minoti Vivek Apte, Associate Professor, Pancreatic Research Group, South Western Sydney Clinical School, the University of New South Wales, Level 2, Thomas and Rachel Moore Education Centre, Liverpool Hospital, New South Wales 2170, Liverpool, Australia

Shen YM, Yang XC, Yang C, Shen JK. Enhanced therapeutic effects for human pancreatic cancer by application K-ras and IGF-IR antisense oligodeoxynucleotides. *World J Gastroenterol* 2008; 14(33): 5176-5185 Available from: URL: <http://www.wjgnet.com/1007-9327/14/5176.asp> DOI: <http://dx.doi.org/10.3748/wjg.14.5176>

INTRODUCTION

Pancreatic cancer is the fatal cancer of the digestive system with the worst prognosis. The 5-year survival rate is approximately 1%-2%, and the median survival time after diagnosis ranges only 4-6 mo^[1-3]. The reasons for poor prognosis include: (1) the difficulty of early diagnosis due to its anatomical location, and lack of specific early syndromes; (2) the high potential to infiltrate to the surrounding tissues and metastasize even in the early stage; and (3) the poor responsiveness to conventional treatments such as chemotherapy, radiotherapy and immunotherapy^[4-6]. Surgery represents the only opportunity for possible cure, but it is restricted to early stage pancreatic cancer and most patients who undergo tumor resection show recurrence or distant metastases and die within a few years. At least, at the present time, an emphasis on early diagnosis alone may not be sufficient for significant improvement in the current poor prognosis of pancreatic cancer, which necessitates the search for novel treatment strategies to improve the prognosis.

Previous studies have demonstrated that a high percentage of pancreatic cancers harbors *K-ras* gene point mutation and overexpresses insulin-like growth factor receptor type 1 (IGF-IR)^[7-11]. These alterations may together contribute to the progression and aggressiveness of pancreatic cancer from different pathways. Consequently, targeting expression of *K-ras* or IGF-IR has a potential value in pancreatic cancer therapy, and has led to the development of new therapeutic strategies based on the use of agents able to selectively inhibit targeted gene expression. In particular, antisense oligodeoxynucleotides (ASODNs) have proved their efficacy as targeted therapy, and are able to modulate target protein expression in pancreatic cancer studies^[12-15]. In the practical application of the ASODN approach, many key problems need to be solved: selection of a single agent does not seem particularly promising because of the multigenic alterations of pancreatic cancer; finding a targeting site of *K-ras* mRNA or IGF-IR mRNA that is likely to be accessible to ASODNs; selection of an adaptable vector for mediating ASODNs; optimization of transfection concentration in a cell line, etc. Based on these considerations, we used polymerase chain reaction with special sequence primers (PCR-SSP) and sequence analysis to detect a *K-ras* point mutation at codon 12, and its mutation style on pancreatic cancer Patu8988 cells, designed and prepared ASODN (*K-ras* ASODN) specific for the *K-ras* point mutation at codon 12, and then combined it with strongest efficient IGF-IR ASODN designed by Resnicoff *et al*^[16] to transfet pancreatic cancer Patu8988 cells with highly efficient vector Lipofectamine 2000. 3-(4,5-dimethylthiazol-2-yl)-2,5-diphenyltetrazolium bromide (MTT) assay, reverse-transcript polymerase chain reaction (RT-PCR), flow cytometry and transmission electron microscope were used to evaluate the effects of cell proliferation, apoptosis and target gene expression. Therapeutic

efficacy of the combination treatment was also evaluated in xenografts.

MATERIALS AND METHODS

Cell culture

Human pancreatic cancer cell lines Patu8988 and BXPC-3 used in this study were preserved in our laboratory. The cells were grown in RPMI 1640 medium (Gibco, USA) supplemented with 10% heat-inactivated fetal bovine serum (Sijiqing, Hangzhou, China), 5 mmol/L HEPES, 100 U/mL penicillin and 100 U/mL streptomycin in 5% atmospheric CO₂ at 37°C. Cells were passaged every 3 d, checked routinely, and found to be free of contamination. When cells grew to 75% confluence, they were digested and used for *in vitro* and *in vivo* studies.

K-ras gene point mutation at codon 12 detected by PCR-SSP and sequence analysis

Genomic DNAs for Patu8988 cells and BXPC-3 cells were extracted according to the protocol. With regard to the sequences of *K-ras* cDNA in Genbank and the three high frequency mutation styles (CGT, GTT and GAT) at codon 12, three kinds of special sequence primers (SSP) for polymerase chain reaction were designed to detect *K-ras* gene point mutation at codon 12 for Patu8988 cells and BXPC-3 cells. Primers were as following: R1: 5'-GGTAGTTGG-AGCTC-3'; R2: 5'-GTAGTTGGAGCTGT-3'; R3: 5'-GTAGITGGAGCTGA-3'; R4: 5'-CTATTGTTGGA TCATATTG-3'. The pairing of R1-R4 amplified CGT mutation with a 89 base pair fragment; the pairing R2-R4 amplified GTT mutation with a 88 base pair fragment; the pairing R3-R4 amplified GAT mutation with a 88 base pair fragment. The amplification products were loaded on 8% acrylamide gels, and stained with ethidium bromide to detect mutation styles. In addition, *K-ras* gene was amplified from Patu8988 cells and BXPC-3 cells using RT-PCR, and the PCR products were directly sequenced.

Proliferation assay of Patu8988 cells treated with *K-ras* ASODN or IGF-IR ASODN alone

Based on the results of PCR-SSP and sequence analysis, the antisense phosphorothioate oligodeoxynucleotides 5'-TACGCCAACAGCTCCAAC-3' (*K-ras* ASODN) specific to the *K-ras* gene point mutation at codon 12 were designed and synthesized. The antisense phosphorothioate oligodeoxynucleotides 5'-TCCTCCGGAGGCCAGACTT-3' (IGF-IR ASODN) specific to IGF-IR gene were synthesized according to the report from Resnicoff *et al*^[16]. Exponentially growing Patu8988 cells at 1 × 10⁵/well were seeded in 96-well microtiter plate, and treated with *K-ras* ASODN or IGF-IR ASODN mediated by LipofectamineTM 2000 at concentration of 2-32 mg/L for 24, 48, 72 and 96 h. The culture medium was changed every 24 h with fresh RPMI 1640 medium, which contained the same

concentration of K-ras ASODN or IGF-IR ASODN. The control cultures were left untreated at 37°C for the same period of time, with triplicate wells for each concentration. After incubating for 24, 48, 72 and 96 h, 20 μ L of 5 g/L MTT (Sigma, USA) in PBS was added to each well, followed by incubation for 4 h at 37°C. Formazan crystals were dissolved in DMSO for 15 min at 37°C. Absorbance was determined with an enzyme-linked immunosorbent assay reader at 570 nm. The cell proliferation curves were drawn according to the absorbance. The optimal concentration able to inhibit cell growth was selected for further experiments.

Proliferation assay of Patu8988 cells treated with combination of K-ras ASODN and IGF-IR ASODN

Patu8988 cells were seeded in a 96-well plate at a concentration of 1×10^5 /well, and divided into three groups: (1) 16 mg/L K-ras ASODN group; (2) 16 mg/L IGF-IR ASODN group; (3) 16 mg/L K-ras ASODN + 16 mg/L IGF-IR ASODN group. The cell cultures were measured for cell proliferation at different time points (0, 24, 48, 72 and 96 h after transfection) using MTT assay as described above. The cell proliferation curves were drawn according to the absorbance.

Apoptosis detection by annexin V-FITC/PI dual staining

Cells at the concentration of 1×10^5 /mL were plated in 6-well plates, divided into three groups as described above. After being incubated for 48 h at 37°C, cells were harvested by trypsinization and rinsed with cold PBS twice. After centrifugation, cells were suspended by 250 μ L conjugated buffer solution and then treated with 5 μ L Annexin V-FITC and 10 μ L propidium iodide (PI) for 15 min in the dark at room temperature. Finally, each sample was added into 300 μ L of conjugated buffer solution and analyzed with flow cytometry. The experiments were performed in triplicate and the results were given as mean \pm SE.

K-ras or IGF-IR protein expression detected by flow cytometry

Patu8988 cells, treated as described above, were removed from the plate by brief trypsinization with 0.25% trypsin, and then washed with PBS twice, stained with primary K-ras Ab or IGF-IR Ab, followed by FITC-conjugated goat anti-mouse IgG. After two rinses with PBS containing 2% FBS, these cells were analyzed with flow cytometry. Controls consisted of incubation with no antibodies or incubation with only the secondary antibody. The experiment was repeated three times.

K-ras or IGF-IR mRNA expression detected by semi-quantitative RT-PCR

Cells were plated in 6-well plates and performed as described above. Total cellular RNA was extracted by using Trizol Reagent (Invitrogen, USA) according to the manufacturer's instructions. The purity and concentration were determined by measuring the absorbance (A) at 260 nm and 280 nm (A_{260}/A_{280}). To

generate first-strand cDNA, an oligo (dT) 18 was used as primer, and 2 μ g RNA was reverse-transcribed in the light of MMLV First Strand cDNA Synthesis Kit (Fermentas, USA) protocols. Amplification of human β -actin served as an internal control. The primers used were 5'-GGACCTGACTGACTACCTC-3' (forward) and 5'-TCATACTCCTGCTGCTG-3' (reverse). The amplification products were 540 bp. The primers for K-ras were 5'-CGCGGATCCATGACTGAATATAACTTGTG-3' (forward) and 5'-CGCAAGCTT TTACATAATTACACACTTGT-3' (reverse). The amplification products were 585 bp. The primers for IGF-IR were 5'-CCAAAATGAAAGCCGAGAAG-3' (forward) and 5'-TGCAGCTGTGGATATCGATG-3' (reverse). The amplification products were 300 bp. K-ras was amplified 35 cycles under the following conditions: denaturing at 94°C for 5 min followed by 94°C for 1 min, annealing at 51°C for 30 s and extension at 72°C for 1 min; the final extension was at 72°C for 10 min. IGF-IR gene and β -actin were amplified 30 cycles under the following conditions: denaturing at 94°C for 5 min followed by 94°C for 1 min, annealing at 55°C for 1 min and extension at 72°C for 90 s; the final extension was at 72°C for 10 min. PCR products were separated in 1.5% agarose gels, stained with ethidium bromide, and visualized by UV absorption. Densitometric scanning of the bands was performed, and the relative amount of each gene mRNA expression was estimated by normalization to the β -actin mRNA detected in the same sample.

Transmission electron microscopic examination

Patu8988 cells treated with the combination of K-ras ASODN and IGF-IR ASODN for 48 h were harvested, and washed in PBS. The cell pellets were prefixed in 2.5% glutaraldehyde, postfixed in 1% osmic acid, dehydrated in gradient acetone and embedded in the resin. Ultrathin sections were cut, stained with lead citrate and assessed for the morphological changes under transmission electron microscope.

Colony assays

Twenty Patu8988 cells treated with 16 mg/L K-ras ASODN, 16 mg/L IGF-IR ASODN or 16 mg/L K-ras ASODN + 16 mg/L IGF-IR ASODN were seeded in 6-well plate and cultured in 5% atmospheric CO₂ at 37°C for 2 wk. The control was with the same volume of culture medium.

Treatment in vivo

To investigate whether the combination of K-ras ASODN with IGF-IR ASODN would alter the tumorigenicity of Patu8988, male 4-wk-old BALB/c nude mice were purchased from the Animal Center of Shanghai. 1×10^7 cells in 0.1 mL PBS were injected subcutaneously into the right flank of nude mice. Fourteen days later, 16 mice with about the same tumor size were divided into four groups randomly. Intratumoral injections were given with K-ras ASODN, IGF-IR ASODN or K-ras ASODN + IGF-IR

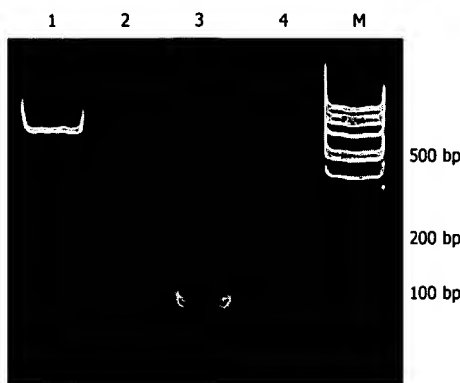


Figure 1 Detection of K-ras point mutation at 12 codon and its style in pancreatic cancer cell line Patu8988 by PCR-SSP. 1: β -actin; 2: R1-R4 pairing (CGT mutation); 3: R2-R4 pairing (GTT mutation); 4: R3-R4 pairing (GAT mutation); M: 100 bp DNA marker.

ASODN, and the control with 100 μ L physiological saline. The injection was repeated every 48 h and 5 times in all. Tumor sizes were measured every 7 d and calculated by the formula: volume (mm^3) = 1/2(width) 2 \times length. After a 49-d follow-up period, mice were sacrificed. The tumors were removed, fixed by 4% polyformaldehyde, paraffin embedded and sectioned for immunohistochemical analysis.

Statistical analysis

All experiments were performed in triplicate and data were expressed as mean \pm SD. Statistical analyses were conducted by one-factor analysis of variance and performed with SPSS 10.0 software. $P < 0.05$ was considered statistically significant.

RESULTS

K-ras point mutation at codon 12 of Patu8988 cell line

Detection of K-ras point mutation at codon 12 in the pancreatic cancer cell line Patu8988 is shown as Figure 1. The pairing R2-R4 had the amplification product of GTT mutation with an 88 bp fragment. But, the pairings of R1-R4 and R3-R4 had no amplification product of any mutation. Therefore, K-ras point mutation at codon 12 was found in pancreatic cancer cell line Patu8988, and the mutation style was GTT; no other mutation styles were found. For wild type pancreatic cancer cell line BXPC-3, no amplification products were found in pairings of R1-R4, R2-R4 and R3-R4. The direct sequencing results were consistent with the results from the PCR-SSP (Figure 2).

Inhibition of Patu8988 cell proliferation by K-ras ASODN and IGF-IR ASODN alone or combination

As shown in Figure 3A and B, when Patu8988 cells were exposed to K-ras ASODN and IGF-IR ASODN respectively, the growth of the cells was suppressed as compared to untreated cells ($P < 0.01$) except at the concentration of 2 mg/L. Moreover, when cells were exposed to different doses of K-ras ASODN

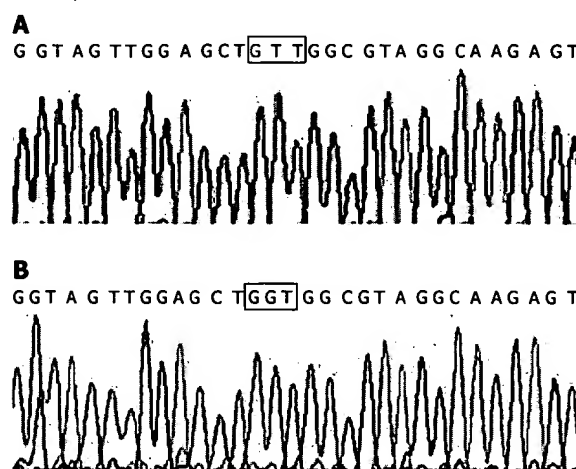


Figure 2 Sequence analysis of pancreatic cancer cell line Patu8988 (A) and BXCP-3 (B). Patu8988 had K-ras point mutation at codon 12 and its style was GGT \rightarrow GTT (indicated in the square). BXCP-3 was a K-ras gene wild type cell line with normal GGT at codon 12; No other mutation styles were found.

and IGF-IR ASODN individually, growth inhibition was dose dependent: obvious inhibition was seen at the concentration of 16 mg/L, and the greatest effect was seen at a concentration of 32 mg/L. However, no statistical significance was found between 16 mg/L and 32 mg/L ($P > 0.05$). So, combination treatment with 16 mg/L K-ras ASODN and 16 mg/L IGF-IR ASODN was employed, and the ASODNs were transfected into Patu8988 cells for 24, 48, 72 and 96 h. Patu8988 cell growth was inhibited at a significantly higher rate in the combination treatment than that in K-ras ASODN or IGF-IR ASODN alone at different transfection times ($P < 0.01$) (Figure 3C). The inhibition peak was reached at 48 h. Subsequently, the inhibition ability wore off, and the tumor cells recovered proliferation. Further experiments were conducted to assess the combined effects on the expression of K-ras or IGF-IR mRNA and protein, apoptosis, clone formation and tumor growth inhibition *in vivo* with the combination treatment of 16 mg/L K-ras ASODN and 16 mg/L IGF-IR ASODN at 37°C for 48 h.

Inhibition of colony formation by K-ras ASODN and IGF-IR ASODN alone or combination

Patu8988 cell proliferation treated in different groups was analyzed by soft agar colony formation assays. The average numbers of colonies in the control, K-ras ASODN, IGF-IR ASODN and combination group were 18.8, 11, 12 and 3, respectively. The Patu8988 cells in the combination groups formed significantly fewer colonies (6 fold decrease) in soft agar than those in the control groups did ($P < 0.05$ vs control). However, there were no statistical differences between K-ras ASODN groups and IGF-IR ASODN groups, although the number of colonies of IGF-IR ASODN groups was a little larger than those of K-ras ASODN groups ($P > 0.05$). At the same time, we noticed that the size of most of the colonies in the combination groups were much smaller than those in the control groups.

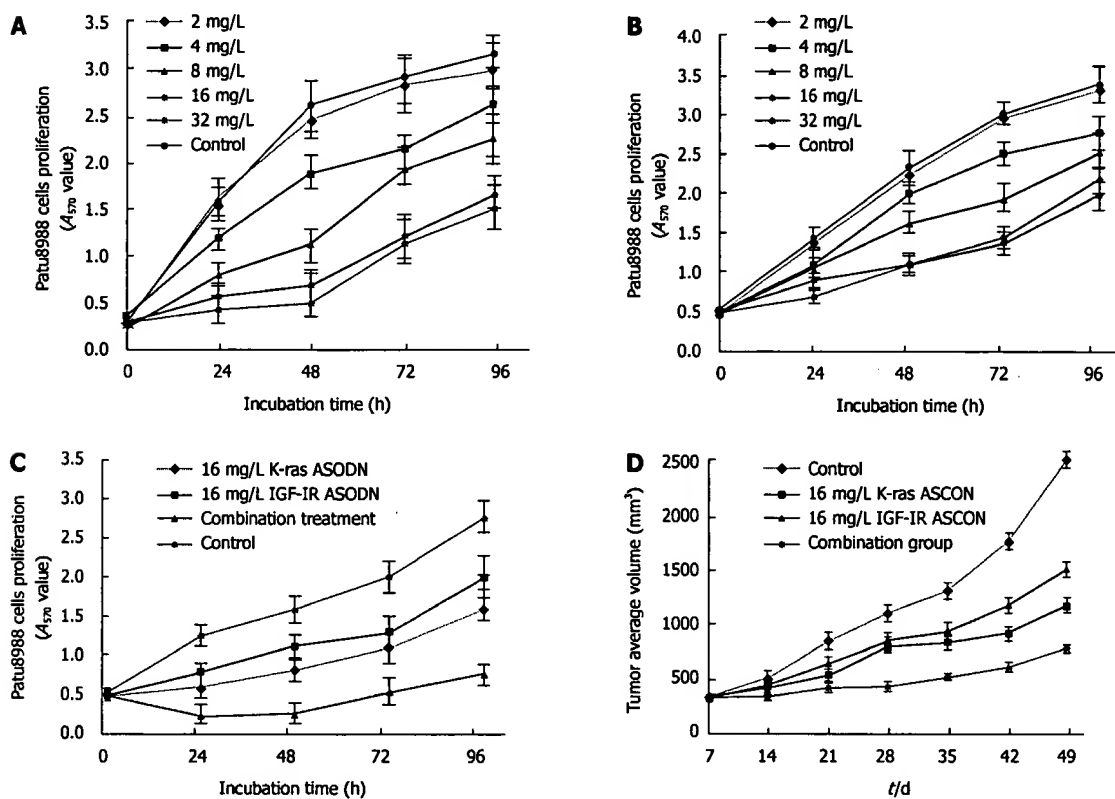


Figure 3 Each value represents the mean \pm SD from triplicate determinations. **A:** Growth curves of Patu8988 cells treated with different concentrations of K-ras ASODN at different incubation times; **B:** Growth curves of Patu8988 cells treated with different concentrations of IGF-IR ASODN at different incubation times; **C:** Growth curves of Patu8988 cells treated with the combination treatment of 16 mg/L K-ras ASODN and 16 mg/L IGF-IR ASODN at different incubation times; **D:** The inhibition effect of the combination treatment with K-ras ASODN and IGF-IR ASODN on tumor growth in nude mice.

Table 1 Protein expression for K-ras and IGF-IR on Patu8988 cells detected by flow cytometry (%)

Groups	Positive rate	
	K-ras protein	IGF-IR protein
K-ras ASODN	25.95 \pm 0.18 ^b	85.25 \pm 0.99
IGF-IR ASODN	69.18 \pm 0.87	40.78 \pm 1.42 ^b
Combination	19.69 \pm 1.15 ^b	38.25 \pm 1.22 ^b
Control	76.15 \pm 1.62	91.53 \pm 1.62

All values are presented as mean \pm SD of triplicate determinations. ^bP < 0.01 vs control group.

Apoptotic influence of Patu8988 cells treated with combination treatment of K-ras ASODN and IGF-IR ASODN

To further confirm the occurrence of apoptosis, we subjected the ASODNs-treated cells (48 h of ASODNs exposure) to annexin V-FITC/PI dual staining followed by flow cytometry analyses. The ratios of apoptosis cells were 21.54% \pm 0.93%, 12.76% \pm 0.74%, 8.43% \pm 0.51% and 1.60% \pm 0.19% in combination group, K-ras ASODN group, IGF-IR group and control group, respectively. Compared with the control group, statistically significant differences were observed (P < 0.01). The apoptotic rate of combination group was significantly higher than that of K-ras ASODN group alone or IGF-IR ASODN alone (P < 0.05). No

difference existed between K-ras ASODN group and IGF-IR group (P > 0.05) (Figure 4).

K-ras and IGF-IR protein expression of Patu8988 cells detected by flow cytometry

Flow cytometry results showed that the positive rate of K-ras protein was 76.15% \pm 1.62% and 69.18% \pm 0.87% in control group and IGF-ASODN group, respectively. No statistical difference was found between the two groups (P > 0.05). But, in K-ras ASODN group and the combination group, K-ras protein was significantly decreased by 25.95% \pm 0.18% and 19.69% \pm 1.15%, respectively, compared with that of control group (P < 0.01). Flow cytometric analysis by using IGF-IR antibody showed that there was high expression in K-ras ASODN group, and control group with a positive rate of 91.53% \pm 1.62% and 85.25% \pm 0.99%, respectively. But, in IGF-IR ASODN, and combination group, IGF-IR protein expression was reduced to 40.78% \pm 1.42% and 38.25% \pm 1.22%, respectively. Significant differences were found when compared with control group (P < 0.01). All above results revealed that antisense oligodeoxynucleotides can inhibit corresponding protein expression. But, K-ras ASODN can not obviously inhibit the expression of IGF-IR protein, and IGF-IR ASODN can not obviously inhibit the expression of K-ras protein (Table 1).

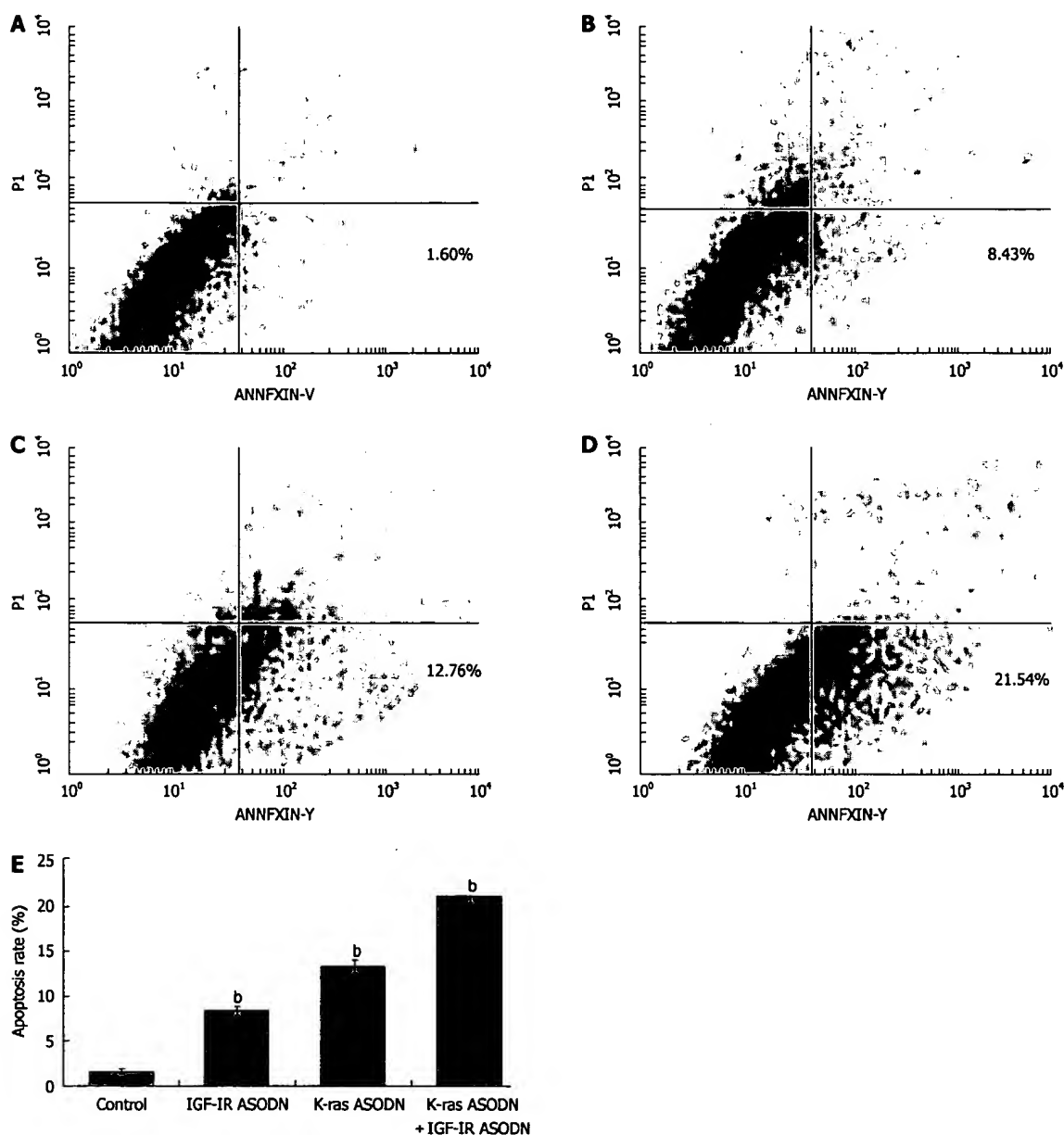


Figure 4 Apoptosis of Patu8988 cells detected by flow cytometry with Annexin V-FITC dual staining. **A:** Control group; **B:** IGF-IR ASODN group; **C:** K-ras ASODN group; **D:** K-ras ASODN + IGF-IR ASODN group; **E:** Apoptosis rate of Patu8988 cells for different groups. $^bP < 0.01$, vs control group. Each value represents the mean \pm SD from triplicate determinations.

K-ras and IGF-IR mRNA expression of Patu8988 cells detected by RT-PCR

The mRNA expression intensities of *K-ras* gene and *IGF-IR* gene were analyzed by semiquantitative RT-PCR. The mRNA levels were normalized by internal control β -actin. At 48 h post-transfection, *K-ras* mRNA intensity levels were 0.389 ± 0.018 for IGF-IR ASODN group, 0.213 ± 0.027 for K-ras ASODN + IGF-IR ASODN group, 0.275 ± 0.023 for K-ras ASODN group and 0.391 ± 0.021 for control group. The statistical analysis showed that *K-ras* mRNAs of Patu8988 cells in K-ras ASODN group, and combination group were reduced significantly, compared with that of control group

($P < 0.05$). The inhibition rate reached 45.5% in the combination group. IGF-IR ASODN had no significant inhibitory effect on the expression of *K-ras* mRNA ($P > 0.05$, vs control) (Figure 5). As for *IGF-IR* gene, the relative mRNA levels were 0.642 ± 0.017 for K-ras ASODN, 0.355 ± 0.020 for the combination group, 0.387 ± 0.025 for IGF-IR ASODN group, and 0.630 ± 0.029 for control group. The statistical analysis showed that both IGF-IR ASODN group, and combination group could have a significant down-regulation effect on the mRNA expression of *IGF-IR* in Patu8988 cells ($P < 0.05$, vs control). The inhibition rate was 43.7% in the combination group. However, K-ras ASODN showed

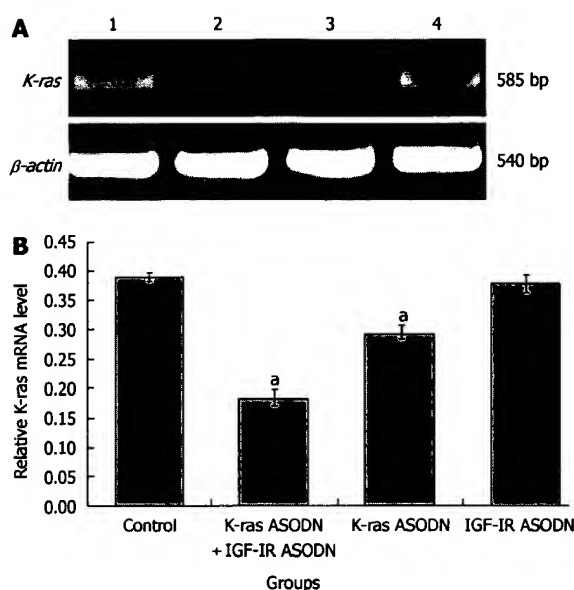


Figure 5 mRNA expression of *K-ras* gene in Patu8988 cells at 48 h post-transfection. **A:** RT-PCR analysis for *K-ras* gene in different groups. The β -actin gene was included as internal control. 1: IGF-IR ASODN group; 2: K-ras ASODN + IGF-IR ASODN; 3: K-ras ASODN group; 4: Control group; **B:** *K-ras* products quantified relative to the internal control β -actin. $^aP < 0.05$, vs control. Each value represents the mean \pm SD from triplicate determinations.

no obvious inhibition for *IGF-IR* mRNA expression ($P > 0.05$ vs control) (Figure 6).

Inhibition of *in vivo* tumor growth by *K-ras* and *IGF-IR* downregulation

All nude mice were bearing pancreatic tumors from 7 to 10 d, and survived during the therapy with no red swelling, and disruption at the inoculation point. Before therapy, there were no significant difference for nude mice in weight and volume. As shown in Figure 3D, the tumor volume increased gradually in control group. The long diameter reached above 1.0 cm, and the volume reached $2230.0 \pm 65.6 \text{ mm}^3$ on the 49th d after inoculation. The tumor growth in K-ras ASODN group, IGF-IR ASODN group and combined group was inhibited with significant difference when compared with control group ($P < 0.01$). The therapeutic effect in the combined group was greater than that of K-ras ASODN or IGF-IR ASODN alone ($P < 0.01$). These results indicated that combination group exerted a strong growth-suppressive effect on pancreatic cancer. However, between K-ras ASODN and IGF-IR ASODN group, there was no obvious difference ($P > 0.05$). The results of immunohistochemical showed that K-ras and IGF-IR protein expression decreased in tumor tissues (data not shown).

Morphologic change under transmission electron microscopy

Using transmission electron microscope, we saw that the normal Patu8988 cells had intact cell membranes and nuclear membranes, distributed nuclear chromosomes,

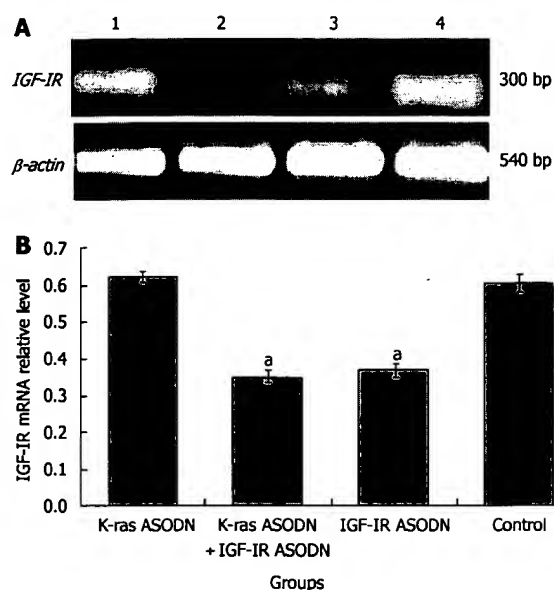


Figure 6 mRNA expression of *IGF-IR* gene in Patu8988 cells at 48 h post-transfection. **A:** RT-PCR analysis for *IGF-IR* gene in different groups. The β -actin gene was included as internal control. 1: K-ras ASODN group; 2: K-ras ASODN + IGF-IR ASODN; 3: IGF-IR ASODN group; 4: Control group; **B:** *IGF-IR* products quantified relative to the internal control β -actin. $^aP < 0.05$ vs control. Each value represents the mean \pm SD from triplicate determinations.

distinct organelles, big nuclei and excessive nuclear division, which indicated that Patu8988 cells were highly malignant (Figure 7A). When Patu8988 cells were treated with K-ras ASODN combined with IGF-IR ASODN for 48 h, changes such as apoptosis, cell shrinkage, separation from neighboring cells, plasma condensation, plasma vacuolation, karyopyknosis, margination of condensed chromatin and membrane-bounded apoptotic bodies were observed (Figure 7B); some cells exhibited distinct deformation and disruption (Figure 7C).

DISCUSSION

The rapid development of molecular techniques has made it clear that tumorigenesis is actually a process of gene abnormalities. The strong invasiveness and rapid diffusive ability of pancreatic cancer are also closely associated with gene abnormalities. The study results of many years show that many genes' cooperation and many factors' participation contribute to the development of pancreatic cancer. Gene therapy brings hope for patients of pancreatic cancer. But, single gene therapy does not achieve ideal results. If two or more genes are combined to treat pancreatic cancer, in theory therapeutic effects will be better.

Since Almoguera *et al*^[17] first reported that K-ras mutation occurred in patients with pancreatic cancer, 85%-95% patients with pancreatic cancer have been found to have K-ras mutation, and most of these were point mutations at codon 12. Among those point mutations, GAT, GTT and CGT mutation styles comprised more than 95% of the point mutations at

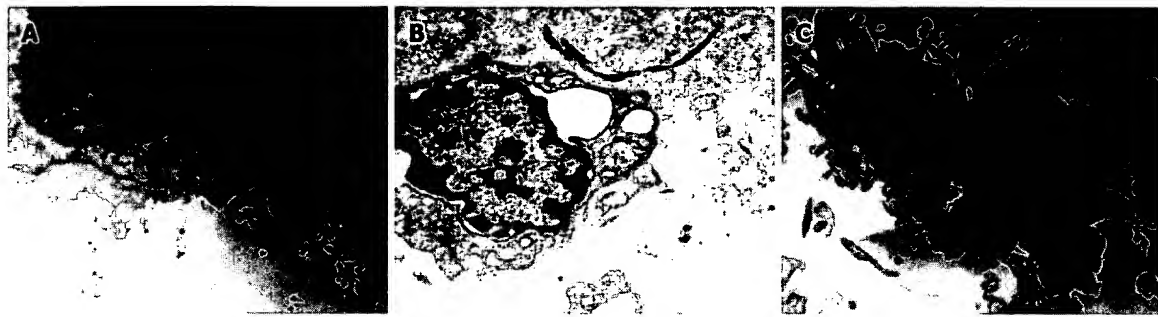


Figure 7 Transmission electron microscopic appearance of Patu8988 cell. A: Normal Patu8988 cell with intact cell membrane and nuclear membrane ($\times 12000$); B: Patu8988 cell treated with K-ras ASODN + IGF-IR ASODN for 48 h. The margination of condensed chromatin and membrane-bounded apoptotic bodies are observed ($\times 15000$); C: Necrotic cell ($\times 15000$).

codon 12^[18]. Therefore, K-ras point mutation at codon 12 is an early event for pancreatic cancer, which can be used as a target for early diagnosis and gene therapy^[19,20]. K-ras gene mutation destroys the GTP enzyme activity of ras protein and makes K-ras active constantly, which makes K-ras protein unable to block signals for growth. Recently, K-ras antisense oligodeoxynucleotides (ASODNs) have been transfected into pancreatic cells in China and abroad. Wang *et al*^[21] first detected and confirmed K-ras gene mutation type CGT in human pancreatic carcinoma cell line PC-2. Then, K-ras mutation ASODN specific to CGT at codon 12 was used to explore its inhibitory effects on target gene in cell line PC-2. The results show that ASODN specific to K-ras point mutation CGT had significant inhibitory effects on target gene expression in human pancreatic carcinoma cells *in vitro*. Nakada *et al*^[22] used ASODN specific to K-ras point mutation GAT at codon 12 to transfet into human pancreatic cancer cell line PANC-1 (with GAT mutation at codon 12), and the invasive activity was investigated using *in vitro* chemoinvasion assay. The results show that K-ras mutation ASODN specific to GAT at codon 12 strongly inhibited the invasive activity of the cell line PANC-1, but not in that with a wild type K-ras (BxPC-3). So, ASODNs specific to mutated K-ras genes can inhibit the proliferation and invasiveness of human pancreatic cancer cell lines. Specific antisense therapy to the point mutation of K-ras might be a new anticancer strategy for pancreatic cancer. However, these studies also indicate that adopting K-ras ASODN alone could not eradicate all the tumor cells. For exploring more effective therapy methods, some scholars abroad recently started to explore therapeutic alliance with diverse antisense oligodeoxynucleotides to treat pancreatic cancer, such as simultaneous transfection with mda-7 ASODN and K-ras ASODN into pancreatic cancer *in vitro* and *in vivo*. The results of their studies showed that the therapeutic effects of combination methods were better than that of one alone^[23,24].

IGF-IR is a receptor protein tyrosine kinase (RPTK) expressed in a wide variety of cell types including mesenchymal, epithelial, and hematopoietic cells. The receptor is a transmembrane heterotetramer consisting of two α -subunits and two β -subunits linked by

disulfide bonds. The binding of IGF-I to its receptor results in receptor oligomerization, activation of PTK, inter-molecular receptor autophosphorylation and phosphorylation of cellular substrates that consequently lead to gene activation, DNA synthesis and cell proliferation. Overexpression of IGF-IR stimulated cells not only to transform toward malignancy and sustain malignant phenotype, but also to promote tumor cells' anti-apoptosis, mitosis, proliferation and invasiveness. Min *et al*^[10] reported that IGF-IR overexpressed in pancreatic cancer and down-regulation of IGF-IR expression using monoclonal antibodies or antisense oligodeoxynucleotides could inhibit tumor cell growth both *in vitro* and *in vivo*^[25-27]. However, the inhibition ratio was not high^[24].

Considering the important effects of K-ras gene point mutation at codon 12 in pancreatic cancer and the broad tumorigenesis of IGF-IR gene, our study explored the effects of Patu8988 cell proliferation, apoptosis and target gene expression using combined antisenses with K-ras ASODN against K-ras point mutation at codon 12 and IGF-IR ASODN against insulin-like growth factor-1. We noticed that different doses for K-ras ASODN or IGF-IR ASODN could inhibit Patu8988 cell growth. But, combinations could produce greater effects ($P < 0.01$). The results were also confirmed in animal experiments. Compared with the single method, combination could obviously induce Patu8988 cell apoptosis, and reduce protein and mRNA expression of K-ras and IGF-IR. In our study, the inhibition effects of K-ras ASODN were better than that of IGF-IR ASODN. Ras protein is not only one of the signal pathways of IGF-IR, but also the pathway for many other growth factors, such as VEGF. Therefore, mutated ras protein not only amplifies the IGF-IR signal, but also amplifies signals for many other growth factors to inhibit cell apoptosis, and also induces vascular growth and cell proliferation. IGF-IR ASODN can inhibit only IGF-IR signal. But, K-ras ASODN can inhibit signals for many factors. Therefore, the inhibition effects of K-ras ASODN was better than that of IGF-IR ASODN. So, combined therapy can inhibit signals on two sides. After being treated with K-ras ASODN and IGF-IR ASODN together, some cells appeared in the

form of apoptosis, some others in the shape of edema or deformation, which indicated that antisense not only induced apoptosis, but also promoted cell death directly.

Our study shows that K-ras ASODN combined with IGF-ASODN obviously inhibited Patu8988 cell growth, and induced cell apoptosis and death. The mechanism may be associated with the inhibition of mRNA, and protein expression of K-ras and IGF-IR in Patu8988 cells. Cooperation with two synergistic antisense oligodeoxynucleotides could provide a new gene therapeutic strategy against pancreatic cancer. Meanwhile, the results of our study show that K-ras ASODN and IGF-IR ASODN inhibited tumor growth alone or in combination. However, a rapid cell proliferation tendency was seen in later stage of combined therapy. We speculated that this phenomenon might be associated with the degradation of ASODN in the late stage of treatment. We need to do further study to learn the relationship between dose-effect and time-effect. On the other hand, the development of pancreatic cancer involves many genes; we can not inhibit tumor growth completely by suppressing two genes of *K-ras* and *IGF-IR*, only partial.

COMMENTS

Background

Pancreatic carcinoma is the cancer that has the highest *K-ras* gene mutation rate. 95% of mutations happen at codon 12. Three major mutation types have been reported, including CGT, GAT and GTT. Antisense oligodeoxynucleotides (ASODNs) specific to CGT and GAT point mutations in human pancreatic cancer cell lines were reported; the ASODN against GTT point mutation in pancreatic cancer remains unclear. Some studies reported that type I insulin-like growth factor receptor (IGF-IR) is overexpressed in pancreatic cancer and down-regulation of IGF-IR expression using ASODNs could inhibit tumor cell growth. In this article, whether K-ras ASODN specific to GTT mutation in alliance with IGF-IR ASODN regulate Patu8988 proliferation, apoptosis, target gene expression *in vitro* and *in vivo* was investigated.

Research frontiers

In previous studies, antisense oligodeoxynucleotides (ASODNs) specific to CGT and GAT point mutation of *K-ras* gene were demonstrated to inhibit proliferation in pancreatic cancer.

Innovations and breakthroughs

It was found in the present study that K-ras ASODN combined with IGF-IR ASODN could cooperatively inhibit the growth of Patu8988 cells and induce their apoptosis via reinforcing specific down regulation of *K-ras* and *IGF-IR* mRNA and protein expression.

Applications

Cooperation with two synergistic antisense oligodeoxynucleotides could provide a new gene therapeutic strategy against pancreatic cancer.

Terminology

PCR-SSP is polymerase chain reaction with special sequence primers; K-ras ASODN is an antisense oligodeoxynucleotide against *K-ras* gene; IGF-IR ASODN is an antisense oligodeoxynucleotide against *IGF-IR* gene; GAT, CGT and GTT are three major point mutation types at codon 12 of *K-ras* gene.

Peer review

This is an interesting study that identifies molecular pathways that may be therapeutically targeted to inhibit pancreatic cancer growth.

REFERENCES

- Nitecki SS, Sarr MG, Colby TV, van Heerden JA. Long-term survival after resection for ductal adenocarcinoma of the pancreas. Is it really improving? *Ann Surg* 1995; 221: 59-66
- Coppola D. Molecular prognostic markers in pancreatic cancer. *Cancer Control* 2000; 7: 421-427
- Welsch T, Kleeff J, Friess H. Molecular pathogenesis of pancreatic cancer: advances and challenges. *Curr Mol Med* 2007; 7: 504-521
- Boeck S, Heinemann V. The role of second-line chemotherapy after gemcitabine failure in patients with advanced pancreatic cancer. *Future Oncol* 2008; 4: 41-50
- Brasiuniene B, Juozaityte E. The effect of combined treatment methods on survival and toxicity in patients with pancreatic cancer. *Medicina (Kaunas)* 2007; 43: 716-725
- Plate JM. Current immunotherapeutic strategies in pancreatic cancer. *Surg Oncol Clin N Am* 2007; 16: 919-943, xi
- Deramaudt T, Rustgi AK. Mutant KRAS in the initiation of pancreatic cancer. *Biochim Biophys Acta* 2005; 1756: 97-101
- Fryzek JP, Garabrant DH, Schenk M, Kinnard M, Greenson JK, Sarkar FH. The Association Between Selected Risk Factors for Pancreatic Cancer and the Expression of p53 and K-ras Codon 12 Mutations. *Int J Gastrointest Cancer* 2006; 37: 139-145
- Jiao L, Zhu J, Hassan MM, Evans DB, Abbruzzese JL, Li D. K-ras mutation and p16 and preproenkephalin promoter hypermethylation in plasma DNA of pancreatic cancer patients: in relation to cigarette smoking. *Pancreas* 2007; 34: 55-62
- Min Y, Adachi Y, Yamamoto H, Ito H, Itoh F, Lee CT, Nadaf S, Carbone DP, Imai K. Genetic blockade of the insulin-like growth factor-I receptor: a promising strategy for human pancreatic cancer. *Cancer Res* 2003; 63: 6432-6441
- Liu W, Bloom DA, Cance WG, Kurenova EV, Golubovskaya VM, Hochwald SN. FAK and IGF-IR interact to provide survival signals in human pancreatic adenocarcinoma cells. *Carcinogenesis* 2008; 29: 1096-1107
- Wang YX, Gao L, Ji ZZ. Inhibitory effects of antisense oligonucleotide specific to K-ras point mutation on the target gene expression in human pancreatic carcinoma cells. *Chin Med J (Engl)* 2007; 120: 1448-1450
- Zhou NX, Fen YQ, Huang ZQ, Wang YZ, Xu QS. Growth inhibition of pancreatic cancer by antisense oligonucleotide against the insulin-like factor-I receptor. *Zhonghua Zhong Li Za Zhi* 1999; 29: 247-251
- Masui T, Hosotani R, Ito D, Kami K, Koizumi M, Mori T, Toyoda E, Nakajima S, Miyamoto Y, Fujimoto K, Doi R. Bcl-XL antisense oligonucleotides coupled with antennapedia enhances radiation-induced apoptosis in pancreatic cancer. *Surgery* 2006; 140: 149-160
- Hotz HG, Hines OJ, Masood R, Hotz B, Foitzik T, Buhr HJ, Gill PS, Reber HA. VEGF antisense therapy inhibits tumor growth and improves survival in experimental pancreatic cancer. *Surgery* 2005; 137: 192-199
- Resnicoff M, Coppola D, Sell C, Rubin R, Ferrone S, Baserga R. Growth inhibition of human melanoma cells in nude mice by antisense strategies to the type 1 insulin-like growth factor receptor. *Cancer Res* 1994; 54: 4848-4850
- Almoguera C, Shibata D, Forrester K, Martin J, Arnhem N, Perucchio M. Most human carcinomas of the exocrine pancreas contain mutant c-K-ras genes. *Cell* 1988; 53: 549-554
- Berndt C, Haubold K, Wenger F, Brux B, Muller J, Bendzko P, Hillebrand T, Kottgen E, Zanow J. K-ras mutations in stools and tissue samples from patients with malignant and nonmalignant pancreatic diseases. *Clin Chem* 1998; 44: 2103-2107
- Fleming JB, Shen GL, Holloway SE, Davis M, Brekken RA. Molecular consequences of silencing mutant K-ras in pancreatic cancer cells: justification for K-ras-directed therapy. *Mol Cancer Res* 2005; 3: 413-423
- Zhu H, Liang ZY, Ren XY, Liu TH. Small interfering RNAs targeting mutant K-ras inhibit human pancreatic carcinoma cells growth *in vitro* and *in vivo*. *Cancer Biol Ther* 2006; 5: 1693-1698
- Wang YX, Gao L, Ji ZZ. [The study of the effect of antisense oligonucleotide specific to K-ras point mutation on human

pancreatic carcinoma cell PC-2] *Zhonghua Waike Zazhi* 2005; 43: 1387-1390

22 Nakada Y, Saito S, Ohzawa K, Morioka CY, Kita K, Minemura M, Takahara T, Watanabe A. Antisense oligonucleotides specific to mutated K-ras genes inhibit invasiveness of human pancreatic cancer cell lines. *Pancreatology* 2001; 1: 314-319

23 Su Z, Lebedeva IV, Gopalkrishnan RV, Goldstein NI, Stein CA, Reed JC, Dent P, Fisher PB. A combinatorial approach for selectively inducing programmed cell death in human pancreatic cancer cells. *Proc Natl Acad Sci USA* 2001; 98: 10332-10337

24 Lebedeva IV, Su ZZ, Emdad L, Kolomeyer A, Sarkar D, Kitada S, Waxman S, Reed JC, Fisher PB. Targeting inhibition of K-ras enhances Ad.mda-7-induced growth suppression and apoptosis in mutant K-ras colorectal cancer cells. *Oncogene* 2007; 26: 733-744

25 Maloney EK, McLaughlin JL, Dagdigian NE, Garrett LM, Connors KM, Zhou XM, Blattler WA, Chittenden T, Singh R. An anti-insulin-like growth factor I receptor antibody that is a potent inhibitor of cancer cell proliferation. *Cancer Res* 2003; 63: 5073-5083

26 Pan YZ, Sun CY, Wang YZ. The growth inhibition of human pancreatic cancer cells by lipofectin mediated IGF-1R antisense oligonucleotides. *Zhonghua Heyixue Zazhi*; 2005; 25: 212-215

27 Adachi Y, Lee CT, Carbone DP. Genetic blockade of the insulin-like growth factor 1 receptor for human malignancy. *Novartis Found Symp* 2004; 262: 177-189; discussion 190-192, 265-268

S- Editor Li DL L- Editor Li M E- Editor Zhang WB

The Mammalian Longevity-associated Gene Product p66^{shc} Regulates Mitochondrial Metabolism*[§]

Received for publication, October 26, 2005, and in revised form, February 7, 2006. Published, JBC Papers in Press, February 14, 2006, DOI 10.1074/jbc.M511626200

Shino Nemoto[‡], Christian A. Combs[§], Stephanie French[¶], Bong-Hyun Ahn[‡], Maria M. Fergusson[‡], Robert S. Balaban[¶], and Toren Finkel^{‡†}

From the [‡]Cardiology Branch, NHLBI, National Institutes of Health, Bethesda, Maryland 20892-1622, [§]NHLBI, National Institutes of Health, Light Microscopy Facility, Bethesda, Maryland 20892, and the [¶]Laboratory of Cardiac Energetics, NHLBI, National Institutes of Health, Bethesda, Maryland 20892

Previous studies have determined that mice with a homozygous deletion in the adapter protein p66^{shc} have an extended life span and that cells derived from these mice exhibit lower levels of reactive oxygen species. Here we demonstrate that a fraction of p66^{shc} localizes to the mitochondria and that p66^{shc-/-} fibroblasts have altered mitochondrial energetics. In particular, despite similar cytochrome content, under basal conditions, the oxygen consumption of spontaneously immortalized p66^{shc-/-} mouse embryonic fibroblasts were lower than similarly maintained wild type cells. Differences in oxygen consumption were particularly evident under chemically uncoupled conditions, demonstrating that p66^{shc-/-} cells have a reduction in both their resting and maximal oxidative capacity. We further demonstrate that reconstitution of p66^{shc} expression in p66^{shc-/-} cells increases oxygen consumption. The observed defect in oxidative capacity seen in p66^{shc-/-} cells is partially offset by augmented levels of aerobic glycolysis. This metabolic switch is manifested by p66^{shc-/-} cells exhibiting an increase in lactate production and a stricter requirement for extracellular glucose in order to maintain intracellular ATP levels. In addition, using an *in vivo* NADH photobleaching technique, we demonstrate that mitochondrial NADH metabolism is reduced in p66^{shc-/-} cells. These results demonstrate that p66^{shc} regulates mitochondrial oxidative capacity and suggest that p66^{shc} may extend life span by repartitioning metabolic energy conversion away from oxidative and toward glycolytic pathways.

Generation of ATP in the mitochondria represents the most efficient pathway to meet the energetic needs of a cell. This process, however, requires the consumption of molecular oxygen with a corresponding production of reactive oxygen species (ROS).² Generation of ROS appears to be one of the central mechanisms that contribute to aging in a wide range of organisms (1–3). In contrast, under aerobic conditions, energy generation can also be achieved through glycolytic pathways present in the cytosol. These cytosolic pathways are inherently less efficient but do not produce ROS. Each cell employs a different relative balance between these two major energetic pathways, although

relatively little is known about how this partition is established or maintained.

In lower organisms, such as *Caenorhabditis elegans* and *Drosophila*, a number of longevity-associated genes have been isolated. One prominent and well characterized aging pathway regulates the activity of the transcription factor DAF-16, a member of the Forkhead family of transcriptional regulators. Evidence suggests that DAF-16 is involved in responding to numerous environmental stresses (4). A rise in intracellular ROS is one particular stress that may be relevant to life span determination, and in this regard, it is of interest that both DAF-16 and its closest mammalian ortholog Foxo3a appear to regulate a number of cellular antioxidant proteins (5–9).

In addition to the DAF-16 pathway, RNAi screens performed in *C. elegans* has identified a number of other putative longevity genes (10, 11). Interestingly, functional characterization of these longevity-associated genes have determined that a number of them appear to be important for mitochondrial function. Similarly, direct knockdown of components of the electron transport chain has also been shown to extend the life span of the worm (12). Analysis of these long lived mitochondrial mutants, as well as in depth energetic analysis of the previously characterized DAF-16-related mutants, has led to the proposal that many life span-extending mutants in *C. elegans* slow aging by decreasing mitochondrial metabolism (13). This hypothesis suggests that a shift away from trichloroacetic acid-based mitochondrial metabolism might extend life by a reduction in oxidative stress. Nonetheless, it should be mentioned that the relationship between metabolic rate and ROS production is not straightforward (3).

In contrast to the wealth of information regarding aging in lower organisms, there is relatively little known regarding the genetic control of mammalian life span. Only a handful of genes have to date been documented to be capable of extending either the mean or maximum age of mammalian organisms (14). One previously described knock-out mouse that appears to produce a long-lived but phenotypically normal animal was obtained after deletion of p66^{shc} (15). Shc proteins are alternatively spliced 46-, 52-, and 66-kDa isoforms that were initially viewed as simple adapter molecules linking receptors with downstream effector molecules such as Ras proteins (16). The larger p66^{shc} isoform differs structurally from its two other isoforms by the presence of a 14-kDa N-terminal CH2 domain. Previous studies have demonstrated that animals deficient in p66^{shc} have an approximate 30% extension in life span (15). These animals are resistant to exogenous oxidative stress and also exhibit lower levels of spontaneous oxidative burden (15, 17, 18). Consistent with these *in vivo* observations, p66^{shc-/-} cells have lower levels of ROS (8, 19). One potential explanation for this effect may come from a modest increase in scavenging capacity in these cells (8); however, this is unlikely to explain the much more significant decrease in basal and stress-induced ROS levels.

* This work was supported by intramural funds from the National Institutes of Health. The costs of publication of this article were defrayed in part by the payment of page charges. This article must therefore be hereby marked "advertisement" in accordance with 18 U.S.C. Section 1734 solely to indicate this fact.

† The on-line version of this article (available at <http://www.jbc.org>) contains supplemental Figs. S1–S3.

‡ To whom correspondence should be addressed: National Institutes of Health, Bldg. 10/6N-240, 10 Center Dr., Bethesda, MD 20892-1622. Tel.: 301-402-4081; E-mail: finkel@nih.gov.

[§] The abbreviations used are: ROS, reactive oxygen species; MEF, mouse embryo fibroblast; FCCP, carbonylcyanide 4-(trifluoromethyl)phenylhydrazone; ED-FRAP, enzyme-dependent fluorescence recovery after photobleaching.

p66^{shc} Regulates Mitochondrial Metabolism

Given that the mitochondria represent the largest source of ROS generation within cells and that oxygen consumption and ROS generation represent an important determinant in aging in a number of species, we sought to explore whether *p66^{shc}* might directly regulate ROS production by regulating mitochondrial metabolism.

MATERIALS AND METHODS

Cell Lines and Subcellular Fractionation—Spontaneously immortalized MEFs (+/+) cells and *p66^{shc}-/-* MEFs were a gift of Pier Pelicci and have been previously described (8). PC12 and HeLa cells were obtained from ATCC (Rockville, MD). Cells were maintained in Dulbecco's modified Eagle's medium supplemented with 10% fetal calf serum. To purify the cytosolic and mitochondrial fractions, we used the ApoAlert Cell Fraction kit (Clontech). To assess the distribution of *p66^{shc}*, 30 μ g of mitochondrial or cytosolic fractions were separated by SDS-PAGE, and the purity of the fractions was assessed by probing for the cytosolic gene product tubulin (Santa Cruz Biotechnology, Inc., Santa Cruz, CA) and the mitochondrial gene product COX4 (Clontech). For some experiments, we also collected and analyzed the initial 700 \times g pellet containing plasma membranes. For construction of the R177A mutant, substitution of alanine for arginine residue at amino acid position 177 was performed by standard methods, and both the mutant and wild type were subsequently confirmed by direct sequencing. Reconstitution of *p66^{shc}* into *p66^{shc}-/-* cells was achieved by transfection of the hygromycin resistance plasmid pTK-Hygro only for control cell lines or this resistance plasmid along with an epitope-tagged *p66^{shc}-/-* expression plasmid that has been previously described (8). In both cases, hygromycin-resistant colonies were obtained, and *p66^{shc}* expression was monitored by Western blot analysis employing the epitope tag. For knock-down expression of *p66^{shc}* in PC12 cells, we targeted a 20-nucleotide sequence in *p66^{shc}*: GTACAAACCCACTTCGGAATG. This sequence was incorporated into the psiRNA vector (Invivogen) to enable the continuous, endogenous expression of small interfering RNAs in stable clones. For oxygen consumption measurements, two random knockdown cell lines were compared with two random Zeocin-selected PC12 cell lines transfected with the psiRNA vector alone.

Mitochondrial NADH and NADH Oxidase Measurements—Cellular NADH fluorescence was measured at room temperature using an excitation wavelength of 351 nm with emission monitored using a 385–470-nm band pass filter. Optical slice thickness was set to 1.5 μ m. NADH regeneration was assessed using NADH ED-FRAP as previously described (20–22). In brief, all ED-FRAP data analysis was performed using custom-written programs in the IDL programming language (RSI Inc., Boulder, CO). Initial rates of regeneration were determined using a linear regression of the first five points (2 s) after the photolysis pulse. Before fitting, all recovery points were filtered using a Lee filter algorithm to smooth out additive image noise. To determine NADH consumption in cytosolic or mitochondrial fractions, MEF lysate was fractionated as above, and 30 μ g of either mitochondrial or cytosolic lysate protein was used. Mitochondrial protein was solubilized in lysis buffer (20 mM Tris, pH 7.5, 0.5% Nonidet P-40, 25 mM NaCl, 2.5 mM EDTA) and subsequently diluted 1:20 (v/v) in phosphate buffer (pH 7.5), and the disappearance of 100 μ M NADH was monitored at 340 nm.

Metabolic Measurements—Oxygen consumption was measured using an oxygen electrode standardized to room air (0.2 mM O₂). The data were digitized and stored using an analog to digital conversion system (DASYLab32). All measurements of oxygen consumption were performed in intact cells. In general, one representative experiment performed in triplicate is shown. All oxygen consumption experiments were performed on at least three separate occasions. To maximize oxy-

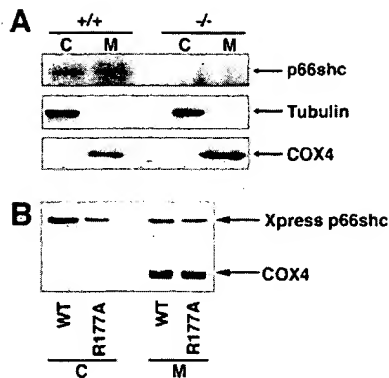


FIGURE 1. A fraction of *p66^{shc}* is associated with the mitochondria. **A**, subcellular fractionation of cytosolic (C) or mitochondrial (M) fractions were prepared from wild type (+/+) or *p66^{shc}-/-* mouse embryonic fibroblasts. Each lane contained 30 μ g of protein. The purity of the fractions was confirmed by assessing the distribution of the cytosolic protein tubulin and the mitochondrial protein cytochrome oxidase subunit 4 (COX4). **B**, subcellular distribution of wild type (WT) Xpress-tagged *p66^{shc}* or a site-directed position 177 mutant (R177A) following transient transfection of HeLa cells.

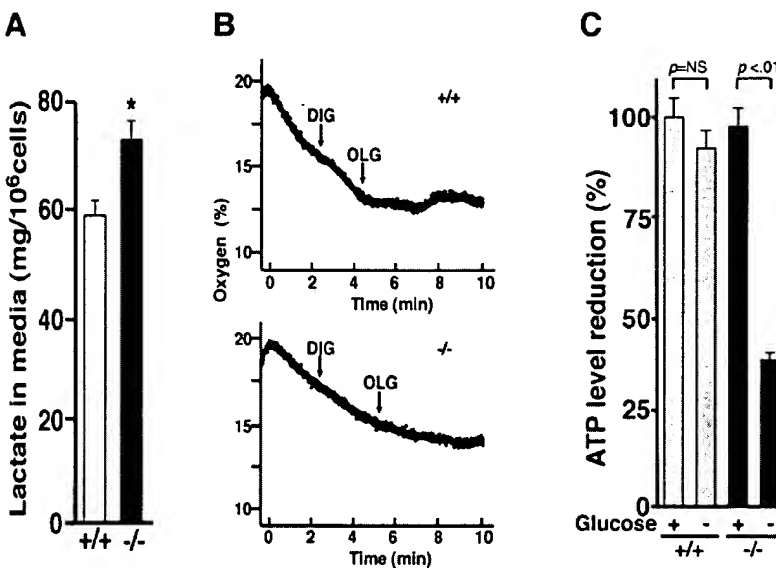
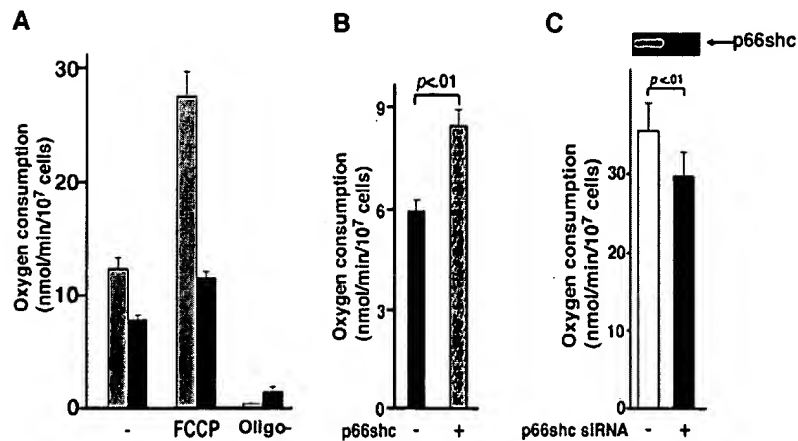
gen consumption, the chemical uncoupler carbonylcyanide 4-(trifluoromethoxy)phenylhydrazone (FCCP; 5.0 μ M) was used. Lactate was measured using the lactate reagent kit (Sigma). Media from wild type MEFs or *p66^{shc}-/-* cells (1×10^6) were conditioned for 24 h prior to lactate determination. For the simultaneous determination of oxygen utilization and lactate levels, we employed the methods previously described (23). The degree of proton leak was calculated by measuring oxygen consumption in permeabilized cells (digitonin, 250 μ g/ml) in the presence of oligomycin (25 μ g/ml). ATP was measured from 1×10^6 cells using the ATP determination kit (Molecular Probes, Inc., Eugene, OR) with cells either maintained in full media or in media lacking glucose. Six hours after glucose withdrawal, cells were lysed in buffer (20 mM Tris, pH 7.5, 0.5% Nonidet P-40, 25 mM NaCl, 2.5 mM EDTA) for ATP determination. Results of ATP and lactate levels are, except where indicated, the results of a single representative experiment performed in triplicate. All experiments were performed at least three separate times.

RESULTS

***p66^{shc}* Localizes to the Mitochondria and Regulates Oxygen Consumption and Oxidative Capacity**—Since Shc proteins were viewed as adapter molecules for cell surface receptor complexes, the subcellular localization of *p66^{shc}* as well as its two other protein isoforms, *p46^{shc}* and *p52^{shc}*, were initially thought to be confined to the plasma membrane. Recent reports have challenged this assumption, and in particular evidence suggests that *p46^{shc}* localizes exclusively to the mitochondria and that a 32-amino acid motif is essential for this targeting (24). This 32-amino acid motif is not unique for *p46^{shc}* and is also contained within *p66^{shc}*. Consistent with these observations, recent evidence suggests that this larger Shc isoform might also be partially localized within the mitochondria (24, 25). As noted in Fig. 1, we also observed that a proportion of *p66^{shc}* was consistently found within the mitochondrial fraction. Based on calculation of the relative mass of the mitochondrial fraction, we estimate that ~10% of *p66^{shc}* is contained within the mitochondria of our wild type MEFs. This estimation is in good agreement with other recent observations (25) as well as indirect immunofluorescence data (supplemental Fig. S1).

As mentioned above, importation of *p46^{shc}* into the mitochondria requires a nonconventional N-terminal 32-amino acid targeting sequence and, in particular, an arginine residue at position 22 of the protein (24). This entire targeting sequence is also contained within the *p66^{shc}* isoform, but because of the N-terminal CH2 domain of *p66^{shc}*, the

FIGURE 2. The role of *p66^{shc}* in oxygen consumption. *A*, levels of oxygen consumption in one of three similar experiments comparing wild type MEFs (gray bars) and *p66^{shc}-/-* cells (black bars). Oxygen consumption was measured in triplicate under base line conditions (−) or following chemical uncoupling with FCCP (5 μ M) or in the presence of the mitochondrial inhibitor oligomycin. *B*, levels of oxygen consumption in seven random *p66^{shc}-/-* stable cell lines transfected with an empty vector expressing hygromycin resistance alone (−), or seven random cell lines with reconstituted wild type *p66^{shc}* (+). *C*, PC12 cells with and without stable expression of a short interfering RNA directed at *p66^{shc}*. Mean oxygen consumption of two control and two knock-down cell lines each measured in duplicate are shown. Inset, expression levels of *p66^{shc}* in one representative control and knockdown PC12 cell line.



critical arginine residue occurs at position 177. Making the corresponding Arg¹⁷⁷ substitution in *p66^{shc}* revealed that this amino acid change did not significantly alter the distribution of *p66^{shc}* (Figs. 1*B* and S1). Thus, importation of *p66^{shc}* into the mitochondria appears to occur via a mechanism that significantly diverges from the *p46^{shc}* isoform.

We next sought to understand whether the absence of *p66^{shc}* in cells alters mitochondrial function. Given the relationship between mitochondrial metabolism and aging, we first sought to characterize oxygen consumption in intact wild type and *p66^{shc}-/-* cells. As noted in Fig. 2*A*, basal oxygen consumption was reduced by ~30–50% in *p66^{shc}-/-* MEFs. This difference could not be explained by differences in mitochondrial number, since cytochrome *a* and *a*₃ content was similar in the two cell types (wild type MEFs, $40 \pm 8 \mu\text{mol}/10^7 \text{ cell}$; *p66^{shc}-/-* MEFs, $50 \pm 5 \mu\text{mol}/10^7 \text{ cell}$, *p* not significant). In an effort to measure maximal oxygen consumption, we treated cells with the chemical uncoupling agent FCCP. Oxygen consumption of wild type and *p66^{shc}-/-* MEFs treated with FCCP demonstrated a bell-shaped concentration effect with maximal uncoupling noted at 5 μM FCCP, a concentration that was subsequently employed in all experiments. As noted in Fig. 2*A*, under these maximally uncoupled conditions, wild type cells more than doubled their oxygen consumption, whereas *p66^{shc}-/-* cells had a much more modest rise in oxygen consumption. In contrast, the addition of the mitochondrial inhibitor oligomycin resulted in a similar and nearly complete reduction in oxygen consumption in both wild type and

p66^{shc}-/- cells. Therefore, under resting conditions, oxygen consumption in both cell types appears to derive almost exclusively from mitochondrial cytochrome chain activity, and the degree of oligomycin-insensitive uncoupled respiration appears low.

To further confirm the role of *p66^{shc}* in regulating oxygen consumption, we generated stable cell lines with reconstituted *p66^{shc}* in an MEF knock-out cell background. Seven random control clones of *p66^{shc}-/-* transfected with an empty vector had levels of oxygen consumption similar to what was previously observed in the *p66^{shc}-/-* parental cell line (Fig. 2*B*). In contrast, seven random clones transfected with a *p66^{shc}* expression vector had increased levels of oxygen consumption (*p* < 0.01). This difference in respiration did not appear to reflect differences in uncoupling, since the level of oligomycin-insensitive respiration did not appreciably differ between the *p66^{shc}*-reconstituted and empty vector clones (supplemental Fig. S2). To potentially extend these observations to other cell types, we also created stable clones of PC12 cells constitutively expressing a short interfering RNA directed at *p66^{shc}*. Compared with two control PC12 lines, PC12 cells with knock-down *p66^{shc}* expression had reduced oxygen consumption (Fig. 2*C* and *inset*).

Absence of p66^{shc} Increases Aerobic Glycolysis—If *p66^{shc}-/-* cells have less oxygen consumption and hence less mitochondria-dependent energy generation, then presumably energetic demands are met through an increase in alternative ATP-generating pathways. One major alternative pathway is aerobic glycolysis, with the ATP-generating step deriving from

p66^{shc} Regulates Mitochondrial Metabolism

TABLE 1

Sources of ATP generation in wild type (+/+) and *p66^{shc}-/-* MEFs
Percentage of ATP derived from mitochondrial respiration is decreased in *p66^{shc}-/-* cells. Calculations are based on the level of coupled respiration and aerobic glycolysis in both cell types according to previous methods (23).

O ₂ consumption	Lactic acid	Total ATP	Percentage of ATP production from	
			Respiration	Glycolysis
nmol/min/mg protein				
+/+	2.3 ± 0.3	10 ± 0.9	24 ± 1.5	54.1 45.9
-/-	1.4 ± 0.1	14 ± 1.4	22 ± 1.6	35.0 65.0

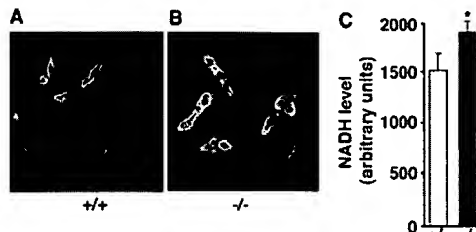


FIGURE 4. *p66^{shc}* alters NADH levels. Shown is endogenous NADH fluorescent intensity in wild type cells (A) or in *p66^{shc}-/-* cells (B). C, quantification in arbitrary units of NADH fluorescent intensity. Data represent the mean ± S.D. from 25 random wild type or *p66^{shc}-/-* cells. *, *p* < 0.05.

the cytosolic conversion of pyruvate to lactate. Measurement of 24-h lactate production revealed that *p66^{shc}-/-* cells did indeed have evidence for increased lactate production (Fig. 3A). To understand the relative balance between aerobic respiration occurring in the mitochondria and glycolysis taking place within the cytosol, we simultaneously measured oxygen consumption and lactate levels using a previously described method (23). As noted in Table 1, using these values, as well as the calculated level of proton leak derived from oligomycin-insensitive respiration (Fig. 3B), we determined that wild type MEFs had over half of their ATP production derived from aerobic respiration. In contrast, for *p66^{shc}-/-* cells, aerobic respiration accounted for closer to one-third of ATP production.

The increased reliance on glycolysis for *p66^{shc}-/-* cells was also demonstrated by the differences in energetic homeostasis in the setting of glucose withdrawal. Under these conditions, oxidative phosphorylation is supported by the remaining carbon substrates, most notably glutamate and fatty acids. As noted in Fig. 3C, 6 h after withdrawing glucose from the media, wild type cells had a modest, but not statistically significant, fall in intracellular ATP levels. In contrast, the same glucose withdrawal resulted in a pronounced reduction in intracellular ATP levels in *p66^{shc}-/-* cells. These results are consistent with the classical Pasteur effect, whereby an inhibition of oxidative metabolism results in an increased reliance on less efficient, glycolytic pathways to meet cellular energetic demands.

Regulation of Mitochondrial NADH Metabolism by *p66^{shc}*—We next sought to further understand the basis for the difference in resting oxygen consumption between wild type and *p66^{shc}-/-* MEF. As noted in Fig. 4, A and B, microfluorometric measurements of the distribution of NADH appeared similar in wild type and *p66^{shc}-/-* cells. This technique predominantly measures protein-bound NAD(P)H and is therefore most reflective of mitochondrial rather than free cytosolic NAD(P)H levels. Quantification of the NADH fluorescent intensity revealed an approximate 20% increase in resting fluorescence in knock-out cells (Fig. 4C). Since the interpretation of resting NADH levels in quiescent cells is difficult, we next sought to assess whether differences existed in NADH turnover between these two cell types. Using a previously

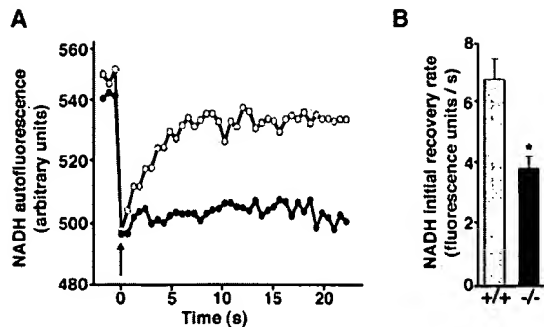


FIGURE 5. *p66^{shc}* alters mitochondrial NADH flux. A, representative NADH ED-FRAP time course from a single wild type (open circles) or *p66^{shc}-/-* cell (closed circles). The arrow indicates the timing of the photolysis pulse. B, composite analysis of the level of initial NADH recovery (first 2 s) following NADH to NAD photolysis in individual wild type (open bar, *n* = 11) and *p66^{shc}-/-* (shaded bar, *n* = 10) cells. *, *p* < 0.03.

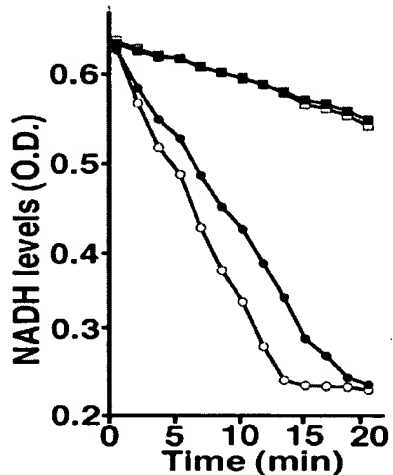


FIGURE 6. Permeabilized *p66^{shc}* mitochondria have reduced NADH consumption. Measurement of *in vitro* consumption of exogenous NADH using either cytosolic (squares) or permeabilized mitochondrial (circles) extracts from wild type MEFs (open symbols) or *p66^{shc}-/-* cells (closed symbols). Whereas cytosolic consumption of NADH is indistinguishable, consumption of exogenous NADH is reduced for *p66^{shc}-/-* mitochondria.

described NADH photolysis technique, NADH ED-FRAP (20–22), we noted that *p66^{shc}-/-* cells exhibited an overall reduction in the degree of NADH regeneration following the laser-induced photolysis of NADH to NAD (Fig. 5A). Quantification of the initial recovery rate of NADH regeneration following photolysis demonstrated an approximate 40% reduction in *p66^{shc}-/-* cells (Fig. 5B). These data are consistent with *p66^{shc}-/-* cells having a blockage or slowing of NADH synthesis from NAD, a process that normally occurs either in the Krebs cycle or from reverse electron flow through Site I of oxidative phosphorylation (21).

Whereas the experiments employing ED-FRAP are most consistent with a defect in mitochondrial NADH metabolism, we could not exclude a contribution from less abundant cytosolic NADH-regenerating enzymes. Therefore, to further pursue the question of alterations in NADH metabolism, we prepared cytosolic and mitochondrial extracts from wild type and *p66^{shc}-/-* cells. As noted in Fig. 6, cytosolic consumption of exogenous NADH was similar in the two cell lines. In contrast, compared with wild type cells, permeabilized mitochondria derived from *p66^{shc}-/-* cells had a considerably slower rate of exogenous NADH consumption. As such, these biochemical measurements are consistent with the previously described noninvasive, NADH ED-FRAP measurements and suggest that the defect in NADH metabolism in *p66^{shc}* cells is confined predominantly to the mitochondria.

p66^{shc} Regulates Mitochondrial Metabolism

DISCUSSION

The identification of gene products that regulate life span has provided significant insight into the molecular mechanisms that underlie aging. In contrast to lower organisms, to date, only a handful of mammalian longevity genes have been identified, and it remains unclear as to how these gene products actually regulate life span (14). One dominant theory regarding aging involves the role of overall metabolism and, in particular, the contribution of reactive oxygen species generated by mitochondrial metabolism (1–3). Here we have demonstrated that the mammalian longevity gene product *p66^{shc}* functions as a regulator of mitochondrial metabolism.

The impetus for our investigation began with the initial observation that *p66^{shc}−/−* mice exhibit increased resistance to oxidative stress such as was observed following paraquat exposure (15). There is also evidence that animals lacking *p66^{shc}* have a reduction in other markers of basal oxidative stress (17, 18). Consistent with these observations, cells derived from *p66^{shc}* animals have reduced resting and stress-induced levels of ROS (8, 19). In the process of performing these experiments, a very recent report suggested that *p66^{shc}* can generate hydrogen peroxide in conjunction with reduced cytochrome *c* (25). These authors have argued that this property is essential for the burst of mitochondrial ROS that occurs with the induction of apoptosis. Interestingly, this study identified a region of *p66^{shc}* required for the *in vitro* interaction with cytochrome *c* that is adjacent to but outside the unique CH2 domain of the protein. Since this identified region is also present in *p52^{shc}*, it is unclear whether this ROS-producing property is also shared by the other *Shc* isoforms that are not currently associated with longevity. It also remains unclear how this ability to generate hydrogen peroxide following apoptotic stress relates to the observation that levels of ROS are chronically reduced in *p66^{shc}−/−* cells and animals, especially since under basal conditions, one would not expect a significant rate of apoptosis. One possibility is that nonapoptotic stresses could also activate *p66^{shc}* to produce hydrogen peroxide in a cytochrome *c*-dependent fashion. Although answers to these questions require further study, together they argue that *p66^{shc}* has properties beyond being a simple adapter molecule.

Whereas our data and previous studies suggest that a fraction of *p66^{shc}* localizes to the mitochondria, it is currently unclear how this importation occurs. In the related *p46^{shc}* molecule, an N-terminal stretch of 32 amino acids is responsible for directing this isoform exclusively to the mitochondria (24). This sequence is not recognized by current bioinformatic methods as a mitochondrial targeting sequence. Within this region, arginine 22 is essential for mitochondrial targeting (24). The corresponding 32-amino acid stretch is found in *p66^{shc}*, but as demonstrated here and previously, the majority of *p66^{shc}* is nonmitochondrial. Similarly, as we show here, in contrast to the *p46^{shc}* isoform, mutation of the corresponding arginine in *p66^{shc}* does not alter the subcellular distribution of the protein. It remains possible that our localization of *p66^{shc}* within the mitochondria is spurious and that the mitochondrial fractions used in our subcellular fractionation experiments were contaminated in some fashion, perhaps by the inadvertent inclusion of plasma membranes. Although this remains a possibility, several observations argue against this. First, previous experiments using perhaps the gold standard of subcellular localization, immunogold electron microscopy, have consistently detected *p66^{shc}* within the mitochondria (25, 26). Similarly, *p66^{shc}* has been shown to form a molecular complex with the mitochondrial protein cytochrome *c* (25). Finally, analysis of our fractions suggests that, at least at the level of Western blot detection, the mitochondrial fractions are relatively free of contamination (supplemental Fig. 3). Nonethe-

less, until more information is known regarding the mechanisms underlying mitochondrial localization, we cannot conclusively state that the metabolic effects seen in our *p66^{shc}−/−* cells are due to the absence of *p66^{shc}* in the mitochondria rather than the absence of this protein in another subcellular compartment.

The observations presented here suggest that *p66^{shc}* may regulate the partition of ATP generation in the cell and that in the absence of *p66^{shc}*, mitochondrial oxidative phosphorylation is reduced, whereas the reliance on glycolysis is increased. Given that mitochondrial electron flow is the major producer of cellular ROS, these results may provide an explanation for the previous observation that *p66^{shc}−/−* cells and animals have lower levels of ROS (8, 15, 17–19). It should be noted that our results were predominantly obtained in spontaneously immortalized MEFs. A similar albeit smaller role for *p66^{shc}* in regulating oxygen consumption was also seen in PC12 cells (Fig. 2C). Our preliminary observations of oxygen consumption in primary MEFs derived from *p66^{shc}−/−* animals suggest that the metabolic alterations are significantly less than what we observed in our immortalized MEFs (data not shown). Thus, the role of *p66^{shc}* in mitochondrial metabolism may vary considerably between different cell types and even between primary and immortalized MEFs. Although considerable drift can occur with cell culture, the observation that reconstitution of *p66^{shc}* in our spontaneously immortalized knock-out MEFs increases oxygen consumption (Fig. 2B) provides strong evidence for a continuous role of *p66^{shc}* in the observed metabolic phenotype.

Although to date, relatively few mammalian longevity genes have been determined, there is a much richer literature from other species such as nematodes. Although the requirement for oxygen and the ability to withstand prolonged hypoxia clearly differs between worms and higher mammals, it is interesting to note that a number of previously described *C. elegans* longevity mutants have altered mitochondrial metabolism (10, 11). Included among these is the *isp-1* mutant, which has a defect in Complex III leading to decreased oxygen consumption and extended life (27). Similarly, RNAi methods have determined that inhibition of mitochondrial electron transport or other essential mitochondrial proteins can often result in worms that have reduced oxygen consumption, lower ATP levels, and a corresponding increase in life span (12). Thus, as recently hypothesized, reducing the level of mitochondrial metabolism may be an important way of extending the life span of lower organisms (13). The results presented here, along with previous studies demonstrating an extended life span of *p66^{shc}−/−* mice (15), suggest that this paradigm may also be applicable to mammalian species.

Acknowledgment—We are grateful to P. Pelicci for the gift of *p66^{shc}−/−* MEFs.

REFERENCES

1. Finkel, T., and Holbrook, N. J. (2000) *Nature* **408**, 239–247
2. Wallace, D. C. (2005) *Annu. Rev. Genet.* **39**, 359–407
3. Balaban, R. S., Nemoto, S., and Finkel, T. (2005) *Cell* **120**, 483–495
4. Johnson, T. E., de Castro, E., Hegi de Castro, S., Cypser, J., Henderson, S., and Tedesco, P. (2001) *Exp. Gerontol.* **36**, 1609–1617
5. Murphy, C. T., McCarroll, S. A., Bargmann, C. I., Fraser, A., Kamath, R. S., Ahringer, J., Li, H., and Kenyon, C. (2003) *Nature* **424**, 277–283
6. Lee, S. S., Kennedy, S., Tolonen, A. C., and Ruvkun, G. (2003) *Science* **300**, 644–647
7. McElwee, J., Bubb, K., and Thomas, J. H. (2003) *Aging Cell* **2**, 111–121
8. Nemoto, S., and Finkel, T. (2002) *Science* **295**, 2450–2452
9. Kops, G. J., Dansen, T. B., Polderman, P. E., Saarloos, I., Wirtz, K. W., Coifer, P. J., Huang, T. T., Bos, J. L., Medema, R. H., and Burgering, B. M. (2002) *Nature* **419**, 316–321
10. Lee, S. S., Lee, R. Y., Fraser, A. G., Kamath, R. S., Ahringer, J., and Ruvkun, G. (2003) *Nat. Genet.* **33**, 40–48
11. Hamilton, B., Dong, Y., Shindo, M., Liu, W., Odell, I., Ruvkun, G., and Lee, S. S. (2005)

p66^{shc} Regulates Mitochondrial Metabolism

Genes Dev. **19**, 1544–1555

12. Dillin, A., Hsu, A. L., Arantes-Oliveira, N., Lehrer-Graiwer, J., Hsin, H., Fraser, A. G., Kamath, R. S., Ahringer, J., and Kenyon, C. (2002) *Science* **298**, 2398–2401
13. Rea, S., and Johnson, T. E. (2003) *Dev. Cell* **5**, 197–203
14. Kenyon, C. (2005) *Cell* **120**, 449–460
15. Migliaccio, E., Giorgio, M., Mele, S., Pelicci, G., Rebaldi, P., Pandolfi, P. P., Lanfrancone, L., and Pelicci, P. G. (1999) *Nature* **402**, 309–313
16. Pelicci, G., Lanfrancone, L., Grignani, F., McGlade, J., Cavallo, F., Forni, G., Nicoletti, I., Pawson, T., and Pelicci, P. G. (1992) *Cell* **70**, 93–104
17. Napoli, C., Martin-Padura, I., de Nigris, F., Giorgio, M., Mansueto, G., Sonnma, P., Condorelli, M., Sica, G., De Rosa, G., and Pelicci, P. (2003) *Proc. Natl. Acad. Sci. U. S. A.* **100**, 2112–2116
18. Francia, P., delli Gatti, C., Bachschmid, M., Martin-Padura, I., Savoia, C., Migliaccio, E., Pelicci, P. G., Schiavoni, M., Luscher, T. F., Volpe, M., and Cosentino, F. (2004) *Circulation* **110**, 2889–2895
19. Trinei, M., Giorgio, M., Cicalese, A., Barozzi, S., Ventura, A., Migliaccio, E., Milia, E., Padura, I. M., Raker, V. A., Maccarana, M., Petronilli, V., Minucci, S., Bernardi, P., Lanfrancone, L., and Pelicci, P. G. (2002) *Oncogene* **21**, 3872–3878
20. Combs, C. A., and Balaban, R. S. (2001) *Biophys. J.* **80**, 2018–2028
21. Joubert, F., Fales, H. M., Wen, H., Combs, C. A., and Balaban, R. S. (2004) *Biophys. J.* **86**, 629–645
22. Combs, C. A., and Balaban, R. S. (2004) *Methods Enzymol.* **385**, 257–286
23. Sariban-Sohraby, S., Magrath, I. T., and Balaban, R. S. (1983) *Cancer Res.* **43**, 4662–4664
24. Ventura, A., Maccarana, M., Raker, V. A., and Pelicci, P. G. (2004) *J. Biol. Chem.* **279**, 2299–2306
25. Giorgio, M., Migliaccio, E., Orsini, F., Paolucci, D., Moroni, M., Contursi, C., Pelliccia, G., Luzi, L., Minucci, S., Marcaccio, M., Pinton, P., Rizzuto, R., Bernardi, P., Paolucci, F., and Pelicci, P. G. (2005) *Cell* **122**, 221–233
26. Orsini, F., Migliaccio, E., Moroni, M., Contursi, C., Raker, V. A., Piccini, D., Martin-Padura, I., Pelliccia, G., Trinei, M., Bono, M., Puri, C., Tacchetti, C., Ferrini, M., Mannucci, R., Nicoletti, I., Lanfrancone, L., Giorgio, M., and Pelicci, P. G. (2004) *J. Biol. Chem.* **279**, 25689–25695
27. Feng, J., Bussiere, F., and Hekimi, S. (2001) *Dev. Cell* **1**, 633–644

***p66^{Shc}* gene has a pro-apoptotic role in human cell lines and it is activated by a p53-independent pathway** [☆]

Luca Tiberi ^a, Amir Faisal ^b, Matteo Rossi ^a, Lucia Di Tella ^a,
Claudio Franceschi ^{a,c,d,e}, Stefano Salvioli ^{a,c,d,*}

^a Department of Experimental Pathology, University of Bologna, via S. Giacomo 12, 40126 Bologna, Italy

^b Friedrich Miescher Institute for Biomedical Research, Maulbeerstrasse 66, CH-4058 Basel, Switzerland

^c Centro Interdipartimentale "L. Galvani," via S. Giacomo 12, 40126 Bologna, Italy

^d ER-GenTech laboratory, via Saragat 1, 44100 Ferrara, Italy

^e I.N.R.C.A., Department of Gerontological Sciences, via Birarelli 8, 60121 Ancona, Italy

Received 1 February 2006

Available online 9 February 2006

Abstract

p66^{Shc} protein has been proposed to be an indispensable factor for p53-dependent, mitochondria-mediated apoptosis in mice. Here, we show that *p66^{Shc}* plays a pro-apoptotic role also in cell lines of human origin such as SaOs-2 and HeLa, where p53 is either absent or inactivated, thus, suggesting that *p66^{Shc}* pro-apoptotic role is independent from the presence of a functional form of p53. The active form of *p66^{Shc}* is phosphorylated in Serine 36. We confirm the importance of Serine 36 phosphorylation for *p66^{Shc}* pro-apoptotic role, and our results suggest that the kinase involved in this process is activated independently from p53.

© 2006 Elsevier Inc. All rights reserved.

Keywords: *p66^{Shc}*; Oxidative stress; Apoptosis; Human cell lines; Serine phosphorylation

Shc proteins have been implicated in longevity in mammals [1] and in a variety of processes such as stress response, proliferation, and apoptosis [2]. The *shcA* locus encodes three isoforms *p46*, *p52*, and *p66^{Shc}*, sharing the same modular structure PTB-CH1-SH2 [3]. In particular, *p66^{Shc}* contains a unique amino-terminal region (CH2) [4] which is phosphorylated at Serine 36 residue (Ser36) after UV rays and hydrogen peroxide (H₂O₂) exposure [5]. Activation of ERKs is necessary for Ser36 phosphorylation after H₂O₂ treatment and *p66^{Shc}* seems to inhibit ERKs with a feed-back loop [6]. *p66^{Shc}* is thought to be a crucial

mediator of the apoptotic response to oxidative damage, since it has been observed that *p66^{Shc}-/-* mice have increased resistance to oxidative stress and prolonged lifespan. Mouse embryo fibroblasts (MEFs) derived from *p66^{Shc}-/-* mice display lower levels of intracellular reactive oxygen species (ROS) and increased resistance to oxidative stress [1]. The overexpression of *p66^{Shc}* in Jurkat cells increases the percentage of apoptosis after H₂O₂ exposure [7]. On the whole, these data suggested a pro-apoptotic role for *p66^{Shc}* in response to oxidative stress [7]. In fact, it has been reported that *p66^{Shc}* is required for the elevation of the intracellular oxidants and for cytochrome *c* release [5]. Indeed, *p66^{Shc}* appears to be localized at mitochondrial level, where it forms a complex with mtHsp70 and regulates the transmembrane potential [8]. More recently, a model for *p66^{Shc}* pro-apoptotic action at mitochondrial level has been proposed [9]. As far as the role of p53 in *p66^{Shc}* activation, experimental evidence showed that *p66^{Shc}* protein levels are up-regulated in p53 wt, but not

[☆] Abbreviations: H₂O₂, hydrogen peroxide; MEFs, mouse embryonic fibroblasts; ROS, reactive oxygen species; PI, propidium iodide; MMP, mitochondrial membrane potential; MPT, mitochondrial permeability transition; RNAi, RNA inhibition technique; siRNA, small interfering double-stranded RNA.

* Corresponding author. Fax: +39 051 2094747.

E-mail address: stefano.salvioli2@unibo.it (S. Salvioli).

in *p53*–/– MEFs after H₂O₂ exposure [5]. Taking into account all the above-mentioned data, we wish to investigate if *p66^{Shc}* requires *p53* to play its role in cells of human origin and to investigate the role of *p66^{Shc}* Ser36 in oxidative stress-induced apoptosis. To this aim, we overexpressed or silenced *p66^{Shc}* in human cell lines lacking a functional *p53* and thereafter we evaluated the susceptibility to apoptosis and mitochondrial membrane potential (MMP) after exposure to hydrogen peroxide. Finally we have evaluated the status of Ser36 residue of *p66^{Shc}* protein and the results obtained allowed us to speculate that Ser36 function is independent from *p53* gene function.

Materials and methods

Cell cultures. Human cell lines SaOs-2 and HeLa were grown in Dulbecco's modified Eagle's medium (Sigma, St. Louis, MO, USA) supplemented with 10% fetal bovine serum (Sigma) heat-inactivated for 30 min at 56 °C, 100 µg/ml streptomycin–100 IU/ml penicillin (PenStrep; Bio-Whittaker, Verviers, Belgium), and 2 mM L-Gln (BioWhittaker); cells were kept at 37 °C in a humidified atmosphere (5% CO₂).

Apoptosis was induced by treatment with 50 µM H₂O₂. In the case of transfected cells, H₂O₂ treatment was performed after 24 h from plasmid transfection. In the case of siRNA experiments, treatment was performed after 48 h from siRNA transfection. Before H₂O₂ exposure, culture medium was removed and replaced with PBS + H₂O₂ 50 µM. After 30 min of incubation at 37 °C, PBS and H₂O₂ were discarded, fresh medium was supplied, and cells were allowed to recover for 4 or 24 h.

RNA extraction and reverse transcription. Total RNA was extracted from cells using TRIzolTM Reagent (Invitrogen, Milan, Italy) according to the manufacturer's instructions. Reverse transcription reactions were performed with 2 µg of total RNA using the M-MLV Reverse Transcriptase (Invitrogen), following the manufacturer's instructions.

Protein extraction and Western blot analysis. Total proteins were extracted with Co-IP Buffer (10 mM Tris–HCl, pH 7.6, 140 mM NaCl, 0.5% NP-40, and 5 mM EDTA) added with Protease Inhibitor Cocktail (Sigma). Pellets were resuspended in Co-IP Buffer and incubated on ice for 10 min; after centrifugation, the supernatant containing proteins is recovered. Thirty micrograms of proteins is used in Western blot analysis, using the following antibodies: *p66^{Shc}* antibody (Upstate Biotechnology, Charlottesville, VA, USA), ShcA antibody (BD, S. José, CA, USA), β-actin antibody (Santa Cruz Biotechnology, S. Cruz, CA, USA), and Caspase-3 Antibody (Cell Signaling Technologies, MA, USA).

Plasmid transfection. HeLa and SaOs-2 cells were plated in six-well plates (9.6 cm²/well) and the following day were transfected with 0.2 µg of plasmid DNA/dish using EffecteneTM (Qiagen, Valencia, CA, USA) according to the manufacturer's standard protocol. Plasmids used were *pcDNA3p66Shc* (kindly provided by Dr. Yoshikuni Nagamine, Friedrich Miescher Institute, Basel, Switzerland), *pcDNA3.1* empty vector, and *pcDNA3p66S36A* (S36 A36, provided by Dr. Yoshikuni Nagamine).

siRNA transfection. To perform isoform-specific knockdown, the following 21-mer oligoribonucleotide pairs (Qiagen) were used: *p66^{Shc}* siRNA 5'-gAA UgA gUC UCU gUC AUC gUC-3' and 5'-CgA UgA CAg AgA CUCAUU CCG-3', from nt 236–256 (in the CH2 domain); *non-silencing* siRNA 5'-UUC UCC gAA CgU gUC ACg U-3' and 5'-ACg UgA CAC gUU Cgg AgA A-3' as negative control.

HeLa and SaOs-2 cells were plated in six-well plates in DMEM 10% FBS, 2 mM L-Gln (without antibiotics) at 2 × 10⁵ cells/well. The following day siRNAs were introduced into cells using the OligofectamineTM Reagent (Invitrogen) according to the manufacturer's instructions, using 10 µl of 20 µM siRNA and 3 µl of transfection reagent/well.

Cytofluorimetric analysis. Flow cytometric analyses were performed using a FACScan flow cytometer (FACScalibur, BD). A minimum of 10,000 cells was acquired in list mode for each sample. Analysis was performed using CellQuest software (BD).

The percentage of apoptotic cells was detected by Annexin V-FITC (ANX-V) and PI double staining (rh-annexin V/FITC kit, Bender Med-SystemsTM, Vienna, Austria). Cells were detached by trypsinization, centrifuged, and resuspended in 200 µl of appropriate binding buffer (10 mM Hepes/NaOH, pH 7.4, 140 mM NaCl, and 2.5 mM CaCl₂), and incubated for 10 min at room temperature in the dark with 5 µl of Annexin V-FITC-conjugated. Cells were washed in PBS and finally resuspended in 300 µl of binding buffer plus 10 µg/ml propidium iodide.

Mitochondrial membrane potential was assessed by JC-1 staining (Molecular Probes, Eugene, OR, USA). Briefly, cells were resuspended in 1 ml of complete medium and incubated for 10 min at room temperature in the dark with 5 µM JC-1, then washed and resuspended in 200 µl PBS, and analysed as previously described [9].

Results

p66^{Shc} overexpression in *p53*–/– human cell lines is able to increase H₂O₂-mediated apoptosis

To investigate the apoptotic role of *p66^{Shc}* in cells lacking *p53* function, we evaluated the exposure of phosphatidylserine residues (considered as an early apoptotic marker) in HeLa and SaOs-2 cells transfected with an empty plasmid (*pcDNA3.1*) or a plasmid encoding *p66^{Shc}* (*pcDNA3p66Shc*; provided by Dr. Yoshikuni Nagamine, Friedrich Miescher Institute, Basel, Switzerland [10]). The *p66^{Shc}* sequence present in the *pcDNA3* vector is of mouse origin and it contains a mutation in the potential translation initiator methionine codons of the *p46^{Shc}* and *p52^{Shc}* isoforms (converted into leucine codons), and thus, it is able to express only the *p66^{Shc}* form. Mouse amino acidic *p66^{Shc}* sequence displays a high degree of homology (94%) with human *p66^{Shc}* protein, particularly in CH2 domain (GenBank[®]/Mouse 14211983 and Human NM_183001). Cells were transfected and *p66^{Shc}* protein expression analysed by Western blot. After 24 h from transfection with *pcDNA3p66Shc* plasmid, an increase of *p66^{Shc}* expression was detected by Western blotting in both HeLa and SaOs-2 cells, as compared to cells transfected with the empty vector (data not shown). Cytofluorimetric analysis of cells co-stained with Annexin V-FITC and propidium iodide (PI) showed that a negligible percentage of apoptotic cells was detectable after transfection with the control empty vector (Figs. 1A and E). Similarly, after 24 h from transfection with *pcDNA3p66Shc*, cells did not show any dramatic increase of apoptosis or necrosis (Figs. 1B and F). On the contrary, when treated with 50 µM H₂O₂ for 30 min and allowed to recover for further 24 h, cells transfected with the empty vector showed a consistent percentage of cell death (Figs. 1C and G). When treated with 50 µM H₂O₂ for 30 min and allowed to recover for further 24 h, cells transfected with *pcDNA3p66Shc* showed a greater increase in the percentage of apoptotic and necrotic cells, as compared to cells transfected with the empty vector (Figs. 1D and H, compared with Figs. 1C and G). Fig. 1I summarizes the results of three separate experiments and reports the percentage of cell death (apoptosis + necrosis) in SaOs-2 and HeLa cells transfected with *pcDNA3.1* empty vector or *pcDNA3p66Shc* and treated

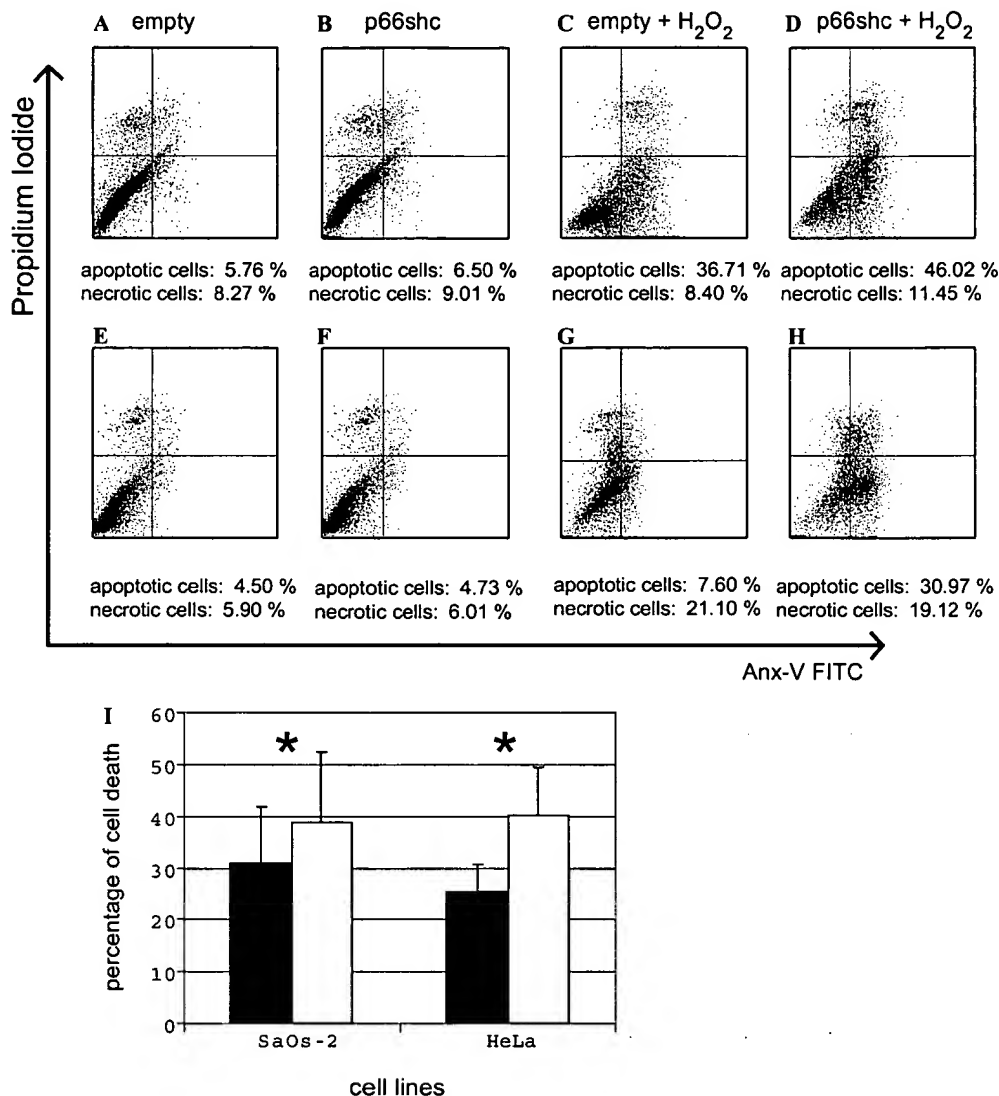


Fig. 1. Cytofluorimetric analysis of apoptosis with ANX V-FITC/PI in SaOs-2 and HeLa cells. (Abscissa: ANX V-FITC fluorescence; Ordinate: PI fluorescence.) A representative experiment out of three is shown. (A) SaOs-2 cells transfected with pcDNA3.1 empty vector. (B) SaOs-2 cells transfected with pcDNA3p66shc plasmid. (C) SaOs-2 cells transfected with pcDNA3.1 and treated with H₂O₂ 50 μM (24 h of recovery). (D) SaOs-2 cells transfected with pcDNA3p66shc and treated with H₂O₂ 50 μM (24 h of recovery). (E) HeLa cells transfected with pcDNA3.1 empty vector. (F) HeLa cells transfected with pcDNA3p66shc plasmid. (G) HeLa cells transfected with pcDNA3.1 and treated with H₂O₂ 50 μM (24 h of recovery). (H) HeLa cells transfected with pcDNA3p66shc and treated with H₂O₂ 50 μM (24 h of recovery). Black columns: cells transfected with pcDNA3.1; white columns: cells transfected with pcDNA3p66shc. Data represent means ± SD of three separate experiments. *p = 0.04, paired Student's *t* test.

with 50 μM H₂O₂. The overexpression of *p66^{Shc}* gene induces a significant increase of oxidative stress-induced cell death in both cell lines.

Oxidative stress-induced apoptosis in *p53*−/− human cell lines is partly *p66^{Shc}*-dependent

To further demonstrate the role of *p66^{Shc}* in oxidative stress-mediated apoptosis in *p53*−/− cells, we used the RNA inhibition technique (RNAi), an in vitro knockdown system (kindly provided by Dr. Yoshikuni Nagamine, Friedrich Miescher Institute, Basel, Switzerland, [10]).

RNAi consists of small interfering double-stranded RNA (siRNA) transfected into HeLa and SaOs-2 cells to inhibit *p66^{Shc}* expression. In these experiments we used two siRNA: siRNAP66Shc, specific for *p66^{Shc}* and a scramble siRNA, which does not recognize any human mRNA, as a control. We checked the *p66^{Shc}* down-regulation by competitive RT-PCR for *p66^{Shc}* mRNA and Western blot analysis (data not shown). HeLa and SaOs-2 cells were then treated with 50 μM H₂O₂ after 48 h from transfection with siRNAP66Shc plasmid. Four hours after oxidative stress, apoptosis has been analysed and a decrease in the percentage of apoptotic cells was found in HeLa cells

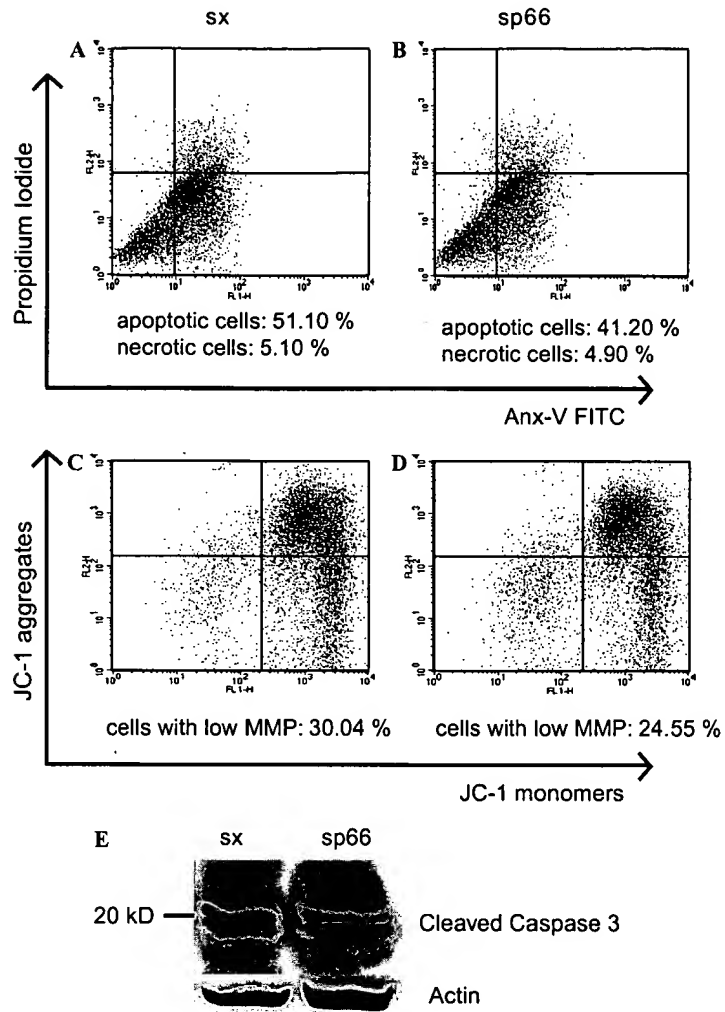


Fig. 2. Cytotoxicity and apoptosis analysis in HeLa cells transfected with siRNAs p66Shc and H₂O₂ 50 μ M (4 h of recovery). (A,B) ANX-FITC/PI analysis (Abscissa: ANX V-FITC fluorescence; Ordinate: PI fluorescence). (A) Cells transfected with scramble siRNA (sx). (B) Cells transfected with siRNAs p66Shc (sp66). (C,D) MMP analysis (JC-1 staining; Abscissa: JC-1 monomers, green fluorescence; Ordinate: JC-1 aggregates, red fluorescence; lower right quadrant: cells with low MMP). (C) Cells transfected with sx. (D) Cells transfected with sp66. (E) Western blot analysis of Caspase 3 cleavage in cells transfected with sx or sp66 and treated with H₂O₂ 50 μ M (4 h of recovery).

(Figs. 2A and B) but not in SaOs-2 cells (data not shown). To confirm these data, other parameters related to apoptosis were assessed, i.e., the MMP, detected by means of the potentiometric cationic dye JC-1 [11], and cleavage of Caspase 3. Also in this case, a mild but consistent decrease of cells with low MMP (Figs. 2C and D) and cleavage of Caspase 3 (Fig. 2E) was observed.

Serine 36 is required for a fully working p66^{Shc} protein

To check for p66^{Shc} Ser36 function in p53^{−/−} human cell lines, we used another plasmid, pcDNA3p66S36A, which encodes a p66^{Shc} protein with an Alanine residue at codon 36 instead of a Serine one. Cytofluorimetric analysis showed that, upon H₂O₂ treatment, both SaOs-2 and HeLa cells, when transfected with pcDNA3p66S36A plasmid, have a decreased percentage of apoptotic cells with

respect to those transfected with pcDNA3p66shc, thus confirming that Ser36 is required for a fully working p66^{Shc} protein (Fig. 3A).

These results were confirmed by measuring MMP. Also in this case, cells transfected with pcDNA3p66S36A showed lower percentage of cells with low MMP with respect to those transfected with pcDNA3p66shc (Fig. 3B). This is in agreement with the observation that p66^{Shc} is important for cytochrome *c* release from mitochondria upon apoptotic stimulation [8].

Discussion

p66^{Shc} is an important component of apoptotic response and life span in mouse. Several studies in mouse have confirmed its pivotal role in oxidative stress response, but only few experiments have been performed in human cells.

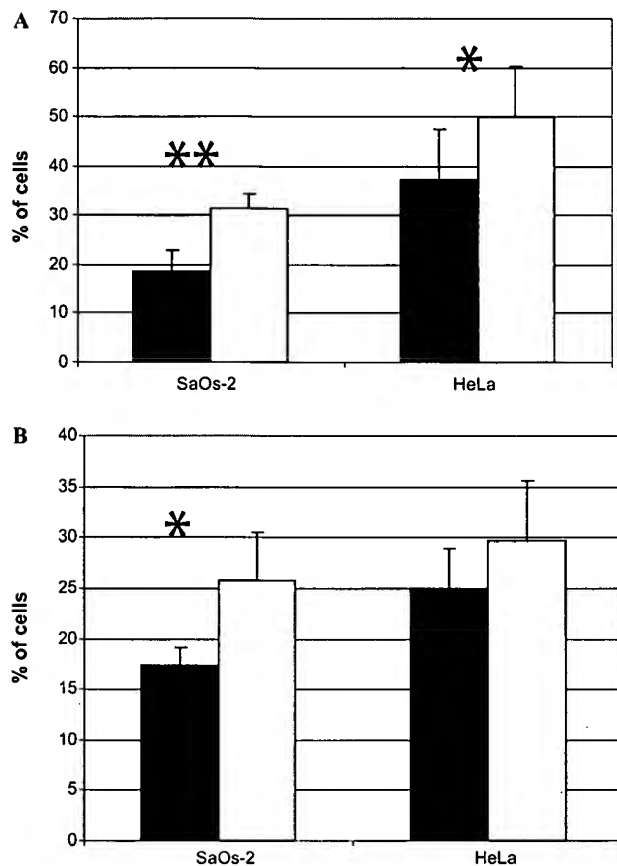


Fig. 3. Cytofluorimetric analysis of SaOs-2 and HeLa cells transfected with pcDNA3p66S36A or pcDNA3p66shc plasmids. (A) Percentage of apoptotic cells as assessed by ANX V-FITC/PI double staining. (B) Percentage of cells with depolarized mitochondrial membrane as assessed by JC-1 staining. Data are expressed as percentage \pm SD of three experiments. Black columns, pcDNA3p66S36A; white columns, pcDNAp66shc. * $p < 0.05$; ** $p < 0.01$, Student's *t* test.

In particular, we reported that dermal fibroblasts from aged subject and centenarians have higher expression of *p66^{shc}* with respect to young people, both as mRNA and protein [12]. Further, in centenarians *p66^{shc}* expression was correlated with a polymorphism of *p53* gene at codon 72, suggesting a functional link of *p53* with *p66^{shc}*.

In this study, we observed an increase in apoptosis imputable to *p66^{shc}* overexpression in cell lines of human origin, thus confirming the proposed *p66^{shc}* pro-apoptotic role also in human cells. Moreover, *p66^{shc}* is not able to induce apoptosis per se, but only after oxidative stress, thus suggesting that it has to be considered not as a direct effector of cell death but rather an adaptor factor that can potentiate (or amplify) an upstream apoptotic signal. Moreover, we could confirm that the Serine at residue 36 is important for mitochondrial *p66^{shc}* action.

Experimental evidence has showed that *p66^{shc}* protein levels are modulated by *p53*, in particular *p66^{shc}* appears to be up-regulated after H_2O_2 treatment in *p53*+/+ cells, but not in *p53*–/– MEFs [5]. In order to investigate if *p66^{shc}* requires physical interaction with *p53* protein (which

is known to localize at mitochondrial level upon apoptotic stimulation) [13,14], we evaluated the susceptibility to apoptosis and the depolarization of mitochondrial membrane after hydrogen peroxide exposure in human cell lines lacking a functional *p53* gene and transiently transfected with plasmid encoding for *p66^{shc}*. In such cells we could observe that even in the absence of functional *p53* protein, *p66^{shc}* maintains a pro-apoptotic function in response to oxidative stress, suggesting that its action is independent from direct or indirect interaction with *p53* protein. Moreover, we could confirm that *p66^{shc}* is responsible, at least to some extent, for the apoptotic response to oxidative stress also in human cells, as we found that in *p66^{shc}* knocked-down cells there is an impaired apoptotic response to H_2O_2 treatment.

It has been recently reported that mitochondria-localized *p66^{shc}* is able to induce mitochondrial permeability transition (MPT), oxidation of cytochrome *c*, and production of H_2O_2 [9]. In our hands, the overexpression of *p66^{shc}* did not induce per se a decrease of MMP, thus it is unlikely that a phenomenon of MPT occurs directly upon *p66^{shc}* overexpression. This suggests that *p66^{shc}* mitochondrial localization is likely to occur only after stress.

Finally, we have evaluated Ser36 function for a fully working *p66^{shc}* protein and we observed that Ser36 modulates not only apoptosis but also MMP, and our data suggest that it is phosphorylated in a *p53*-independent manner. Also, no data are available about the possible mechanisms of action of *p66^{shc}* Ser36. It is to note that Ser36 is contained into a S-P motif that is a possible target of the isomerase Pin1. Pin1 is an enzyme that isomerizes phosphorylated Ser/Thr-Pro bonds and regulates different biological processes and pathological conditions. The importance of this Serine residue could likely be due to the fact that Pin1 isomerization is required for the *p66^{shc}* function in mitochondrial depolarization. Further studies are needed to identify possible interactions of *p66^{shc}* with Pin1 and other proteins.

Acknowledgments

This work was supported by: AIRC (Associazione Italiana Ricerca sul Cancro) Grant, EU (European Union) Grants 'T-CIA' and PROTEOMAGE; the PRRIITT program of the Emilia-Romagna Region and Fondi Strutturali Obiettivo 2; MIUR (Italian Ministry of University) Fondo per gli Investimenti della Ricerca di Base (FIRB) 2001, protocol #RBNE018AAP and #RBNE018R89; Italian Ministry of Health Grant (Ricerche Finalizzate 2002 and 2003) to CF; University of Bologna Ricerca Fondamentale Orientata (RFO ex 60%) 2005 and Roberto and Cornelia Pallotti Legacy for Cancer Research Grants to CF and SS.

References

- [1] E. Migliaccio, M. Giorgio, S. Mele, G. Pelicci, P. Rebaldi, P.P. Pandolfi, L. Lanfrancone, P.G. Pelicci, The *p66^{shc}* adaptor protein

controls oxidative stress response and life span in mammals, *Nature* 402 (1999) 309–313.

[2] L. Bonfini, E. Migliaccio, P.G. Pelicci, L. Lanfrancone, P.G. Pelicci, Not all Shc's roads lead to Ras, *Trends Biochem. Sci.* 21 (1996) 257–261.

[3] G. Pelicci, L. Lanfrancone, F. Grignani, J. Mc Glade, F. Cavallo, G. Forni, I. Nicoletti, F. Grignani, T. Pawson, P.G. Pelicci, A novel transforming protein (SHC) with an SH2 domain is implicated in mitogenic signal transduction, *Cell* 70 (1992) 93–104.

[4] G. Pelicci, L. Dente, A. De Giuseppe, B. Verducci-Galletti, S. Giuliani, S. Mele, C. Vetrini, M. Giorgio, P.P. Pandolfi, G. Cesareni, P.G. Pelicci, A family of Shc related proteins with conserved PTB, CH1 and SH2 regions, *Oncogene* 13 (1996) 633–641.

[5] M. Trinei, M. Giorgio, A. Cicalese, S. Barozzi, A. Ventura, E. Migliaccio, E. Milia, I. Martin-Padura, V.A. Raker, M. Maccarana, V. Petronilli, S. Minucci, P. Bernardi, L. Lanfrancone, P.G. Pelicci, A p53-p66Shc signalling pathway controls intracellular redox status, levels of oxidation-damaged DNA and oxidative stress-induced apoptosis, *Oncogene* 21 (2002) 3872–3878.

[6] Y. Hu, X. Wang, L. Zeng, D.Y. Cai, K. Sabapathy, S.P. Goff, E.J. Firpo, B. Li, ERK phosphorylates p66shcA on Ser36 and subsequently regulates p27kip1 expression via the Akt-FOXO3a pathway: implication of p27kip1 in cell response to oxidative stress, *Mol. Biol. Cell.* 16 (2005) 3705–3718.

[7] S. Pacini, M. Pellegrini, E. Migliaccio, L. Patrussi, C. Ulivieri, A. Ventura, F. Carraro, A. Naldini, L. Lanfrancone, P. Pelicci, C.T. Baldari, p66SHC promotes apoptosis and antagonizes mitogenic signaling in T cells, *Mol. Cell. Biol.* 24 (2004) 1747–1757.

[8] F. Orsini, E. Migliaccio, M. Moroni, C. Contursi, V.A. Raker, D. Piccini, I. Martin-Padura, G. Pelliccia, M. Trinei, M. Bono, C. Puri, C. Tacchetti, M. Ferrini, R. Mannucci, I. Nicoletti, L. Lanfrancone, M. Giorgio, P.G. Pelicci, The life span determinant p66Shc localizes to mitochondria where it associates with mtHsp70 and regulates trans-membrane potential, *J. Biol. Chem.* 11 (2004) 25689–25695.

[9] M. Giorgio, E. Migliaccio, F. Orsini, D. Paolucci, M. Moroni, C. Contursi, G. Pelliccia, L. Luzi, S. Minucci, M. Marcaccio, P. Pinton, R. Rizzuto, P. Bernardi, Electron transfer between cytochrome *c* and p66Shc generates reactive oxygen species that trigger mitochondrial apoptosis, *Cell* 122 (2005) 221–233.

[10] M. Kisielov, S. Kleiner, M. Nagasawa, A. Faisal, Y. Nagamine, Isoform-specific knockdown and expression of adaptor protein ShcA using small interfering RNA, *Biochem. J.* 363 (2002) 1–5.

[11] S. Salvioli, A. Ardizzone, C. Franceschi, A. Cossarizza, JC-1, but not DiOC6(3) or rhodamine 123, is a reliable fluorescent probe to assess delta psi changes in intact cells: implications for studies on mitochondrial functionality during apoptosis, *FEBS Lett.* 411 (1997) 77–82.

[12] S. Pandolfi, M. Bonafè, L. Di Tella, L. Tiberi, S. Salvioli, D. Monti, S. Sorbi, C. Franceschi, p66(shc) is highly expressed in fibroblasts from centenarians, *Mech. Ageing Dev.* 126 (2005) 839–844.

[13] M. Bonafe, S. Salvioli, C. Barbi, C. Trapassi, F. Tocco, G. Storci, L. Invidia, I. Vannini, M. Rossi, E. Marzi, M. Mishto, M. Capri, F. Olivieri, R. Antonicelli, M. Memo, D. Uberti, B. Nacmias, S. Sorbi, D. Monti, C. Franceschi, The different apoptotic potential of the p53 codon 72 alleles increases with age and modulates in vivo ischaemia-induced cell death, *Cell Death Differ.* 11 (2004) 962–973.

[14] N.D. Marchenko, A. Zaika, U.M. Moll, Death signal-induced localization of p53 protein to mitochondria. A potential role in apoptotic signaling, *J. Biol. Chem.* 275 (2000) 16202–16212.

Reduction of p66Shc Suppresses Oxidative Damage in Retinal Pigmented Epithelial Cells and Retina

ZHIHAO WU, BRIAN ROGERS, SHU KACHI, SEAN F. HACKETT,
 ANNA SICK, AND PETER A. CAMPOLCIARO*

Departments of Ophthalmology and Neuroscience,
 Johns Hopkins University School of Medicine, Baltimore, Maryland

The largest isoform of the Shc adapter protein, p66Shc, has been implicated in oxidative damage-induced apoptosis in vital organs, because mice deficient in p66Shc have a 30% increase in life span and are resistant to the lethal effects of systemically administered paraquat, a source of severe oxidative damage. In this study, we utilized siRNA directed against the CH2 domain of Shc, to reduce p66Shc, but not p52Shc nor p46Shc in retinal pigmented epithelial (RPE) cells. RPE cells deficient in p66Shc had reduced susceptibility to oxidative stress-induced apoptosis. Compared to control cells, those with reduced p66Shc had increased basal and oxidative stress-induced NF- κ B transcriptional activity, increased levels of antioxidant enzymes, and less generation of reactive oxygen species when challenged with H₂O₂. The increase in oxidative stress-induced NF- κ B activity was mediated by activation of ERK. Compared to eyes injected with GFP siRNA, those injected with p66Shc siRNA showed less loss of retinal function as assessed by electroretinograms from paraquat-induced oxidative stress. These data suggest that p66Shc and molecular signals involved in its regulation provide therapeutic targets for retinal degenerations in which oxidative-damage plays a major role, including age-related macular degeneration and cone cell death in retinitis pigmentosa. *J. Cell. Physiol.* 209: 996–1005, 2006. © 2006 Wiley-Liss, Inc.

Oxidative damage has been implicated in the pathogenesis of age-related macular degeneration (AMD) (The Age-Related Eye Disease Study Research Group, 2001) and in cone cell death after rods degenerate in retinitis pigmentosa (RP) (Shen et al., 2005b). The Age-Related Eye Disease Study (AREDS) has shown that oral administration of antioxidant vitamins and/or zinc has a beneficial effect in patients with AMD, and while the benefit is rather modest, it provided proof-of-concept for bolstering the retina's defense system against oxidative damage as a treatment strategy for AMD (The Age-Related Eye Disease Study Research Group, 2001). One way to improve on the results of AREDS is to identify additional antioxidants that can be added to the AREDS formulation to provide greater protection to the retina against oxidative damage. However, exogenous antioxidants are only one component of the oxidative defense system in any particular tissue. The primary line of defense is an elaborate system of antioxidant enzymes. Thus, a second treatment strategy for AMD and RP is to characterize the endogenous antioxidant defense systems in rods and cones and develop ways to strengthen them. A third, complementary approach is to determine how oxidative damage leads to death of rods and cones and identify ways to intervene at this downstream step.

A major way in which oxidative damage leads to cell death is by inducing apoptosis. Recently a member of the Shc protein family has been identified as a critical molecule linking oxidative damage to apoptosis (Migliaccio et al., 1999). There are three members of the Shc family, ShcA, ShcB, and ShcC, that each has an N-terminal phosphotyrosine binding (PTB) domain and a C-terminal Src homology-2 (SH2) domain (Pelicci et al., 1996). ShcA is expressed in many tissues, while ShcB and ShcC are expressed only in neurons. ShcA (also designated Shc) was identified as an adapter protein that couples activated growth factor receptors to Ras and the mitogen-activated protein (MAP) kinase cascade (Ravichandran, 2001). There are three isoforms of Shc, p66Shc, p52Shc, and p46Shc that are 66, 52, or 46 kDa in size, respectively. All three isoforms have a

central collagen homology domain (CH1) containing tyrosine residues that when phosphorylated in p52Shc or p46Shc mediate MAP kinase signaling. Thus p52Shc and P46Shc function to amplify signaling through tyrosine kinase receptors to enhance mitogenesis and other growth factor functions. The longest isoform, p66Shc, does not enhance actions of growth factors, but rather serves as a negative modulator by acting as a dominant-negative inhibitor of p52Shc- and p46Shc-mediated stimulation of MAP kinase (Migliaccio et al., 1997).

An N-terminal CH2 domain that is not present in the two shorter isoforms mediates a second function of p66Shc. This domain contains a serine residue at position 36 (Ser36) that is phosphorylated in cells that are exposed to ultraviolet (UV) light or H₂O₂ (Migliaccio et al., 1999). Mice with a targeted mutation of the exon encoding the CH2 domain of Shc are deficient in p66Shc, but not p52Shc nor p46Shc. The mutant mice had a 30% increase in life span compared to wild-type mice and were resistant to the lethal effects of systemic injection of paraquat, a source of severe oxidative damage. Embryonic fibroblasts from the mutant mice were protected against UV light- or H₂O₂-induced apoptosis. Thus, the phosphorylation of the unique Ser36 in p66Shc plays a critical role in linking oxidative stress to apoptosis.

Contract grant sponsor: NEI; Contract grant numbers: EY05951, EY12609, EY11498, P30EY1765, P30EY0572; Contract grant sponsor: Macula Vision Foundation; Contract grant sponsor: Dr. and Mrs. William Lake, and Ms. Beth Myers.

*Correspondence to: Dr. Peter A. Campochiaro, Maumenee 719, The Johns Hopkins University School of Medicine, 600 N. Wolfe Street, Baltimore, MD 21287-9277. E-mail: pcampo@jhmi.edu

Received 6 April 2006; Accepted 6 July 2006

DOI: 10.1002/jcp.20819

It is not known if p66Shc mediates death of retinal cells from oxidative damage. As noted above, ShcB and ShcC are selectively expressed in neurons and in some neurons ShcA is low or undetectable, but it is unclear what the level of expression of ShcA is in retinal neurons or non-neuronal cells such as retinal pigmented epithelial (RPE) cells or Muller cells, which are derived from neural ectoderm, but are not neurons. In this study we investigated the role of p66Shc in oxidative damage in the RPE and retina.

MATERIALS AND METHODS

Reagents and cells

The inhibitors PD98059, LY294002, p38 inhibitor, and PP2 were purchased from Calbiochem (San Diego, CA) and used at the concentrations of 50, 20, 10, and 5 μ M, respectively. These concentrations were found to be effective in previous studies (Ceryak et al., 2004; Lee et al., 2004a,b; Hayashi et al., 2005). Rabbit polyclonal anti-Shc antibody generated from human Shc SH2 domain was obtained from Transduction Laboratories (Hanover, MD). Anti-phospho-p44/42 Map kinase, anti-Map kinase, and anti-Akt antibodies were obtained from Cell Signaling (Beverly, MA). Human RPE cells were isolated as previously described (Campochiaro et al., 1986) and grown in Dulbecco's modified Eagle's medium (DMEM) supplemented with 10% fetal bovine serum.

Small interfering RNA (siRNA)

Two siRNAs that specifically target both human and mouse p66Shc and not p52Shc nor p46Shc, 5'-UGA GUC UCU GUC AUC GCU GdTdT-3' and 5'-CAG CGA UGA CAG AGA CUC AdTdT-3', were designed using the "siRNA Target Finder and Design Tool" provided on the website (www.ambion.com) for Ambion, Inc. (Austin, TX). To provide a control, siRNAs directed against GFP were designed, 5'-ACG ACU UCU UCA AGU CCU UdTdT-3' and 5'-AAG GAC UUG AAG AAG UCG UdGdC-3'. RPE cells were plated in 6-well plates and when the cells were 30–50% confluent, siRNAs directed against p66Shc or GFP were added in final concentration of 1 μ M with oligofectAMINE (Invitrogen, Carlsbad, CA) or X-tremeGENE siRNA Transfection Reagent (Roche, Nutley, NJ) using the manufacturer's instructions.

Immunoblots

At various times after addition of siRNAs, the levels of Shc isoforms were assessed by immunoblots. Other immunoblots were done to assess for phosphorylated p44/42 MAP kinase. RPE cells were seeded in 6-well plates (10^5 cells per well) and after various treatments they were lysed in pre-warmed Laemmli buffer (Bio-Rad, Hercules, CA). For each sample, the entire pre-cleared cell lysate was added to a well of a 12% acrylamide gel and resolved by SDS-PAGE. The separated proteins were transferred to a nitrocellulose membrane (Hybond-ECL, Amersham Biosciences, Piscataway, NJ). Non-specific binding was blocked by incubation with 5% non-fat milk at room temperature for 2 h and then the membranes were incubated with primary antibody overnight at 4°C. The various primary antibodies used were rabbit polyclonal anti-human Shc (1:500, Transduction Laboratories), rabbit polyclonal anti-phospho-p44/42 MAP kinase (1:1,000, Cell Signaling), and rabbit polyclonal anti-Akt (1:1,000, Cell Signaling). The proteins were detected by SuperSignal western Pico lumino/Enhancer solution using horseradish peroxidase-linked anti-rabbit IgG (Pierce, Rockford, IL). Blots were quantified by densitometry using a Bio-Rad Molecular Imager FX and Quantity One software.

Cell viability assays

Cells were plated in 6-well plates and using oligofectAMINE (Invitrogen) as a carrier were transfected with either *p66shc* siRNA or *GFP* siRNA as a control. At 24, 48, or 72 h after addition of siRNA, cells were placed in serum-free medium and 0.8 mM H₂O₂ was added. Cell viability was determined 24 h after addition of H₂O₂ by Trypan Blue exclusion. Trypan Blue

(0.4%) (Sigma, St. Louis, MO) is a dye that is taken up by dead cells and excluded by living cells. Cultures were trypsinized and the number of stained and unstained cells per ml was counted in a hemocytometer allowing calculation of the number of viable cells per well. For long-term survival assays, the cells were placed in serum-free medium and treated with 0.8 mM H₂O₂ 72 h after initial transfection. Cells were trypsinized and counted with a Coulter Counter at indicated time points after H₂O₂ exposure.

Determination of intracellular ROS levels

Seventy-two hours after addition of siRNAs, cells were placed in serum-free medium containing various concentrations of H₂O₂ for 30 min and then 30 μ M 2',7'-dichlorofluorescein diacetate (DCFDA; Molecular probes, Inc. Eugene, OR), an efficient probe for identification of free radicals (Yoshida et al., 2003), was added. After 30 min, the cells were examined with an inverted fluorescence microscope (Nikon Eclipse TE2000U). In similar experiments, 5 μ M hydroethidine was added to RPE cell cultures 30 min after addition of H₂O₂ and after an additional 30 min fluorescence microscopy was done.

In situ terminal deoxynucleotidyltransferase-mediated deoxy-UTP nick end labeling (TUNEL)

The commercially available Apoptag Plus Fluorescein In Situ Apoptosis Detection kit (Chemicon International, Inc. Temecula, CA) was used to detect apoptotic cells. Seventy-two hours after lipofection with siRNAs, cells were placed in serum-free medium for 24 h and then incubated for 5 h in the presence or absence of H₂O₂. Cells were fixed and apoptotic cells were determined with the Apoptag kit using the manufacturer's instructions. The percentage of the total number of cells that were apoptotic was quantified with Scion image software.

Quantitative real-time PCR

Total RNA was isolated at the indicated time using the RNAeasy kit (Qiagen, Valencia, CA) and incubated with rDNase I (DNA-freeTM kit, Ambion, Inc.) to remove any traces of contaminating DNA. Reverse transcription was performed at 50°C for 1 h using 2 μ g of total RNA, 1 μ l of SuperscriptTM III reverse transcriptase, 1 μ l of oligo(dT)₂₀ (50 μ M), 1 μ l of 10 mM dNTP, 4 μ l of 5 \times First-stand buffer, 1 μ l of 0.1 M DTT, and 1 μ l of RNaseOUT (Invitrogen). Each 20 μ l of PCR reaction mixture was prepared using the LightCycler FastStart DNA Master^{PULS} SYBR Green I kit (Roche). The primer pairs used for each mRNA that was measured is shown in Table 1; they were designed to hybridize in two different exons or at exon/intron boundaries to prevent amplification of any remaining genomic DNA. The amplification conditions were optimized for each primer set, but in general the following conditions were used for most primer sets; denaturation at 95°C for 15 sec, annealing at 55°C for 5 sec, and extension at 72°C for 12 sec for a total of 40 cycles. Under optimized conditions there was a single melting curve and no primer–dimer formation. The copy number for each mRNA was determined using a standard curve generated with external standards of known copy number. The transcript of human ribosome protein (Large Po subunit) was used as an internal control.

Luciferase assays for NF- κ B activity

RPE cells were plated in 6-well plates and co-transfections were done at 80–90% confluence. An NF- κ B-responsive reporter plasmid (pTAL-NF- κ B, BD Biosciences Clontech, Mountain View, CA) and a *Renilla* luciferase vector (pRL-SV40 vector, Promega, Madison, WI) were co-transfected with either *p66shc* or *GFP* siRNA using X-tremeGENE siRNA Transfection Reagent (Roche). Seventy-two hours after transfection, cells were placed in serum-free medium for 24 h, treated with H₂O₂ for 5 h, and lysed with passive lysis buffer (Promega). For inhibitor studies, cells were pre-treated with PD98059, LY294002, p38 inhibitor, or PP2 for 30 min before the addition of H₂O₂. Luciferase activity was measured using the Dual-luciferase reporter assay system with a luminometer according to the manufacturer's instructions. Firefly luciferase

TABLE 1. Sequences of real-time PCR primers

Gene	Genebank accession number	Primer	PCR product (bp)
<i>SOD1</i>	AY835629	Forward: 5'-agggcatcatcaattcgag-3' Reverse: 5'-acattgccaagtctccaac-3'	216
<i>SOD2</i>	BC035422	Forward: 5'-tgaacaacctgaaactcacc-3' Reverse: 5'-ccatcgaggcactcttcta-3'	241
<i>SOD3</i>	AY787834	Forward: 5'-ctgggtcaggtcttttc-3' Reverse: 5'-acatgtcggatcaactcc-3'	183
<i>Catalase</i>	NM_001752	Forward: 5'-gcctgggaccataatctt-3' Reverse: 5'-gaatctccgacttccag-3'	202
<i>MT-1E</i>	BC009699	Forward: 5'-atggacccaactgtctt-3' Reverse: 5'-acagcagtcacttctcc-3'	179
<i>MT-2A</i>	NM_005953	Forward: 5'-atggatcccaactgtctt-3' Reverse: 5'-caggagtcgacttgc-3'	178
<i>GPX1</i>	BC007865	Forward: 5'-ccttcgagaaatgtcgaggt-3' Reverse: 5'-tcgatgtcaatgtctggaa-3'	235
<i>GPX3</i>	NM_002084	Forward: 5'-tgcaccaatttggaaaaca-3' Reverse: 5'-tcaatgggttcccgaaagag-3'	223
<i>GPX4</i>	BC058329	Forward: 5'-tcaagatgtcgactgtgaac-3' Reverse: 5'-ggggcagggtcttcttctatc-3'	194
<i>GSTM1</i>	AY510272	Forward: 5'-atgcccataactgggta-3' Reverse: 5'-gtgagccccatcaatcaagt-3'	203
<i>GSTM2</i>	NM_000848	Forward: 5'-agcagatcgccgaaacatt-3' Reverse: 5'-cgcataaatccacaaagg-3'	201
<i>GSTM3</i>	NM_000849	Forward: 5'-taatggatttccgcacacaa-3' Reverse: 5'-ccttcagggttgggaactca-3'	236
<i>GSTM4</i>	BC108729	Forward: 5'-ttggagaaccagggtatgg-3' Reverse: 5'-ggacatcataggcgaggaa-3'	193
<i>GSTM5</i>	BC058881	Forward: 5'-gactctgggtactggaca-3' Reverse: 5'-gtgagccccatcaatcaagt-3'	195
<i>GSTP1</i>	BT019950	Forward: 5'-ggagacccatcacctgtacca-3' Reverse: 5'-ggcagttgccttcacatag-3'	197
<i>GSTT1</i>	BT019951	Forward: 5'-ggcttccttaactggcttc-3' Reverse: 5'-tggcttcagaatgaccc-3'	188
<i>GSTT2</i>	NM_000854	Forward: 5'-gcccgttcatgatgaccc-3' Reverse: 5'-aacttgtcccaaggccatg-3'	172
<i>Shc</i>	NM_183001	Forward: 5'-gcgcgatgtgcgcctatgt-3' Reverse: 5'-ggggggcttcgggtt-3'	149

activities were normalized to *Renilla* luciferase activities for transfection efficiency.

Subretinal injections

Adult female BalbC mice (6- to 8-week-old) were treated humanely in strict compliance with the Association for Research in Vision and Ophthalmology statement on the use of animals in research. They were kept in a 12:12 h light/dark cycle. Subretinal injections were done with a Harvard pump apparatus and pulled glass micropipettes as previously described (Mori et al., 2001). Micropipettes were calibrated to deliver 1 μ l of vehicle upon depression of a foot switch. Mice were anesthetized, pupils were dilated, and the pipette tip was passed through the sclera posterior to the limbus. The retina was visualized using a condensing lens system on the dissecting microscope and a plastic ring filled with GONAK (AKORN, Buffalo Grove, IL) that served as a contact lens. The pipette tip was positioned just above the retina and depression of the foot switch caused a jet of injection fluid to penetrate the retina. This technique is very atraumatic and the direct visualization allows confirmation of successful subretinal injection by the appearance of a small retinal detachment (bleb). The blebs were quite uniform in size and involved about 1/4 of the retina.

The siRNA was mixed with oligofectAMINE (Invitrogen) in Opti-MEM medium (Invitrogen) and incubated at room temperature to allow stable complexes to form. One microliter of 4% oligofectamine containing 1 pmol of either *GFP* or *p66Shc* siRNA was injected under the retina.

Electroretinograms (ERG)

Single-flash, scotopic ERG were performed as previously described (Okoye et al., 2003). Mice were dark-adapted overnight for 12 h, and recordings were performed under dim red illumination with an Espion ERG Diagnosys machine (Diagnosys LLL, Littleton, MA). Mice were anesthetized by

intraperitoneal injection of Avertin (Aldrich, Milwaukee, WI) and corneas were anesthetized with a drop of 0.5% proparacaine hydrochloride (Alcon Labs, Forth Worth, TX). Pupils were dilated with a drop of 1% tropicamide (Alcon Labs). Mice were placed on a pad heated to 39°C, and platinum loop electrodes were placed on each cornea after application of Gonioscopic prism solution (Alcon Labs). A reference electrode was placed subcutaneously in the anterior scalp between the eyes, and a ground electrode was inserted into the tail. The head of the mouse was held in a standardized position in a ganzfeld bowl illuminator that ensured equal illumination of the eyes. Electrical impedance was balanced for each pair of eyes measured. Simultaneous recordings from both eyes were made for 11 intensity levels of white light ranging from -3.00 to 1.40 log cd-sec/m². The Espion ERG apparatus measures the ERG response six times at each flash intensity and records the average value.

RESULTS

Knockdown of p66Shc reduces RPE cell susceptibility to oxidative stress-induced apoptosis

Substantial levels of the three isoforms of Shc were present in RPE cells (Fig. 1A). To selectively knockdown p66Shc, a siRNA was designed that targets the first exon of *Shc* that encodes the N-terminal CH2 domain, which is present in the mRNA for p66Shc, but not the mRNA for p52Shc and p46Shc. After addition of the siRNA directed against GFP to RPE cells, immunoblots showed that all three isoforms of Shc increased over the ensuing 72 h (Fig. 1A). There was a similar increase in p52Shc and p46Shc protein for 72 h after addition of siRNA directed against p66Shc to RPE cells, but there was a decrease in p66Shc mRNA confirmed by densitometry (Fig. 1B). Compared to cells incubated with *GFP* siRNA, cells incubated with *p66Shc* siRNA showed a decrease in

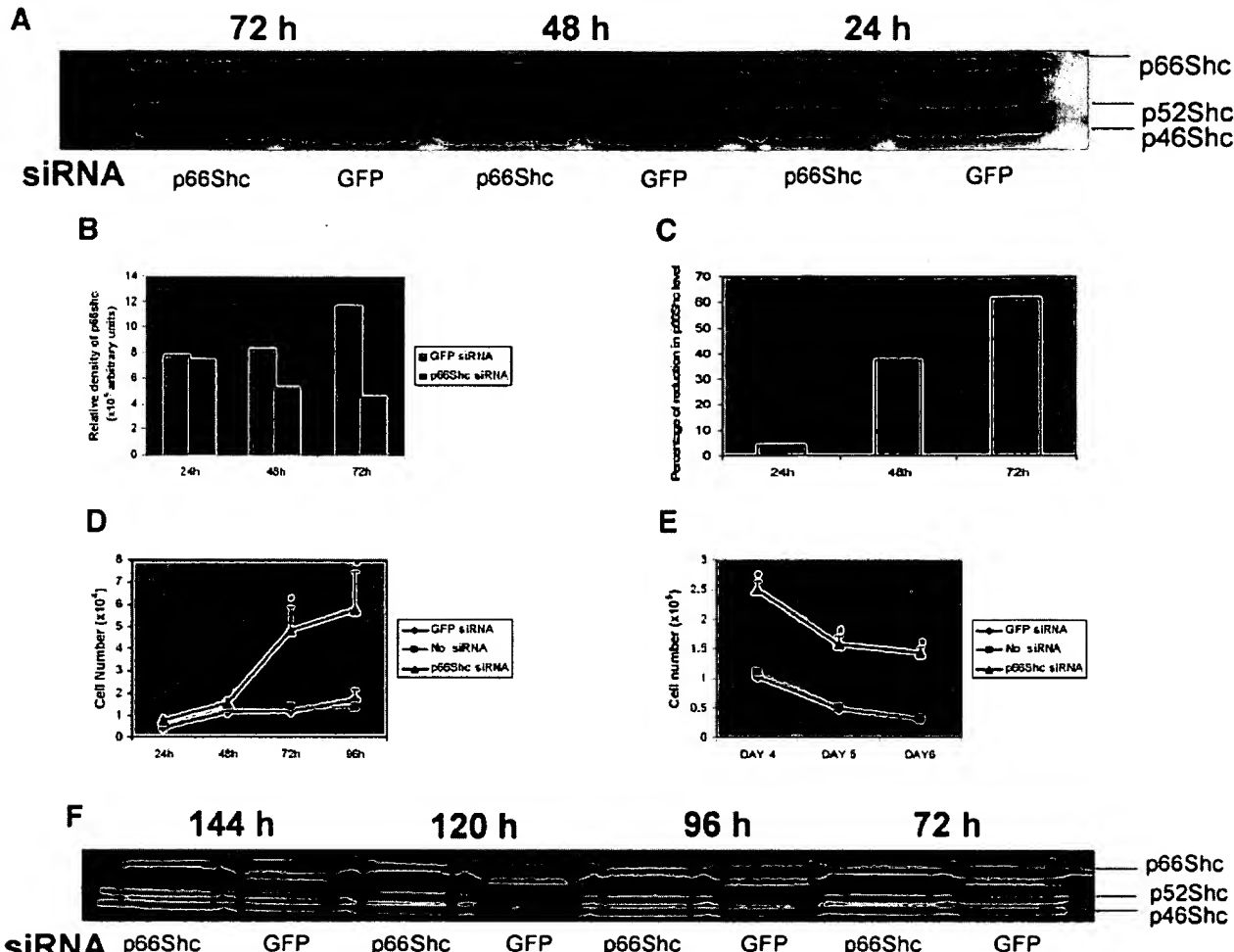


Fig. 1. Lipofection of retinal pigmented epithelial (RPE) cells with *p66Shc* siRNA selectively reduces *p66Shc* and decreases oxidative stress-induced cell death. RPE cells (10^5 cells per well) were seeded in 6-well plates and transfected with siRNA directed against *p66Shc* or *GFP* mRNA. At 24, 48, or 72 h after transfection, the entire lysate from wells transfected with *p66Shc* siRNA or corresponding wells of control cells transfected with *GFP* mRNA were harvested and run in immunoblots using an antibody directed against Shc. Cells transfected with *GFP* siRNA showed an increase in all three isoforms of Shc between 24 and 72 h after transfection, while cells transfected with *p66Shc* siRNA showed a selective decrease in *p66Shc* (A). Densitometry confirmed that *p66Shc* increased in RPE cells during the 72 h after transfection of *GFP* siRNA, but decreased in RPE cells transfected with *p66Shc* siRNA (B). Compared to control cells, cells treated with *p66Shc* siRNA showed reductions in *p66Shc* of roughly 40% at 48 h and 60% at 72 h (C). These data were confirmed in an independent experiment. RPE cells were plated in 6-well plates at

10^5 cells per well and at 50% confluence they were transfected with *p66Shc* or *GFP* siRNA. As an additional control, some cells were not transfected (no siRNA). At 24, 48, 72, or 96 h after transfection (D) or 4, 5, or 6 days after transfection (E), cells (triplicate wells for each group) were placed in serum-free medium containing 0.8 mM H_2O_2 for 24 h. The cells were then washed and after incubation in Trypan Blue, the percentage of unstained cells per well was determined by counting stained and unstained cells in a hemocytometer. For both D and E, a single experimental value was derived from the mean of triplicates and the mean ($\pm SD$) of three experimental values from independent experiments was plotted. F: To determine whether siRNA knockdown persisted for the duration of the experiment shown in (E), additional immunoblots were performed. The procedure was the same as that described in (A), except that cell lysates were collected 72, 96, 120, and 144 h after transfection. * $P < 0.05$ by unpaired *t*-test for difference from *GFP* siRNA-treated cells

p66Shc protein that was roughly 40% at 48 h and 60% at 72 h (Fig. 1C).

At 24, 48, or 72 h after addition of *GFP* or *p66Shc* siRNA, or no siRNA, RPE cells were incubated with 0.8 mM H_2O_2 for 24 h and viability was assessed by Trypan Blue exclusion. The number of viable cells was similar when H_2O_2 was added 24 or 48 h after no additions or addition of *GFP* or *p66Shc* siRNA, but when H_2O_2 was added 72 or 96 h after addition of siRNA, cells incubated with *p66Shc* siRNA showed significantly more viable cells 24 h after addition of H_2O_2 than *GFP* siRNA-treated or -untreated cells (Fig. 1D). To determine the effect of prolonged exposure to H_2O_2 , RPE cells were treated with *GFP* or *p66Shc* siRNA and after 72 h the cells were placed in serum-free medium containing

0.8 mM H_2O_2 . The number of surviving cells was counted at 4, 5, and 6 days after exposure to H_2O_2 and at each time point there were significantly more *p66Shc* siRNA-treated cells (Fig. 1E) and less *p66Shc* (Fig. 1F) than *GFP* siRNA-treated or -untreated cells.

Seventy-two hours after no treatment or treatment with *GFP* or *p66Shc* siRNA, RPE cell cultures were placed in serum-free medium for 24 h and then incubated with 0, 0.8, or 1 mM H_2O_2 for 5 h. TUNEL showed rare stained cells in cultures not exposed to H_2O_2 (Fig. 2A, top row). In untreated or *GFP* siRNA-treated cultures incubated with 0.8 or 1 mM H_2O_2 there were numerous stained cells, but after exposure to either concentration of H_2O_2 there were few stained cells in *p66Shc* siRNA-treated cultures (Fig. 2A, middle

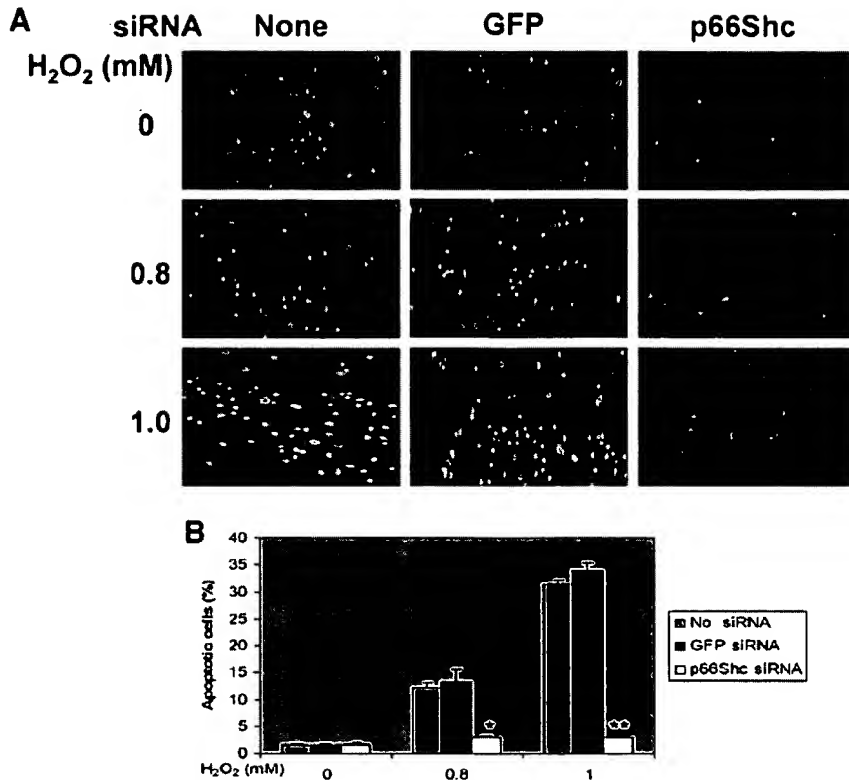


Fig. 2. Knock-down of p66Shc protects RPE cells from oxidative stress-induced apoptosis. Seventy-two hours after transfection with p66Shc or GFP siRNA, RPE cells were washed, incubated in serum-free medium for 24 h, and then incubated in 0, 0.8, or 1.0 mM H_2O_2 for 5 h. Cells were fixed and the percentage of apoptotic cells per well was determined by the Apoptag assay. Cells were counterstained with propidium iodide to determine the total number of cells. A: Fluorescence microscopy shows hyperfluorescent nuclei of apoptotic cells among faint background illumination of nuclei of normal cells. There are few apoptotic cells in p66Shc siRNA-treated cells incubated with 0, 0.8, or 1.0 mM H_2O_2 . Untransfected cells (none) or GFP siRNA-

treated cells incubated with 0 mM H_2O_2 also had few apoptotic cells, but those incubated with 0.8 or 1.0 mM H_2O_2 showed many apoptotic cells. The mean percentage (\pm SD) of apoptotic cells calculated from 6-wells for each condition is shown in (B). Treatment with 0.8 or 1.0 mM H_2O_2 resulted in significantly less apoptosis in p66Shc-deficient cells compared to controls. There was essentially no difference between untransfected cells and those transfected with GFP siRNA. Therefore, statistical comparisons were made between cells transfected with p66Shc siRNA or GFP siRNA using a two-tailed *t*-test. (* $P < 0.018$; ** $P < 0.00035$.)

and bottom rows). Quantification confirmed that these were significantly fewer TUNEL-positive cells in p66Shc SiRNA-treated cultures (Fig. 2B).

Knockdown of p66Shc reduces ROS levels in H_2O_2 -treated cells

We sought to determine if reduction of p66Shc has its effect solely to block initiation of apoptosis or whether it has any effects upstream that could reduce stimuli that lead to apoptosis. We hypothesized that knockdown of p66Shc would not reduce oxidative stress-induced levels of ROS. To test this hypothesis, we used DCFDA, which is a non-fluorescent, membrane permeable molecule that is hydrolyzed inside cells to become impermeable and thereby trapped, and in the presence of ROS forms a fluorescent product, 2',7'-dichlorofluorescein, allowing assessment of the level of ROS by fluorescence microscopy. We also used hydroethidine, which is converted to ethidium in the presence of superoxide radicals. Seventy-two hours after no treatment or lipofection with GFP or p66Shc siRNA, RPE cells were placed in serum-free medium for 24 h and then treated with various concentrations of H_2O_2 for 30 min and incubated with 30 μM DCFDA or 5 μM hydroethidine for an additional 30 min. In untreated RPE cell cultures and those that had been treated with GFP siRNA and not exposed to H_2O_2 , there were several fluorescent cells, some of which were brightly fluorescent, suggesting a

basal level of oxidative stress (Fig. 3, top row). There were few fluorescent cells and none that were brightly fluorescent in RPE cell cultures that had been treated with p66Shc siRNA (Fig. 3, top right of each major column). Exposure of non-transfected or GFP siRNA-treated cells to 0.8 mM H_2O_2 for 30 min resulted in a substantial increase in the number of fluorescent cells (Fig. 3, middle row) compared to unexposed cells, and there was a greater increase by exposure to 1.0 mM H_2O_2 (Fig. 3, bottom row). In contrast, there was little increase in the number of fluorescent cells or the intensity of fluorescence per cell in p66Shc-treated RPE cell cultures exposed to 0.8 mM (Fig. 3, middle row, right panel of each major column) or 1.0 mM H_2O_2 (bottom row, right panel of each major column). Thus, contrary to our expectations, p66Shc knockdown reduced basal and oxidative stress-induced levels of ROS in RPE cells.

Knockdown of p66Shc causes increased expression of several antioxidant enzymes

Antioxidant enzymes are a major component of the defense system utilized by cells to counter ROS produced secondary to cellular metabolism or from exposure to oxidative stress. Quantitative real-time RT-PCR was used to assess the impact of p66Shc knockdown on mRNA levels for several antioxidant enzymes, including Superoxide Dismutase 1 (SOD1), SOD2, SOD3,

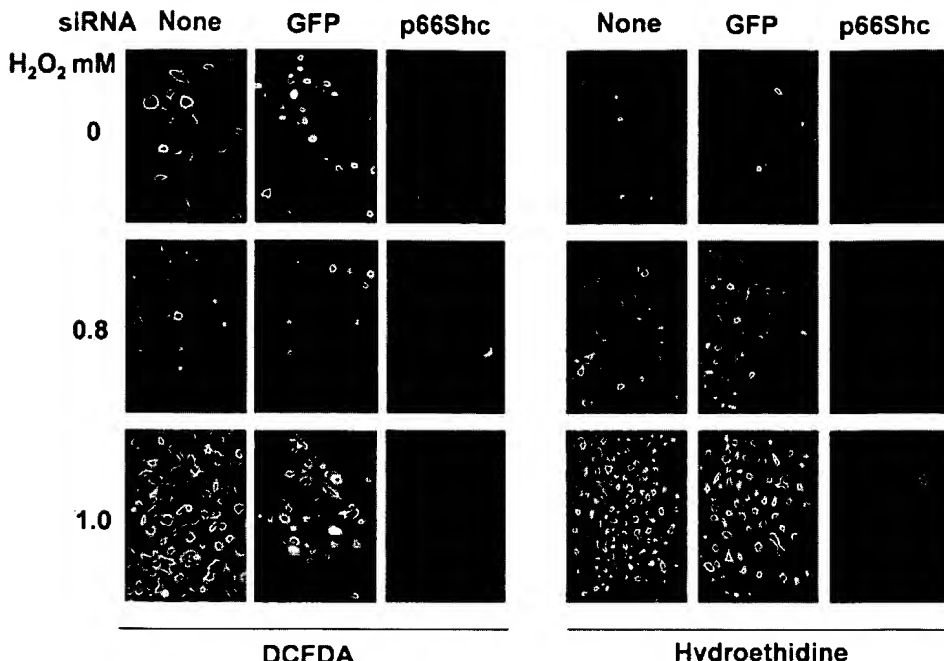


Fig. 3. Knockdown of p66Shc reduces ROS in RPE cells under basal conditions and in the presence of oxidative stress. Seventy-two hours after transfection with *p66Shc* or *GFP* siRNA, RPE cells were placed in serum-free medium for 24 h, and then treated with 0, 0.5, or 1.0 mM H_2O_2 for 30 min. After an additional 30 min incubation in 30 μM 2',7'-dichlorofluorescein diacetate (DCFDA) or 5 μM hydroethidine, which

Glutathione Peroxidase 1 (GPx1), GPx3, GPx4, Catalase, Glutathione S-Transferase M1 (GST-M1), GST-M2, GST-M3, GST-M4, GST-M5, GST-T1, GST-T2, GST-P1, Metallothionein 1E (MT-1E), and MT-2A (Table 1). Seventy-two hours after treatment with siRNA directed against *p66Shc* or *GFP*, RPE cells were exposed to 0.75 mM H_2O_2 for 24 h, RNA was isolated, and quantitative real-time RT-PCR was performed. Measurement of *p66Shc* mRNA levels confirmed that compared to *GFP* siRNA-treated RPE cells, *p66Shc* siRNA-treated cells had significantly less *p66Shc* mRNA (Fig. 4A). This reduction in *p66Shc* mRNA was associated with significant increases in mRNA for four antioxidant enzymes, GPx3, MT-1E, MT-2A, and GST-P1 (Fig. 4B-E). There was no significant difference in levels of *SOD1* or *SOD2* mRNA, however, when RPE cells were exposed to 0.75 mM H_2O_2 , there was a substantial increase in *SOD1* and *SOD2* mRNA in *p66Shc* siRNA-treated cells, but not *GFP* siRNA-treated RPE cells (Fig. 4F,G). Exposure to H_2O_2 also increased GPx3 mRNA in *p66Shc* siRNA-treated cells relative to controls accentuating the difference between them. Conversely, exposure to H_2O_2 increased MT-1E and MT-2A mRNA in control cells relative to *p66Shc* siRNA-treated cells abrogating the difference that was seen under basal conditions. The remainder of the genes listed above showed no differences in expression between *p66Shc* siRNA and *GFP* siRNA-treated RPE cells. Only catalase mRNA was reduced in both control and *p66Shc*-deficient cells after H_2O_2 exposure (Fig. 4H), which is consistent with a study in AML-2/DX100 cells, in which exposure to H_2O_2 caused down-regulation of catalase and upregulation of other antioxidant enzymes (Oh et al., 2004). With the exception of catalase, our data suggest that reduction of *p66Shc* results in upregulation of some antioxidant enzymes under basal conditions and others in the presence of

generate fluorescent molecules in the presence of ROS, the cells were visualized and photographed under a fluorescence microscope. Compared to control cells, *p66Shc*-deficient cultures showed fewer highly fluorescent cells and an overall lower level of fluorescence under basal conditions or in the presence of 0.5 or 1.0 mM H_2O_2 .

oxidative stress. This could contribute to reduction of oxidative stress-induced ROS levels and apoptosis seen in *p66Shc* siRNA-treated cells.

Knockdown of *p66Shc* in RPE cells increases basal and oxidative stress-induced NF- κ B transcriptional activity

Several antioxidant enzymes are upregulated by NF- κ B, a transcription factor that is activated by oxidative stress. We used an NF- κ B-dependent luciferase reporter construct containing three NF- κ B binding sites to investigate the effect of *p66Shc* on NF- κ B activity. RPE cells were co-transfected with the NF- κ B reporter construct and either *p66Shc* or *GFP* siRNA and after 72 h they were incubated with 0.8 mM H_2O_2 for 5 h. Western blots confirmed a significant reduction in *p66Shc* levels after co-transfection of the NF- κ B reporter construct and *p66Shc* siRNA, similar to that seen with *p66Shc* siRNA alone, indicating that the siRNA knockdown efficiency had not been compromised by co-transfection with the NF- κ B reporter construct (Fig. 5A). RPE cells demonstrated a high basal level of NF- κ B activity that was not significantly changed by incubation with H_2O_2 (Fig. 5B). Compared to controls, RPE cells with reduced levels of *p66Shc* showed a significant increase in basal and H_2O_2 -stimulated NF- κ B activity.

Activation of ERK by oxidative-stress mediates the increase in NF- κ B activity in *p66Shc*-deficient RPE cells

Various kinases such as Src, PI-3K and kinases in the MAPK pathway have been implicated in regulation of some responses to oxidative stress in some cells. We utilized inhibitors of several kinases to explore whether any were involved in the increase in NF- κ B activity that occurs in *p66Shc*-deficient RPE cells. RPE cells

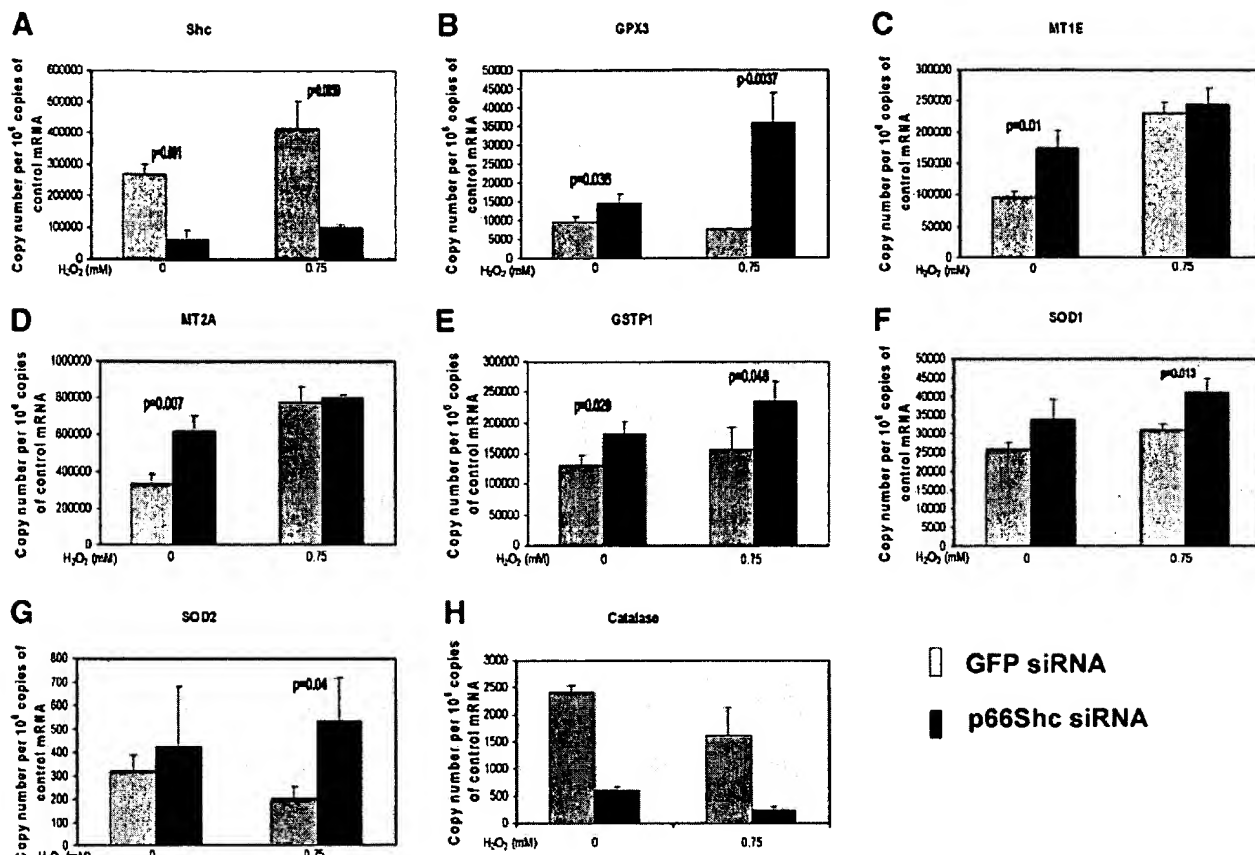


Fig. 4. Effect of downregulation p66Shc on mRNA levels of genes involved in defense against oxidative stress. Seventy-two hours after lipofection with *p66Shc* or *GFP* siRNA, RPE cells were placed in serum-free medium and exposed to 0.75 mM H_2O_2 for 24 h. Total RNA was isolated and cDNA was prepared. Quantitative real-time PCR was performed as described in Methods Section. The bars represent the mean ($\pm SD$) calculated for six experimental values.

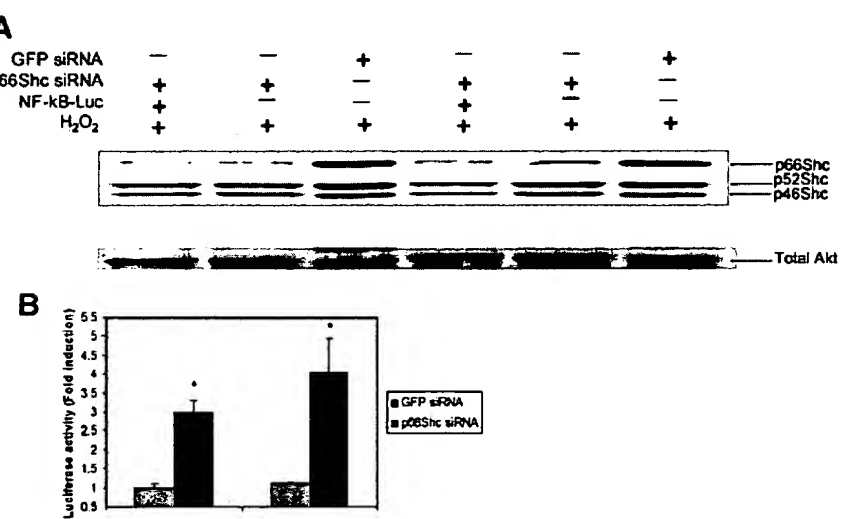


Fig. 5. NF- κ B activity is modulated by p66Shc levels. A: Seventy-two hours after co-transfection of *NF-κB-Luc* and *p66Shc* or *GFP* siRNA, cells were placed in serum-free medium for 24 h and then incubated in 0.8 mM H_2O_2 for 5 h. The entire cell lysate from each well was run in immunoblots using antibodies directed against Shc and total Akt. Cells co-transfected with *NF-κB-Luc* and *p66Shc* showed efficient knockdown of *p66Shc* similar to that seen in cells treated with only

p66Shc siRNA in Figure 1. B: Seventy-two hours after co-transfection of *NF-κB-Luc* and *p66Shc* or *GFP* siRNA, cells were placed in serum-free medium for 24 h and then incubated in 1 mM H_2O_2 for 5 h. Cells lysates were assayed using the Dual-luciferase reporter system. Bars represent the mean ($\pm SD$) calculated from three experimental values. * $P < 0.05$ by unpaired *t*-test for difference from *GFP* siRNA-treated cells.

were co-transfected with the NF- κ B reporter construct and either *p66Shc* or *GFP* siRNA. Seventy-two hours after co-transfection, RPE cells were treated with an inhibitor of ERK (PD98059), PI-3K (LY294002), p38 MAPK, or Src (PP2) and then incubated with 0.8 mM H₂O₂ for 5 h. The increase in NF- κ B activity induced by oxidative stress was unaffected by inhibitors of p38 MAPK, PI-3K, or Src, but was significantly reduced by the inhibitor of ERK (Fig. 6A). Western blots using an antibody that specifically recognizes phosphorylated ERK1/2 showed that the basal level of ERK1/2 phosphorylation in RPE cells (Fig. 6B, lane 6) was not altered by knockdown of *p66Shc* in the absence of oxidative stress (lane 5), but in its presence, phosphorylation was increased (lane 2). This increase was not seen in control RPE cells exposed to oxidative stress (lane 3). The ERK inhibitor reduced phosphorylated ERK1/2 to very low levels in *p66Shc*-deficient cells in the presence (lane 1) or absence (lane 4) of H₂O₂. These data indicate that knockdown of *p66Shc* results in activation of MAP kinase signaling in the presence of oxidative stress, and the activation is effectively blocked by the MAP kinase inhibitor. The MAP kinase inhibitor also eliminated the oxidative stress-induced increase in NF- κ B activity seen in *p66Shc*-deficient RPE cells exposed to oxidative stress (Fig. 6C), suggesting that MAP kinase signaling is involved. The basal increase in NF- κ B activity that occurs from reduction of *p66Shc* in the absence of oxidative stress was not altered by the inhibitor suggesting that the basal increase is independent of the ERK pathway.

Intraocular injection of *p66Shc* siRNA reduces paraquat-induced retinal damage

We have previously demonstrated that efficient knockdown of proteins can be achieved in the retina by intraocular injection of siRNA (Shen et al., 2005a). We have also established and characterized a model of oxidative damage-induced retinal degeneration (Cingolani et al., 2006). Since the target sequence for the *p66Shc* is identical in humans and mice, we tested the effects of intraocular injection of *p66Shc* and *GFP* siRNA in this model. Compared to injection of *GFP* siRNA, injection of *p66Shc* siRNA resulted in significant preservation of ERG a- and b-wave amplitudes in eyes injected with paraquat (Fig. 7, Table 2). This indicates that knockdown of *p66Shc* in retinal cells preserves retinal function in the presence of oxidative stress.

DISCUSSION

Mice deficient in *p66Shc* have a longer life span than wild-type mice with the same genetic background and are less susceptible to the lethal effects of systemic administration of paraquat, a strong oxidizing agent (Migliaccio et al., 1999). This suggests that in one or more vital organs *p66Shc* mediates oxidative damage-induced cell death. In this study, we sought to determine if *p66Shc* also contributes to oxidative damage in the RPE and retina. The three isoforms of ShcA are abundantly expressed in RPE cells and using siRNA directed against *p66Shc*, the level of *p66Shc* was substantially reduced without affecting the other two

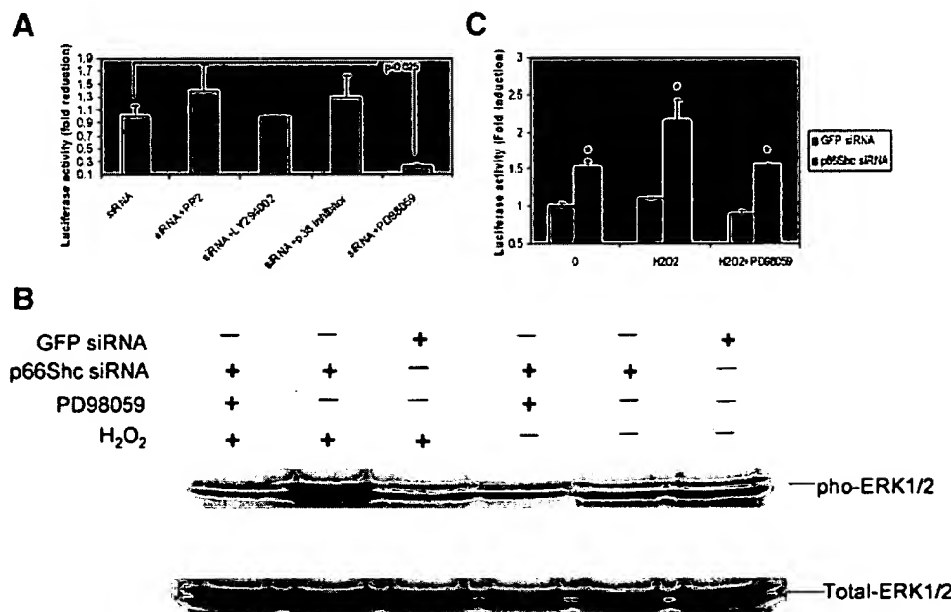


Fig. 6. ERK kinase is involved in the regulation of NF- κ B activity by *p66Shc*. **A:** Seventy-two hours after co-transfection of *NF- κ B-Luc* and *p66Shc* or *GFP* siRNA, cells were placed in serum-free medium for 24 h and then treated for 30 min with an inhibitor of Src kinase (PP2), p38 MAPK (p38 inhibitor), PI-3 kinase (LY294002), or ERK1/2 (PD98059). The cells were then treated with 0.8 mM H₂O₂ for 5 h and cells lysates were assayed using the Dual-luciferase reporter system. Bars represent the mean (\pm SD) calculated from three experimental values. Statistical comparisons were made by ANOVA with Bonferroni correction for multiple comparisons. **B:** Seventy-two hours after co-transfection of *NF- κ B-Luc* and *p66Shc* or *GFP* siRNA, cells were placed in serum-free medium for 24 h. The cells were pre-treated with buffer or PD98059 (inhibitor of ERK1/2) for 30 min and then incubated in the presence or absence of 0.8 mM H₂O₂ for 20 min.

The entire cell lysate from each well was run in an immunoblot using an antibody that specifically recognizes phosphorylated ERK (p44/42). The blots were stripped and rehybridized with an antibody directed against total ERK to control for loading. Compared to control cells, cells deficient in *p66Shc* showed similar levels of phosphorylated ERK (p44/42) under basal conditions, but they were substantially reduced in the presence of oxidative stress. **C:** Seventy-two hours after co-transfection of *NF- κ B-Luc* and *p66Shc* or *GFP* siRNA, cells were placed in serum-free medium for 24 h and then treated for 30 min with buffer or PD98059. The cells then were treated with or without 0.8 mM H₂O₂ for 5 h and cells lysates were assayed using the Dual-luciferase reporter system. Bars represent the mean (\pm SD) calculated from three experimental values. Statistical comparisons were made by unpaired *t*-test.

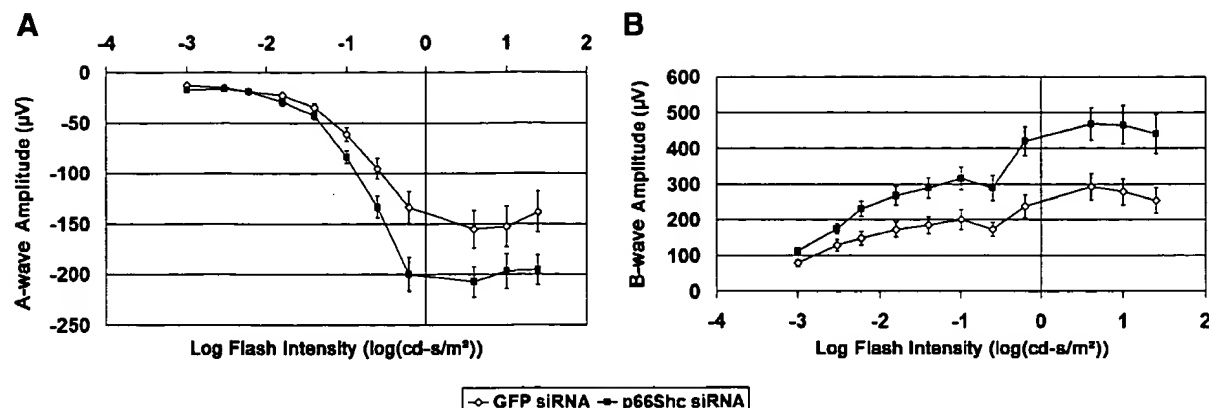


Fig. 7. Knockdown of p66Shc protein preserves retinal function in a model of oxidative stress-induced retinal degeneration. Adult Balb/C mice were given a subretinal injection of 1 μ l of 4% oligofectAMINE containing 1 pmol of p66Shc or GFP siRNA and after 3 days they received an intravitreous injection of 0.75 mM of paraquat in both eyes. Scotopic electroretinograms were performed 5 days after

injections of paraquat. Plots of a-wave amplitudes (A) or b-wave amplitudes (B) versus flash intensity showed a significant increase in both a- and b-wave amplitudes in paraquat-injected eyes that had received p66Shc siRNA compared to those that had received GFP siRNA.

isoforms. RPE cells deficient in p66Shc were less susceptible to oxidative stress-induced apoptosis than appropriate control cells. Conversely, it has been shown that overexpression of p66Shc increases oxidative stress-induced apoptosis in T cells (Pacini et al., 2004). Thus, p66Shc may promote oxidative damage-induced death in several cell types.

The ability to selectively reduce p66Shc without affecting p52Shc and p46Shc in cultured RPE cells demonstrated that p66Shc plays an important role in oxidative stress-induced death of these cells that are critical for retinal function, and also provided a system to investigate the mechanism of the effect. Other Shc proteins act as adapters for growth factor receptors and enhance cell growth and proliferation. Cycling cells are more susceptible to apoptosis and therefore it seems reasonable to hypothesize that p66Shc acts as an adapter switch that in the presence of oxidative stress diverts mitogenic signals to initiate apoptosis. If this were the sole mechanism by which p66Shc promotes cell death in the presence of oxidative stress, then the generation of ROS should be unaffected by the cellular level of p66Shc. We were surprised to find that this was not the case; p66Shc-deficient RPE cells showed substantially lower ROS generation than appropriate control cells when challenged with H_2O_2 . This is due, at least in part, to enhancement of levels of antioxidant enzymes in p66Shc-deficient RPE cells. The expression of some antioxidant enzymes is upregulated by NF- κ B (Hayes and Pulford, 1995; Pahl, 1999) and therefore a reporter system was used to assess the effect of p66Shc levels on NF- κ B activity in RPE cells. Cells deficient in p66Shc had increased basal and oxidative stress-induced NF- κ B transcriptional activity. The increase in oxidative stress-induced NF- κ B activity, but not the

basal activity, was mediated by activation of ERK. These in vitro findings are relevant to the situation in vivo, because compared to eyes injected with GFP siRNA, those injected with p66Shc siRNA showed less loss of retinal function as assessed by ERG from paraquat-induced oxidative stress.

These data indicate that p66Shc is a critical permissive factor for oxidative damage in the retina. One way that p66Shc enhances the damaging effects of oxidative stress is through downregulation of NF- κ B. It is well established that NF- κ B is upregulated during inflammation and stimulates expression of many inflammatory cytokines (Tak and Firestein, 2001; Karin et al., 2002; Karin and Greten, 2005). Evidence for a potential role of NF- κ B in the antioxidant defense system is just emerging (Storz and Toker, 2003; Kratovnik et al., 2005). NF- κ B is sensitive to the cellular redox state (Kabe et al., 2005) and its activation increases expression of several components of the antioxidant defense system in RPE cells. This is consistent with recent demonstrations that NF- κ B mediates induction of SOD2 by TNF (Guo et al., 2003), upregulates SOD1 in PC12 cells in response to activation of the PI3K/Akt pathway (Rojo et al., 2004), and increases expression of GPx in H_2O_2 -exposed skeletal muscle cells (Zhou et al., 2001). It was recently demonstrated that p66Shc acts as a downstream effector of the tumor suppressor p53 and is critical in p53-dependent apoptosis (Trinei et al., 2002; Pellegrini et al., 2005). This may also provide a link with NF- κ B, because there is reciprocal inhibition between NF- κ B and p53 (Culmsee et al., 2003; Gurova et al., 2005).

The manner in which NF- κ B levels are regulated during inflammation is well understood (Tak and Firestein, 2001). The activity of NF- κ B is controlled by

TABLE 2. Deficiency of p66Shc preserves retinal function in the setting of paraquat-induced oxidative stress

Flash intensity (log (cd·sec/m ²))	n	Treatment	a-wave (μV)	P-value	b-wave (μV)	P-value
(1a) -2.6	13	GFP siRNA	-15.58 ± 2.40	0.6980	128.74 ± 15.75	0.0441
(2a) -2.6	15	p66Shc siRNA	-16.76 ± 1.89		174.03 ± 14.51	
(1b) -0.6	13	GFP siRNA	-95.31 ± 10.32	0.0190	172.42 ± 19.84	0.0116
(2b) -0.6	15	p66Shc siRNA	-133.06 ± 10.83		288.56 ± 35.86	
(1c) 1.4	13	GFP siRNA	-138.16 ± 20.25	0.0289	253.42 ± 35.30	0.0098
(2c) 1.4	15	p66Shc siRNA	-195.47 ± 15.00		440.72 ± 54.57	

Statistical comparisons were made by two-tailed t-test.

I κ B, which when bound to NF- κ B prevents its translocation to the nucleus. Phosphorylation of I κ B by I κ B kinase (IKK) promotes ubiquitination and proteasomal degradation of I κ B, allowing NF- κ B to translocate to the nucleus and stimulate transcription of responsive genes. IKK is phosphorylated and activated by several serine/threonine kinases, including MEKK1 (mitogen-activated protein kinase kinase 1), NIK (NF- κ B-inducing kinase), and NAK (NF- κ B-activating kinase). The regulation of NF- κ B during oxidative stress is less clear. Exposure of HeLa cells to H₂O₂ leads to activation of Src and c-Abl kinases, which then converge on the IKK complex, resulting in NF- κ B activation (Storz et al., 2004a,b). Oxidative stress activates MAPKs such as ERK, JNK, and p38 MAPK (Wang et al., 1998). In p66Shc-deficient RPE cells, exposure to H₂O₂-increased phosphorylation of ERK1/2 and an inhibitor of ERKs blocked H₂O₂-induced NF- κ B activation, but inhibitors of Src kinase or p38 MAPK had no effect. This observation is consistent with findings in other cell systems suggesting that NF- κ B is activated by ERK in the presence of oxidative stress (Bai et al., 2004; Je et al., 2004; Lee et al., 2004c). Knockdown of p66Shc also results in activation of NF- κ B activation in the absence of exogenous oxidative stress, but this is not mediated by ERK, because unchallenged RPE cells deficient in p66Shc show no difference in ERK activity. The mechanism by which p66Shc regulates NF- κ B activity in RPE cells in the absence of exogenous oxidative stress deserves further study.

This study has important clinical implications. It suggests that reduction of p66Shc levels in the retina and RPE may provide benefit in diseases in which oxidative damage occurs, including AMD and RP. An siRNA directed against VEGF receptor 1 has been shown to inhibit choroidal neovascularization in mouse models (Shen et al., 2005a) and a phase I clinical trial investigating its effects in patients with advanced choroidal neovascularization is underway. If siRNA-based treatments are shown to provide benefit for other indications in the eye, then targeting p66Shc in retinal degenerations should be explored. In addition, further work is needed to explore the effects of NF- κ B activation in models of retinal degeneration, because this could provide a complementary approach to treatment.

ACKNOWLEDGMENTS

PAC is the George S. and Dolores Dore Eccles Professor of Ophthalmology.

LITERATURE CITED

Bai XC, Lu D, Bai J, Zheng H, Ke ZY, Li XM, Luo SQ. 2004. Oxidative stress inhibits osteoblastic differentiation of bone cells by ERK and NF- κ p α B. *Biochem Biophys Res Comm* 314:197–207.

Campochiaro PA, Jerdan JA, Glaser BM. 1986. The extracellular matrix of human retinal pigmented cells in vivo and its synthesis in vivo. *Invest Ophthalmol Vis Sci* 27:1615–1621.

Ceryak S, Zingarello C, O'Brien T, Patierno SR. 2004. Induction of pro-apoptotic and cell cycle-inhibiting genes in chromium (VI)-treated human lung fibroblasts: Lack of effect of ERK. *Mol Cell Biochem* 255:139–149.

Cingolani C, Rogers B, Lu L, Kachi S, Shen J, Campochiaro PA. 2006. Retinal degeneration from oxidative damage. *Free Radic Biol Med* 40:660–669.

Culmsee C, Siewe J, Junker V, Retiounskia M, Schwartz S, Camandola S, El-Metainy S, Behnke H, Mattson MP, Krigstein J. 2003. Reciprocal inhibition of p53 and nuclear factor- κ p α B transcriptional activities determines cell survival or death in neurons. *J Neurosci* 23:8586–8595.

Guo Z, Boekhoudt GH, Boss JM. 2003. Role of the intronic enhancer in tumor necrosis factor-mediated induction of manganese superoxide dismutase. *J Biol Chem* 278:23570–23578.

Gurova KV, Hill JE, Guo C, Prokvolit A, Burdelya LG, Samoilova E, Khodyakova AV, Ganapathi R, Ganapathi M, Tararova ND, Bosykh D, Lvovskiy D, Webb TR, Starl GR, Gudkov AV. 2005. Small molecules that reactivate p53 in renal cell carcinoma reveal a NF- κ p α B-dependent mechanism of p53 suppression in tumors. *Proc Natl Acad Sci USA* 102:17448–17453.

Hayashi H, Matsuzaki O, Muramatsu S, Tsuchiya Y, Harada T, Suzuki Y, Sugano S, Matsuda A, Nishida E. 2006. Centaurin-alpha 1 is a PI3K dependent activator of ERK1/2 map kinases. *J Biol Chem* Nov 14 281:1332–1337.

Hayes JD, Pulford DJ. 1995. The glutathione S-transferase supergene family: Regulation of GST and the contribution of the isoenzymes to cancer chemoprotection and drug resistance. *Crit Rev Biochem Mol Biol* 30:445–600.

Je JH, Lee JY, Jung KJ, Sung B, Go EK, Yu BP, Chung HY. 2004. NF- κ p α B activation mechanism of 4-hydroxyhexenal via NIK/IKK and p38 MAPK pathway. *FEBS Lett* 566:183–189.

Kabe Y, Ando K, Kira S, Yoshida M, Handa H. 2005. Redox regulation of NF- κ p α B activation: Distinct redox regulation between the cytoplasm and the nucleus. *Antioxid Redox Signal* 7:395–403.

Karin M, Greten FR. 2005. NF- κ p α B: Linking inflammation and immunity to cancer development and progression. *Nat Rev Immunol* 5:749–759.

Karin M, Cao Y, Greten FR, Li ZW. 2002. NF- κ p α B in cancer: From innocent bystander to major culprit. *Nat Rev Cancer* 2:301–310.

Kratzovnik E, Bromberg Y, Sperling O, Zoref-Shani E. 2005. Oxidative stress activates transcription factor NF- κ B-mediated protective signaling in primary rat neuronal cultures. *J Mol Neurosci* 26:27–32.

Lee KW, Jung JW, Kang KS, Lee HJ. 2004a. p38 is a key signaling molecule for H-ras-induced inhibition of gap junction intercellular communication in rat liver epithelial cells. *Ann NY Acad Sci* 1030:258–263.

Lee MC, Kim JY, Koh WS. 2004b. Apoptotic effect of PP2, a Src tyrosine kinase inhibitor, in murine cell leukemia. *J Cell Biochem* 93:629–638.

Lee YJ, Kang IJ, Bunger R, Kang YH. 2004c. Enhanced survival effect of pyruvate correlates with MAPK and NF- κ p α B activation in hydrogen peroxide-treated human endothelial cells. *J Appl Physiol* 96:793–801.

Migliaccio E, Mele S, Salcini AE, Pellicci G, Lai KM, Superti-Furga G, Pawson T, DiFiore PP, Lanfrancone L, Pellicci PG. 1997. Opposite effects of the p52shc and p66shc splicing isoforms on the EGF receptor-MAP kinase-fos signalling pathway. *EMBO J* 16:706–716.

Migliaccio E, Giorgio M, Mele S, Pellicci G, Rebaldi P, Pandolfi PP, Lanfrancone L, Pellicci PG. 1999. The p66^{shc} adaptor protein controls oxidative stress response and life span in mammals. *Nature* 402:309–313.

Mori K, Duh E, Gehlbach P, Ando A, Takahashi K, Pearlman J, Mori K, Yang HS, Zack DJ, Etyreddy D, Brough DE, Wei LL, Campochiaro PA. 2001. Pigment epithelium-derived factor inhibits retinal and choroidal neovascularization. *J Cell Physiol* 188:253–263.

Oh YK, Lee TB, Choi CH. 2004. Anti-oxidant adaptation in the AML cells supersensitive to hydrogen peroxide. *Biochem Biophys Res Comm* 319:41–45.

Okoye G, Zimmer J, Sung J, Gehlbach P, Deering T, Nambu N, Hackett SF, Melia M, Esumi N, Zack DJ, Campochiaro PA. 2003. Increased expression of BDNF preserves retinal function and slows cell death from rhodopsin mutation or oxidative damage. *J Neurosci* 23:4164–4172.

Pacini S, Pellegrini M, Migliaccio E, Patrussi L, Ulivieri C, Ventura A, Carraro F, Naldini L, Lanfrancone L, Pellicci PG, Baldari CT. 2004. p66SHC promotes apoptosis and antagonizes mitogenic signaling in T cells. *Mol Cell Biol* 24: 1747–1757.

Pahl HL. 1999. Activators and target genes of Rel/NF- κ p α B. *Oncogene* 18:6853–6866.

Pellicci G, Dente L, De Giuseppe A, Verducci-Galletti B, Giuli S, Mele S, Vetrani C, Giorgio M, Pandolfi PP, Cesareni G, Pellicci PG. 1996. A family of Shc related proteins with conserved PTB, CH1 and SH2 regions. *Oncogene* 13:633–641.

Pellegrini M, Pacini S, Baldari CT. 2005. p66SHC: The apoptotic side of Shc proteins. *Apoptosis* 10:13–18.

Ravichandran KS. 2001. Signaling via Shc family adapter proteins. *Oncogene* 20:6322–6330.

Rojo AI, Salinas M, Martin D, Perona R, Cuadrado A. 2004. Regulation of Cu/Zn-superoxide dismutase expression via the phosphatidylinositol 3 kinase/Akt pathway and nuclear factor- κ p α B. *J Neurosci* 24:7324–7334.

Shen J, Samul R, Lima e Silva R, Akiyama H, Liu H, Saishin Y, Hackett SF, Zinnen S, Kossen K, Fosnaugh K, Vargeese C, Aitchison R, Pavco P, Campochiaro PA. 2005a. Suppression of ocular neovascularization with siRNA targeting VEGF receptor 1. *Gene Ther* 13:225–234.

Shen J, Yan X, Dong A, Petters RM, Peng Y-W, Wong F, Campochiaro PA. 2005b. Oxidative damage is a potential cause of cone cell death in retinitis pigmentosa. *J Cell Physiol* 203:457–464.

Storz P, Toker A. 2003. Protein kinase D mediates a stress-induced NF- κ p α B activation and survival pathway. *EMBO J* 22:109–120.

Storz P, Doppler H, Toker A. 2004a. Activation loop phosphorylation controls protein kinase D-dependent activation of nuclear factor κ p α B. *Mol Pharmacol* 66:870–879.

Storz P, Doppler H, Toker A. 2004b. Protein kinase C δ selectively regulates protein kinase D-dependent activation of NF- κ p α B in oxidative stress signaling. *Mol Cell Biol* 24:2614–2626.

Tak PP, Firestein GS. 2001. NF- κ p α B: A key role in inflammatory diseases. *J Clin Invest* 107:7–11.

The Age-Related Eye Disease Study Research Group. 2001. A randomized, placebo-controlled, clinical trial of high-dose supplementation with vitamins C and E, beta carotene, and zinc for age-related macular degeneration and vision loss. *Arch Ophthalmol* 119:1417–1436.

Trinei M, Giorgio M, Cicalese A, Barozzi S, Ventura A, Migliaccio E, Milia E, Padura IM, Raker VA, Maccarone M, Petronilli V, Minucci S, Bernardi P, Lanfrancone L, Pellicci PG. 2002. A p53-p66Shc signaling pathway controls intracellular redox status, levels of oxidation-damaged DNA and oxidative stress-induced apoptosis. *Oncogene* 21:3872–3878.

Wang X, Martindale JL, Liu Y, Holbrook NJ. 1998. The cellular response to oxidative stress: Influences of mitogen-activated protein kinase signalling pathways on cell survival. *Biochem J* 333(Pt 2):291–300.

Yoshida Y, Shimakawa S, Itoh N, Niki E. 2003. Action of DCFH and BODIPY as a probe for radical oxidation in hydrophilic and lipophilic domain. *Free Radic Res* 37:861–872.

Zhou SZ, Johnson AP, Rando TA. 2001. NF kappa B and AP-1 mediate transcriptional responses to oxidative stress in skeletal muscle cells. *Free Radic Biol Med* 31:1405–1416.

Expression of p66^{Shc} protein correlates with proliferation of human prostate cancer cells

Suresh Veeramani^{1,5}, Tsukasa Igawa^{1,5,6}, Ta-Chun Yuan¹, Fen-Fen Lin¹, Ming-Shyue Lee^{1,7}, Jamie S Lin^{1,8}, Sonny L Johansson^{2,3} and Ming-Fong Lin^{*,1,3,4}

¹Department of Biochemistry and Molecular Biology, University of Nebraska Medical Center, 985870 Nebraska Medical Center, Omaha, NE 68198, USA; ²Department of Pathology, University of Nebraska Medical Center, Omaha, NE 68198, USA; ³Eppley Institute for Cancer Research, University of Nebraska Medical Center, Omaha, NE 68198, USA; ⁴Section of Urologic Surgery, College of Medicine, University of Nebraska Medical Center, Omaha, NE 68198, USA

p66^{Shc}, an isoform of Shc adaptor proteins, is shown to mediate various signals, including cellular stress. However, little is known about its involvement in carcinogenesis. We previously showed that p66^{Shc} protein level is upregulated by steroid hormones in human carcinoma cells and is higher in prostate cancer (PCa) specimens than adjacent noncancerous cells. In this study, we investigated the role of p66^{Shc} protein in PCa cell proliferation. Among different PCa cell lines tested, p66^{Shc} protein level showed positive correlation with cell proliferation, that is, rapid-growing cells expressed higher p66^{Shc} protein than slow-growing cells. Exposure of slow-growing LNCaP C-33 cells to epidermal growth factor (EGF) and 5 α -dihydrotestosterone (DHT) led to upregulation of proliferation and p66^{Shc} protein level. Conversely, growth suppression of fast-growing cells by cellular form of prostatic acid phosphatase (cPAcP) expression, a negative growth regulator, downregulated their p66^{Shc} protein level. Additionally, increased expression of p66^{Shc} protein by cDNA transfection in LNCaP C-33 cells resulted in increased cell proliferation. Cell cycle analyses showed higher percentage of p66^{Shc}-overexpressing cells at S phase (24%) than control cells (17%), correlating with their growth rates. On the other hand, transient knock-down of p66^{Shc} expression by RNAi in rapidly growing cells decreased their proliferation as evidenced by the reduced cell growth as well as S phase in p66^{Shc}-knocked down cells. The p66^{Shc} signaling in cell growth regulation is apparently mediated by extracellular signal-regulated kinase/mitogen-activated protein kinase (ERK/MAPK). Thus, our results indicate a novel role for p66^{Shc} in prostate carcinogenesis, in part, promoting cell proliferation.

Oncogene (2005) 24, 7203–7212. doi:10.1038/sj.onc.1208852; published online 19 September 2005

Keywords: p66^{Shc}; prostatic acid phosphatase; prostate cancer; cell proliferation

Introduction

Shc (Src homolog and collagen homolog) proteins are adaptor molecules that contain SH2 and PTB domains (Ravichandran, 2001). They exist in three different isoforms with molecular masses of 46, 52 and 66 kDa. Shc proteins are conventionally known to transduce the mitogenic signals from receptor tyrosine kinases to downstream targets, such as, extracellular signal-regulated kinases/mitogen-activated protein kinases (ERK/MAPK) (Ravichandran, 2001). All the isoforms contain three functional domains – an SH2 domain, a PTB domain and a CH1 domain with three conserved tyrosine residues that are phosphorylated with respect to various signals (Ravichandran, 2001). Additionally, p66^{Shc} has a unique CH2 domain at the N-terminus of the protein, which contains a serine residue that could be phosphorylated under stress signals (Migliaccio *et al.*, 1999).

Different members of the Shc proteins exhibit distinct expression patterns and biological functions. For example, p52^{Shc} and p46^{Shc} are expressed in most of the cells, while p66^{Shc} protein is expressed predominantly in epithelial cells (Migliaccio *et al.*, 1997). Both p52^{Shc} and p66^{Shc} are distributed throughout the cytosol, whereas p46^{Shc} localizes to mitochondria (Ventura *et al.*, 2004). Nevertheless, recent studies indicate that in response to stress signals, such as, H₂O₂ treatment, a fraction of cytosolic p66^{Shc} is translocated to mitochondria, where it is associated with heat-shock protein to mediate apoptotic response (Orsini *et al.*, 2004). Despite that p66^{Shc}, like p52^{Shc}/p46^{Shc}, is phosphorylated at its tyrosine residues during epidermal growth factor (EGF) treatment and forms complexes with Grb-2, there are certain functional differences between p66^{Shc} and the other two Shc members. First, p66^{Shc}, unlike p52^{Shc}, could not transform NIH3T3 mouse fibroblast cells *in vitro* (Migliaccio *et al.*, 1997). Second,

*Correspondence: M-F Lin; E-mail: mlin@unmc.edu

¹These two authors contributed equally to this article

²Current address: Department of Urology, Nagasaki University School of Medicine, Sakamoto 1-7-1 Nagasaki 852-8501, Japan

³Current address: Lombardi Cancer Center, Georgetown University Medical Center, Washington, DC 20057, USA

⁴Current address: School of Arts and Sciences, University of Pennsylvania, Philadelphia, PA 19104, USA

Received 17 December 2004; revised 4 May 2005; accepted 4 May 2005; published online 19 September 2005

overexpression of p66^{Shc} protein in cell lines, such as, HeLa, CHO and COS-1 cells, does not increase EGF-induced ERK/MAPK activation (Migliaccio *et al.*, 1997; Okada *et al.*, 1997). Third, p66^{Shc} is phosphorylated at Ser³⁶ in its CH2 domain under various stress signals such as H₂O₂, UV radiation and exposure to chemicals, such as, Taxol, and thus could serve as an apoptotic sensitizer to stress signals (Migliaccio *et al.*, 1999; Yang and Horwitz, 2000). Finally, p66^{Shc} acts as a negative regulator of human and mouse T-cell survival and proliferation (Pacini *et al.*, 2004) and has been implicated in the control of lifespan in mammals (Migliaccio *et al.*, 1999). Thus, data from the above studies clearly indicate p66^{Shc} as a transducer of signals in response to cellular stress. However, its role in human carcinogenesis is not understood.

In human carcinoma cells, p66^{Shc} may be involved in regulating their proliferation. Among ErbB-2-positive ovarian cancer cell lines, a positive correlation between p66^{Shc} and ErbB-2 is observed (Xie and Hung, 1996). In breast cancer cell lines, elevated expression of p66^{Shc} protein is observed in those with highly metastatic ability and similar phenomenon is seen in lymph node-positive breast tumors (Jackson *et al.*, 2000). However, another study shows that p66^{Shc} protein level inversely correlates with the expression of ErbB-2, a prognostic marker for breast cancer cell lines (Xie and Hung, 1996). Additionally, studies on archival breast cancer specimens have showed that the expression of p66^{Shc} protein inversely correlates with the relapse of breast cancer (Davol *et al.*, 2003). Hence, the role of p66^{Shc} in carcinogenesis requires further investigations.

We previously showed that sex steroid hormones including estrogens and androgens upregulate p66^{Shc} protein level in human carcinoma cell lines (Lee *et al.*, 2004a). These data suggest the role of p66^{Shc} protein in sex hormone-regulated cancer cell proliferation. Furthermore, p66^{Shc} level is significantly elevated in cancerous cells compared to the neighboring noncancerous cells in clinical archival prostate cancer (PCa) specimens (Lee *et al.*, 2004a). Therefore, p66^{Shc} might play a role in the development and/or progression of PCa. Hence, in this study, we explored the role of p66^{Shc} in the regulation of PCa cell proliferation that could lead to cancer progression.

Results

Expression of p66^{Shc} protein in different human PCa cell lines

Based on our previous observations on archival PCa specimens that p66^{Shc} protein level is elevated in cancerous cells, we analysed the expression profile of p66^{Shc} in different PCa cell lines, which exhibit different growth rates. As shown in Figure 1, Western blot analyses with an anti-Shc antibody (Ab) recognizing all three isoforms of Shc protein showed that rapid-growing PC-3, DU 145 and TSU-Pr1 PCa cells expressed higher levels of p66^{Shc} protein as compared

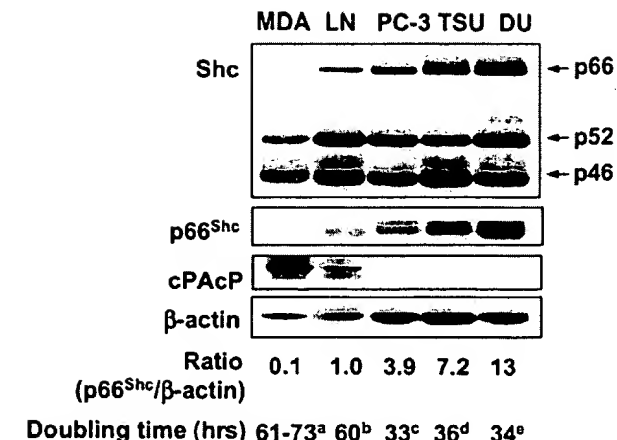


Figure 1 Expression of p66^{Shc} protein in different PCa cells. LNCaP C-33, PC-3, TSU-Pr1 and DU 145 cells were plated in a medium supplemented with 5% fetal bovine serum (FBS), while MDA PCa2b cells were plated in a medium containing 20% FBS for the experiments. An aliquot of total cell lysates from MDA PCa2b (MDA), LNCaP C-33 (LN), PC-3 (PC), TSU-Pr1 (TSU), and DU145 (DU) cells was electrophoresed, transferred to nitrocellulose membranes, and incubated with Abs against Shc, p66^{Shc} and cPAcP proteins, respectively. The level of β-actin protein was detected as an internal loading control. The intensity of hybridization band was semiquantified using a densitometer. The relative level of p66^{Shc} protein to the corresponding β-actin protein was calculated and then normalized to that of LNCaP C-33 cells. The ratio was shown at the bottom of the figure. Similar results were observed in three sets of independent experiments. The doubling time of each cell line has been given as a measure of their growth rates (^aNavone *et al.*, 1997; ^bHoroszewicz *et al.*, 1983; ^cKaighn *et al.*, 1979; ^dIizumi *et al.*, 1987; ^eStone *et al.*, 1978)

to slow-growing MDA PCa2b and LNCaP C-33 cells. The low level of p66^{Shc} protein in MDA PCa2b cells was detected only after prolonged exposure (data not shown). The protein levels of p52^{Shc} and p46^{Shc} were similar in all the cell lines examined. The phenomenon that rapidly growing cells express high level of p66^{Shc} protein was also observed with another Ab that specifically reacts with p66^{Shc} protein alone (Figure 1). p66^{Shc} protein levels in the rapid-growing cells were approximately 4–13-fold higher than that in slow-growing LNCaP C-33 cells and over 10-fold higher than in MDA PCa2b cells. Interestingly, among those PCa cells, the p66^{Shc} protein level inversely correlated with the expression level of cellular form of prostatic acid phosphatase (cPAcP) (Figure 1), the major protein tyrosine phosphatase and a negative growth regulator in prostatic epithelia (Lin *et al.*, 1998, 2001).

To examine further the correlation of p66^{Shc} protein expression with cell growth, we analysed p66^{Shc} protein level in different passages of LNCaP cells, utilizing Ab recognizing all the three isoforms of Shc protein. As reported earlier (Lin *et al.*, 1998; Igawa *et al.*, 2002), the growth ratio of C-81 cells was approximately three times higher than that of C-33 cells, while C-51 cells exhibit a growth rate faster than C-33 cells but slower than C-81 cells (Figure 2a). Western blot analyses revealed that p66^{Shc} protein expression was higher in C-81 cells than in

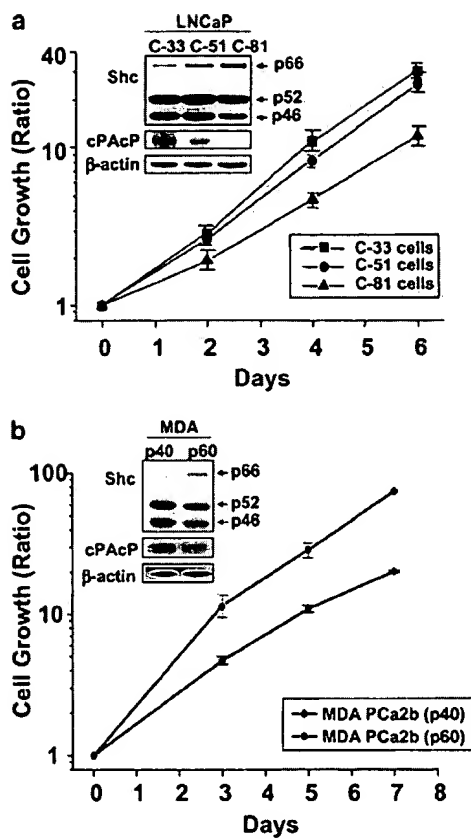


Figure 2 The growth rate and the expression of p66^{Shc} protein in different passages of LNCaP and MDA PCa2b cells. (a) Different LNCaP cells were seeded and maintained as described in Materials and methods. The total cell number was counted on day 2, 4 and 6. Similar results were observed in three sets of independent experiments performed in duplicates (mean \pm s.d.). Western blot analyses of Shc, cPAcP and β -actin proteins in LNCaP C-33, C-51 and C-81 cells were performed by incubating with the corresponding Abs (inner panel). (b) Different MDA PCa2b cells were seeded and maintained as described in Materials and methods. The total cell number was counted on day 3, 5 and 7. Similar results were observed in two sets of independent experiments done in duplicates (mean \pm s.d.). Immunoblot analyses of Shc, cPAcP and β -actin proteins in both low (MDA p40) and high (MDA p60) passage MDA PCa2b cells were performed by incubating with the corresponding Abs (inner panel).

C-51 and C-33 cells, whereas p52^{Shc} protein level was approximately similar in all cells (Figure 2a, inner panel). Since Shc family members are tyrosine phosphorylated in mediating the growth signals from tyrosine phosphorylated receptor tyrosine kinases (Ravichandran, 2001; Lee et al., 2004b), we analysed the tyrosine phosphorylation level of p66^{Shc} protein by Western blotting, following immunoprecipitation with anti-Shc antibody, in different LNCaP cells. Unexpectedly, we could not detect any tyrosine phosphorylation of p66^{Shc} protein in different passages of LNCaP cells by the enhanced chemiluminescence (ECL) method (data not shown, Lee et al., 2004b). Similar negative results were obtained by using the antibody against pY239 or pY317 of p52^{Shc} that could also react with the corresponding sites in p66^{Shc} protein with the total cell

lysate proteins (Lee et al., 2004b). Nevertheless, cPAcP was highly expressed in C-33 cells, while it was only barely detected in C-81 cells, thus, inversely correlating with their relative p66^{Shc} protein levels (Figure 2a, inner panel). Similarly, MDA PCa2b cells of passage number 60 (MDA p60) grew faster than those of passage number 40 (MDA p40) (Figure 2b). Concurrently, MDA p60 cells expressed a higher level of p66^{Shc} protein than MDA p40 cells (Figure 2b, inner panel). The low level of p66^{Shc} protein in MDA p40 cells could be detected only after prolonged exposure (data not shown). Furthermore, the elevated level of p66^{Shc} protein in MDA p60 cells corresponded to the decreased cPAcP protein (Figure 2b, inner panel). Thus, the data collectively indicate that the expression level of p66^{Shc} protein correlates, positively with PCa cell proliferation rate and, inversely with cPAcP expression.

Effects of growth manipulation on p66^{Shc} protein level in different PCa cells

Since p66^{Shc} protein level positively correlates with the PCa cell growth, we analysed whether manipulation of PCa cell growth would alter the expression level of p66^{Shc} protein. We used EGF and 5 α -dihydrotestosterone (DHT), which could upregulate the proliferation of LNCaP C-33 cells and downregulate the cPAcP (Lin et al., 1992, 1998; Meng and Lin, 1998; Lee et al., 2004b), and examined their effects on the protein levels of p66^{Shc} in those cells. As shown in Figure 3a, p66^{Shc} protein level was upregulated in LNCaP C-33 cells treated for 24 h with 10 ng/ml EGF or 10 nM DHT, approximately 2.5–3-fold higher than that in the corresponding control cells.

Owing to the inhibitory effect of cPAcP on PCa cell proliferation (Lin et al., 1998, 2001), we examined whether increased proliferation by inhibiting cPAcP activity would lead to the elevation of p66^{Shc} protein in those cells. LNCaP C-33 cells that express endogenous cPAcP were exposed to different concentrations of L(+)tartrate, a classical inhibitor of PAcP (Lin et al., 1992; Meng and Lin, 1998). In the presence of 2.5 mM L(+)tartrate, the expression level of p66^{Shc} protein was elevated by approximately 2.5-fold (Figure 3b), corresponding to the decrease in cPAcP activity (data not shown). 5 mM L(+)tartrate had the similar effect as 2.5 mM concentration. Furthermore, the increase of p66^{Shc} in L(+)tartrate-treated cells correlated with increased ERK/MAPK activation (Figure 3b) and cell proliferation (data not shown). It should be noted that L(+)tartrate had no effect on the levels of p52^{Shc} and p46^{Shc} proteins. Thus, elevated p66^{Shc} protein level correlates with ERK/MAPK activation as well as cell proliferation in cPAcP-inhibited PCa cells.

As an additional approach, we examined the p66^{Shc} protein expression in PAcP cDNA-transfected stable subclones of LNCaP C-81 cells that have reduced proliferation rates (Lin et al., 1998, 2001; Meng and Lin, 1998). Western blot analyses showed that LN-23 and LN-40 subclone cells, which express exogenous cPAcP, had lower levels of p66^{Shc} protein when

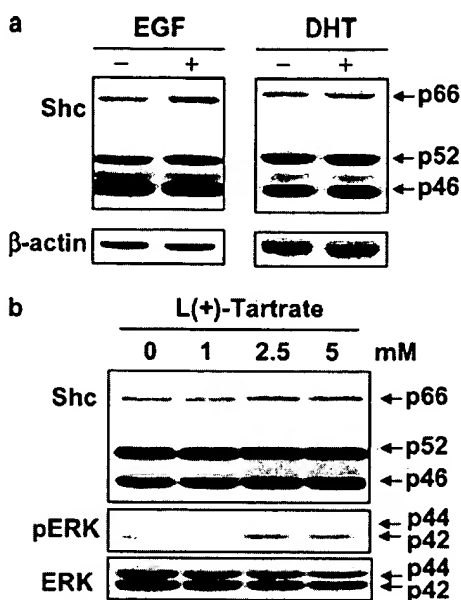


Figure 3 Effects of EGF, DHT and L(+)-tartrate on p66^{Shc} protein expression in LNCaP C-33 cells. (a) LNCaP C-33 cells were preincubated in a steroid-reduced medium for 48 h and then treated with EGF (10 ng/ml) or DHT (10 nM) for 24 h. Control cells received the solvent alone. Total cell lysates were used for Western blot analyses of Shc protein level. The level of β -actin protein was detected as a loading control. Similar results were obtained from three sets of independent experiments. (b) LNCaP C-33 cells were treated with 0, 1, 2.5 and 5 mM of L(+)-tartrate for 16 h. Total cell lysates were used for analysing the protein levels of Shc and ERK/MAPK as well as the phosphorylation level of ERK/MAPK. Similar results were obtained from two sets of independent experiments

compared to C-81 parental (Figure 4a). Similarly, PAcP cDNA-transfected PC-3 stable subclone cells that had slower growth rates compared to their parental cells (Lin *et al.*, 1998; Meng and Lin, 1998) also expressed lower levels of p66^{Shc} protein than their parental cells (Figure 4b). Taken together, the results indicated that manipulation of PCa cell growth leads to a corresponding change in p66^{Shc} expression level.

Effect of p66^{Shc} protein expression on the growth of PCa cells

We determined the effect of p66^{Shc} protein on the growth rate of PCa cells. Initially, LNCaP C-33 cells were transiently transfected with a cDNA encoding the wild-type p66^{Shc} protein and cell growth was analysed. Results indicated that transient elevation of p66^{Shc} protein in LNCaP C-33 cells resulted in a reduction in the doubling time by approximately 26%, indicating an increased cell proliferation, which correlated with the increased activation of ERK/MAPK (data not shown). We subsequently established stable subclones of LNCaP C-33 cells, that is, S-32 and S-36 cells, which stably express the exogenous p66^{Shc} protein. For experimental control, the vector alone-transfected stable subclone cells, that is, V-1 cells were established as well. Despite that different passages of LNCaP cells exhibit morpho-

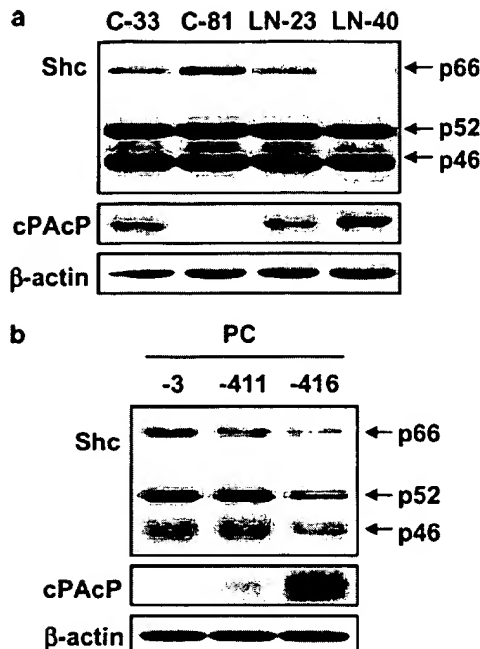


Figure 4 Expression of p66^{Shc} protein in the PAcP cDNA-transfected LNCaP C-81 and PC-3 stable subclone cells. (a) The protein levels of Shc and cPAcP in LNCaP C-33 and C-81 cells as well as LN-23 and LN-40 cells were analyzed by Western blot analyses. The level of β -actin protein was analysed as a loading control. (b) Western blot analyses of Shc, cPAcP and β -actin proteins in PC-3, PC-411 and PC-416 cells. Similar results were obtained from two sets of independent experiments

logical changes, we did not observe any noticeable morphological difference between the subclone cells overexpressing p66^{Shc} and V-1 and LNCaP C-33 cells (data not shown). As shown in Figure 5a (left panel), in S-32 and S-36 subclone cells, elevated levels of p66^{Shc} protein correlated with the activation of ERK/MAPK, indicated by increased levels of phosphorylation. The cell growth was initially evaluated by analysing the doubling time of those cells. Results showed that elevated p66^{Shc} protein levels correlated with rapid cell growth with a reduction in the doubling time of p66^{Shc}-overexpressing stable subclones, that is, approximately 30 h for S-36 cells and 33 h for S-32 cells compared to the control cells, that is, 45 h for V-1 and C-33 parental cells (Figure 5a, right panel). We subsequently analysed the cell cycle distribution of those cells with flow cytometry. The S-32 and S-36 cells exhibited higher proliferation rates than the parental C-33 and V-1 cells, as indicated by the percentage of cell population in the S phase of cell cycle, that is, 17, 17.6, 22.3 and 24.1% for LNCaP C-33, V-1, S-32 and S-36 cells, respectively (Figure 5b). The data collectively suggest that elevated p66^{Shc} protein in PCa cells, possibly through the activation of ERK/MAPK, plays a role in promoting their proliferation resulting in an increased percentage of cells in the S phase of the cell cycle.

To further confirm the role of p66^{Shc} in PCa cell growth regulation, we determined whether downregulation of p66^{Shc} protein, using a plasmid-based RNAi

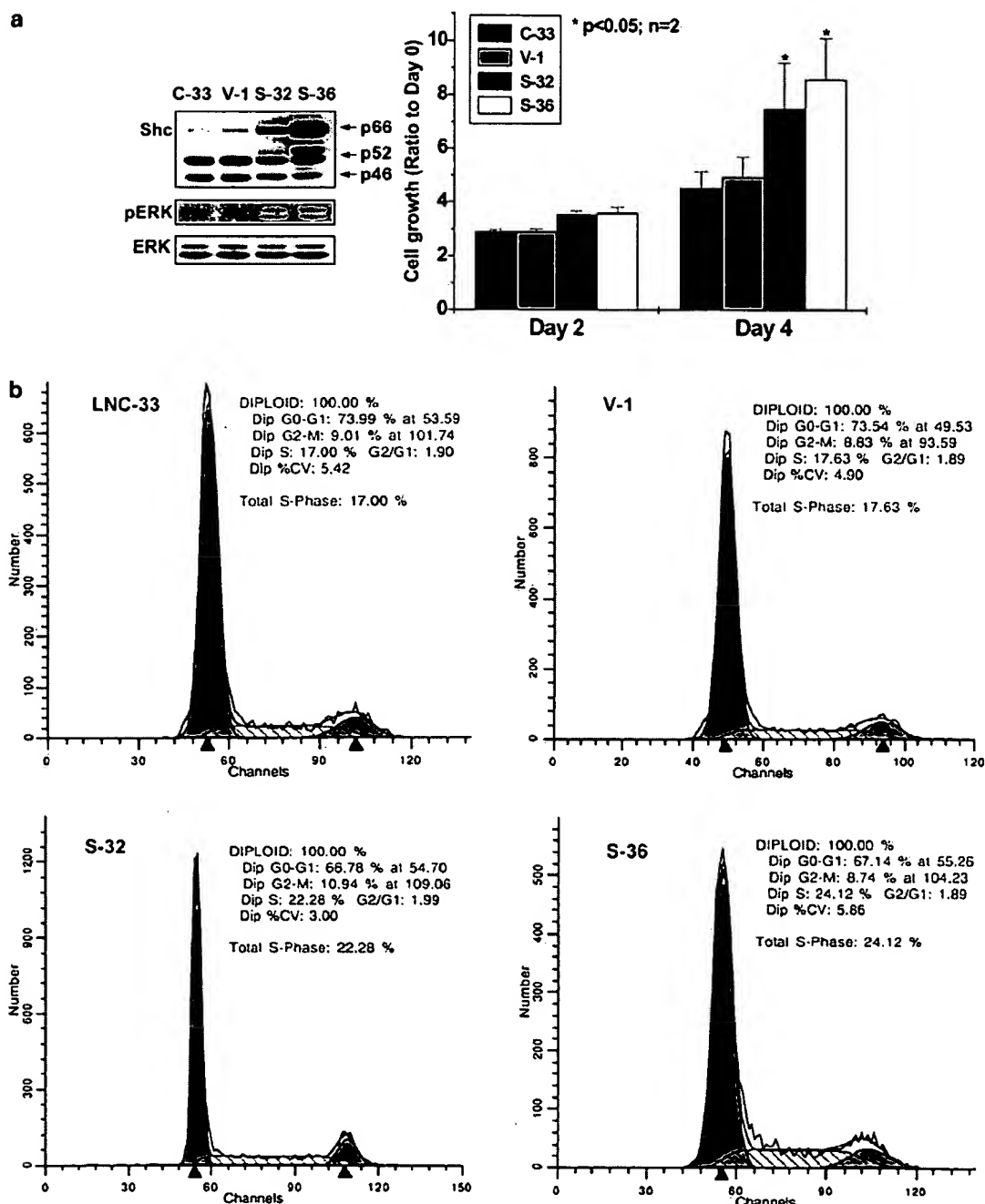


Figure 5 p66^{Shc} protein expression, phosphorylation of ERK/MAPK, and the growth of stable subclones of p66^{Shc} cDNA-transfected LNCaP C-33 cells. (a) Western blot analyses of Shc (left panel) and cell growth (right panel) in LNCaP C-33, vector alone-transfected (V-1), and two stable subclones of p66^{Shc} cDNA-transfected LNCaP C-33 cells (S-32 and S-36). Aliquots of the same set of whole-cell lysates were immunoblotted with an anti-phospho-ERK/MAPK Ab and, after stripping, followed by an anti-ERK/MAPK Ab. The cell growth data are the representative of two sets of independent experiments in duplicates (b) Histograms of cell cycle distributions of S-32 and S-36 cells by flow cytometric analyses. LNCaP C-33 parental and V-1 cells were used as controls. Similar results were obtained from two sets of independent experiments

approach, would lead to a decrease in their growth rate. We transfected LNCaP C-81 and PC-3 cells with pSUP-p66 to knock down their p66^{Shc} expression. In order to normalize the differences in the transfection efficiency of those cells, we cotransfected with pTRACER-CMV along with pSUP-p66. As shown in Figure 6a (left panel), transient knock-down of p66^{Shc} in C-81 cells

correlated with the decrease in activation of ERK/MAPK, indicated by decreased levels of phosphorylation. Transient knock-down of p66^{Shc} protein by about 40% in rapid-growing LNCaP C-81 cells using pSUP-p66 resulted in an approximately 30% decrease in cell proliferation (Figure 6a, right panel). Cell cycle distribution of p66^{Shc}-knocked-down C-81 cells indicated

that they exhibited approximately 30% decrease in their proliferation rates than the vector-alone transfected cells, as indicated by the decrease in the percentage of cell population in the S phase of cell cycle, that is, 14.8% for p66^{Shc}-knocked-down cells vs 22.6% for vector-alone-transfected cells (Figure 6b). Similarly, in PC-3 cells, an approximately 45% knock-down of p66^{Shc} protein by RNAi led to the decrease in ERK/MAPK activation, as indicated by its decreased phosphorylation (Figure 6c, left panel) that correlated with approximately 35% reduction in their proliferation rate as determined by the cell counting (Figure 6c, right panel).

Cell cycle analysis of those p66^{Shc}-knocked-down PC-3 cells showed that there was a decrease in S phase from 18.3% in vector-alone-transfected cells to 13.6% for p66^{Shc}-knocked-down cells (Figure 6d). Thus, the data collectively indicate that p66^{Shc} protein plays a critical role in regulating the proliferation of PCa cells.

Discussion

Shc proteins play a critical role in regulating PCa cell proliferation, in part by mediating tyrosine phosphorylation

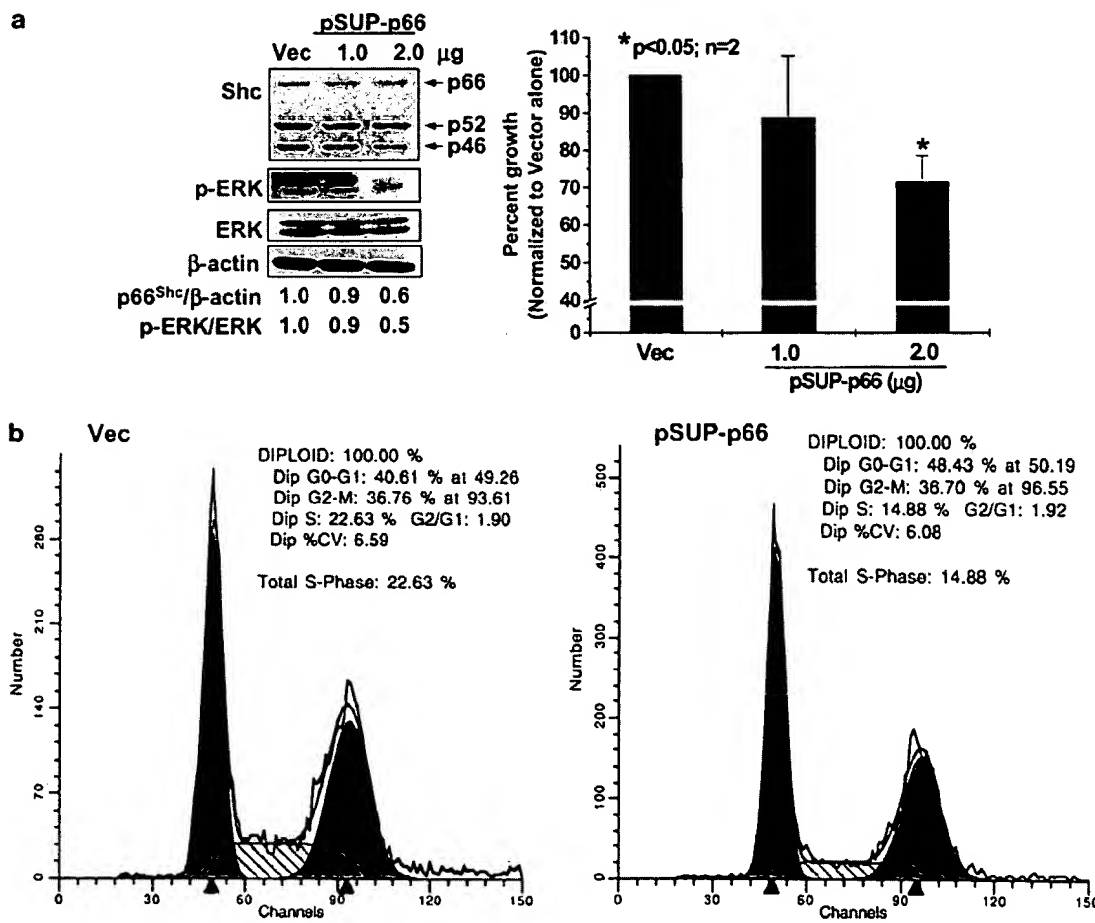


Figure 6 Effect of knock-down of p66^{Shc} expression by siRNA on PCa cell growth. (a) Western blot and cell growth analyses of p66^{Shc}-knocked-down LNCaP C-81 cells. LNCaP C-81 cells were plated at a density of 1×10^3 cells/well of a six-well plate for 48 h. The cells were transiently transfected with pSUP-p66. Control cells were transfected with pSUPER vector alone (Vec). After 3 days following transfection, cells were harvested by trypsinization and counted in a Coulter cell counter (right panel). Cell lysates were analysed for p66^{Shc} protein level and ERK1/2 phosphorylation. To normalize the transfection efficiency, cells were cotransfected with pTRACER-CMV, a plasmid expressing green fluorescent protein (GFP). The figure is a representative of three sets of independent experiments in duplicates. (b) Cell cycle analysis of p66^{Shc}-knocked-down LNCaP C-81 cells. 7.5×10^3 LNCaP C-81 cells were plated in regular medium on 100 mm dishes and transfected with pSUP-p66. Control cells were transfected with vector alone (Vec). After 3 days, cells were trypsinized, fixed with 70% ethanol and stained with propidium iodide. Cells were analysed with a flow cytometer for the distribution of cell cycle. Cells were cotransfected with pTRACER-CMV for estimating the transfection efficiency. The figure is a representative of three sets of independent experiments. (c) Western blot and cell growth analyses of p66^{Shc}-knocked-down PC-3 cells. PC-3 cells were transfected with pSUP-p66, as described for LNCaP C-81 cells. Cell growth was analysed 3 days post-transfection. To normalize the transfection efficiency, cells were cotransfected with pTRACER-CMV. The figure is a representative of two sets of independent experiments performed in duplicates. (d) Cell cycle analysis of p66^{Shc}-knocked-down PC-3 cells. 7.5×10^3 PC-3 cells were plated in regular medium on 100 mm dishes and transfected with pSUP-p66. Control cells were transfected with vector alone. To normalize the transfection efficiency, cells were cotransfected with pTRACER-CMV. After 3 days, cells were trypsinized, fixed with 70% ethanol and stained with propidium iodide. Cells were analysed with a flow cytometer for the distribution of cell cycle. The figure is a representative of two sets of independent experiments

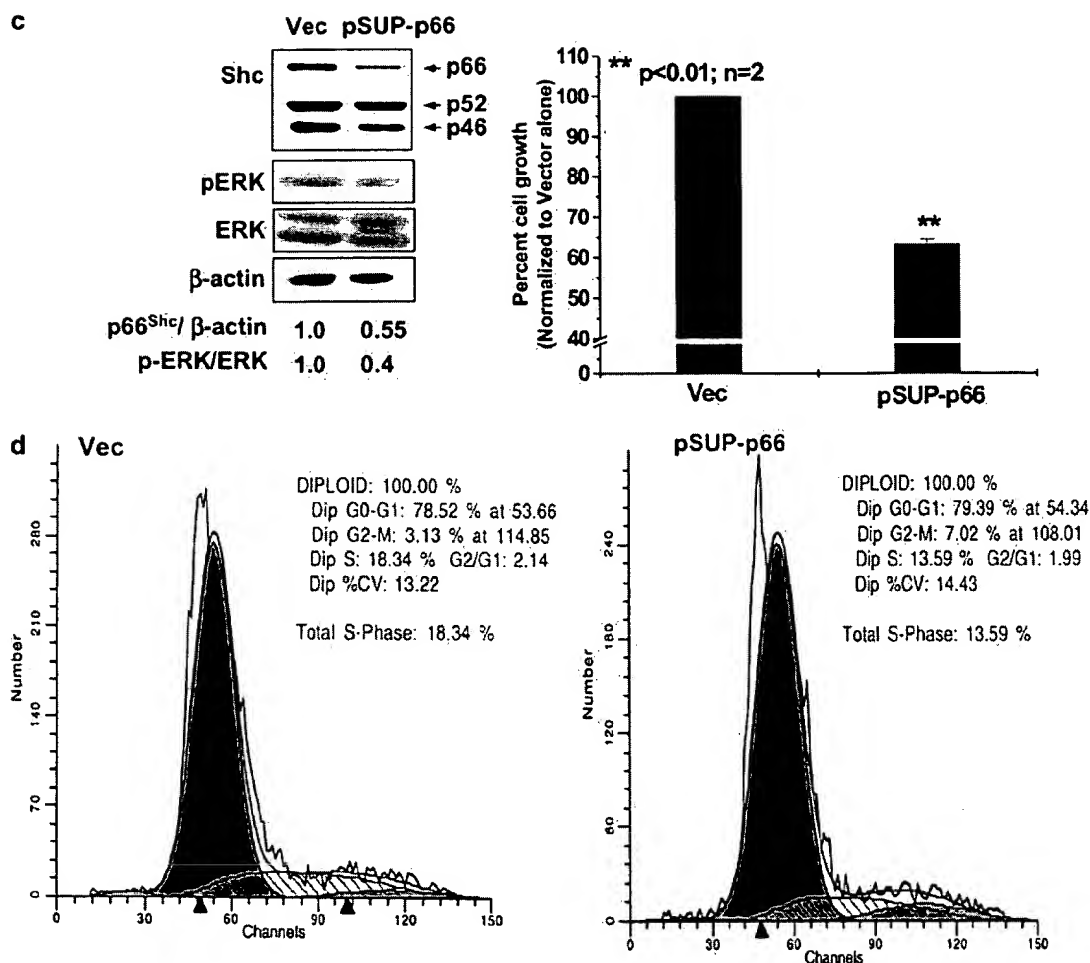


Figure 6 *Continued*

signals. For example, treatment of LNCaP C-33 cells with androgens leads to increased phosphorylation of p52^{Shc} at Y317 residue, which is required for DHT-induced proliferation, but not that of EGF (Lee *et al.*, 2004b). Apart from p52^{Shc}, the role of other Shc members in the proliferation of PCa cells remains an enigma. Interestingly, androgen stimulation of PCa cells is accompanied with the upregulation of p66^{Shc} protein levels, but not its tyrosine phosphorylation levels (Lee *et al.*, 2004a, b; Figure 3a). Furthermore, p66^{Shc} protein level is significantly elevated in archival human PCa specimens, higher in the cancerous cells compared to the adjacent noncancerous cells (Lee *et al.*, 2004a). Hence, we hypothesize that p66^{Shc} protein is also involved directly in the regulation of PCa cell proliferation.

Our data in different PCa cell lines clearly show that p66^{Shc} protein level, but not p52^{Shc} or p46^{Shc} protein levels, consistently correlates with cell proliferation (Figures 1–4). Additionally, elevated expression of p66^{Shc} protein by cDNA transfection in LNCaP C-33 cells correlates with increased cell proliferation (Figure 5). Conversely, knock-down of p66^{Shc} protein level by its siRNA leads to decreased cell growth (Figure 6). Our

cell line data corroborate our observations on the archival PCa tissue specimens that p66^{Shc} expression is lower in benign glandular cells, whereas in adjacent adenocarcinomatous cells, the expression of p66^{Shc} is higher (Lee *et al.*, 2004a). Thus, we further propose that normal differentiated prostate epithelial cells, which have a slow growth rate, would express a low level of p66^{Shc} protein, whereas its elevated expression might contribute to prostate carcinogenesis. It should also be noted that the protein levels of other Shc isoforms, that is, p46^{Shc} and p52^{Shc}, do not consistently correlate with the PCa cell growth. Hence, we propose that p66^{Shc} protein level, but not p46^{Shc} or p52^{Shc} protein level, is directly involved in the regulation of cell growth. Nevertheless, a similar growth rate of the stable subclone cells that overexpress p66^{Shc} might be due to that the growth stimulation by high levels of p66^{Shc} reached the plateau (Figure 5a, right panel). This is comparable to the rapid-growing PCa cells, such as PC-3, TSU-Pr1 and DU 145 cells, which express increasingly higher levels of p66^{Shc} protein, but still have a similar doubling time (Figure 1). Collectively, the data support our hypothesis that elevated p66^{Shc} protein in prostate carcinomas plays a critical role in upregulating

the proliferation of those cancer cells and, thus, contributes to the tumorigenicity of human PCa.

Similarly, elevation of p66^{Shc} protein is observed in breast cancer specimens, where p66^{Shc} protein is elevated in the lymph node-positive breast carcinomas (Jackson *et al.*, 2000). Nevertheless, other studies show that the level of p66^{Shc} protein in relapsed breast cancers is decreased, significantly lower than that in primary, nonrelapsed tumors (Davol *et al.*, 2003). The data collectively implicate that p66^{Shc} protein plays a role in the tumorigenicity of those breast cancer cells, although the correlative relationship requires further clarification. It should be noted that the level of p66^{Shc} protein in human carcinoma cells is altered by various treatments including steroids and growth factors (Figure 3a; Lee *et al.*, 2004a). Hence, it is possible that the inconsistency in the correlative relationship in breast cancer studies may partly be related to the different treatment regimens that those patients were in, prior to obtaining the specimens. As described, some of those relapsed tumors had been obtained from patients who were under adjuvant hormonal therapy (Davol *et al.*, 2003). It is thus expected that those hormone-ablated specimens would have a decreased level of p66^{Shc} protein. In such case, a substantial number of cancer specimens that have low levels of p66^{Shc} protein may tip the results of statistical analyses. Nevertheless, due to the small sample size in our study, we are unable to determine if the elevated p66^{Shc} protein level could serve as a surrogate marker for PCa progression. The clinical application of p66^{Shc} protein in PCa deserves further investigations.

The molecular mechanism by which p66^{Shc} protein is involved in regulating cell proliferation deserves careful analyses. In PCa cells, p66^{Shc} protein level inversely correlates with cPAcP and positively correlates with ERK/MAPK activation. In p66^{Shc} cDNA-transfected stable subclone cells, ERK/MAPKs are activated, correlating with increased cell proliferation (Figure 5). Conversely, in p66^{Shc}-knocked-down LNCaP C-81 and PC-3 cells, ERK/MAPKs are inhibited that correlate with decreased cell proliferation (Figure 6). This p66^{Shc}-activated ERK/MAPK in p66^{Shc} cDNA-transfected LNCaP cells is consistent with the observations that in cPAcP-inhibited LNCaP C-33 cells by L(+)-tartrate, p66^{Shc} protein level is elevated and ERK/MAPK are activated (Figure 3b). We propose that the negative effect of cPAcP on p66^{Shc} protein level is not through a direct mechanism, such as cPAcP-p66^{Shc} protein interaction, although it requires further investigation. It should be noted that the inverse correlation of the level of cPAcP to p66^{Shc} and ERK/MAPK phosphorylation is clinically significant, because in clinical PCa specimens, cPAcP is decreased (Loor *et al.*, 1981; Pontes *et al.*, 1981; Solin *et al.*, 1990; Sakai *et al.*, 1993; Lin *et al.*, 2001) and p66^{Shc} protein level and ERK/MAPK phosphorylation are elevated (Gioeli *et al.*, 1999; Price *et al.*, 1999; Lee *et al.*, 2004a). This phenomenon is also similar to the observation in breast cancer cells that increased expression of p66^{Shc} protein correlates with ERK/MAPK activation (Jackson *et al.*, 2000). The observation that elevated p66^{Shc} protein reduces the

degree of EGF-induced ERK/MAPK activation in HeLa, CHO or COS-1 cells (Migliaccio *et al.*, 1997; Okada *et al.*, 1997) could be due in part to different cell types. Alternatively, it should be noted that in those p66^{Shc}-elevated cells, the basal activity of ERK/MAPKs was upregulated. Thus, it could be expected that the degree of further stimulation of ERK/MAPK by EGF in those p66^{Shc}-elevated cells is reduced. The mechanism of p66^{Shc} activating ERK/MAPK requires further analysis.

Increased oxidative stress, through the generation of reactive oxygen species (ROS), in rapid-growing PCa cells might also account for the elevated expression of p66^{Shc} protein in those cells. It is generally accepted that rapid-growing cells have activated metabolic reactions that lead to increased production of ROS (Klaunig and Kamendulis, 2004), which results in the elevation of p66^{Shc} protein to mediate oxidative stress signals. This notion is supported by the observations that the expression of p66^{Shc} protein is increased by raising intracellular ROS level, for example, by H₂O₂ treatment (Trinei *et al.*, 2002; Pacini *et al.*, 2004). Interestingly, treatment of cells with steroid hormones and growth factors, such as, DHT and EGF, results in the upregulation of ROS in those cells (Ripple *et al.*, 1997, 1999; Meng *et al.*, 2002) and the increased ROS could serve as a positive regulator of cell growth as observed in human hepatoma cells (Liu *et al.*, 2002). Importantly, around 80% of the prostate tumor specimens showed an increase in NADPH oxidase 1 and intracellular ROS levels when compared to the adjacent noncancerous tissue (Lim *et al.*, 2005). Thus, it could be speculated that the upregulation of p66^{Shc} protein by DHT or EGF treatment in PCa cells might be through the upregulation of ROS in those stimulated cells. In summary, our data clearly support for a novel functional role of p66^{Shc} protein in prostate carcinogenesis probably through promoting cell proliferation, although the detailed molecular mechanism(s) by which p66^{Shc} protein upregulates PCa cell proliferation require(s) further studies. Further, the potential role for p66^{Shc} protein in serving as a target for PCa therapy deserves further investigations.

Materials and methods

Materials

FBS, RPMI 1640 culture medium, glutamine and gentamicin were purchased from Invitrogen (Carlsbad, CA, USA). Charcoal/dextran-treated, certified FBS was obtained from HyClone (Logan, UT, USA). BRFF-HPC1 medium was obtained from Athena Environment Science, Inc. (Baltimore, MD, USA). Polyclonal Abs (#06-203) recognizing all three isoforms of Shc protein and the Ab (#07-150) specifically recognizing p66^{Shc} protein were from Upstate Biotechnology Inc. (Lake Placid, NY, USA). Rabbit anti-PAcP antiserum was obtained as described previously (Lin *et al.*, 1993). Polyclonal Abs against phospho-ERK/MAPK (Thr202/Tyr204) and ERK/MAPK were from Cell Signaling (Beverly, MA, USA). Anti- β -actin Ab, EGF and DHT were obtained

from Sigma (St Louis, MO, USA). Horseradish peroxidase-conjugated anti-rabbit and anti-mouse IgG were purchased from Santa Cruz Biotechnology, Inc. (Santa Cruz, CA, USA). All other chemicals were as described previously (Lin *et al.*, 1998; Meng and Lin, 1998; Lee *et al.*, 2004a, b).

Cell culture

Human prostate carcinoma cell lines including LNCaP-FGC (doubling time 60 h) (Horoszewicz *et al.*, 1983), MDA PCa2b (doubling time 61–73 h) (Navone *et al.*, 1997), DU 145 (doubling time 34 h) (Stone *et al.*, 1978) and PC-3 (doubling time 33 h) (Kaighn *et al.*, 1979) were purchased from the American Type Culture Collection (Rockville, MD, USA). TSU-Pr1 cells (doubling time 36 h) (Iizumi *et al.*, 1987) were obtained from Dr Jin-Tang Dong at Emory University School of Medicine (Atlanta, GA, USA). Human PCa cells except MDA PCa2b cells were routinely maintained in the regular culture medium, that is, phenol red-positive RPMI 1640 medium supplemented with 5% FBS, 1% glutamine and 0.5% gentamicin (Meng and Lin, 1998). Cells were split once per week, which was defined as one passage. LNCaP cells with passage numbers less than 33 were designated as C-33, those with numbers greater than 81 as C-81, and those with numbers between 34 and 80 as C-51 (Lin *et al.*, 1998; Meng *et al.*, 2000; Igawa *et al.*, 2002). LNCaP C-33 cells express endogenous PAcP, while C-81 cells have lost PAcP expression (Lin *et al.*, 1998). PAcP-cDNA-transfected C-81 stable subclone cells, that is, LN-23 and LN-40 cells, have slower growth rates (doubling time 72 and 90 h, respectively) than C-81 parental cells (doubling time 49 h) in a steroid-reduced condition (Meng and Lin, 1998). PC-3 cells do not express endogenous PAcP (Kaighn *et al.*, 1979; Lin *et al.*, 1998). PC-411 and PC-416 cells were PAcP cDNA-transfected PC-3 stable subclone cells with doubling time 40 and 54 h, respectively (Lin *et al.*, 1998). MDA PCa2b cells were routinely maintained in the culture medium, that is, BRFF-HPC1 medium supplemented with 20% FBS, 1% glutamine and 0.5% gentamicin. For EGF or DHT treatment, LNCaP C-33 cells were steroid-starved for 48 h in a steroid-reduced medium, that is, phenol red-free RPMI 1640 medium containing 5% charcoal/dextran-treated, heat-inactivated certified FBS, 1% glutamine and 0.5% gentamicin. Cells were then exposed to EGF (10 ng/ml) or DHT (10 nM) for 24 h.

Cell growth determination

To determine the growth of different passages of LNCaP and MDA PCa2b cells, 3.2×10^4 of different LNCaP cells or 1×10^5 of different MDA PCa2b cells were seeded on six-well culture plates with duplicate wells and maintained in their respective culture medium. After 3 days, one set of attached cells was harvested and counted as day 0 with a Z1 model Coulter Counter (Coulter Corporation, Miami, FL, USA). The remaining attached cells were fed with fresh medium, and the total cell numbers were counted on days 2, 4 and 6 for LNCaP cells or day 3, 5 and 7 for MDA PCa2b cells. The fresh medium was added to the remaining LNCaP cells on days 2 and 4 or MDA PCa2b cells on days 3 and 5.

Immunoblotting

Subconfluent cells were harvested by scraping. After being spun at 4°C, the pelleted cells were rinsed with ice-cold 20 mM HEPES-buffered saline, pH 7.0, and then lysed in ice-cold cell lysis buffer containing protease and phosphatase inhibitors. The detailed protocols for immunoblotting were as described previously (Lin *et al.*, 1998; Meng and Lin, 1998; Lee *et al.*, 2004a, b). The p66^{shc} protein level was semiquantified by

densitometric analyses of autoradiograms with different exposure time periods using Molecular Dynamics equipment and its software program (ImageQuant 3.0). The relative protein level was then normalized to the corresponding β -actin protein level.

Construction of p66^{shc} cDNA expression vector

The wild-type p66^{shc} cDNA constructed in the PINCO retroviral expression vector was from Dr A Raymond Frackelton Jr at the Brown University (Providence, RI, USA) with the approval from Dr Pier Giuseppe Pelicci at the European Institute of Oncology (Milan, Italy) (Migliaccio *et al.*, 1999). The p66^{shc} coding region was amplified using this p66^{shc} PINCO plasmid as the template and two oligonucleotide primers: 5'-GAATTCAACT ATGGATCTCCTGCC-3' and 5'-AAGCTT^{TTAGGGCAGATCACAGTTT-CC-3'} (*Eco*RI and *Hind*III sites are, respectively, underlined). This PCR fragment was digested by restriction enzymes *Eco*RI and *Hind*III and then ligated with the *Eco*RI/*Hind*III-cut pcDNA 3.1A vector (designated as pcDNA 3.1A-p66^{shc}). The sequence of p66^{shc} cDNA coding region was confirmed by DNA sequencing at the UNMC Molecular Biology Core Facility.

Establishment of stable subclones of p66^{shc} cDNA-transfected LNCaP C-33 cells

LNCaP C-33 cells were transfected with pcDNA 3.1A-p66^{shc} plasmid encoding the wild-type p66^{shc} protein and subsequently selected by G418, as described previously (Lin *et al.*, 1998). Two stable subclone cell lines, S32 and S36, were established and characterized in this study. V-1 cells were a subclone cell line of LNCaP C-33 cells transfected with the vector alone.

Flow cytometry

For experiments, cells were seeded at a density of 5×10^5 cells per T25 flask in the regular medium for 3 days. At 48 h after feeding with fresh medium, cells were trypsinized, harvested and washed twice by Hank's balanced salt solution. Cells were treated with 70% ethanol at 4°C for 1 h, washed with PBS, and spun down by centrifugation. The DNA of ethanol-fixed cells was stained by the PI staining reagent at 4°C for 30 min. The PI staining reagent was prepared in PBS, pH 7.4, containing 0.1% Triton X-100, 0.1 mM EDTA disodium salt, 0.05 mg/ml RNase A (50 U/ml), and 50 μ g/ml propidium iodide (Telford *et al.*, 1991). The determination of cell cycle distribution for single cell was carried out using a Becton-Dickinson fluorescence-activated cell sorter (FACSCalibur, Becton Dickinson, San Jose, CA, USA) at the UNMC Flow Cytometry Core Facility.

Construction of vector coding for p66^{shc} siRNA transcripts and transfection

To knock down p66^{shc} expression in PCa cells, pSUPER vector (OligoEngine Inc., USA) was used, which involves a plasmid-based RNAi approach. Sense and antisense strand oligonucleotides that code for p66^{shc} siRNA transcripts were designed, according to the instructions by OligoEngine Inc., USA, and were synthesized in the Molecular Biology core facility at UNMC. The target sequence was 5'-TGAGTCTCTGT CATCGCTG-3' that lies in the CH₂ region of p66^{shc} (GenBank Acc. No. U73377). The oligos were annealed to each other and ligated with pSUPER vector predigested with *Bg*II and *Hind*III. The plasmid was designated as pSUP-p66.

LNCaP C-81 cells and PC-3 cells were plated at a density of 1×10^5 cells/well of a six-well plate for 48 h. Cells were then transfected with different amounts of siRNA-encoding

pSUPER plasmid using LipofectAmine Plus reagent (Invitrogen, USA). After 4 h, cells were replenished with RPMI-1640 medium containing 10% FBS overnight and then fed with regular medium. The cells were harvested after 3 days by trypsinization and were counted using a Coulter counter. Owing to the differences in transfection efficiency of those cells, we cotransfected them with pSUP-p66 and pTRACER-CMV, a plasmid expressing full-length GFP (Invitrogen Inc., USA), in the ratio of 3:1. Cells were harvested after 3 days for analysis of cell growth and cell cycle.

Abbreviations

Ab, antibody; cPAcP, cellular form of prostatic acid phosphatase; DHT, 5 α -dihydrotestosterone; ECL, enhanced chemiluminescence; EGF, epidermal growth factor; ERK/MAPK, extracellular signal-regulated kinases/mitogen-activated protein kinases; FBS, fetal bovine serum; GFP, green

References

Davol PA, Bagdasaryan R, Elfenbein GJ, Maizel AL and Frackelton Jr AR. (2003). *Cancer Res.*, **63**, 6772–6783.

Gieli D, Mandell JW, Petroni GR, Frierson Jr HF and Weber MJ. (1999). *Cancer Res.*, **59**, 279–284.

Horoszewicz JS, Leong SS, Kawinski E, Karr JP, Rosenthal H, Chu TM, Mirand EA and Murphy GP. (1983). *Cancer Res.*, **43**, 1809–1818.

Igawa T, Lin FF, Lee MS, Karan D, Batra SK and Lin MF. (2002). *Prostate*, **50**, 222–235.

Iizumi T, Yazaki T, Kanoh S, Kondo I and Koiso K. (1987). *J. Urol.*, **137**, 1304–1306.

Jackson JG, Yoneda T, Clark GM and Yee D. (2000). *Clin. Cancer Res.*, **6**, 1135–1139.

Kaighn ME, Narayan KS, Ohnuki Y, Lechner JF and Jones LW. (1979). *Invest. Urol.*, **17**, 16–23.

Klaunig JE and Kamendulis LM. (2004). *Annu. Rev. Pharmacol. Toxicol.*, **44**, 239–267.

Lee MS, Igawa T, Chen SJ, Van Bemmel D, Lin JS, Lin FF, Johansson SL, Christman JK and Lin MF. (2004a). *Int. J. Cancer*, **108**, 672–678.

Lee MS, Igawa T and Lin MF. (2004b). *Oncogene*, **23**, 3048–3058.

Lim SD, Sun C, Lambeth JD, Marshall F, Amin M, Chung L, Petros JA and Arnold RS. (2005). *Prostate*, **62**, 200–207.

Lin MF, DaVolio J and Garcia-Arenas R. (1992). *Cancer Res.*, **52**, 4600–4607.

Lin MF, Garcia-Arenas R, Chao YC, Lai MM, Patel PC and Xia XZ. (1993). *Arch. Biochem. Biophys.*, **300**, 384–390.

Lin MF, Lee MS, Zhou XW, Andressen JC, Meng TC, Johansson SL, West WW, Taylor RJ, Anderson JR and Lin FF. (2001). *J. Urol.*, **166**, 1943–1950.

Lin MF, Meng TC, Rao PS, Chang C, Schonthal AH and Lin FF. (1998). *J. Biol. Chem.*, **273**, 5939–5947.

Liu SL, Lin X, Shi DY, Cheng J, Wu CQ and Zhang YD. (2002). *Arch. Biochem. Biophys.*, **406**, 173–182.

Loor R, Wang MC, Valenzuela L and Chu TM. (1981). *Cancer Lett.*, **14**, 63–69.

Meng TC, Fukada T and Tonks NK. (2002). *Mol. Cell*, **9**, 387–399.

Meng TC, Lee MS and Lin MF. (2000). *Oncogene*, **19**, 2664–2677.

Meng TC and Lin MF. (1998). *J. Biol. Chem.*, **273**, 22096–22104.

Migliaccio E, Giorgio M, Mele S, Pelicci G, Rebaldi P, Pandolfi PP, Lanfrancone L and Pelicci PG. (1999). *Nature*, **402**, 309–313.

Migliaccio E, Mele S, Salcini AE, Pelicci G, Lai KM, Superti-Furga G, Pawson T, Di Fiore PP, Lanfrancone L and Pelicci PG. (1997). *EMBO J.*, **16**, 706–716.

Navone NM, Olive M, Ozen M, Davis R, Troncoso P, Tu SM, Johnston D, Pollack A, Pathak S, von Eschenbach AC and Logothetis CJ. (1997). *Clin. Cancer Res.*, **3**, 2493–2500.

Okada S, Kao AW, Ceresa BP, Blaikie P, Margolis B and Pessin JE. (1997). *J. Biol. Chem.*, **272**, 28042–28049.

Orsini F, Migliaccio E, Moroni M, Contursi C, Raker VA, Piccini D, Martin-Padura I, Pelliccia G, Trinei M, Bono M, Puri C, Tacchetti C, Ferrini M, Mannucci R, Nicoletti I, Lanfrancone L, Giorgio M and Pelicci PG. (2004). *J. Biol. Chem.*, **279**, 25689–25695.

Pacini S, Pellegrini M, Migliaccio E, Patrussi L, Ulivieri C, Ventura A, Carraro F, Naldini A, Lanfrancone L, Pelicci P and Baldari CT. (2004). *Mol. Cell. Biol.*, **24**, 1747–1757.

Pontes JE, Rose NR, Ercole C and Pierce Jr JM. (1981). *J. Urol.*, **126**, 187–189.

Price DT, Rocca GD, Guo C, Ballo MS, Schwinn DA and Luttrell LM. (1999). *J. Urol.*, **162**, 1537–1542.

Ravichandran KS. (2001). *Oncogene*, **20**, 6322–6330.

Ripple MO, Henry WF, Rago RP and Wilding G. (1997). *J. Natl. Cancer Inst.*, **89**, 40–48.

Ripple MO, Henry WF, Schwarze SR, Wilding G and Weindruch R. (1999). *J. Natl. Cancer Inst.*, **91**, 1227–1232.

Sakai H, Yogi Y, Minami Y, Yushita Y, Kanetake H and Saito Y. (1993). *J. Urol.*, **149**, 1020–1023.

Solin T, Kontturi M, Pohlmann R and Vihko P. (1990). *Biochim. Biophys. Acta*, **1048**, 72–77.

Stone KR, Mickey DD, Wunderli H, Mickey GH and Paulson DF. (1978). *Int. J. Cancer*, **21**, 274–281.

Telford WG, King LE and Fraker PJ. (1991). *Cell Prolif.*, **24**, 447–459.

Trinei M, Giorgio M, Cicalese A, Barozzi S, Ventura A, Migliaccio E, Milia E, Padura IM, Raker VA, Maccarana M, Petronilli V, Minucci S, Bernardi P, Lanfrancone L and Pelicci PG. (2002). *Oncogene*, **21**, 3872–3878.

Ventura A, Maccarana M, Raker VA and Pelicci PG. (2004). *J. Biol. Chem.*, **279**, 2299–2306.

Xie Y and Hung MC. (1996). *Biochem. Biophys. Res. Commun.*, **221**, 140–145.

Yang CP and Horwitz SB. (2000). *Cancer Res.*, **60**, 5171–5178.

fluorescent protein; PCa, prostate cancer; ROS, reactive oxygen species.

Acknowledgements

We thank Dr Pier Giuseppe Pelicci at European Institute of Oncology (Milan, Italy) and Dr A Raymond Frackelton Jr at Brown University (Providence, RI) for the gift of the wild-type p66^{shc} cDNA; Dr Jin-Tang Dong at Emory University School of Medicine (Atlanta, GA) for TSU-Pr1 cell line. We thank Ms Jacquelynn Dahl's help for screening p66^{shc} stable subclone cells. We also thank the supports from the core facilities, including Molecular Biology, DNA sequencing, Tissue Procurement and Flow Cytometry at UNMC. This study was supported in part by NIH grant CA88184, P20RR017675, P20RR018759, NCI P30 CA36727, Department of Defense PC040587 and PC05096, and the Graduate Student Fellowship of UNMC.

THERAPEUTIC APPLICATIONS OF OLIGONUCLEOTIDES

Stanley T. Crooke

ISIS Pharmaceuticals, 2280 Faraday Avenue, Carlsbad, California 92008

KEY WORDS: oligonucleotides, RNA, molecular pharmacology, pharmacodynamics, pharmacokinetics

INTRODUCTION

First proposed in 1978 by Zamencik & Stephenson (1), oligonucleotide therapeutics represent a new paradigm for drug discovery. The technology focuses on a class of chemicals, oligonucleotides, that has not been studied as potential drugs before and employs them to intervene in biological processes that likewise have not been studied previously as sites at which drugs might act.

The paradigm has resulted in substantial enthusiasm because oligonucleotides may display dramatic increases in affinity and selectivity for their nucleic acid targets compared to traditional drugs. Furthermore, antisense technology may facilitate rational drug design. Table 1 compares affinities and the potential for selectivity of oligonucleotides versus traditional drugs. The comparison is based on average affinities of typical traditional drugs in optimized assays with purified receptors and data derived from a 21-mer phosphorothioate oligonucleotide in binding assays performed in 1M NaCl. Hybridization varies substantially as a function of ionic strength, and the affinities at 100 mM NaCl in the presence of Mg²⁺ for the 21-mer are significantly lower. Furthermore, affinities may be lower in physiological systems with RNA that has secondary structure, so these comparisons present the opportunity in its broadest dimensions.

A number of terms have been coined and often misused to describe various

Table 1 Affinity and selectivity of traditional and oligonucleotide drugs. Affinity constants were determined as described in text

Traditional drug	Oligonucleotide drug (1M NaCl)		
Affinity for receptor	10^8	Affinity for receptor sequence	10^{29}
Affinity for isotype	10^6 – 10^8	Affinity for one base mismatch	10^{26}
Maximum affinity for other proteins	10^6 – 10^8	Maximum affinity for nucleic acid binding proteins	10^{12} – 10^{13}
ΔK_d	1 – 10^2	Δk_D	10^4 – 10^{11}

components of the overall approach to using oligonucleotides as therapeutic agents. *Antisense* describes the interaction between oligonucleotides complementary to (sense) pre-mRNA¹ or mRNA molecules; these inhibit the oligonucleotides production of the protein product. The term has been broadened to describe any therapeutic oligonucleotide interaction with nucleic acids. *Triplex* denotes the interaction between oligonucleotides and double-stranded DNA that may result in inhibition of transcription. RNA structures display double-stranded regions, however, and thus the formation of triple-stranded structures in RNA is also possible. *Aptamers* describes the use of oligonucleotides to bind to nucleic acid binding proteins.

SCOPE AND OBJECTIVES OF THE REVIEW

This review focuses strictly on the use of oligonucleotides designed to interact with nucleic acids as therapeutics. The objectives are to place oligonucleotide therapeutics in the context of modern drug discovery and development and to summarize recent progress.

¹Abbreviations: BFGF, basic fibroblast growth factor; cAMP, cyclic AMP; CH₃-P, methylphosphonate oligonucleotides; EGF, epidermal growth factor; ELAM, endothelial cell adhesion molecule; G-CSF, granulocyte colony-stimulating factor; GM-CSF, granulocyte macrophage colony-stimulating factor; HB, hepatitis B; HIV, human immunodeficiency virus; HSV, herpes simplex virus; HTLV, human T-cell lymphotropic virus; ICAM, intracellular adhesion molecule; IGF, insulin-like growth factor; IL-1, interleukin 1; introns, intervening sequences; IV, influenza virus; mRNA, messenger ribonucleic acid; P, phosphodiester oligonucleotides; P-acridine, phosphodiester oligonucleotide conjugated with acridine moiety; PCNA, proliferating cell nuclear antigen; PLA₂, phospholipase A₂; P-lipid, phosphodiester oligonucleotide conjugated with lipid moiety; PMA, phorbol myristic acid; P-S, phosphorothioate oligonucleotides; Rev, regulation of virion protein expression; RSV, Rous sarcoma virus; TAR, Tat response element; TBE, tick-borne encephalitis; Tm, thermal transition point; VSV, vesicular stomatitis.

BASIC CONSIDERATIONS

Conceptually, oligonucleotide drug effects can be rationalized by traditional receptor theory and basic concepts concerning drug action. Within the broad context of pharmacological theory, however, a number of differences influence rational drug design and the potential utility of these agents.

Pharmacodynamics

RNA INTERMEDIARY METABOLISM Oligonucleotides are designed to modulate the information transfer from the gene to protein—in essence, to alter the intermediary metabolism of RNA. Figure 1 summarizes these processes.

RNA intermediary metabolism is initiated with transcription. The transcription initiation complex contains proteins that recognize specific DNA sequences and locally denature double-stranded DNA, thus allowing a member of the RNA polymerase family to transcribe one strand of the DNA (the antisense strand) into a sense pre-mRNA molecule. Usually during transcription, the 5' end of the pre-mRNA is capped by adding a methyl-guanosine and most often by methylation of one or two adjacent sugar residues. This enhances the stability of the pre-mRNA and may play a role in a number of key RNA processing events (2). Between the 5' cap and the site at which translation is initiated is usually a stretch of nucleotides; this area may play a key role in regulating mRNA half-life (3).

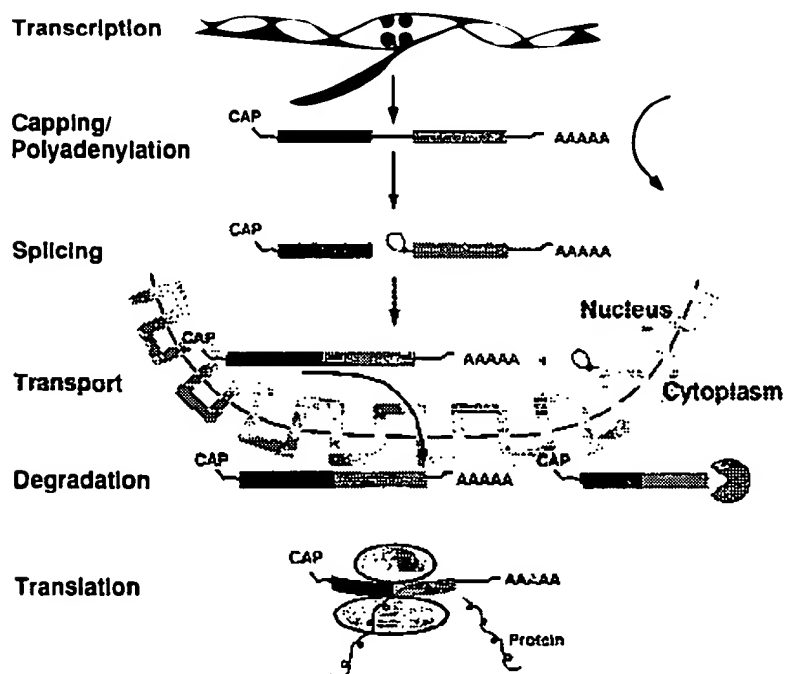


Figure 1 RNA processing.

Similarly, the 3' end of the pre-mRNA usually has a stretch of several hundred nucleotides beyond the translation termination signal. This area often plays an important role in determining mRNA half-life. Moreover, post transcriptionally, most pre-mRNA species are polyadenylated. Polyadenylation stabilizes the RNA, is important in transport of mature mRNA out of the nucleus, and may play important roles in the cytoplasm as well (4, 5).

Because eukaryotic genes usually contain intervening sequences (introns), most pre-mRNA species must have these sequences excised and the mature RNA spliced together. Splicing reactions are complex, highly regulated, and involve specific sequences, small molecular weight RNA species, and numerous proteins. Alternative splicing processes are often used to produce different mature mRNAs and, thus, different proteins. Even though introns are often considered waste, important sequences are conserved, and some introns may play a variety of regulatory roles.

Mature mRNA is exported to the cytoplasm and engages in translation. mRNA half-life varies from a few minutes to many hours and appears to be highly regulated (3).

Each step shown in the pathway is a composite of numerous steps, and each step is theoretically amenable to intervention with oligonucleotides. For virtually no mRNA is the pathway fully defined, however, and available information is insufficient to determine the rate-limiting steps in the intermediary metabolism of any mRNA species (6, 7).

AFFINITY The affinity of oligonucleotides for their receptor sequences results from hybridization interactions. The two major contributors to the free energy of binding are hydrogen bonding (usually Watson-Crick base pairing) and base stacking in the double helix that is formed. As mentioned, affinity is affected by ionic strength. Affinity results from hydrogen bonding between complementary base pairs; the reduction in entropy results from the stacking of the coplanar bases. Consequently, affinity increases as the length of the oligonucleotide receptor complex increases. Affinity also varies as a function of the sequence in the duplex. Nearest neighbor rules allow the prediction of the free energy of binding for DNA-DNA and RNA-RNA hybrids with relatively high precision (8, 9). Less information is available to develop predictions for DNA-RNA duplexes. A common misconception is that DNA-RNA duplexes are more stable than DNA-DNA duplexes. In fact, the relative stability of these duplexes varies as a function of the sequence. RNA-RNA duplexes are typically the most stable (S. M. Freier, unpublished results).

As with other drug-receptor interactions, activity requires a minimum level of affinity. For many targets and types of oligonucleotides, the minimum length of an oligonucleotide may be 12–14 nucleotides.

SPECIFICITY Specificity derives from the selectivity of Watson-Crick or other types of base pairing. The decrease in affinity associated with a mismatched base pair varies as a function of the specific mismatch, the position of the mismatch in a region of complementarity, and the sequence surrounding the mismatch. As an example, Table 2 compares the impact of various mismatches centered in two complementary 18-mers. The $\Delta\Delta G_{37}^0$ or change in Gibbs free energy of binding induced by a single mismatch varies from $+0.2$ to $+4.9$ kcal/mol per-modification at 100 mM NaCl. Thus, a single base mismatch results in a change in affinity of approximately 500-fold (10). Modifications of oligonucleotides may alter specificity. In fact, we have synthesized modified bases with substantially enhanced selectivity and others that display virtually no preferences for different bases.

Table 2 Effects of single-base mismatches on duplex stability. Absorbance vs temperature profiles were measured at 4 μ M each strand in 100 mM Na⁺, 10 mM phosphate, 0.1 mM, EDTA, pH 7.0.

X strand: 5'-d(CTC GTA CC _x TTC CCG TCC)-3'		fully phosphorothioate		
		X = dA, dC, dG, or T		
Y strand: 5'-(GGA CCG GAA yGG TAC GAG)-3'		fully RNA		
X	Y	T_m^1 (°C)	ΔT_m (°C)	ΔG_{37}^0 (kcal/mol)
dT	rA	53.6	—	-11.6
dT	rC	40.8	-12.8	-8.9
dT	rG	50.0	-3.6	-10.5
dT	rU	41.9	-11.7	-9.1
dG	rC	56.9	—	-13.1
dG	rA	42.3	-14.6	-8.9
dG	rG	45.0	-11.8	-9.3
dG	rU	45.7	-11.1	-9.8
dC	rG	59.0	—	-12.5
dC	rA	43.3	-15.7	-9.3
dC	rC	39.5	-19.4	-8.7
dC	rU	40.0	-19.0	-8.7
dA	rU	52.7	—	-11.4
dA	rA	42.7	-10.0	-9.3
dA	rC	42.7	-10.0	-9.1
dA	rG	44.5	-8.1	-9.3

¹ T_m s and free energies of duplex formation were obtained from fits of the absorbance vs. temperature data to a two-state model with linear sloping baselines. Reported parameters are averages of at least three experiments.

Based on the differences in affinity of oligonucleotides for their complementary target sequence, calculations suggest that unmodified oligodeoxy-nucleotides between 11–15 in length should be able to bind selectively to a single RNA species in the cell (11). Studies in our laboratories have demonstrated that affinities predicted by nearest neighbor analyses are highly useful in rational drug design (10). For example, by using strategies based on nearest neighbor predictions, oligonucleotides can be designed that selectively inhibit the production of mutant RAS containing a single base change in the mRNA vs. normal RAS in cells in tissue culture (B. P. Monia et al, manuscript submitted).

NUCLEIC ACID SELECTIVITY The 2'-hydroxyl in RNA results in the sugar assuming a different conformation from that in DNA. RNA-RNA duplexes assume an A-form double helix whereas DNA-DNA duplexes assume a B-form double helix. Consequently, oligonucleotides can be modified to bind more tightly to RNA or DNA sequences. For example, Table 2 shows the effect of 2'-modifications at every position of a 15-mer on T_m and ΔG_{37}^0 for DNA and RNA targets and demonstrates that 2'-O-methyl substitutions increase T_m for RNA by 1.4° per modification compared to DNA (12).

RNA STRUCTURE RNA can assume a variety of secondary structures deriving from intramolecular base pairing. The simplest structures are stem-loops in which double-stranded regions are interspersed with loops and random coils. More complex structures described as *pseudoknots* also form (13). These structures are profoundly important in determining RNA function and influencing the ability of oligonucleotides to bind to their RNA targets. The types of effects of bound oligonucleotides on RNA function are affected by RNA structures as well.

Pharmacokinetics

As with any other class of drugs, oligonucleotide drugs must attain a sufficient concentration at their receptor for a sufficient period to display activity. Inasmuch as most of the targets for oligonucleotides are intracellular, oligonucleotides must be relatively stable in and outside the cell and must be able to traverse the cellular membrane.

NUCLEASE STABILITY Oligonucleotides may be degraded by nucleases. Nucleases that degrade DNA or RNA from either the 5' or 3' terminus are known as *exonucleases*; those that cleave internally are *endonucleases*. Numerous nucleases exist and have been shown to degrade oligonucleotides. Although in serum the dominant nuclease activity is 3' exonuclease, in cells and other bodily fluids 3' and 5' exonucleases and endonucleases are present.

In serum, phosphodiester oligodeoxynucleotides are rapidly degraded. The rate of degradation varies as function of the sequence and length of the oligonucleotide and the type of serum (14–16). Typically, half-lives of phosphodiester oligodeoxynucleotides range from 15 to 60 min in most sera. Heat inactivation of serum reduces the rate of degradation of oligonucleotides. Oligoribonucleotides are significantly less stable than oligodeoxynucleotides.

Work from many laboratories has demonstrated that a wide range of modifications may be used to enhance the stability of oligonucleotides. Phosphate modifications have been shown to result in marked increases in stability (see Table 3). Phosphorothioate oligonucleotides have been shown to be extremely stable in media, cells and cell extracts, serum, various tissues, urine and stable to most nucleases (16–20). The half-life of phosphorothioate oligonucleotides is greater than 24 hr in nearly all environments tested. Furthermore, phosphorothioates have been shown to be stable to various restriction endonucleases when in duplexes. In general, one of the diastereomers is cleaved slowly and the other is entirely resistant (21–24).

The non-ionic methylphosphonate analogs have also been shown to be extremely stable to nucleases (25–31). Again, these oligonucleotides are diastereomeric at each modified phosphate, and the R isomer is slightly more sensitive than the S isomer to degradation by nucleases (16, 32).

Table 3 Effects of 2' modifications on hybridization and stability. Duplex hybridization was evaluated from absorbance vs. temperature profiles at 260 nm in 100 mM Na⁺, 10 mM phosphate, 0.1 mM EDTA, pH 7.0 at 8 μ M strand concentration.

Modification ¹	Positions	Hybridization		Serum stability
		T_m ² vs DNA (°C)	T_m vs RNA (°C)	
Phosphodiester	All	50.5	39.0	1 h
Phosphorothioate	All	43.2		>24 h
2'-O-nonyl dA	12 13 14		41.3	60 h
2'-O-allyl	12 13 14	50.3	40.8	10 h
2'-O-benzyl	12 13 14	45.5	37.8	18 h
2'-O-aminopropyl	12 13 14	53.7	42.0	
2'-fluoro P + S	2'F in 12 13 14 P = S in all	47.2	36.5	1 h >>24 h

¹15 mer: CGA CTA TGC AAA AAC

² T_m is the temperature at which half the strands are in the duplex state and half are in the coil state. T_m was obtained from a nonlinear least squares fit of the experimental data to a modified two-state model with linear sloping baselines (224)

Other classes of modifications that have been reported to result in substantial nuclease stability include the phosphoramidates (19, 33) and isopropyl phosphate triesters (34, 35). Interestingly, ethylphosphate triesters were shown to be cleaved after being deethylated in cells (27, 36). Oligonucleotides containing α -anomers in the sugar moiety are substantially more stable in serum and cells than natural phosphodiesters (14-15, 37-41).

Modifications at the 2'-position of the sugar have also been shown to enhance nuclease stability (42). 2'-O-methyl-oligonucleotides were shown to be significantly more resistant than unmodified oligonucleotides, and 2'-O-allyl modified oligonucleotides were even more stable (43). In studies in our laboratory, a large number of 2'-modifications have been characterized. 2'-O-methyl analogs were highly resistant to nucleases in serum and cells. Modifications as bulky as nonyl groups were shown to have only a minor negative effect on hybridization and to impart high levels of nuclease stability. In contrast, 2'-fluoro derivatives were nearly as sensitive to nucleases as unmodified oligoribonucleotides (12, 44). Table 3 provides a comparison of affinities to RNA and stabilities in serum for several 2' modified oligonucleotides (45). Although numerous other modifications have been studied, either insufficient data concerning hybridization properties or nuclease stabilities have been reported to support conclusions or their hybridization properties were unattractive. For example, open ring sugar analogs of adenosine were reported to be nuclease stable (46). Acyclic pentofuranosyl modified oligonucleotides were reported to be nuclease resistant, but the T_m for these oligonucleotides was reduced 9-15 degrees per modification (47). Other acyclic sugars have been reported but, again, the hybridization properties were poor (48). Carbocyclic modified oligothymidylates were reported to be nuclease resistant and to hybridize to oligodeoxyadenosine with higher affinity than natural oligodeoxy-thymidylate (49, 50), but studies on mixed sequences have not been reported.

A wide variety of phosphate replacements have also been studied. In earlier work, the phosphodiester was replaced with esters, amides, and various polymeric materials, but these modifications were not designed to be used as antisense oligonucleotides and, therefore, are largely unattractive (12, 16). More recently, formacetal replacement of the phosphate has been reported by two groups to result in oligonucleotides with acceptable hybridization properties and nuclease resistance (51-53).

Other modifications for which little information is available include sulfonamide replacement of phosphate (54), diphosphonate dinucleotides (55), acetamide linkages (56, 57), and phosphonyl methyl linkages (58). These and other modifications are discussed in detail in two recent reviews (12, 16). In our laboratories, a number of other novel backbone modifications have been synthesized. Given the number of novel synthetic approaches and molecules

and the number of laboratories now involved, a substantial increase in the repertoire of backbone-modified oligonucleotides with desirable properties is likely in the near future.

In addition to uniform modifications, a number of pendant groups at the 5' and/or 3' termini and more recently in internal positions of oligonucleotides have been reported to enhance nuclease stability. Modifications include intercalating agents (59–62) and poly-L-lysine (63, 64) at the 5' or 3' terminus and a number of modifications such as amino-alkoxy (65), anthraquinone (66), and alkyl groups (45). Moreover, heterocycle modifications, including pendant groups from the N2 site of guanine (67, 68), pendant groups from 3-deazaguanine (69), and 5- and 6-position modifications of deoxycytidine and thymidine (70), have shown increased stability to nucleases of varying levels.

In conclusion, numerous medicinal chemical strategies can be employed to create oligonucleotides with varying degrees of nuclease stability. The choice of the modification(s) employed is dictated by the level of stability desired and other desired properties of the oligonucleotides. It is now possible to design oligonucleotides that display excellent hybridization characteristics and half-lives, that range from minutes to several days when oligonucleotides are incubated with nucleases, serum, cells, or cell extracts.

INTRACELLULAR STABILITY Although considerable confusion and controversy exist with regard to the stability of oligonucleotides in cells in tissue culture and the ability to predict intracellular stability of oligonucleotides based on stability in sera, a consensus opinion is emerging. The nuclease activity of sera derived from different species varies. Fetal calf serum is more active than mouse serum, and human serum appears to have the least nuclease activity (G. D. Hoke, unpublished observations). All sera display substantial nuclease activity, however, and there are significant lot-to-lot variations. In all sera tested, 3' exonucleases constitute the primary nuclease activity (12, 16, 71). In a number of publications, fetal calf serum used in tissue culture experiments has been heated to inactivate nucleases. Again, however, conditions were not standardized, and in some lots of sera, heating to 65°C for 30 min does not inactivate all nucleases (16).

Another factor that has contributed to confusion is that a variety of labeling methods and analytical techniques have been employed. Studies have employed 3'³²P and 5'³²P labeled oligonucleotides, 5'³⁵S labeled oligonucleotides, and oligonucleotides labeled with fluorescent pendant groups at the 5' terminus (14–16, 72). Relatively few studies have used uniformly labeled oligonucleotides. Furthermore, relatively few studies have rigorously separated intact oligonucleotides from degradation products, and even fewer have performed careful kinetic studies.

Studies in our laboratory have employed either phosphodiester oligonucleotides uniformly labeled with ^{32}P or phosphorothioate oligonucleotides uniformly labeled with ^{35}S . The kinetics of degradation have been studied with several cell lines *in vitro* and cytoplasmic and nuclear extracts derived from HeLa cells. In contrast to a number of studies, in all cells studied to date, phosphodiester oligonucleotides were degraded within 15–30 min of incubation (71, 73). In contrast, phosphorothioate oligonucleotides of 15, 21, and 30 nucleotides in length and various sequences were stable for at least 24 hr when incubated with various cells. In studies in HeLa cells in which ISIS 1082, a 21-mer phosphorothioate, was incubated with the cells, then extracted from cells at various time points and analyzed on polyacrylamide gels, the compound was intact for four days (73).

Methylphosphonate oligonucleotides have also been shown to be stable in a variety of cell lines and extracts (14). No other class of oligonucleotides, however, has been sufficiently studied to allow definitive conclusions.

CELLULAR UPTAKE AND DISTRIBUTION Antisense oligonucleotides typically are 15–30 nucleotides long and thus have molecular weights that range from 4500–9000 daltons. The charge carried by phosphodiesters is, of course, negative and they are highly water soluble. The charge and hydrophilicity of modified oligonucleotides vary depending on the modifications. Consequently, membrane transport and cellular distribution are likely to vary widely as a function of the modifications introduced into oligonucleotides. For the two classes of modified oligonucleotides for which significant data have been reported—methylphosphonates and phosphorothioates—this is clearly the case. For both classes of oligonucleotides, the evidence is compelling that they do enter many cells at pharmacologically relevant concentrations.

Methylphosphonates are uncharged and lipophilic. Although thought to be taken up by most cells in tissue culture via passive diffusion, detailed studies of the kinetics of cellular uptake, distribution, and metabolism of uniformly labeled methylphosphonates have not been reported. Studies in Syrian hamster fibroblasts on oligonucleotides 3–9 nucleotides in length showed linear cell association for 1 hr, then reduced uptake. At equilibrium, the intracellular concentration of oligonucleotide was reported to be equivalent to the extracellular concentration (27, 74). In another study, a 21-mer methylphosphonate labeled with ^{32}P at the 5' terminus was reported to be taken up by CV-1 cells. Cell association was linear for 2 hr. Unfortunately, however, studies proving that the cell-associated radioactivity represented intact oligonucleotide were not presented. Nor were detailed studies on characteristics of uptake or intracellular distribution presented (75).

Phosphorothioates are negatively charged, but because of the sulfur atoms

they may be slightly more lipophilic than phosphodiesters and tend to bind nonspecifically to serum proteins. Studies in our laboratories have shown that phosphorothioate oligonucleotides bind to serum albumin and that in the presence of serum albumin, cell-association is reduced (73; G. D. Hoke et al, unpublished observations).

Studies employing a 28-mer phosphorothioate deoxycytidine that was uniformly labeled with ^{35}S demonstrated that when HeLa cells were incubated with 1 μM of the drug, significant intracellular concentrations were achieved. Cellular uptake was linear, reaching a plateau of 60 p mole/10⁶ cells in 6 hr. Adsorption to the cell membrane was minimal. Uptake was also concentration-dependent, reaching a plateau at approximately 1 μM . The drug associated with HeLa cells was intact for 24 hr and was located in both nuclei and cytoplasm. Infection with herpes simplex virus type 2, but not type 1, increased cellular uptake (76).

Studies in our laboratories have confirmed and extended the observations on phosphorothioate oligonucleotides. The cellular uptake, distribution, and metabolism of ISIS 1082, a uniformly ^{35}S labeled 21-mer phosphorothioate with a mixed antisense sequence, have been characterized in HeLa cells and HeLa S₃ cells, a variant line conditioned to growth in suspension. Incubation of HeLa cells with 5 μM of the drug resulted in approximately 8% of input radioactivity being associated with the cells. Cell association was linear for approximately 8 hr, and approximately 20% of the cell-associated radioactivity appeared to be adsorbed to the membrane. Uptake was temperature-dependent, required viable cells, and was inhibited by metabolic poisons. Uptake was concentration-dependent, and was linear to 10 μM . Uptake was influenced slightly by calcium and magnesium and was saturable. Natural oligonucleotides and methylphosphonates did not compete for uptake while other phosphorothioates competed; however, different length and sequence phosphorothioates competed differently (73, 77).

We have also studied other phosphorothioates of various lengths and other cell lines. HL 60 cells appear to take up less phosphorothioate oligonucleotides than HeLa cells and HeLa S₃ cells take up very little drug (73). Although not directly compared, human umbilical vein endothelial cells also appear to take up less drug than HeLa cells. Thus, there is considerable variation in the extent of uptake as a function of cell type.

In all cells studied, and with all uniformly labeled phosphorothioate oligonucleotides of varying size and sequences, we have shown that these drugs are stable in cells and cytoplasmic and nuclear extracts. In HeLa cells, no degradation of intracellular ISIS 1082 was observed for four days (73). Preliminary studies confirmed that these oligonucleotides distributed to both cytoplasm and nuclei and showed that there is an active temperature-dependent efflux process as well (77, 78).

When incubated with cells in the absence of serum or heat-inactivated serum, several laboratories have reported the apparent uptake of phosphodiester deoxyoligonucleotides. Moreover, a number of laboratories have reported activities for phosphodiester oligonucleotides that apparently were due to cellular uptake and intracellular activities. The studies on cellular uptake are not fully convincing, however Loke et al (79) studied deoxythymidine oligonucleotides ranging from 3–20 nucleotides in length and labeled with acridine at the 3' terminus. They incubated HL60 and three other hematopoietic cell lines with 12.5 μ M of the acridine labeled drug and used flow-cytometric analyses of acridine fluorescence to quantitate cellular uptake. Uptake was reported to decrease as the length of the oligonucleotide increased and to vary as a function of the cell type. Uptake achieved a plateau in HL60 cells in 50 hr and was inhibited by polynucleotides of any length. The authors concluded that the oligonucleotides were taken up by an endocytotic mechanism. Unfortunately, the stability of the oligonucleotide-acridine conjugate was not rigorously documented. Nor were possible effects of acridine in the uptake of the oligonucleotide rigorously explored. Additionally, possible quenching or enhancement of the fluorescence of acridine by cellular interactions was not explored. Finally, extrapolations from homopolymers to mixed sequences have not been proven to be valid.

Another study employing phosphodiester oligonucleotides reached similar conclusions (80). Again, for most of the experiments, oligodeoxythymidines of 8 to 16 nucleotides in length were incubated with L929 mouse fibroblasts in the absence of serum. Maximal uptake occurred within 2 hr and upon incubation with fresh medium, cell-associated 32 P was released. Substantial degradation of the 5' labeled oligonucleotide was observed within 2 hr, and the authors concluded that approximately 20% of the radioactivity was in nuclei. Again, the authors concluded that the most likely mechanism of uptake was endocytosis (80).

Other pendant modifications of phosphodiester oligonucleotides have also been studied. A 9-mer labeled with acridine at the 3' terminus was reported to be taken up by *Trypanosome brucei* (61). More recently, the same group has reported that a 9-mer coupled at the 3' terminus to acridine via a dodecanal linker was more active in cells expressing mutated RAS than a 9-mer with a 3' acridine only (81). 3' poly-L-lysine-oligonucleotides have been reported to be stable to serum nucleases and to have enhanced activity as compared to phosphodiesters. Uptake was not studied, however, (63, 82, 83). In a later publication, the uptake of a poly-L-lysine oligonucleotide conjugate was enhanced compared to the unmodified oligonucleotide (84). When used to treat cells other than L929 cells, however, poly-L-lysine conjugates were inactive (64).

A number of lipid conjugates have also been studied. 5' linked triethylam-

monium 1,2 di-O-hexadecyl-rac-glycerol-3-H-phosphonate oligonucleotides were taken up 8–10-fold more than unmodified oligonucleotides by L929 cells and were more active against varicella zoster viral infections, albeit at high concentrations (85). An oligonucleotide linked at the 5' terminus to an undecyl residue was reported to be active, but no uptake or stability studies were reported (86).

The intracellular fate of oligonucleotides injected into oocytes and the uptake of oligonucleotides into oocytes have also been studied. When injected into *Xenopus* oocytes, unmodified oligonucleotides were degraded within 1 min primarily by 3' exonuclease digestion, but other nucleolytic activities were also present (87, 88). Interestingly, in this system, even phosphorothioate oligonucleotides were reported to be degraded, albeit much more slowly than phosphodiesters (89). These observations were extended in studies on oligodeoxynucleotides injected into CV-1 endothelial cells. A 28-mer oligonucleotide of either phosphodiester, phosphorothioate, or methylphosphonate type was injected into the cytoplasm of these cells. All three types of oligonucleotides localized to the nucleus in a temperature- but not energy-dependent fashion. The methylphosphonate oligonucleotide concentrated in regions of genomic DNA, in contrast to the two other oligonucleotides that co-localized with small nuclear ribonucleoproteins (90). Uptake of unmodified oligonucleotides by pre-implantation embryos was reported to be virtually nil (91).

Liposomes and related formulations have been shown to enhance cellular uptake of oligonucleotides in vitro. Loke et al (92) compared the uptake of phosphodiester and phosphorothioate deoxythymidine heptamers into HL-60 cells by using oligonucleotides coupled to 2-methoxy-6-chloro 9-(5-hydroxypentyl) amino acridine and monitoring with flow cytometry. They did not determine the integrity of the oligonucleotides, but reached the conclusion that phosphodiester dT₇ was taken up by HL-60 cells much more effectively than phosphorothioate d-T₇, and that uptake plateaued at 50 hr. They reported increased anti-c-myc activity of phosphorothioate oligonucleotides after loading them in phosphatidyl serine liposomes. The uptake of a tetramer 2'-5' deoxyadenylate into L1210 cells was reported to be increased by loading the oligo-adenylate into *Staphylococcus aureus* protein A-crosslinked phospholipid vesicles (93). In our laboratories, we have shown that lipofectin, a cationic lipid mixture, can significantly increase the uptake and activity of phosphorothioate oligonucleotides in several cell lines. It also alters the intracellular distribution of these nucleotides (78).

With the exception of methylphosphonates, the conclusion from studies that have addressed the mechanisms of uptake of oligonucleotides is that the most likely mechanism is receptor-mediated endocytosis. In fact, in one study an 80-kd protein that appeared to bind oligonucleotides was partially purified

and postulated to be a "receptor" (79). The evidence supporting this mechanism is limited, however, and data are insufficient to conclude that receptor-mediated endocytosis is the most common or only mechanism of uptake of charged oligonucleotides in most cells.

In conclusion, although many questions remain to be answered, it appears that many cells in tissue culture may take up oligonucleotides at pharmacologically relevant concentrations. Clearly, oligonucleotides of different types behave differently and there are substantial variations as a function of cell type. Moreover, length and specific sequences may alter uptake, and pendant modifications may profoundly influence cellular uptake.

Once in the cell, it would seem that oligonucleotides distribute to the cytoplasm and the nuclei. In most if not all cells, phosphodiester oligonucleotides are rapidly degraded whereas methylphosphonates and phosphorothioates are much more stable. Again, pendant modifications may alter the rate of intracellular degradation and distribution.

Mechanisms of uptake and distribution are poorly understood. Clearly, however, multiple mechanisms may play a role, and different types of oligonucleotides may behave very differently.

Novel formulations may enhance cellular uptake. Liposomes and cationic lipids significantly enhance uptake and may alter the mechanisms of uptake and intracellular fate of oligonucleotides.

IN VIVO PHARMACOKINETICS Preliminary *in vivo* pharmacokinetic data are now available on methylphosphonate and phosphorothioate oligonucleotides. A 12-mer ^3H -labeled methylphosphonate injected in the tail vein of mice was rapidly cleared as intact oligonucleotide and distributed broadly to all tissues except the brain (94).

More extensive studies have been performed on ^{35}S -labeled phosphorothioates in rats. A true distribution phase of 15–25 min was observed after a single IV dose of a 27-mer followed by a prolonged elimination phase of 20–40 hr (94). The prolonged elimination phase may result from the binding of phosphorothioates to serum proteins. Phosphorothioates distributed broadly to all tissues except the brain and were eliminated in the urine intact. Phosphorothioates were rapidly and extensively absorbed after IM and IP administration (94).

Repeated daily doses of 50 mg/kg of a 27-mer phosphorothioate to mice resulted in similar distribution and elimination kinetics but slight differences in tissue concentrations from single dose studies. Liver, kidney, spleen, and lung were the organs with highest concentrations. Again, the drug was excreted intact in the urine (94).

Continuous osmotic pump administration of the same compound subcutaneously for 4 wk at doses of 50–150 mg resulted in similar pharmacokinetics (94).

Studies with ISIS 1082, a 21-mer phosphorothioate, in mice showed that when applied to the cornea in a sodium acetate buffer, significant adsorption to the cornea and absorption into the aqueous and vitreous humors occurred. Moreover, significant systemic bioavailability was observed (78). In rabbit, as much as 25% of an applied ocular dose was systemically bioavailable (unpublished observations). Post absorption pharmacokinetics were equivalent to IV pharmacokinetics.

Recently, a 20-mer phosphodiester was administered intravenously to rabbits. Clearance from blood was rapid and, after 90 min, 16% of the dose was found in the urine and was intact. In blood, at least 17% of the drug was estimated to be completely degraded within 5 min (95).

Toxicology

IN VITRO

Phosphodiesters Very little information has been published on the in vitro toxicities of unmodified oligonucleotides. In most systems, the oligonucleotides are thought to be rapidly degraded. When a 15-mer complementary to a c-myc sequence was incubated with human lymphocytes at 30 μ M for 4 hr, no toxicity was observed. Longer incubation (24 hr) in 10% serum resulted in reduced 3 H-thymidine incorporation, but the authors concluded that this was probably due to dilution of the thymidine pool by thymidine liberated after rapid degradation of the oligonucleotide (96).

The incubation of a transformed leukemic cell line with 50 μ M of a 20-mer complementary to a sequence in the BCL-1 proto-oncogene was reported to result in no decrease in viability as judged by trypan blue exclusion (97).

Methylphosphonates Incubation of Vero cells with 30 μ M and lower concentrations of an 8-mer methylphosphonate for 24 hr resulted in no decrease in growth rate or cell count; however, 48 hr incubation resulted in 40% inhibition of growth rate (98). Similarly, neither of three 9-mers had any effect on L929 cell plating efficiency or protein synthesis after 16 or 40 hr incubations with 150 μ M of drug (99). Incubation of T15 cells with 80 μ M of a 9-mer directed against N-ras for 48 hr produced no effect on protein synthesis or viability (100). Similar results were reported for HT29 cells.

Inasmuch as methylphosphonate oligonucleotides have, when they have displayed activity, effective concentrations of 50–100 μ M, the therapeutic index in vitro may be rather modest. Much more detailed studies are required before reaching final conclusions, however.

Phosphorothioates Phosphorothioate oligonucleotides bind to a variety of proteins, including serum albumin. In cell free protein translation experiments, they have been shown to induce nonspecific inhibition of protein synthesis (11, 101, 102). In wheat germ and rabbit reticulocyte lysate assays,

concentrations as high as 100 nM of a 17-mer phosphorothioate targeted to the protein mRNA inhibited globin synthesis relatively specifically. At 10 μ M, nonspecific effects were observed (103). The nonspecific effects of phosphorothioates in these assays are length-dependent, as a 5-mer was much less potent than the 14-mers and dC28 appeared to be the most potent phosphorothioate oligonucleotide tested. In studies in our laboratories, we have made similar observations with a number of phosphorothioate oligonucleotides (G. D. Hoke et al, unpublished observations).

Phosphorothioate oligonucleotides have also been shown to inhibit DNA polymerases, reverse transcriptases, and nucleases when incubated in cell free systems (76, 77, 104).

Despite the potential nonspecific interactions of phosphorothioate oligonucleotides with cellular proteins, a wide variety of compounds have been shown to have excellent therapeutic indices. Microinjection of nanomolar concentrations of a 17-mer into *Xenopus* oocytes inhibited β -globin synthesis. When 16 μ M of the compound were injected, however, protein synthesis was aborted and the oocytes underwent extensive cytolysis (89).

Incubation of cells in vitro with phosphorothioate oligonucleotides has likewise resulted in toxicities only at concentrations much higher than those at which therapeutic activities were observed. Human mononuclear cells were unaffected after 20 hr of incubation with 25 μ M of several 15-mers (105). T697 cells were unaffected by a three-day exposure to 25 μ M of a 20-mer (97, 106).

In our laboratories, we have determined the effects of ISIS 1082, a 21-mer phosphorothioate that inhibits herpes simplex virus types 1 and 2 infections in HeLa cells at 200-400 nM, on HeLa cell viability, DNA synthesis, RNA synthesis, protein synthesis, and energy metabolism. At no concentration below 500 μ M were statistically significant effects observed after incubation for 96 hr. Exposure of HeLa cells to 500 μ M ISIS for 48 hr resulted in 20% inhibition of protein synthesis (77). Similar results were observed in other cell lines.

Table 4 presents results from studies on 20 phosphodiester or phosphorothioate oligonucleotides targeted to various regions in the 5-lipoxygenase gene. Again, most of the phosphorothioates displayed toxicities only at 50 μ M and greater. The exceptions to this rule were three 30-mers that inhibited cell growth at 10-35 μ M. Clearly, one can conclude from this study that toxicity was time- and concentration-dependent and that, with longer exposures in particular, phosphorothioates were more toxic than their phosphodiester analogs (73).

We have identified other factors that influence the toxicity of phosphorothioates. Cell type may alter toxicity significantly. A comparison of the toxic effects of a 15-mer phosphorothioate on HL60 cells, U937 cells, and RBL-1

Table 4 In vitro toxicities of 5.

Compound	Oligonucleotide Class ^b	Length	Sequence	AT:GC	24 hr	48 hr	72 hr	96 hr
1787	PD	15	5'GTTGCCACCGAG-3'	1:2	21.5	18.5	16.0	14.4
1788	PS	15	AATGGTGAATCTCAC	>100	35.0	25.0	19.0	
1789	PD	30	GTGTGCCACAGCAG	>100	>100	>100	>100	
1790	PS	30		>100	>100	15.0	11.8	
1795	PD	15	TGCCAGTGATTCAATG	1:0.88	63.0	39.5	34.0	26.0
1796	PS	15	GGTCTTCCGCCAGT	>100	>100	50.0	35.0	
1797	PD	30	GATTCAATGACCCGCT	1:1.31	>100	20.0	50.0	74.0
1789	PS	30				10.0	10.0	
1799	PD	15	GTCCTGATGGCTTC	1:1.5	28.0	25.0	22.0	22.0
1800	PS	15	GTCCTGATGGCTTC	>50.0	50.0	50.0	50.0	34.0
1801	PD	30	CACACCAGGAGCCCCG	1:2.0	>50.0	>50.0	>50.0	>50.0
1802	PS	30			27.0	21.0	21.0	3.9
1812	PD	15	GTTGCTGCTGGTGT	1:1.14	29.0	17.0	16.0	18.0
1813	PS	15	ATTGCTGTTGCTGC	>50.0	32.0	25.0	43.0	
1814	PD	30	TRGGTGTGGAAATGC	>50.0	32.0	25.0	43.0	
1815	PS	30			9.0	10.0	10.0	11.0
1816	PD	15	AGGTGTCCGCATCTA	1:1.14	>50.0	>50.0	>50.0	>50.0
1817	PS	15			32.0	>50.0	>50.0	>50.0
1818	PD	30	TCGGCGGGGTCC	1:2.33	>50.0	>50.0	>50.0	>50.0
1819	PS	30	AGGTGTCCGCATCTA		15.0	19.0	19.0	20.0

^aHL 60 cells were incubated in 96 well plates with increasing concentrations of oligonucleotides (1–50 or 100 μ M) in the presence of 10% fetal bovine serum. Viability of the cells was determined at each time point by trypan blue exclusion. IC₅₀ values were obtained by plotting percentage control cell number vs. drug concentration.

^bPD = Phosphodiester; PS = Phosphorothioate.

cells showed considerable variation in sensitivity; HL60 cells were the most sensitive. As phosphorothioates bind to serum albumin, in the presence of 10% fetal calf serum, a 15-mer produced no cytotoxicity after 24 hr of incubation at 100 μ M. In the presence of 2.5% fetal calf serum, the IC₅₀ was 19 μ M. Finally, the purity of the oligonucleotide has a significant effect. Purification of oligonucleotides in triethyl ammonium buffers with trityl-on HPLC followed by removal of the trityl groups in triethyl ammonium may result in substantial contamination with triethyl ammonium ions, which are toxic to cells (73). Others have alluded to batch-to-batch variations and the potential that contaminants might contribute to toxicities, but they have not identified potential toxins (60, 97, 106-108).

Pendant group modified oligonucleotides Limited information is available concerning the effects of pendant groups on the toxicities of oligonucleotides. An acridine conjugated 7-mer phosphodiester was reported to produce no toxicities at 100 μ M even though the free acridine had an IC₅₀ for cell viability of 2 μ M (109). Two 11-mer phosphodiesters that were covalently attached to an undecyl group at the 5' terminus had no apparent toxic effect on MDCK cells at 100 μ M (86). 5' terminal phospholipid conjugates of both phosphodiester and phosphorothioate oligonucleotides produced little toxicity in L292 cells when incubated at 50 to 100 μ M (85). In contrast, a phosphodiester 15 mer linked to poly-L-lysine was toxic to L929 cells at 1 μ M (84).

Table 5 summarizes published data concerning the in vitro toxicology.

IN VIVO Although only preliminary toxicologic data are available, considerably more information should soon be available, as several compounds are currently in preclinical development.

Single-dose toxicity studies in mice were reported for phosphodiester (19), methylphosphonate (110), phosphomorpholidate, and phosphorothioate oligonucleotides. Unmodified oligonucleotides resulted in deaths in two of four treated mice at 160 mg/kg and all four mice treated with 640 mg/kg IV. Within three days after injection, a phosphorothioate oligonucleotide resulted in equivalent toxicities to the phosphodiester. The other analogs produced similar toxicologic effects with slight differences in doses.

Single doses of as much as 3.5 mg of a 27-mer complementary to the REV gene of HIV given IV or IP produce no toxicities in rats. Daily injections of 50 mg/kg IV of the same compound for 12 days in mice resulted in no observable toxicities. This 27-mer was also administered via a subcutaneous osmotic pump designed to administer up to 150 mg at a constant rate for 4 wk to rats. Again, no toxicities in any organ were observed (94).

ISIS 1082, a 21-mer phosphorothioate targeted to inhibit herpes virus types 1 and 2, has been administered topically to mouse and rabbit eyes for as much

as 21 days and resulted in no ocular toxicities. In rabbits, other organs were examined, and no effects were observed. Given the extensive bioavailability of ISIS 1082 in rabbits after ocular administration, this constitutes a significant observation.

Single doses of ISIS 2105, a 20-mer phosphorothioate active against human papilloma viruses, were administered intradermally and resulted in no local or systemic toxicities.

Consequently, a growing body of data supports the contention that at least single doses of phosphorothioate oligonucleotides may be given to mice, rats, and rabbits without significant acute or subacute toxicities.

MUTAGENICITY Virtually no data have been published on the potential mutagenicity of oligonucleotides. A 27-mer phosphorothioate was reported to be negative in an Ames assay in the presence or absence of a liver metabolic activation system at doses as high as 5 mg/plate (101).

P. Iverson (personal communication; 101) compared a number of oligonucleotide types and related chemicals in hamster lung fibroblasts. Unfortunately, although this study has been cited, the primary data have never been published, and thus it is difficult to draw any conclusion.

Mechanisms of Action of Oligonucleotides Interacting with Nucleic Acid Targets

The mechanisms by which interactions of oligonucleotides with nucleic acids may induce biological effects are complex and potentially numerous. Furthermore, very little is currently understood about the roles of various mechanisms or the factors that may determine which mechanisms are involved after oligonucleotides bind to their receptor sequences. Consequently, a discussion of mechanisms remains largely theoretical. Although a number of potential schemes to classify mechanisms of action might be employed, I prefer a scheme based on drug-receptor concepts.

OCCUPANCY-ONLY MEDIATED MECHANISMS Classic competitive antagonists are thought to alter biological activities because they bind to receptors, thereby preventing natural agonists from binding and inducing normal biological processes. Binding of oligonucleotides to specific sequences may inhibit the interaction of the RNA or DNA with proteins, other nucleic acids, or other factors required for essential steps in the intermediary metabolism of the RNA or its utilization by the cell.

Transcriptional arrest Oligonucleotides may bind to DNA and prevent either initiation or elongation of transcription by preventing effective binding of factors required for transcription, thus producing transcriptional arrest.

Table 5 In Vitro toxicology of antisense oligonucleotides

Oligonucleotide class	Length	Concentration	Target	Cell type	Time	Toxicity assessment	References
Phosphodiester	15	30 μ M	c-myc	Human T cells	4 hours	Nontoxic	99
Phosphodiester	20	150 μ M	β CL2	697 cells	3 days	Nontoxic	100
Phosphorothioate	20	25 μ M	β CL2	697 cells	3 days	Nontoxic	
Phosphodiester	23	1-30 ng	Vg 1	Xenopus oocytes	2 days	Nontoxic @ low concentrations, i.e. <5 ng	92
Phosphorothioate	23	1-30 ng	Vgl	Xenopus oocytes	2 days	Toxic @ 15-30 ng	
Phosphodiester-acridine conjugate	7	50-100 μ M	Type A influenza	MDCK	3 days	Nontoxic	
Acridine alone		2 μ M		MDCK	3 days	Toxic	
Methylphosphonate	9	150 μ M	VSV	L929	16-40 hours	Nontoxic	102
Methylphosphonate	9	80 μ M	N-ras	T15	4.8 hours	Nontoxic	103
Methylphosphonate	9	80 μ M	N-ras	HT29	48 hours	Nontoxic	
Phosphodiester	14	1-25 μ M	HIV	ATH8	7 days	Minor toxicity @ all conc. (<35%)	20
Methylphosphonate	14	1-25 μ M			7 days	Minor toxicity @ all conc. (<27%)	

Phosphorothioate (heteropolymer)	14	1-25 μ M			7 days	Nontoxic
Phosphorothioate (homopolymer)	14-28	1-25 μ M			7 days	Nontoxic
Phosphorothioate (homooligomer)	28	3-50 μ M	HSV-2	HeLa S ₃	72 hours	Nontoxic
Phosphorothioate (antisense)	20	4-100 μ g/ml	HIV	H9, MOLT3	96 hours	Nontoxic
Phosphorothioate (nonsense)	20	4-100 μ g/ml		H9, MOLT3	96 hours	Nontoxic (4 μ g/ml)
						Toxic (20 μ g-5% 100 μ g-67%)
Phosphodiester homooligomer (dT)	15	4-100 μ g/ml		H9, MOLT3	96 hours	Toxic
Phosphodiester homooligomer (dA)	15	4-100 μ g/ml		H9, MOLT3	96 hours	Minor toxicity
Phosphornorpholidate homooligomer (dT)	15	4-100 μ g/ml		H9, MOLT3	96 hours	Toxic
Phosphornorpholidate homooligomer (dG)	15	4-100 μ g/ml		H9, MOLT3	96 hours	Toxic
Phosphorothioate	17	16 μ M	β -Globin	<i>Xenopus</i> oocytes	>6 hours	Toxic
Phosphorothioate	15	0.1-25 μ M	IL1 β	Human blood monocytes	20 hours	Nontoxic

It is possible that oligonucleotides could bind to segments of DNA that are partially denatured by the transcription complex, although this is highly unlikely. The initiation and elongation of transcription require a complex set of proteins and other factors, and it is difficult to conceive of a mechanism by which oligonucleotides might compete effectively against the transcriptional machinery for these single-stranded regions. Nevertheless, despite the improbability of such an event, reports of activities have been made that can be explained most simply by this mechanism (112, 113). Additionally, Helene and colleagues (114) reported that hexanucleotides to nonanucleotides with acridine derivatives at the 3' terminus inhibited transcription of the β -lactamase gene. When the RNA polymerase was preincubated with the oligonucleotide-acridine adducts, however, they observed nonspecific inhibition (115).

The alternative to seeking transient single-stranded regions or to attempting to denature a double-stranded region of DNA is to inhibit transcription by interacting with double-stranded DNA, i.e. forming triple-stranded structures. To form triple-stranded structures, hydrogen bonds other than Watson-Crick must be formed. In most current triple-strand motifs, the oligonucleotide becomes the third strand by recognizing hydrogen bonding donor/receptor sites on a purine reference strand and lying in the major groove (116-124). Alternative motifs have also been proposed. For example, Hogan and colleagues (125) proposed that a purine-rich oligonucleotide can form a triplex structure based upon the purines in the oligonucleotide base pairing in parallel fashion with the purines in the duplex DNA. Studies by Dervan's group (126), however, suggested that the purine-rich oligonucleotide bound to the duplex DNA with an antiparallel orientation.

The formation of triple-stranded structures by using natural nucleosides requires runs of purines Watson-Crick-hydrogen-bonded to their complementary pyrimidines. When cytidine is used to form a triple strand with a G-C base pair, it must be protonated; this occurs at nonphysiological acidic conditions (121). Furthermore, all motifs employ one or more "weak" hydrogen bonds. Thus, to achieve sufficient stability, relatively long triple-strand structures are required.

The principal theoretical advantage of triple helical inhibition schemes is that transcription represents the first step in the intermediary metabolism of RNA and may, therefore, provide substantial leverage for drug therapy. The other advantages that have been suggested are much more speculative. For example, it has been suggested that the smaller number of genes (one or two) compared to the number of mRNA molecules (usually less than 1000) per cell is an advantage for approaches that inhibit transcription. This suggestion ignores the kinetics of the targets, however. Genes have an infinite half-life relative to cell life. RNA molecules are synthesized and degraded with

varying kinetics. Furthermore, a variety of mechanisms exist to assure that even covalent modifications of DNA are repaired. Another concept has been that triple helices in DNA might produce permanent biological effects. That even alkylating and DNA-cleaving anticancer drugs do not produce permanent effects points to the speciousness of this notion.

A number of theoretical disadvantages of triple helical inhibition of transcription have also been enumerated. Sequence specific binding is not yet possible, as runs of homopyrimidines are required. These sequences may play important regulatory roles in DNA, as they are much more abundant than statistically predicted (16). Longer term, a more substantial problem may simply be gaining sequence-specific access to DNA in chromatin. Additionally, deliberate interactions with the genome raise concerns about mutagenicity, carcinogenicity, and teratogenicity, which, in most therapeutic settings, are of considerable importance.

Several strategies have been developed to circumvent the requirement for purine-pyrimidine runs and other limitations. For example, purine oligonucleotides form triplex structures at higher pH values than pyrimidine-rich oligonucleotides (125, 126). Similarly, pyrimidine-rich oligonucleotides, in which 2'-O-methyl pseudouridine was substituted for 2' deoxycytidine, formed triplex structures at neutral pH (127). Oligonucleotides with linkers that allow crossover of the oligopyrimidine from one strand of the duplex to the other have been reported and this motif suggested to be a solution to a broader sequence repertoire (128). To enhance the stability of triple helices, intercalators and photoactivatable crosslinkers and alkylators have been conjugated to oligo pyrimidines (129–131). To increase potency and enable identification of sites of binding, a number of cleavage moieties have been conjugated to oligopyrimidines (132–137). Finally, to enhance nuclease stability, methylphosphonates (138) and α -oligonucleotides (136) have been shown or suggested to form triple helices.

In addition to cleavage of DNA *in vitro* by triplex-forming oligonucleotides coupled to cleavage reagents and alkylation induced by oligonucleotide-coupled alkylators, several other methods have been used to show triplex formation. These include agarose affinity column purification (139), NMR (140), protection from uv dimerization (141), solution hybridization (142), inhibition of binding of DNA-binding proteins (143), inhibition of restriction endonucleases (144), and repression of c-myc transcription *in vitro* (125). Recently, a 28-mer phosphodiester stabilized at the 3' end by alanine and directed to enhancer elements for the IL-2 receptor gene was shown to inhibit the transcription of the gene when incubated with human lymphocytes. The authors reported evidence for selectivity to oligonucleotides as well (145).

Obviously, triple-helix-based inhibition of transcription is of potential therapeutic importance, particularly for targets that for a variety of reasons

may be difficult to inhibit at the post-transcriptional level. Substantial medicinal chemistry must be completed, however, to create oligonucleotides that can interact with duplex structures in a sequence-specific fashion without requiring special motifs. Once this is accomplished, of course, additional studies must show that the other theoretical limitations discussed above can be overcome.

Inhibition of splicing A key step in the intermediary metabolism of most mRNA molecules is the excision of introns. These "splicing" reactions are sequence-specific and require the concerted action of spliceosomes. Consequently, oligonucleotides that bind to sequences required for splicing may prevent binding of necessary factors or physically prevent the required cleavage reactions. This then would result in inhibition of the production of the mature mRNA. Although there are several examples of oligonucleotides directed to splice junctions, none of the studies presented data showing inhibition of RNA processing, accumulation of splicing intermediates, or a reduction in mature mRNA. Nor are there published data in which the structure of the RNA at the splice junction was probed and the oligonucleotides demonstrated to hybridize to the sequences for which they were designed (146-149). Activities have been reported for anti-c-myc and antiviral oligonucleotides with phosphodiesters, methylphosphonates, and phosphorothioates.

Translational arrest Without question, the mechanism for which the majority of oligonucleotides have been designed is translational arrest. Oligonucleotides have been designed to bind to the translational initiation codon. The positioning of the initiation codon within the area of complementarity of the oligonucleotide and the length of the oligonucleotide used have varied considerably. Again, unfortunately, only in relatively few studies have the oligonucleotides been shown to bind to the sites for which they were designed, and other data that support translation arrest as the mechanism reported.

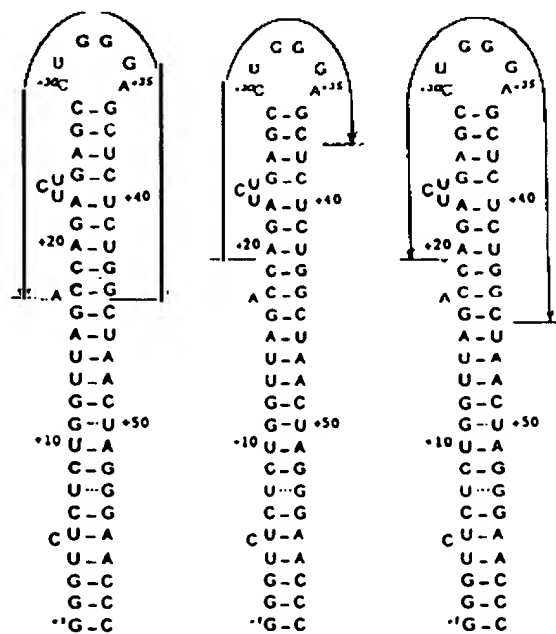
Target RNA species that have been reported to be inhibited include HIV (19), vesicular stomatitis virus (VSV) (82), n-myc (150), and a number of normal cellular genes (151-154).

In our laboratories, we have shown that a significant number of targets may be inhibited by binding to translation initiation codons. For example, ISIS 1082 hybridizes to the AUG codon for the UL13 gene of herpes virus types 1 and 2. Studies with RNaseH confirmed that ISIS 1082 binds selectively in this area. In vitro protein synthesis studies confirmed that ISIS 1082 inhibited the synthesis of the UL13 protein, and studies in HeLa cells showed that it inhibited the growth of herpes type 1 and type 2 with an IC₅₀ of 200-400 nm.

by translation arrest (155). Similarly, ISIS 1753, a 30-mer phosphorothioate complementary to the translation initiation codon and surrounding sequences of the E2 gene of bovine papilloma virus, was highly effective, and its activity was shown to be due to translation arrest. ISIS 2105, a 20-mer phosphorothioate complementary to the same region in human papilloma virus, was shown to be a very potent inhibitor. Compounds complementary to the translation initiation codon were the most potent of the more than 50 compounds studied complementary to various other regions in the RNA (156).

In conclusion, translation arrest represents an important mechanism of action for antisense drugs. A number of examples purporting to employ this mechanism have been reported. Recent studies on several compounds have provided data that unambiguously demonstrate that this mechanism can result in potent antisense drugs.

Disruption of necessary RNA structure RNA adopts a variety of three-dimensional structures induced by intramolecular hybridization, the most common of which is the stem loop (Figure 2). These structures play crucial roles in a variety of functions. They are used to provide additional stability for



length	28	18	26
P=S	1972	1308	1307
P=O	1971	1116	1118

Figure 2 Antisense oligonucleotides directed against the HIV TAR element. The oligonucleotide sequences are complementary to the tar sequences where indicated.

RNA and as recognition motifs for a number of proteins, nucleic acids, and ribonucleoproteins that participate in the intermediary metabolism and activities of RNA species. Thus, given the potential general activity of the mechanism, it is surprising that occupancy-based disruption RNA has not been more extensively exploited.

As an example, we designed a series of oligonucleotides that bind to the important stem-loop in all RNA species in HIV, and TAR element. We synthesized a number of oligonucleotides designed to disrupt TAR, and showed that several indeed did bind to TAR, disrupt the structure, and inhibit TAR-mediated production of a reporter gene (157). Furthermore, general rules useful in disrupting stem-loop structures were developed as well.

Although designed to induce relatively nonspecific cytotoxic effects, two other examples are noteworthy. Oligonucleotides designed to bind to a 17 nucleotide loop in *Xenopus* 28S RNA, required for ribosome stability and protein synthesis, inhibited protein synthesis when injected into *Xenopus* oocytes (158). Similarly, oligonucleotides designed to bind to highly conserved sequences in 5.8S RNA inhibited protein synthesis in rabbit reticulocyte and wheat germ systems (159).

OCCUPANCY-ACTIVATED DESTABILIZATION RNA molecules regulate their own metabolism. A number of structural features of RNA are known to influence stability, various processing events, subcellular distribution, and transport. As RNA intermediary metabolism is better understood, many other regulatory features and mechanisms will probably be identified.

5' Capping A key early step in RNA processing is 5' capping (Figure 1). This stabilizes pre-mRNA and is important for the stability of mature mRNA. It also is important in binding to the nuclear matrix and nuclear transport of mRNA. As the structure of the cap is unique and understood, it presents an interesting target.

Several oligonucleotides that bind near the cap site have been shown to be active, presumably by inhibiting the binding of proteins required to cap the RNA. Again, however, this putative mechanism has not been rigorously demonstrated in any published study. In fact, none of the oligonucleotides have been shown in any published study to bind to the sequences for which they were designed. For example, the synthesis of SV40 T-antigen was reported to be most sensitive to an oligonucleotide linked to polylysine and targeted to the 5' cap site of RNA (160).

In studies in our laboratory, we have designed oligonucleotides to bind to 5' cap structures and reagents to specifically cleave the unique 5' cap structure (161).

Inhibition of 3' polyadenylation In the 3' untranslated region of pre-mRNA molecules, there are sequences that result in the post-transcriptional addition of long (hundreds of nucleotides) tracts of polyadenylate. Polyadenylation stabilizes mRNA and may play other roles in the intermediary metabolism of RNA species. Theoretically, interactions in the 3' terminal region of pre-mRNA could inhibit polyadenylation and destabilize the RNA species. Although there are a number of oligonucleotides that interact in the 3' untranslated region and display antisense activities, to date no study has reported evidence for alterations in polyadenylation.

Other mechanisms In addition to 5' capping and 3' adenylation, clearly other sequences in the 5' and 3' untranslated regions of mRNA affect the stability of the molecules. Again, a number of antisense drugs may work by these mechanisms.

Zamecnik & Stephenson (1) reported that a 13-mer targeted to untranslated 3' and 5' terminal sequences in Rous sarcoma viruses was active. Oligonucleotides that were conjugated to an acridine derivative and targeted to a 3'-terminal sequence in type A influenza viruses were reported to be active (109, 162, 163). Against several RNA targets, studies in our laboratories have shown that sequences in the 3' untranslated region of RNA molecules are often the most sensitive. For example, ISIS 1939, a 20-mer phosphorothioate that binds to and appears to disrupt a predicted stem-loop structure in the 3' untranslated region of the mRNA for ICAM, is a potent antisense inhibitor. However, inasmuch as a 2'-O-methyl analog of ISIS 1939 was much less active, it is likely that in addition to destabilization to cellular nucleolytic activity, activation of RNase H (see below) is also involved in the activity of ISIS 1939 (164).

ACTIVATION OF RNase H RNase H is an ubiquitous enzyme that degrades the RNA strand of an RNA-DNA duplex. It has been identified in organisms as diverse as viruses and human cells (for review see 165). At least two classes of RNase H have been identified in eukaryotic cells. Those in yeast and multiple enzymes with RNase H activity have been observed in prokaryotes (165). Furthermore, data suggest that there are multiple isozymes in eukaryotic cells.

Although RNase H is involved in DNA replication, it may play other roles in the cell and is found in the cytoplasm as well as the nucleus (166). The concentration of the enzyme in the nucleus is thought to be greater, however, and some of the enzyme found in cytoplasmic preparations may be due to nuclear leakage.

RNase H activity is quite variable. It is absent or minimal in rabbit reticulocytes (167) but present in wheat germ extracts (165) in a wide range of

cells (16). The level of RNase H varies as a function of development, differentiation, and rate of cell division (165). In HL60 cells, for example, the level of activity in undifferentiated cells is greatest; it is relatively high in DMSO and vitamin D-differentiated cells, and much lower in PMA-differentiated cells (G. D. Hoke et al, unpublished observations).

The precise recognition elements for RNase H are unknown; however, it has been shown that oligonucleotides with DNA-like properties as short as tetramers can activate RNase H (168). Changes in the sugar influence RNase H activation, as sugar modifications that result in RNA-like oligonucleotides, e.g. 2'-fluoro or 2'-O-methyl, do not appear to serve as a substrate for RNase H (44, 169). Alterations in the orientation of the sugar to the base can also affect RNase H activation, as α -oligonucleotides are unable to induce RNase H or may require parallel annealing (41, 170). Additionally, backbone modifications influence the ability of oligonucleotides to activate RNase H. Methylphosphonates are not substrates for RNase H (74, 143). In contrast, phosphorothioates are excellent substrates (106, 155, 171; G. D. Hoke unpublished observations). More recently, chimeric molecules have been studied as substrates for RNase H (172, 173). A single ribonucleotide in a sequence of deoxyribonucleotides was recently shown to be sufficient to serve as a substrate for RNase H when bound to its complementary deoxyoligonucleotide (174).

Despite the information about RNase H and the demonstrations that many oligonucleotides may activate RNase H in lysate and purified assays (168, 175–177), relatively little is known about the role of structural features in RNA targets in activating RNase H. There is little direct proof that RNase H activation is, in fact, the mechanism of action of oligonucleotides in cells. Recent studies in our laboratories provide additional, albeit indirect, insights into these questions. ISIS 1939 is a 20-mer phosphorothioate complementary to a sequence in the 3' untranslated region of ICAM-1 RNA. It inhibits ICAM production in human umbilical vein endothelial cells, and northern blots demonstrate that ICAM-1 mRNA is rapidly degraded. A 2'-O-methyl analog of ISIS 1939 displays higher affinity for the RNA than the phosphorothioate, is stable in cells, but inhibits ICAM-1 protein production much less potently than ISIS 1939. It is likely that ISIS 1939 destabilizes the RNA and activates RNase H. In contrast, ISIS 1570, an 18-mer phosphorothioate that is complementary to the translation initiation codon of the ICAM-1 message, inhibited production of the protein but caused no degradation of the RNA. Thus, two oligonucleotides that are capable of activating RNase H had different effects, depending on the site in the mRNA to which they bound (164).

COVALENT MODIFICATION OF THE TARGET NUCLEIC ACID BY THE OLIGO-NUCLEOTIDE A large number of oligonucleotides conjugated to alkylating

and photoactive alkylating species have been synthesized and tested for effects on purified nucleic acids and intracellular nucleic acid targets (162, 178). The potential advantage of such modifications is, of course, enhanced potency. The potential disadvantages are equally obvious: nonspecific alkylation *in vivo* and resulting toxicities.

A variety of alkylating agents have been used to modify single-stranded DNA covalently and have been shown to induce alkylation at sequences predicted by the complementary oligonucleotide to which they were attached (178–182). Similar alkylators have been employed to modify double-stranded DNA covalently after triplex formation (125, 137, 183, 184).

Photoactivatable crosslinkers and platinates have been coupled to oligonucleotides and shown to crosslink sequence-specifically as well. Photoactivatable crosslinkers coupled to phosphodiesters, methyl-phosphonates, and phosphorothioates have been shown to produce sequence-specific crosslinking (59, 130, 185–190). Photoreactive crosslinking has also been demonstrated for double-stranded DNA after triplex formation (136, 191).

Preliminary data suggesting that covalent modifications of nucleic acids in cells is feasible and may enhance the potency of oligonucleotides have also been reported. Psoralen-linked methylphosphonate oligonucleotides were reported to be significantly more potent than methylphosphonate oligonucleotides in inhibiting rabbit globin mRNA in rabbit reticulocyte lysate assay (33). Psoralen-linked methylphosphonates were also reported to be more potent in inhibiting herpes simplex virus infection in HeLa cells in tissue culture (147). Additionally, although it did not produce covalent modification, a 9-mer phosphodiester conjugated with an intercalator inhibited mutant Ha-ras synthesis in T-24 bladder carcinoma cells (81).

OLIGONUCLEOTIDE-INDUCED CLEAVAGE OF NUCLEIC ACID TARGETS

Another attractive mechanism by which the potency of oligonucleotides might be increased is to synthesize derivatives that cleave their nucleic acid targets directly. Several potential chemical mechanisms are being studied, and positive results have been reported.

The mechanism that has been most broadly studied is to conjugate oligonucleotides to chelators of redox-active metals and generate activated oxygen species that can cleave nucleic acids. Dervan and colleagues have developed EDTA-conjugated oligonucleotides that cleave double-stranded DNA sequence specifically after triplex formation (124, 137). Dervan and others have employed EDTA-oligonucleotide conjugates to cleave single-stranded DNA (192, 193). It is thought that EDTA chelates iron, which generates hydroxyl radicals that cleave the DNA; however, the cleavage occurs at several nucleotides near the nucleotide at which EDTA is attached.

In the presence of copper, oligonucleotides that are conjugated to 2,10-phenanthroline also cleave DNA with some sequence specificity (129,

133–135, 194, 195), as do porphyrin-linked oligonucleotides when exposed to light (196–198). Porphyrin-linked oligonucleotides, however, oxidize bases and induce crosslinks as well as cleave the phosphodiester backbone.

To date, no reports have demonstrated selective cleavage of an RNA or enhanced potency of oligonucleotides in cells using oligonucleotides and cleaving moieties that employ these mechanisms. Studies in progress in a number of laboratories will probably soon explore this question.

Another mechanism that may be intrinsically more attractive for therapeutic applications, particularly for cleavage of RNA targets, is a mechanism analogous to that used by many ribonucleases, nucleotidyltransferases, phosphotransferases, and ribozymes.

Ribozymes are oligoribonucleotides or RNA species capable of cleaving themselves or other RNA molecules (199). Furthermore, the Tetrahymena ribozyme has been shown to cleave DNA, but at a slower rate than RNA (200). Although several classes of ribozymes have been identified that differ with regard to substrate specificity, the use of internal or external guanosine, and other characteristics, they all employ similar enzymatic mechanisms. Cleavage and ligation involve a Mg^{2+} -dependent transesterification with nucleophilic attack by the 3'-hydroxyl of guanosine (200).

The notion that we might design a relatively small ribozyme that could interact with desired sequences as a therapeutic was given impetus by studies that showed activity for ribozymes as short as a 19-mer (201) and by the demonstration that ribozyme activity can be retained after substitutions such as phosphorothioates are introduced (200).

Other approaches to creating oligonucleotides that cleave RNA targets are to synthesize oligonucleotides with appropriate adducts positioned to catalyze degradation via acid-base mechanisms. Substantial progress is being made in this area as well (P. D. Cook et al, unpublished observations).

A few studies have attempted to compare activities of oligonucleotides targeted to different receptor sequences in the same RNA. In our laboratories, we have shown that the most sensitive site in ICAM mRNA appears to be the 3' untranslated region (164). Against PLA₂, the most active molecules are also directed to sequences in the 3' untranslated region. In contrast, the most active molecules against ELAM are in the 5' untranslated region (C. F. Bennett et al, unpublished observations). However, oligonucleotides directed to the 5' cap site, translation initiation codon, and coding regions have also shown activity (for review see 202, 203).

In conclusion, an array of potential post-binding mechanisms have already been identified for oligonucleotides. For specific oligonucleotides, however, insufficient data are available to draw firm conclusions about mechanisms. More than one mechanism may very well play a role in the activity of a given oligonucleotide. Many additional mechanisms are likely to be identified as

progress continues. It is important to consider the structure and function of receptor sequences in designing oligonucleotides and to continue to study potential mechanisms in detail. Clearly, RNase H may play a role in the mechanisms of many oligonucleotides, but, equally clearly, it is not critical for the activity of others. In the future, the mechanisms for which oligonucleotides are designed will probably be optimized for each target and class of oligonucleotide.

MEDICINAL CHEMISTRY

The core of any rational drug discovery program is medicinal chemistry. Although the synthesis of modified nucleic acids has been a subject of interest for some time, the intense focus on the medicinal chemistry of oligonucleotides dates perhaps to no more than three years prior to this writing. Consequently, the scope of medicinal chemistry has recently expanded enormously, but the biological data to support conclusions about synthetic strategies are only beginning to emerge. As several excellent reviews have been published recently, I focus here strictly on design features and progress in evaluating various approaches to enhance the properties of oligonucleotides as drugs (12, 16, 202, 203).

Modifications in the base, sugar, and phosphate moieties of oligonucleotides have been reported. The subject of medicinal chemical programs include approaches to create enhanced affinity and more selective affinity for RNA or duplex structures; the ability to cleave nucleic acid targets; enhanced nuclease stability, cellular uptake, and distribution; and *in vivo* tissue distribution, metabolism and clearance.

Modifications of the Phosphate

Table 6 shows the structures of various phosphate analogs. The properties of phosphodiester, phosphorothioate, and methylphosphonate analogs have been discussed extensively. More recently, phosphorodithioates have been synthesized and reported to be nuclease-resistant and to form stable duplexes with complementary DNA (204). Of course, a potential advantage of the phosphorodithioates is the lack of a chiral center. Another interesting recent modification is the replacement of one of the nonbonding oxygen atoms with a borane group (205). A dimer was reported to be nuclease-resistant, but little additional information is available.

Modifications of the Pentofuranose Linker

Modifications of oligonucleotides that replace phosphorous may be attractive because they support the design of oligonucleotides that may have a range of

Table 6 Phosphate modifications and analogs

Structure	R	Name
1	O^-	Phosphodiester
2	S^-	Phosphorothioate
3	Me	Methyl phosphonate
4	N (alkyl)	Phosphoramidate
5	S and $\text{O} \rightarrow \text{S}$	Phosphorodithioate
6	H_3B	Boranophosphate

charges from nonionic to negatively or positively charged. In theory, reducing the anionic character of oligonucleotides may enhance hybridization and pharmacokinetic properties.

As discussed above, earlier modifications were not specifically directed to the needs of oligonucleotide drugs. Recent modifications have attempted to maintain the geometry and spacing required to support hybridization. Replacement of the phosphorous dioxygen moiety with a methylene group has been reported by two groups (51–53). This “formacetal” linkage forms a stable duplex with DNA and to be nuclease-resistant, but it is not amenable to additional modifications without creating chiral centers and would result in a water-insoluble molecule if fully substituted throughout an oligonucleotide. Other one-for-one substitutions have been reported, but the substitutions are either less interesting or have not been evaluated sufficiently to determine their potential (for review see 12).

More complex substitutions have also been reported recently, including two atom substitutions in which the phosphorous and 5' oxygen atoms were replaced by a sulfonamide linkage (54) or methyl sulfoxyl linkage (206). A thymine tetramer in which the phosphate backbone structure was replaced with dimethylene sulfonate was recently found to hybridize with natural oligonucleotides (207). Additionally, an acetamide group has been substituted for the backbone phosphate structure in a dinucleoside (207). Finally, a great many other substitutions in the backbone have been made and will probably be published in the next year, so the repertoire of compounds should continue to increase.

Pentofuranose (Sugar) Modifications

A significant number of modifications have recently been reported. In essence, these derive from two strategies with different objectives. Oligonucleotides in which the sugars are modified uniformly throughout are designed to enhance affinity to RNA targets by facilitating the formation of a more stable helix. They also may enhance nuclease stability and membrane permeability, but these outcomes are usually secondary to the hybridization goals. In contrast, pendant modifications have also been synthesized primarily to enhance pharmacokinetics or to introduce alkylating or cleaving moieties. In any event, the sugar at the 2' position is clearly an attractive site for medicinal chemistry. Some of the properties of a few of the 2' modified oligonucleotides are shown in Table 3. This remains a fertile area for medicinal chemistry, and additional advances are likely.

More substantive alterations in sugar and even replacement of sugar are also possible. Of course, α -oligonucleotides represent one type of modification (41), but numerous other approaches are feasible. Carbocyclic (49, 50) and acyclic (47, 48) structures have been reported.

Heterocyclic Modifications

Numerous heterocyclic modifications have also been described. Many of these have been designed to enhance affinity and/or alter specificity (224). Other modifications have been developed to attach pendant modifications that may alkylate, intercalate, or cleave, as well as others that may enhance pharmacokinetic properties.

Conclusions

In conclusion, it is clear that an enormous scope for medicinal chemistry exists and that the major programs are already beginning to pay dividends.

ACTIVITIES OF OLIGONUCLEOTIDES

In the past several years, scores of articles have been published demonstrating the activity of a large number of oligonucleotides in a variety of systems. A number of excellent reviews have summarized the activities of these compounds (16, 202, 203, 208). The activities of oligonucleotides in assays of cell-free protein synthesis and after injection into cells of several types have also been summarized. Consequently, I provide a brief summary of the activities of oligonucleotides in cell-based assays and a comment on the limited *in vivo* data reported to date.

Activities in Cells in Tissue Culture

To date, oligonucleotides have been found to inhibit the growth of a large number of viruses in tissue culture, the expression of numerous oncogenes, a variety of normal cellular genes, and a number of transfected reporter genes controlled by several regulatory elements. The oligonucleotides used, the cells employed, and the receptor sequences, concentrations, and conditions have differed widely. Only a few of the studies have reported detailed dose response curves and conditions. Studies for which sufficient information was presented are summarized in Table 7.

The data presented in Table 7 support only a few generalizations, as follows:

1. Even though phosphodiesters are relatively rapidly degraded, a number of laboratories have reported activities for unmodified phosphodiester oligonucleotides in cells incubated in the absence of serum. The concentrations required to display activity were typically greater than 10 μ M.
2. A variety of modified oligonucleotides have been reported to be active. Methylphosphonates appear to be less potent than phosphorothioates, but considerable variation has been noted, depending on the system. Conjugation of alkylators and intercalators to phosphodiesters and methylphosphates increases potency. Lipophilic and poly-lysine conjugates have also displayed enhanced activities.
3. Oligonucleotides have demonstrated a broad array of activities against viral targets, oncogenes, normal host gene products, and various transfected genes. Thus, clear evidence supports the broad, potential applicability of these drugs.
4. Although the data from studies incorporated in Table 7 are limited, when combined with the in vitro toxicologic data, the therapeutic indexes of phosphorothioates appear to be quite high in vitro. Methylphosphonates appear to have lower therapeutic indexes. Too few data are available to draw conclusions about other classes of oligonucleotides.
5. Very few data support putative mechanisms of action, and generalizations concerning desired mechanisms of action are not possible. Nevertheless, a variety of mechanisms of action may be employed by oligonucleotides to result in significant biological activities.

In Vivo Activities

Two earlier investigations have suggested in vivo activities of antisense drugs against viral infections. Although no data were reported, a methylphosphonate oligonucleotide was indicated to have been active in a mouse model of herpes simplex virus I infection (147). Another study claimed in vivo activity against tick-borne encephalitis virus (213).

Table 7 Summary of antisense oligonucleotide Activities (in vitro)^a

Target	Cell type	Serum	Oligo types	Length	Concentration	Reference
Viruses						
HTLV-III	H9 cells	—	P	12-26	5-50 mg/ml	148
HIV	H-T cells	+	PS	14-28	0.5-1 μ M	20
HIV (gag/pol)	H-T cells	+	PS	18-24	1-10 μ M	211
HIV	H9 cells	+	PS, others	20	4-20 μ g/ml	19
HIV	CZM cells	+	PS	18-28	10 μ M	157
Herpes simplex	Vero cells	+	CH ₃ P	7	50-100 μ M	98
Herpes simplex	HeLa cells	+	PS	28	1-10 μ M (non-antisense)	76
Herpes simplex	Vero cells	+	CH ₃ P	12	20-50 μ M	15
Herpes simplex	Vero cells	+	CH ₃ P psoralen	12	5 μ M	15
Herpes simplex	HeLa cells	+	PS	21	0.2-4 μ M	155
Vesicular stomatitis	L929 cells	+	CH ₃ P	9	25-50 μ M	99
Vesicular stomatitis	L929 cells	+	P-lipid	11	50-150 μ M	85
Vesicular stomatitis	L929 cells	+	P-poly L-lysine	10-15	0.1 μ M	212
Influenza	MDCK cells	+	P-acridine	11	50 μ M	109
Tick-borne encephalitis	—	+	Various	Var.	0.1-1 μ M	213
SV40	MDCK cells	+	CH ₃ P	6-9	25 μ M	214
Rous	Chicken fibroblasts	+	Various	Var.	10 μ M	■
Hepatitis B	Alexander	+	P	15	8.5 μ M	215
Bovine papilloma virus	C-127 cells	+	PS	4-30	0.01-1 μ M	209
Oncogenes						
c-myc	T-lymphocytes	+	P	15	30 μ M	96
c-myc	HL-60 cells	+	P, PS	15	10 μ M	216
c-myc	Burkitt cells	■	P	21	100 μ M	146

c-myc	PMBC	+	P	18	40 mg/ml	217	
BCI-2	L697 cells	■	P, PS	20	25-150 μ M	97	
N-myc	Neuroblastoma cells	+	P	15	1-5 μ M	155	
N-ras	T15 cells	+	CH ₃ P	9	Inactive	100	
Host genes							
Multiple drug Resistance	MCF-1 cells	+	PS	15		218	
PCNA (cyclin)	3T3	+	P	18	30 μ M	219	
Prothymosin	Human myeloma cells	-	P	22		153	
T cell receptor	T cells	+	P	22		153	
Gm CSF	Endothelial cells	-	P	15, 18	10 ⁻⁵ M	153	
CSF-1	FL-ras/myc cells	+	P	?	?	220	
EGF receptor	+	+	P	13	30 μ M	221	
BFGF	Human astrocytes	-	P	15	10-75 μ M	229	
β Globin	Rabbit reticulocytes	+	CH ₃ P	9	100 μ M	222	
TAU	Neurons	-	P	20-25	3-50 μ M	228	
cAMP-Protein kinase II	HL-60 cells	+	P	21	15 μ M	210	
β	Myeloblastin	HL-60 cells	+	P	18	■	227
	Phospholipase A ₂	BC3H ₁	+	P	25	25 μ M	233
	activating protein						
ICAM-1	A549 HVEC	-	PS	18-20	0.01-1 μ M	154	
	lymphocytes						
IL-2	T-lymphocytes	-	P	15	5 μ M	72	
IL-1 α	HUVEC	+	P	18	10 μ M	154	
IL-1 β	Monocytes	+	PS	15	0.1-2.5 μ M	105	

Table 7 (Continued)

Target	Cell type	Serum	Oligo types	Length	Concentration	Reference
IGF-1	Myoblasts	P		15	10 μ M	225
Perforin	T-lymphocytes	P		18	5-35 μ M	226
Other						
Chloramphenicol acetyl transferase	CV-1 cells	+	P, PS, CH ₃ P	21	5-30 μ M	75
Placental alkaline phosphatase driven by HIV TAR	SK-mel-2 cells	+	PS	18-28	0.25-5 μ M	157
Chloramphenicol Acetyl transferase	C-127 and CV-1 cells	+	PS	14-20	1-10 μ M	209
Driven by human papilloma virus E2 responsive element						

* Abbreviations: cAMP, cyclic AMP; CH₃P, methylphosphonate oligonucleotides; EGF, epidermal growth factor; G-CSF, granulocyte colony-stimulating factor; GM-CSF, granulocyte macrophage colony-stimulating factor; HB, hepatitis B; HIV, human immunodeficiency virus; HSV, herpes simplex virus; HTLV, human T-cell lymphotropic virus; IV, influenza virus; P, phosphodiester oligonucleotides; P-acridine, phosphodiester oligonucleotide conjugated with acridine moiety; P-lipid, phosphodiester oligonucleotide conjugated with lipid moiety; P-S, phosphorothioate oligonucleotides; PCNA, proliferating cell nuclear antigen; PMA, phorbol myristic acid; RSV, Rous sarcoma virus; TAR, Tat response element; TBE, tick-borne encephalitis; VSV, vesicular stomatitis.

Topical application of ISIS 1082 in an aqueous buffer to the cornea of mice infected with herpes virus I inhibited viral growth in a concentration-dependent fashion and cured the infection at concentrations greater than 1% (230). The activity of ISIS 1082 was equivalent to trifluorothymidine and was associated with no local or systemic toxicities.

CONCLUSIONS

Oligonucleotides designed to interact with nucleic acid receptors represent a potentially revolutionary advance in pharmacotherapy. Advances in the recent past and the intense, current focus assure that the paradigm will be fully explored.

Oligonucleotides have already been shown to work *in vitro* and have proven to be invaluable pharmacologic tools. The progress in resolving the basic pharmacological questions relating to oligonucleotide therapeutics and in resolving issues that will influence the commercialization of new drugs of this class has been impressive. Moreover, advances in medicinal chemistry are exciting and argue that exciting new classes of these drugs are forthcoming.

Much remains to be learned; a great deal remains to be accomplished before the paradigm is fully proven and the opportunity it represents realized. In the coming years, the key tasks will be (*a*) to place oligonucleotide therapeutics on a solid pharmacological footing by performing careful dose response curves in well-designed experiments, and (*b*) to advance the development of oligonucleotide pharmaceutical products to the point that the paradigm can be tested in man.

There is now cause for considerable optimism that the promise of oligonucleotide therapeutics may be realized.

ACKNOWLEDGMENTS

The author acknowledges the excellent typographical and administrative assistance by Mrs. Colleen Matzinger and critical reviews by C. Frank Bennett, P. Dan Cook, Rosanne M. Crooke, David J. Ecker and Tom Briuce.

Literature Cited

1. Zamecnik, P. C., Stephenson, M. L., 1978. Inhibition of Rous sarcoma virus replication and cell transformation by a specific oligodeoxynucleotide. *Proc. Natl. Acad. Sci. USA* 75:280
2. Mizumoto, K., Kaziro, Y. 1987. Messenger RNA capping enzymes from eukaryotic cells. *Prog. Nucleic Acids Res. Mol. Biol.* 34:1
3. Ross, J. 1988. Messenger RNA turnover in eukaryotic cells. *Mol. Biol. Med.* 5:1
4. Friedman, D. I., Imperiale, M. J. 1987. RNA 3' end formation in the control of gene expression. *Annu. Rev. Genet.* 21:453
5. Manley, J. L. 1988. Polyadenylation of mRNA precursors. *Biochim. Biophys. Acta* 950:1

6. Padgett, R. A., Grabowski, P. J., Konarska, M. M., Seiler, S., Sharp, P. A. 1986. Splicing of messenger RNA precursors. *Annu. Rev. Biochem.* 55: 1119

7. Green, M. R. 1986. Pre-mRNA splicing. *Annu. Rev. Genet.* 20:671

8. Freier, S. M., Kierzek, R., Jaeger, J. A., Sugimoto, N., Caruthers, M. H., Neilson, T. 1986. Improved free-energy parameters for predictions of RNA duplex stability. *Proc. Natl. Acad. Sci. USA* 83:9373

9. Breslauer, K. J., Frank, R., Blocker, H., Marky, L. A. 1986. Predicting DNA duplex stability from base sequence. *Proc. Natl. Acad. Sci. USA* 83:3746

10. Freier, S. M., Lima, W. F., Sanghvi, Y. S., Vickers, T., Zounes, M., et al. 1991. Thermodynamics of antisense oligonucleotide hybridization. In *Gene Regulation by Antisense Nucleic Acids*, ed. J. Ivant, R. Erickson. New York: Raven. In press

11. Cazenave, C., Helene, C. 1991. Antisense oligonucleotides. See Ref. 203, p. 47

12. Cook, P. D. 1991. Medicinal chemistry of antisense oligonucleotides—future opportunities. *Anti-Cancer Drug Design*. In press

13. Puglisi, J. D., Wyatt, J. R., Tinoco, I., Jr. 1990. Conformation of an RNA Pseudoknot. *J. Mol. Biol.* 214:437

14. Wickstrom, E. 1986. Oligodeoxynucleotide stability in subcellular extracts and culture media. *J. Biochem. Biophys. Methods* 13:97

15. Cazenave, C., Chevrier, M., Thuong, N. T., Helene, C. 1987. Rate of degradation of alpha and beta-oligodeoxynucleotides in *Xenopus* oocytes: Implications for anti-messenger strategies. *Nucleic Acids Res.* 15:10507

16. Uhlmann, E., Peyman, A. 1990. Antisense oligonucleotides: A new therapeutic principle. *Chem. Rev.* 90:543

17. Campbell, J. M., Bacon, T. A., Wickstrom, E. 1990. Oligodeoxynucleoside phosphorothioate stability in subcellular extracts, culture media, sera and cerebrospinal fluid. *J. Biochem. Biophys. Methods* 20:259

18. Cohen, J. S. 1990. Antisense oligonucleotides as an approach towards anti-AIDS therapy. In *Design of Anti-AIDS Drugs*, ed. E. De Clercq, p. 195. Amsterdam: Elsevier

19. Agrawal, S., Goodchild, J., Civeira, M. P., Thornton, A. T., Sarin, P. M., Zamecnik, P. C. 1988. Oligodeoxynucleoside phosphoramidites and phosphorothioates as inhibitors of human immunodeficiency virus. *Proc. Natl. Acad. Sci. USA* 85:7079

20. Matsukura, M., Shinozuka, K., Zon, G., Mitsuya, H., Reitz, M., et al. 1987. Phosphorothioate analogs of oligodeoxynucleotides: Inhibitors of replication and cytopathic effects of human immunodeficiency virus. *Proc. Natl. Acad. Sci. USA* 84:7706

21. Eckstein, F. 1983. Phosphorothioate analogs of nucleotides—tools for the investigation of biochemical processes. *Angew. Chem.* 22:423

22. Eckstein, F. 1985. Nucleoside phosphorothioates. *Annu. Rev. Biochem.* 54: 367

23. Stec, W. J., Zong, G., Egan, W., Stec, B. 1984. Automated solid-phase synthesis, separation and stereochemistry of phosphorothioate analogues of oligodeoxynucleotides. *J. Am. Chem. Soc.* 106:6077

24. Gallo, K. A., Shao, K., Phillips, L. R., Regan, J. B., Koziolkiewicz, M., et al. 1986. Alkyl phosphotriester modified oligodeoxyribonucleotides. V. Synthesis and absolute configuration of R_p and S_p diastereomers of an ethyl phosphotriester (Et) modified Eco RI recognition sequence, d[GGAA(Et)TTCC]. A synthetic approach to regio- and stereospecific ethylation-interference studies. *Nucleic Acids Res.* 14:7405

25. Miller, P. S., Agris, C. H., Aurelian, L., Blake, K. R., Lin, S.-B., et al. 1985. Control of gene expression by oligonucleotide methylphosphonates. In *Interrelationship Among Aging, Cancer and Differentiation*, ed. B. Pullman, p. 207. Dordrecht: Reidel

26. Miller, P. S., Agris, C. H., Blake, K. R., Murakami, A., Spitz, S. A., et al. 1983. Nonionic oligonucleotide analogs as new tools for studies of the structure and function of nucleic acids inside living cells. In *Nucleic Acids: The Vectors of Life*, ed. B. Pullman, J. Jortner, p. 521. Dordrecht: Reidel

27. Miller, P. S., McParland, K. B., Jayaraman, K., Ts'o, P. O. P. 1981. Biochemical and biological effects of non-ionic nucleic acid methylphosphonates. *Biochemistry* 20:1874

28. Miller, P. S., Ts'o, P. O. P. 1987. A new approach to chemotherapy based on molecular biology and nucleic acid chemistry: Matagen (masking tape for gene expression). *Anti-Cancer Drug Design* 2:117

29. Ts'o, P. O. P., Miller, P. S., Aurelian, L., Murakami, A., Agris, C., et al. 1987. An approach to chemotherapy based on base sequence information and

nucleic acid chemistry. Matagen (masking tape for gene expression). *Ann. NY Acad Sci.* 507:220.

30. Agrawal, S., Goodchild, J. 1987. Oligodeoxynucleoside methylphosphonates: Synthesis and enzymic degradation. *Tetrahedron Lett.* 28:3539

31. Agrawal, K. L., Riftina, F. 1979. Synthesis and enzymatic properties of deoxyribonucleotides containing methyl and phenylphosphonate linkage. *Nucleic Acids Res.* 6:3009

32. Miller, P. S., Dreon, N., Pulord, S. M., McParland, K. B. 1980. Oligothymidylate analogues having stereoregular, alternating methylphosphonate/phosphodiester backbones. *J. Biol. Chem.* 255:9659

33. Kean, J. M., Murakami, A., Blake, K. R., Cushman, C. D., Miller, P. S. 1988. Photochemical cross-linking of psoralen-derivatized oligonucleotide methylphosphonates to rabbit globin messenger RNA. *Biochemistry* 27:9113

34. Koziolkiewicz, M., Uznanski, B., Stec, W. J., Zon, G. 1986. P-Chiral analogues of oligodeoxyribonucleotides: Synthesis, stereochemistry and enzyme studies. *Chem. Sci.* 26:251

35. Miller, P. S., Ts'o, P. O. P. 1988. Oligonucleotide inhibitors of gene expression in living cells: New opportunities in drug design. *Ann. Rep. Med. Chem.* 23:295

36. Miller, P. S., Chandrasegaran, S., Dow, D. L., Pullford, S. M., Kan, L. S. 1982. Synthesis and template properties of an ethyl phosphotriester modified deoxyribonucleotide. *Biochemistry* 21: 5468

37. Bacon, T. A., Morvan, F., Rayner, B., Imbach, J. L., Wickstrom, E. 1988. α -Oligodeoxynucleotide stability in serum, subcellular extracts and culture media. *J. Biochem. Biophys. Methods* 16:311

38. Morvan, F., Rayner, B., Imbach, J. L., Thenet, S., Bertrand, J. R., et al. 1987. Alpha-DNA. II. Synthesis of unnatural alpha-anomeric oligodeoxyribonucleotides containing the four usual bases and study of their substrate activities for nucleases. *Nucleic Acids Res.* 15:3421

39. Morvan, F., Genu, C., Rayner, B., Imbach, J. L. 1990. Sugar modified oligonucleotides. III: Synthesis nuclease resistance and base pairing properties of α and β -L-octathymidylates. *Biochem. Biophys. Res. Commun.* Submitted

40. Thenet, S., Morvan, F., Bertrand, J. R., Gauthier, C., Malvy, C. 1988. α -Anomer oligonucleotides are more stable than β ones in 3T3 cellular extracts. *Biochimie* 70:1729

41. Morvan, F., Rayner, B., Imbach, J. L. 1991. α -Oligonucleotides: A unique class of modified chimeric nucleic acids. *Anti-Cancer Drug Design.* In press

42. Sproat, B. S., Lamond, A. L., Beijer, B., Neuner, P., Ryder, U. 1990. Rat brain expresses a heterogeneous family of calcium channels. *Proc. Natl. Acad. Sci. USA* 87:3391

43. Iribarren, A. M., Sproat, B. S., Neuner, P., Sulston, I., Ryder, U., Lamond, A. I. 1990. 2'-O-alkyl oligoribonucleotides as antisense probes. *Proc. Natl. Acad. Sci. USA* 87:7747

44. Kawasaki, A. M., Martin, J. F., Guinozzo, C. J., Zounes, M. C., Springer, R. S., et al. 1991. Synthesis and biophysical studies of 2'-d-ribo-f modified oligonucleotides. *Intl. Union Biochem. Conf. Nucleic Acid Ther.*, p. 71

45. Guinozzo, C. J., Hoke, G. D., Ecker, D. J., Mirabelli, C. K., Crooke, S. T., Cook, P. D. 1991. Synthesis and biophysical and biological evaluation of 2'-modified antisense oligonucleotides. *Nucleosides Nucleotides* 10:259

46. Hakimelahi, G. H., Zarrinehzad, M., Jarrahpour, A. A., Shargi, H. 1987. *Helv. Chim. Acta* 70:219

47. Schneider, K. C., Benner, S. A. 1990. Building blocks for oligonucleotide analogs with dimethylene-sulfide, sulfoxide and sulfone groups replacing phosphodiester linkages. *Tetrahedron Lett.* 31:335

48. Augustyns, K., Van Aershot, A., Urbanke, C., Herdewijn, P. 1991. Synthesis of oligonucleotides with a hexose or with an acyclic sugar moiety. *Intl. Union Biochem. Conf. Nucleic Acid Ther.*, p. 53

49. Perbost, M., Lucas, M., Chavis, C., Pompon, A., Baumgartner, H., et al. 1989. Sugar modified oligonucleotides: Carbo-oligodeoxynucleotides as potential antisense agents. *Biochem. Biophys. Res. Commun.* 165:742

50. Szemzo, A., Szecski, J., Sagi, J., Otvos, L. 1990. First synthesis of carbocyclic oligothymidylates. *Tetrahedron Lett.* 31:1463

51. Matteucci, M. 1990. Deoxyliogonucleotide analogs based on formacetal linkages. *Tetrahedron Lett.* 31:2385

52. Veeneman, G. H., van der Marel, G. H., van den Elst, H., van Boom, H. J. 1990. Synthesis of oligonucleotides containing thymines linked via an internucleosidic-(33'-5')-methylene bond. *Rec. Trav. Chim. Pays-Bas* 109:449

53. Veeneman, G. H., van der Marel, G. H., van den Elst, H., van Boom, H. J.

1991. An efficient approach to the synthesis of thymine derivatives containing phosphate-isoteric methylene acetal linkages. *Tetrahedron Lett.* 47:1547

54. Kirshenbaum, M. R., Huie, E. M., Trainor, G. L. 1991. Novel oligonucleotide analogues with a sulfur based linkage. *Colloq. Gene Regulation by Antisense RNA and DNA, CD 210:19 Keystone Symp. Mol. Cell. Biol.*, Feb. 2-7, Frisco, CO

55. Jones, G. H., Albrecht, H. P., Damodaran, N. P., Moffatt, J. G. 1970. Synthesis of isoteric phosphonate analogs of some biologically important phosphodiesters. *J. Am. Chem. Soc.* 92:5510

56. Nyilas, A., Glemarec, C., Chattapadhyaya, J. 1990. Synthesis of [$3'(\text{O})\text{Æ}5'(\text{c})$]-oxyacetamido linked nucleosides. *Tetrahedron* 46:2149

57. Gait, M. J., Jones, A. S., Walker, R. 1974. Synthetic analogues of polynucleotides. Part XII. Synthesis of thymidine derivatives containing an oxyacetamido- or an oxyformamido-linkage instead of a phosphodiester group. *Chem. Soc. Perkin I*, p. 1684

58. Rosenberg, I., Holy, A. 1987. Synthesis of phosphonylmethyl analogues of d-ribonucleoside monophosphates containing modified internucleotide bond. *Collec. Czech. Chem. Commun.* 52:2572

59. Praseuth, D., Doan, T. L., Chassignol, M., Decourt, J.-L., Habhou, N., et al. 1988. Sequence-targeted photosensitized reactions in nucleic acids by oligo- α -deoxynucleotides and oligo- β -deoxynucleotides covalently linked to proflavin. *Biochemistry* 27:3031

60. Stein, C. A., Mori, K., Loke, S. L., Subasinghe, C., Shinozuka, K., et al. 1988. Phosphorothioate and normal oligodeoxyribonucleotides with 5'-linked acridine: Characterization and preliminary kinetics of uptake. *Gene* 72:333

61. Vespieren, P., Cornelissen, A. W. C. A., Thuong, N. T., Helene, C., Toulme, J. J. 1987. An acridine-linked oligodeoxynucleotide targeted to the common 5' end of trypanosome mRNAs kills cultured parasites. *Gene* 61:307

62. Toulme, J. J., Krisch, H. M., Loreau, N., Thuong, N. T., Helene, C. 1986. Specific inhibition of mRNA translation by complementary oligonucleotides covalently linked to intercalating agents. *Proc. Natl. Acad. Sci. USA* 83:1227

63. Lemaitre, M., Bisbal, C., Bayard, B., Lebleu, B. 1987. Biological activities of oligonucleotides linked to poly(L-lysine). *Nucleosides Nucleotides* 6:311

64. Leonetti, J. P., Rayner, B., Lemaitre, M., Gagnor, C., Milhaud, P. G., et al. 1988. Antiviral activity of conjugates between poly(L-lysine) and synthetic oligodeoxyribonucleotides. *Gene* 72:323

65. Manoharan, M., Guinoss, C. J., Cook, P. D. 1991. Novel functionalization of the sugar moiety of nucleic acids for diagnostic and therapeutic applications. *Tetrahedron Lett.* In press

66. Yamanai, K., Nishijima, Y., Ikeda, T., Gokota, T., Ozaki, H., et al. 1990. Synthesis and interactive properties of an oligonucleotide with anthraquinone at the sugar fragment. *Bioconjugate Chem.* 1:319

67. Ramasamy, K., Springer, R. S., Martin, J. F., Freier, S. M., Hoke, G. D., et al. 1991. Synthesis and biophysical evaluation of N^2 -substituted guanine and adenine modified oligonucleotides as catalytic cleavers of RNA. *Intl. Union Biochem. Conf. Nucleic Acid Ther.*, p. 82

68. Casale, R., McLaughlin, L. W. 1990. Synthesis and properties of an oligodeoxynucleotide containing a polycyclic aromatic hydrocarbon site specifically bound to the N^2 amino group of a 2'-dcoxy guanosine residue. *J. Am. Chem. Soc.* 112:5264

69. Acevedo, O. L., Hoke, G. D., Freier, S., Zounes, M., Guinoss, C. G., et al. 1991. Synthesis and biological evaluation of antisense oligonucleotides containing 3-deaza-3-substituted guanines. *Intl. Union Biochem. Conf. Nucleic Acid Ther.*, p. 50

70. Sanghvi, Y. S., Hoke, G. D., Zounes, M., Chan, H., Acevedo, O., et al. 1991. Synthesis and biological evaluation of antisense oligonucleotides containing modified pyrimidines. *Nucleosides Nucleotides* 10:345

71. Hoke, G. D., Draper, K., Freier, S. M., Gonzalez, C., Driver, V. B., et al. 1991. Effects of phosphorothioate capping on antisense oligonucleotide stability, hybridization and antiviral efficacy versus herpes simplex virus infection. *Nucleic Acids Res.* In press

72. Harel-Bellan, A., Durum, S., Muegge, K., Abbas, A. K., Farrar, W. L. 1988. Specific inhibition of lymphokine biosynthesis and autocrine growth using antisense oligonucleotides in Th1 and Th2 helper T cell clones. *J. Exp. Med.* 168:2309

73. Crooke, R. M. 1991. In vitro toxicology and pharmacokinetics of antisense oligonucleotides. *Anti-Cancer Drug Design*. In press

74. Miller, P. S., 1989. Non-ionic antisense oligonucleotides. See Ref. 202, p. 79

75. Marcus-Sekura, C. J., Woerner, A. M., Shinozuka, K., Zon, G., Quinnan, G.

V. Jr. 1987. Comparative inhibition of chloramphenicol acetyltransferase gene expression by antisense oligonucleotide analogues having alkyl phosphotriester, methylphosphonate and phosphorothioate linkages. *Nucleic Acids Res.* 15:5749

76. Gao, W., Stein, C. A., Cohen, J. S., Dutschman, G. E., Cheng, C.-Y. 1989. Effect of phosphorothioate homo-oligodeoxy-nucleotides on herpes simplex virus type 2-induced DNA polymerase. *J. Biol. Chem.* 264:11521

77. Crooke, R. M., Shoemaker, J., Graham, M., Ecker, D. J. 1991. *In vitro* pharmacokinetic analysis of ISIS 1082, a novel anti-herpetic therapeutic. Submitted

78. Bennett, C. F., Chiang, M.-Y., Chan, H., Shoemaker, J., Mirabelli, C. K. 1991. Cationic lipids enhance cellular uptake and activity of antisense oligonucleotides. *Mol. Pharmacol.* Submitted

79. Loke, S. L., Stein, C. A., Zhang, X. H., Mori, K., Nakanishi, M., et al. 1989. Characterization of oligonucleotide transport into living cells. *Proc. Natl. Acad. Sci. USA* 86:3474

80. Yakubov, L. A., Deeva, E. A., Zarytova, V. F., Ivanova, E. M., Ryte, A. S., et al. 1989. Mechanism of oligonucleotide uptake by cells: Involvement of specific receptors. *Proc. Natl. Acad. Sci. USA* 86:6454

81. Saison-Behmoaras, T., Tocque, B., Rey, I., Chassignol, M., Thuong, N. T., Helene, C. 1991. Short modified oligonucleotides directed against Ha-ras point mutation induce selective cleavage of the mRNA and inhibit T24 cells proliferation. *Embo. J.* Submitted

82. Lemaitre, M., Bayard, B., Lebleu, B. 1987. Specific antiviral activity of a poly(L-lysine)-conjugated oligodeoxyribonucleotide sequence complementary to vesicular stomatitis virus N-protein mRNA initiation site. *Proc. Natl. Acad. Sci. USA* 84:648

83. Leonetti, J. P., Degols, G., Milhaud, P., Gagnor, C., Lemaitre, M., Lebleu, B. 1989. Antiviral activity of antisense oligonucleotides linked to poly(L-lysine): targets on genomic RNA and/or mRNA of vesicular stomatitis virus. *Nucleosides Nucleotides* 8:825

84. Leonetti, J. P., Degols, G., Lebleu, B. 1990. Biological activity of oligonucleotide-poly-(L-lysine) conjugates: Mechanism of cell uptake. *Bioconjugate Chem.* 1:149

85. Shea, R. G., Marsters, J. C., Bischofberger, N. 1990. Synthesis, hybridization properties and antiviral activity of lipid-oligodeoxynucleotide conjugates. *Nucleic Acids Res.* 18:3777

86. Kabanov, A. V., Vinogradov, S. V., Ovcharenko, A. V., Krivonos, A. V., Melik-Nubarov, N. S., et al. 1990. A new class of antivirals: Antisense oligonucleotides combined with a hydrophobic substituent effectively inhibit influenza virus reproduction and synthesis of virus-specific proteins in MDCK cells. *FEBS Lett.* 259:327

87. Dagle, J. M., Walder, J. A., Weeks, D. L. 1990. Targeted degradation of mRNA in *Xenopus* oocytes and embryos directed by modified oligonucleotides: Studies of An2 and cyclin in embryogenesis. *Nucleic Acids Res.* 18:4751

88. Dagle, J. M., Weeks, D. L., Walder, J. A. 1991. Pathways of degradation and mechanism of action of antisense oligonucleotides in *Xenopus laevis* embryos. *Antisense Res. Dev.* 1:11

89. Woolf, T. M., Jennings, C. G., Rebagliati, M., Melton, D. A. 1990. The stability, toxicity and effectiveness of unmodified and phosphorothioate antisense oligodeoxynucleotides in *Xenopus* oocytes and embryos. *Nucleic Acids Res.* 18:1763

90. Chin, D. J., Green, G. A., Zon, G., Szoka, F., Straubinger, R. M. 1990. Rapid nuclear accumulation of injected oligodeoxyribonucleotides. *New Biol.* 2:1091

91. Ao, A., Erickson, R. P., Bevilacqua, A., Karolyi, J. 1991. Antisense inhibition of β -glucuronidase expression preimplantation mouse embryos: A comparison of transgenes and oligodeoxynucleotides. *Antisense Res. Dev.* 1:1

92. Loke, S. L., Stein, C., Zhang, X., Avigan, M., Cohen, J., Neckers, L. 1988. Delivery of c-myc antisense phosphorothioate oligodeoxynucleotides to hematopoietic cells in culture by liposome fusion: Specific reduction in c-myc protein expression correlates with inhibition of cell growth and DNA synthesis. *Curr. Top. Microbiol. Immunol.* 141: 282

93. Bisbal, C., Bayard, B., Lemaitre, M., Leserman, L., Lebleu, B. 1987. Intracellular delivery of (2'-5') oligo(adenylated). *Drugs Future* 12:793

94. Iversen, P. 1991. In vivo studies with phosphorothioate oligonucleotides: Pharmacokinetics prologue. *Anti-Cancer Drug Design.* In press

95. Goodchild, J., Kim, B., Zamecnik, P. C. 1991. The clearance and degradation of oligodeoxynucleotides following intravenous injection into rabbits. *Antisense Res. Dev.* 1:153

96. Heikkila, R., Schwab, G., Wickstrom, E., Loke, S. L., Pluznik, D. H., et al. 1987. A c-myc antisense oligonucleotide inhibits entry into S phase but not progress from G0 to G1. *Nature* 328:445

97. Reed, J. C., Cuddy, M., Halder, S., Croce, C., Nowell, P., et al. 1990. BCL2-mediated tumorigenicity of a human T-lymphoid cell line: Synergy with myc and inhibition by BCL2 antisense. *Proc. Natl. Acad. Sci. USA* 87:3660

98. Smith, C. C., Aurelian, L., Reddy, M. P., Miller, P. S., Ts'o, P. O. P. 1986. Antiviral effect of an oligonucleoside methylphosphonate complementary to the splice junction of herpes simplex virus type 1 immediate early pre-mRNAs 4 and 5. *Proc. Natl. Acad. Sci. USA* 83:2787

99. Agris, C. H., Blake, K. R., Miller, P. S., Reddy, M. P., Ts'o, P. O. P. 1986. Inhibition of vesicular stomatitis virus protein synthesis and infection by sequence-specific oligodeoxyribonucleoside methylphosphonates. *Biochemistry* 25:6268

100. Tidd, D. M., Hawley, P., Warenius, H. M., Gibson, I. 1988. Evaluation of N-ras oncogene antisense, sense and non-sense sequence methylphosphonate oligonucleotide analogues. *Anti-Cancer Drug Design* 3:117

101. Zon, G. 1989. Pharmaceutical considerations. See Ref. 202, p. 233

102. Neckers, L. M. 1989. Antisense oligodeoxynucleotides as a tool for studying cell regulation: Mechanism of uptake and application to the study of oncogene function. See Ref. 202, p. 211

103. Cazenave, C., Loreau, N., Toulme, J. J., Helene, C. 1986. Anti-messenger oligodeoxynucleotides: Specific inhibition of rabbit β -globin synthesis in wheat germ extracts and *Xenopus* oocytes. *Biochimie* 68:1063

104. Majumdar, C., Stein, C. A., Cohen, J. S., Broder, S., Wilson, S. H. 1989. Stepwise mechanism of HIV reverse transcriptase: Primer function of phosphorothioate oligodeoxynucleotide. *Biochemistry* 28:1340

105. Manson, J., Brown, T., Duff, G. 1990. Modulation of interleukin 1 β gene expression using antisense phosphorothioate oligonucleotides. *Lymphokine Res.* 9:35

106. Stein, C. A., Cohen, J. S. 1989. Phosphorothioate oligodeoxynucleotide analogues. See Ref. 202, p. 97

107. O'Keefe, S. J., Wolfes, H., Kiessling, A. A., Cooper, G. M. 1989. Microinjection of antisense c-mos oligonucleotides prevents meiosis II in the maturing mouse egg. *Proc. Natl. Acad. Sci. USA* 86:7038

108. Zaia, J. A., Rossi, J. J., Murakawa, G. J., Spallone, P. A., Stephens, D. A., et al. 1988. Inhibition of human immunodeficiency virus by using an oligonucleoside methylphosphonate targeted to the tat-3 gene. *J. Virol.* 62:3914

109. Zerial, A., Thuong, N. T., Helene, C. 1987. Selective inhibition of the cytopathic effect of type A influenza viruses by oligodeoxynucleotides covalently linked to an intercalating agent. *Nucleic Acids Res.* 15:9909

110. Goodchild, J., Agrawal, S., Civeira, M. P., Sarin, P. S., Sun, D., Zamecnik, P. C. 1988. Inhibition of human immunodeficiency virus replication by antisense oligonucleotides. *Proc. Natl. Acad. Sci. USA* 85:5507

111. Sarin, P. S., Agrawal, S., Civeira, M. P., Goodchild, J., Ikeuchi, T., Zamecnik, P. C. 1988. Inhibition of acquired immunodeficiency syndrome virus by oligodeoxynucleoside methylphosphonates. *Proc. Natl. Acad. Sci. USA* 85:7448

112. Gasparro, F., O'Malley, M., Amici, L., Edelson, R. 1990. Photoactivatable antisense DNA: UVA photoactivation enhances the effects of antisense DNA. *J. Invest. Dermatol.* 94:527 (Abstr.)

113. Gasparro, F. P., Wong, H. H., Ugent, S. J., O'Malley, M. E., Edelson, R. L. 1989. Design of photoactivatable antisense oligonucleotides. *Clin. Res.* 37: 30A (Abstr.)

114. Helene, C., Montenay-Garestier, T., Saison, T., Takasugi, M., Toulemc, J. J., et al. 1985. Oligodeoxynucleotides covalently linked to intercalating agents: A new class of gene regulatory substances. *Biochimie* 67:777

115. Helene, C. 1987. Specific gene regulation by oligodeoxynucleotides covalently linked to intercalating agents. In *DNA-Ligand Interactions*, ed. W. Buschbauer, W. Saenger, p. 127. London/New York: Plenum

116. Felsenfeld, G., Davies, D. R., Rich, A. 1957. Formation of a three-stranded polynucleotide molecule. *J. Am. Chem. Soc.* 79:2023

117. Lipsett, M. N. 1963. The interactions of poly C and guanine trinucleotide. *Biochem. Biophys. Res. Commun.* 11: 224

118. Howard, F. B., Frazier, J., Lipsett, M. N., Miles, H. T. 1964. Infrared demonstration of two- and three-strand helix formation between poly C and guanosine mononucleotides and oligonucleotides. *Biochem. Biophys. Res. Commun.* 17:93

119. Miller, J. H., Sobell, H. M. 1966. A molecular model for gene repression. *Proc. Natl. Acad. Sci. USA* 55:1201
120. Lee, J. S., Johnson, D. A., Morgan, A. R. 1979. Complexes formed by (pyrimidine)_n (purine)_n DNAs on lowering the pH are three-stranded. *Nucleic Acids Res.* 6:3073
121. Morgan, A. R., Wells, R. D. 1968. Specificity of the three-stranded complex formation between double-stranded DNA and single-stranded RNA containing repeating nucleotide sequences. *J. Mol. Biol.* 37:63
122. Arnott, S., Bond, P. J., Selsin, E., Smith, P. J. C. 1976. Models of triple-stranded polynucleotides with optimised stereochemistry. *Nucleic Acids Res.* 3: 2459
123. Hoogsteen, K. 1959. The structure of crystals containing a hydrogen-bonded complex of 1-methylthymine and 9-methyladenine. *Acta Crystallogr.* 12: 822
124. Dervan, P. B. 1989. Oligonucleotide recognition of double-helical DNA by triple-helix formation. See Ref. 202, p. 197
125. Cooney, M., Czernuszewicz, G., Postel, E. H., Flint, S. J., Hogan, M. E. 1988. Site-specific oligonucleotide binding represses transcription of the human c-myc gene *in vitro*. *Science* 241:456
126. Beal, P. A., Dervan, P. B. 1991. Second structural motif for recognition of DNA by oligonucleotide-directed triple helix formation. *Science* 251:1360
127. Ono, A., Ts'o, P. O. P., Kan, L. 1991. Triplex formation of oligonucleotides containing 2'-O-methyl pseudouridine in substitution for 2'-deoxycytidine. *J. Am. Chem. Soc.* 113:4032
128. Horne, D. A., Dervan, P. G. 1990. Recognition of mixed sequence duplex DNA by alternate strand triple helix formation. *J. Am. Chem. Soc.* 112:2435
129. Sun, J. S., Francois, J. C., Montenay-Garestier, T., Saison-Behmoaras, T., Roig, V., et al. 1989. Sequence-specific intercalating agents: Intercalation at specific sequences on duplex DNA via major groove recognition by oligonucleotide-intercalator conjugates. *Proc. Natl. Acad. Sci. USA* 86:9198
130. Praseuth, D., Perrouault, L., Le Doan, T., Chassignol, M., Thuong, N., Helene, C. 1988. Sequence-specific binding and photocrosslinking of [alpha] and [beta]-oligodeoxynucleotides to the major groove of DNA via triple helix formation. *Proc. Natl. Acad. Sci. USA* 85:1349
131. Vlassov, V. V., Gaidamakov, S. A., Zarytova, V. F., Knorre, D. G., Levina, A. S., et al. 1988. Sequence-specific chemical modification of double-stranded DNA with alkylating oligodeoxyribonucleotides. *Gene* 72:313
132. Francois, J. C., Saison-Behmoaras, T., Chassignol, M., Thuong, N. T., Helene, C. 1988. Nucleases artificielles: Coupures spécifiques de la double hélice d'ADN par des oligonucléotides liés au complexe cuivre-phenanthroline. *CR Acad. Sci. III* 307(20):849
133. Francois, J. C., Saison-Behmoaras, T., Barbier, C., Chassignol, M., Thuong, N. T., Helene, C. 1989. Sequence-specific recognition and cleavage of duplex DNA via triple helix formation by oligonucleotides covalently linked to a phenanthroline-copper chelate. *Proc. Natl. Acad. Sci. USA* 86:9702
134. Francois, J. C., Saison-Behmoaras, T., Chassignol, M., Thuong, N. T., Helene, C. 1989. Sequence-targeted cleavage of single- and double-stranded DNA by oligothymidylates covalently linked to 1,10-phenanthroline. *J. Biol. Chem.* 264:5891
135. Francois, J. C., Saison-Behmoaras, T., Chassignol, M., Thuong, N. T., Sun, J. S., Helene, C. 1988. Periodic cleavage of poly(dA) by oligothymidylates covalently linked to 1,10-phenanthroline-copper complexes. *Biochemistry* 27:2272
136. Perrouault, L., Asseline, U., Rivalle, C., Thuong, N. T., Bisagni, E., et al. 1990. Sequence-specific artificial photo-induced endonucleases based on triple-helix forming oligonucleotides. *Nature* 344:358
137. Moser, H. E., Dervan, P. B. 1987. Sequence specific cleavage of double helical DNA by triple helix formation. *Science* 238:650
138. Hauseer, F. H., Singh, U. C., Saxe, J. D., Colvin, O. M., Ts'o, P. O. P. 1990. Can oligonucleoside methylphosphonates form a stable triplet with a double DNA helix? *Anti-Cancer Drug Design* 5:159
139. Letai, A. G., Palladine, M. A., Fromm, E., Rizzo, V., Fresco, J. R. 1988. Specificity in formation of triple-stranded nucleic acid helical complexes: Studies with agarose-linked polyribonucleotide affinity columns. *Biochemistry* 27:9108
140. Sklenar, V., Feigon, J. 1990. Formation of a stable triplex from a single DNA strand. *Nature* 345:836
141. Lyamichev, V. I., Frank-Kamenetskii, M. D., Soyfer, V. N. 1990. Protection against UV-induced pyrimidine dimer-

ization in DNA by triplex formation. *Nature* 344:568

142. Broitman, S. L., Im, D. D., Fresco, J. R. 1987. Formation of the triple-stranded polynucleotide helix, poly (AAU) *Proc. Natl. Acad. Sci. USA* 84: 5120

143. Maher, J. L. III, Wold, B., Dervan, P. G. 1989. Inhibition of DNA binding properties by oligonucleotide-directed triple helix formation. *Science* 245:725

144. Hanvey, J. C., Shimizu, M., Wells, R. D. 1989. Site-specific inhibition of EcoRI restriction/modification enzymes by a DNA triple helix. *Nucleic Acids Res.* 18:157

145. Orson, F. M., Thomas, D. W., McShan, W. M., Kessler, D. J., Hogan, M. E. 1991. Oligonucleotide inhibition of IL2R α mRNA transcription by promoter region collinear triplex formation in lymphocytes. *Nucleic Acids Res.* 19:3435

146. McManaway, M. E., Neckers, L. M., Loke, S. L., Al-Nasser, A. A., Redner, R. L., et al. 1990. Tumour-specific inhibition of lymphoma growth by an antisense oligodeoxynucleotide. *Lancet* 335:808

147. Kulka, M., Smith, C. C., Aurelian, L., Fishelevich, R., Meade, K., Miller, P., Ts'o, P. O. P. 1989. Site specificity of the inhibitory effects of oligo(nucleoside methylphosphonates) complementary to the acceptor splice junction of herpes simplex virus type 1 immediately early mRNA. *Proc. Natl. Acad. Sci. USA* 86:6868

148. Zamecnik, P. C., Goodchild, J., Taguchi, Y., Sarin, P. S. 1986. Inhibition of replication and expression of human T-cell lymphotropic virus type III in cultured cells by exogenous synthetic oligonucleotides complementary to viral RNA. *Proc. Natl. Acad. Sci. USA* 83:4143

149. Smith, C. C., Aurelian, L., Reddy, M. P., Miller, P. A., Ts'o, P. O. P. 1985. Antiviral effect of an oligo(nucleoside methylphosphonate) complementary to the splice junction of herpes simplex virus type 1 immediate early pre-mRNAs 4 and 5. *Proc. Natl. Acad. Sci. USA* 83:2787

150. Rosolen, A., Whitesell, L., Olegalo, M., Lennett, R. H., Neckers, L. M. 1990. Antisense inhibition of single copy N-myc expression results in decreased cell growth without reduction of c-myc protein in a neuroepithelioma cell line. *Cancer Res.* 50:6316

151. Vasanthakumar, G., Ahmed, N. K. 1989. Modulation of drug resistance in a daunorubicin resistant subline with oligonucleoside methylphosphonates. *Cancer Commun.* 1:225

152. Sburlati, A. R., Manrow, R. E., Berger, S. L. 1991. Prothymosin α antisense oligomers inhibit myeloma cell division. *Proc. Natl. Acad. Sci. USA* 88:253

153. Zheng, H., Sahai, B. M., Kilgannon, P., Fotedar, A., Green, D. R. 1989. Specific inhibition of cell-surface T-cell receptor expression by antisense oligodeoxynucleotides and its effect on the production of an antigen-specific regulatory T-cell factor. *Proc. Natl. Acad. Sci. USA* 86:3758

154. Maier, J. A. M., Voulalas, P., Roeder, D., Maciag, T. 1990. Extension of the life-span of human endothelial cells by an interleukin-1 α antisense oligomer. *Science* 249:1570

155. Draper, K. G., Driver, V. B., Hoke, G., Gonzalez, C., Anderson, K. P. 1991. Inhibition of herpes simplex virus replication using phosphorothioate oligonucleotides complementary to viral mRNA. Submitted

156. Cowser, L. M., Fox, M. C. 1991. Inhibition of bovine papilloma E₂ transactivation by antisense oligonucleotides. *Virology*. Submitted

157. Vickers, T., Baker, B. F., Cook, P. D., Zounes, M., Buckheit, R. W. Jr. et al. 1991. Inhibition of HIV-LTR gene expression by oligonucleotides targeted to the TAR element. *Nucleic Acids Res.* 19:3359

158. Saxena, S. K., Ackerman, E. J. 1991. Microinjected oligonucleotides complementary to the α -sarcin loop of 28 S RNA abolish protein synthesis in xenopus oocytes. *J. Biol. Chem.* 265:3263

159. Walker, K., Elela, S. A., Nazar, R. N. 1990. Inhibition of protein synthesis by anti-5.8 S rRNA oligodeoxyribonucleotides. *J. Biol. Chem.* 265:2428

160. Westerman, P., Gross, B., Hoinkis, G. 1989. Inhibition of expression of SV40 virus large T-antigen by antisense oligodeoxyribonucleotides. *Biomed. Biochim. Acta* 48:85

161. Baker, B. 1991. Analysis of reactive moieties for the chemical alteration of the 5' cap structure of mRNA. Submitted

162. Thuong, N. T., Asseline, U., Montenay-Garestier, T. 1989. Oligodeoxynucleotides covalently linked to intercalating and reactive substances: Synthesis, characterization, and physicochemical studies. See Ref. 202, p. 25

163. Helene, C., Toulme, J. J. 1989. Control of gene expression by oligodeoxynucleotides covalently linked to intercalat-

ing agents and nucleic acid-cleaving agents. See Ref. 202, p. 137

164. Chiang, M. Y., Chan, H., Zounes, M. A., Freier, S. M., Lima, W. F., Bennett, C. F. 1991. Antisense oligonucleotides inhibit ICAM-1 expression by two distinct mechanisms. *J. Biol. Chem.* 266:18162
165. Crouch, R. J., Dirksen, M.-L. 1990. Ribonucleases H. In *Nucleases*, ed. S. M. Linn, R. J. Roberts, p. 211. Cold Spring Harbor, NY: Cold Spring Harbor Lab.
166. Crum, C., Johnson, J. D., Nelson, A., Roth, D. 1988. Complementary oligodeoxynucleotide mediated inhibition of tobacco mosaic virus RNA translation *in vitro*. *Nucleic Acids Res.* 16:4569
167. Haeuptle, M. T., Frank, R., Dobberstein, B. 1986. Translation arrest by oligodeoxynucleotides complementary to mRNA coding sequences yields polypeptides of predetermined length. *Nucleic Acids Res.* 14:1427
168. Doris-Keller, H. 1979. Site specific enzymatic cleavage of RNA. *Nucleic Acids Res.* 7:179
169. Sproat, B. S., Lamond, A. L., Beijer, B., Neuner, P., Ryder, U. 1989. Highly efficient chemical synthesis of 2'-O-methyloligonucleotides and tetra-biotinylated derivatives; novel probes that are resistant to degradation by RNA or DNA specific nucleases. *Nucleic Acids Res.* 17:3373
170. Gagnor, C., Rayner, B., Leonetti, J. P., Imbach, J.-L., Leubleu, B. 1989. α -DNA IX. Parallel annealing of α -anomeric oligodeoxynucleotides to natural mRNA is required for interference in RNaseH mediated hydrolysis and reverse transcription. *Nucleic Acids Res.* 17:5107
171. Cazenave, C., Stein, C. A., Loreau, N., Thuong, N. T., Neckers, L. M., et al. 1989. Comparative inhibition of rabbit globin mRNA translation by modified antisense oligodeoxynucleotides. *Nucleic Acids Res.* 17:4255
172. Quartin, R., Brakel, C., Wetmur, J. 1989. Number and distribution of methylphosphonate linkages in oligodeoxynucleotides affect exo- and endonuclease sensitivity and ability to form RNase H substrates. *Nucleic Acids Res.* 17:7253
173. Furdon, P., Dominski, Z., Kole, R. 1989. RNase H cleavage of RNA hybridized to oligonucleotides containing methylphosphonate, phosphorothioate and phosphodiester bonds. *Nucleic Acids Res.* 17:9193
174. Eder, P. S., Walder, J. A. 1991. Ribonuclease H from K562 human erythroleukemia cells. *J. Biol. Chem.* 266:6472
175. Walder, R. Y., Walder, J. A. 1988. Role of RNase H in hybrid-arrested translation by antisense oligonucleotides. *Proc. Natl. Acad. Sci. USA* 85: 5011
176. Minshull, J., Hunt, T. 1986. The use of single-stranded DNA and RNase H to promote quantitative hybrid arrest of translation of mRNA/DNA hybrids in reticulocyte lysate cell-free translations. *Nucleic Acids Res.* 14:6433
177. Gagnor, C., Bertrand, J., Thenet, S., Lemaitre, M., Morvan, F., et al. 1987. Alpha-DNA VI: Comparative study of alpha- and beta-anomeric oligodeoxyribonucleotides in hybridization to mRNA and in cell free translation inhibition. *Nucleic Acids Res.* 15:10419
178. Knorre, D. G., Vlassov, V. V., Zarytova, V. F. 1989. Oligonucleotides linked to reactive groups. See Ref. 202, p. 173
179. Knorre, D. G., Vlassov, V. V., Zarytova, V. F. 1985. Reactive oligonucleotide derivatives and sequence-specific modification of nucleic acids. *Biochimie* 67:785
180. Vlassov, V. V., Zarytova, V. F., Kutyavin, I. V., Mamave, S. V. 1988. Sequence-specific chemical modification of a hybrid bacteriophage M13 single-stranded DNA by alkylating oligonucleotide derivatives. *FEBS Lett.* 231:352
181. Summerton, J., Bartlett, P. A. 1978. Sequence-specific crosslinking agents for nucleic acids. Use of 6-bromo-5,5-dimethoxyhexanohydrazide for crosslinking cytidine to guanosine and crosslinking RNA to complementary sequences of DNA. *J. Mol. Biol.* 122: 145
182. Webb, T. R., Matteucci, M. D. 1986. Hybridization triggered crosslinking of deoxynucleotides. *Nucleic Acids Res.* 14:7661
183. Le Doan, T., Perrouault, L., Praseuth, D., Habhou, N., Decout, J., et al. 1987. Sequence-specific recognition, photocrosslinking and cleavage of the DNA double helix by an oligo-[alpha]-thymidylate covalently linked to an azidoproflavine derivative. *Nucleic Acids Res.* 15:7749
184. Federova, O. S., Knorre, D. G., Podust, L. M., Zarytova, F. V. 1988. Complementary addressed modification of double-stranded DNA within a ternary complex. *FEBS Lett.* 228:273
185. Le Doan, T., Perrouault, L., Chassignol, M., Thuong, N. T., Helene, C. 1987. Sequence-targeted chemical mod-

ifications of nucleic acids by complementary oligonucleotides covalently linked to porphyrins. *Nucleic Acids Res.* 15:8643

186. Le Doan, T., Perrouault, L., Thuong, N. T., Helene, C. 1989. Sequence-specific chemical and photochemical reactions on nucleic acids by oligonucleotides linked to porphyrins. *J. Inorg. Biochem.* 36:274 (Abstr.)

187. Le Doan, T., Praseuth, D., Perrouault, L., Chassignol, M., Thuong, N. T., Helene, C. 1991. Sequence-targeted photochemical modifications of nucleic acids by complementary oligonucleotides covalently linked to porphyrins. *Bioconj. Chem.* 1:108

188. Lee, B. L., Blake, K. R., Miller, P. S. 1988. Interaction of psoralen-derivatized oligodeoxyribonucleoside methylphosphonates with synthetic DNA containing a promoter for T7 RNA polymerase. *Nucleic Acids Res.* 16:10681

189. Lee, B. L., Murakami, A., Blake, K. R., Lin, S.-B., Miller, P. S. 1988. Interaction of psoralen-derivatized oligodeoxyribonucleoside methylphosphonates with single-stranded DNA. *Biochemistry* 27: 3197

190. Praseuth, D., Chassignol, M., Takasugi, M., Le Doan, T., Thuong, N. T., Helene, C. 1987. Double helices with parallel strands are formed by nuclease-resistant oligo-[alpha]-deoxynucleotides and oligo-[alpha]-deoxynucleotides covalently linked to an intercalating agent with complementary oligo-[beta]-deoxynucleotides. *J. Mol. Biol.* 196:939

191. Helene, C. 1989. Artificial control of gene expression by oligonucleotides covalently linked to intercalating agents. *Br. J. Cancer* 60:157

192. Chu, B. C. F., Orgel, L. E. 1985. Nonenzymatic sequence-specific cleavage of single-stranded DNA. *Proc. Natl. Acad. Sci. USA* 82:963

193. Boutorin, A. S., Vlassov, V. V., Kazakov, S. A., Kutiaviv, I. V., Podyminogin, M. A. 1984. Complementary addressed reagents carrying EDTA-Fe(II) groups for directed cleavage of single-stranded nucleic acids. *FEBS Lett.* 172:43

194. Chen, C.-H. B., Sigman, D. S. 1986. Nuclease activity of 1,10-phenanthroline-copper: Sequence-specific targeting. *Proc. Natl. Acad. Sci. USA* 83:7147

195. Sun, J. S., Francois, J. C., Lavery, R., Saison-Behmoaras, T., Montenay-Garestier, et al. 1988. Sequence-targeted cleavage of nucleic acids by oligo-[α]-thymidylate-phenanthroline conjugates: Parallel and anti-parallel double helices are formed with DNA and RNA, respectively. *Biochemistry* 27:6039

196. Helene, C., Le Doan, T., Thuong, N. T. 1989. Sequence-targeted photochemical reactions in single-stranded and double-stranded nucleic acids by oligonucleotide-photosensitizer conjugates. In *Photochemical Probes in Biochemistry*, ed. P. E. Nielsen, p. 219. Paris: Kluwer Academic

197. Helene, C., Thuong, N. T. 1987. Oligodeoxynucleotides covalently linked to intercalating agents and to nucleic acid-cleaving reagents. New families of gene regulatory substances. In *Working Group on Molecular Mechanisms of Carcinogenic and Antitumor Activity*, ed. C. Chagas, B. Pullman, p. 205. Vatican City: Pontificiae Acad. Scientiarum Scripta Varia

198. Helene, C., Thuong, N. T. 1989. Control of gene expression by oligonucleotides covalently linked to intercalating agents. *Genome* 31:413

199. Cech, T. R. 1987. The chemistry of self-splicing RNA and RNA enzymes. *Science* 236:1532

200. McSwiggen, J. A., Cech, T. R. 1989. Stereochemistry of RNA cleavage by the *Tetrahymena* ribozyme and evidence that the chemical step is not rate-limiting. *Science* 244:679

201. Herschlag, D., Cech, T. R. 1990. DNA cleavage catalysed by the ribozyme from *Tetrahymena*. *Nature* 344:405

202. Cohen, J. S., 1989. *Oligodeoxynucleotides. Antisense Inhibitors of Gene Expression*. Boca Raton, FL: CRC Press. 255 pp.

203. Mol, J. N. M., van der Krol, A. R., eds. 1991. *Antisense Nucleic Acids and Proteins. Fundamentals and Applications*. New York: Dekker. 231 pp.

204. Caruthers, M. H., Beaton, G., Cummings, L., Dellinger, D., Graff, D., et al. 1991. Chemical and biochemical studies with dithioate DNA. *Nucleosides and Nucleotides* 10:47

205. Spielvogel, B. F., Sood, A., Shaw, B. R., Hall, I. H. 1991. From boron analogues of amino acids to boranated DNA: Potential for new pharmaceuticals and neutron capture agents. *Pure Appl. Chem.* 63:415

206. Musicki, B., Widlanski, T. S. 1991. Synthesis of nucleoside sulfonates and sulfones. *Tetrahedron Lett.* 32:1267

207. Huang, Z., Benner, S. T. 1991. Non-ionic antisense oligonucleotides containing sulfide and sulfone linkages in place of phosphodiester groups in natural oligonucleotides. *Colloq. Gene Regulation by Antisense RNA and DNA, CD* 210:19.

Keystone Symp. Mol. Cell. Biol. Feb. 2-7, Frisco, CO

208. Mirabelli, C. K. 1991. Activities of antisense oligonucleotides. *Anti-Cancer Drug Design*. In press

209. Cowser, L. M., Fox, M. C. 1991. Inhibition of human papillomavirus type II E2 transactivation by antisense oligonucleotides. *Antimicrob. Agents Chemother.* Submitted

210. Tortora, G., Clair, T., Cho-Chung, Y. S. 1990. An antisense oligodeoxynucleotide targeted against the type II β regulatory subunit mRNA of protein kinase inhibits cAMP-induced differentiation in HL-60 leukemia cells without affecting phorbol ester effects. *Proc. Natl. Acad. Sci. USA* 87:705

211. Kinchington, D., Galpin, S. 1989. GAG and POL antisense oligodeoxynucleotides as inhibitors of HIV-1. *Meet. Oligodeoxynucleotides as Antisense Inhibitors of Gene Expression: Therapeutic Implications*, June 18-21, Rockville, MD

212. Lemaitre, M., Bayard, B., Lebleu, B. 1987. Specific antiviral activity of a poly(L-lysine)-conjugated oligodeoxyribonucleotide sequence complementary to vesicular stomatitis virus N protein mRNA initiation site. *Biochemistry* 84:648

213. Vlassov, V. V. 1989. Inhibition of tick-borne viral encephalitis expression using covalently linked oligonucleotide analogs. See Ref. 211

214. Miller, P. S., Agris, C. H., Aurelian, L., Blake, K. R., Murakami, A., et al. 1985. Control of ribonucleic acid function by oligonucleoside methylphosphonates. *Biochimie* 67:769

215. Goodarzi, G., Gross, S. C., Tewari, A., Watabe, K. 1990. Antisense oligodeoxyribonucleotides inhibit the expression of the gene for hepatitis B virus surface antigen. *J. Gen. Virol.* 71:3021

216. Wickstrom, E. L., Bacon, T. A., Gonzalez, A., Lyman, G. H., Wickstrom, E. 1989. Anti-c-myc DNA increases differentiation and decreases colony formation by HL-60 cells *in vitro*. *Cell Dev. Biol.* 25:297

217. Gewirtz, A. M., Anfossi, G., Venturelli, D., Valpreda, S., Sims, R., Calabretta, B. 1989. A c-myb antisense oligodeoxynucleoside inhibits normal human hematopoiesis *in vitro*. *Science* 245:1303

218. Jaroszewski, J. W., Kaplan, O., Syi, J. L., Sehested, M., Faustino, P. J., Cohen, J. S. 1990. Concerning antisense inhibition of the multiple drug resistance gene. *Cancer Commun.* 2:287

219. Jaskulski, D., DeRiel, J. K., Mercer, W. E., Calabretta, B., Baserga, R. 1989. Inhibition of cellular proliferation by antisense oligodeoxynucleotides to PCNA cyclin. *Science* 240:1544

220. Birchenall-Roberts, M. C., Falk, L. A., Ferrer, C., Ruscetti, F. W. 1989. A CSF-1 antisense oligodeoxynucleotide inhibits proliferation of immortalized murine monocytes establishment of a autocrine regulation. *J. Cell. Biochem. Suppl.* 13 (Pt. C):18

221. Yeoman, L. C., Daniels, Y. J., Lynch, M. J. 1989. Inhibition of colon tumor cell growth by direct addition of anti-EGF receptor oligodeoxyribonucleotides. See Ref. 211

222. Blake, K. R., Murakami, A., Miller, P. S. 1985. Inhibition of rabbit globin mRNA translation by sequence-specific oligodeoxyribonucleotides. *Biochemistry* 24:6132-34

223. Clark, M. A., Ozgur, L. E., Conway, T. M., Dispoto, J., Crooke, S. T., Bomalaski, J. S. 1991. Cloning of a phospholipase A₂-activating protein. *Proc. Natl. Acad. Sci. USA* 88:5418

224. Petersheim, M., Turner, D. H. 1983. Base-stacking and base-pairing contributions to helix stability: Thermodynamics of double-helix formation with CCGG, CGGGp, CCGGAp, ACCGGp, CCGGUp and ACCGGUp. *Biochemistry* 22:256

225. Florini, J. R., Ewton, D. Z. 1990. Highly specific inhibition of IGF-I-stimulated differentiation by an antisense oligodeoxyribonucleotide to myogenin mRNA. *J. Biol. Chem.* 265:13435

226. Acha-Orbea, H., Scarpellino, L., Hertig, S., Dupuis, M., Tschoop, J. 1990. Inhibition of lymphocyte mediated cytotoxicity by perforin antisense oligonucleotides. *EMBO J.* 9:3815

227. Bories, D., Raynal, M-C., Solomon, D. H., Darzynkiewicz, Z., Cayre, Y. E. 1989. Down-regulation of serine protease, myeloblastin, causes growth arrest and differentiation of promyelocytic leukemia cells. *Cell* 59:959

228. Caceres, A., Kosik, K. S. 1990. Inhibition of neurite polarity by tau antisense oligonucleotides in primary cerebellar neurons. *Nature* 343:461

229. Morrison, R. S. 1991. Suppression of basic fibroblast growth factor expression by antisense oligodeoxynucleotides inhibits the growth of transformed human astrocytes. *J. Biol. Chem.* 266:728

230. Brandt, C. R., Coakley, L. M., Grau, D. R., Draper, K. G., Mirabelli, C. K. 1991. Treatment of HSV-1 induced ocular disease with a phosphorothioate oligonucleotide, ISIS 1082. Submitted